

**Investigating the Corrosion Behaviour of Carbon Black Steel Rebar in Ordinary
and Limestone Cements with and without Blast Furnace Slag**

by

Shelley Hui Juan Yang

A thesis

presented to the University of Waterloo

in fulfilment of the

thesis requirement for the degree of

Master of Applied Science

in

Civil Engineering

Waterloo, Ontario, Canada, 2022

© Shelley Hui Juan Yang 2022

Author's Declaration

I hereby declare that I am the sole author of this thesis. This is a true copy of the thesis, including any required final revisions, as accepted by my examiners.

I understand that my thesis may be made electronically available to the public.

Abstract

Over the years, strange climate patterns have evolved over the globe, raising flags for concerns of the effects of global warming. Cement production contributes to 8% of the global carbon dioxide emission, primarily by the kiln process which involves heating the ground raw materials into clinker to which chemicals are added to create what is known as cement. In the construction industry, efforts to adopt more sustainable approaches are not uncommon. One such approach is the use of Portland Limestone Cement (PLC) in place of Ordinary Portland Cement (OPC). Unlike the heavy adoption in European countries, North American countries are gradually adopting this alternative for cement, allowing for up to 15% limestone in PLC. Another more common approach is the replacement of cement by ground-granulated blast furnace slag (GBFS). The North American standards, however, limit the replacement by GBFS by 25%.

It is not surprising that with the limited research on the influence of the additional limestone in PLC on the corrosion performance of reinforced concrete, it brings hesitation for its use in North American countries where harsh cold winters last longer than warmer climates. With the cold, comes ice and the need for use of de-icing salts on concrete infrastructure to ensure safety of its users. The disadvantage of the de-icing salts to the durability of reinforced concrete structures is primarily the induced corrosion of the reinforcement. Therefore, the intent of this research is to promote the use of green cement mixes comprising PLC and high levels of GBFS replacement, by investigating the degree of detriment on the corrosion behaviours of carbon (black) steel rebar by the cement replacement.

This research assessed the chemical, physical and electrochemical changes of eight cement mixes, OPC and PLC, with 0%, 25%, 35% and 50% GBFS replacement by mass of the cementitious materials. Two types of samples of the various mixes were investigated: cement pastes for chemical and electrochemical evaluations of rebar directly exposed to simulated environments, and concrete for physical and electrochemical evaluations of embedded rebar. Two carbon steel rebar of different surface conditions, pre-rusted and non-rusted, were used for the control mixes which were OPC or PLC without GBFS, while only the latter rebar type was used in the investigations with the other mixes.

Reinforced concrete structural components can persist for much longer service lives in the absence of salts than in the reality of the use of de-icing salts. It is because of the highly alkaline nature of concrete which facilitates the formation of self-protective passive films on the rebar embedded within. Under the attack of salts in the pore solution of the concrete surrounding the rebar, the passive film becomes pitted, and any discontinuity facilitates corrosion of the exposed area. The pore liquids were squeezed, using high pressure equipment, from the hardened cement pastes of the eight mixes, with varied admixed chloride concentrations. The direct influence of the changes of the pore solution chemistry on the corrosion resistance of the carbon steel rebar in simulated environments of the pore solutions was investigated using the electrochemical technique of linear polarization resistance (LPR). This type of experiment is an accelerated method which mitigates the need for time-dependent ion diffusion in concrete and allows for direct observation of the behaviour of the rebar in contact with chloride-contaminated pore solutions specific to the chemistry of the various mixes. The results showed the chemistry of the pore solutions of the PLC-based mixes to be comparable with the respective OPC-based mixes, while the electrochemical tests showed that the increase of GBFS replacement in the cement resulted in decreased corrosion resistance of the carbon rebar.

The experimental portion involving the reinforced concrete block specimens, which were formed with recesses for ponding wells, comprised primarily of electrochemical measurements. The electrical resistivities and compressive strengths of concrete cylinders, which were cast along with the block specimens of the eight cementitious mixes, were evaluated and the results differed by little to none between the OPC- and PLC-based specimens. The resistivities increased with increasing GBFS replacement. The strengths showed a general decrease with increase in GBFS replacement, particularly for the 50% GBFS replacement, but the strengths of the 25% and 35% GBFS specimens were similar to the strengths of 0% GBFS after day 56. The wetting solution of one of the four/five reinforced concrete replicas of each mix type was left without chlorides while the others were contaminated with 3% NaCl solution for 210 days followed by 5.75% NaCl solution. The electrochemical data showed slight decrease in passive corrosion rates as GBFS replacement level increased. Two chloride-contaminated concrete specimens were autopsied, and it was observed that the chlorides ingress was not yet at the level of the rebar to induce corrosion. The autopsied concretes with GBFS had lesser chloride ion detections, by XRF analyses, than those without GBFS, which was expected with the increased resistivities with GBFS replacement.

Acknowledgements

I once heard the saying, “the future is the present of the past,” and so, had I not crossed paths with Dr. Carolyn Hansson, I would have remained with little confidence in my critical thinking and communication skills. I sincerely thank her not only for the opportunity under her supervision but also for nurturing me with words of wisdom in academics and life and of encouragement as she patiently guided me through the graduate program. Despite the challenges brought by the unprecedented pandemic and downtimes, her kindness and dedication did not waver.

I would like to express my gratitude to our research team: Fook Yee Yang and Ibrahim Ogunsanya, for their help and for sharing their knowledge and lessons learnt. My experiments would not have run smoothly without the help of the very knowledgeable and experienced technical staff at the University of Waterloo: Richard Morrison, Doug Hirst and Rob Kaptein of the structures and materials groups, and Fred Bakker and Rick Forgett of the engineering machine shop (EMS), as they worked to provide alternatives to ensure safety and continued functioning of my experiments.

I would like to thank Joy Hu of the Groundwater Geochemistry and Remediation Group (for the IC/ICP analyses), Phill Laycock of EMS (for the XRF analyses), Mark Merlau (for access to the DWE Water Chemistry lab equipment and chemicals for the pH and titration tests), and the teams at the Centre for Pavement and Transportation Technology (CPATT), Sciences Technical Services and Engineering Student Machine Shop for use of their equipment and for conducting the key analyses for my research. My graduate studies would not have been possible without the financial support by the National Sciences and Engineering Research Council (NSERC) and Department of Civil and Environmental Engineering at the University of Waterloo, as well as the supply of materials by Max Aicher North America (MANA), HarrisRebar and Ash Grove Cement Company.

Needless to say, my motivation and state of mind would have wavered if it were not for the unconditional support by my dearest parents and family in Trinidad and Canada. I thank my brethren Alex, Kelly and Karen for being there to push me out of my slumps and for believing that I could excel in what I do. Last but not least, I would like to express my sincerest thanks to my friends in Trinidad and Canada: Kiana, Shalini, Linglin and Debbie, for being there for me always and for encouraging me to have faith in my capabilities for excellence.

Finally, I wish to encourage others to be open to learning: "Learn from yesterday, live for today, hope for tomorrow. The important thing is not to stop questioning." _ by *Albert Einstein*.

Table of Contents

Author's Declaration.....	ii
Abstract.....	iii
Acknowledgements.....	v
List of Figures.....	ix
List of Tables.....	xii
List of Abbreviations.....	xiii
1.0 Introduction.....	1
1.1 Background.....	1
1.2 Research Objectives.....	5
2.0 Literature Review.....	6
2.1 Cement Production.....	6
2.1.1 Hardened Cement Paste and Concrete.....	7
2.1.1 Effect of Cement Replacement on Hydration.....	9
2.1.2 Effect of Water-to-Cementitious Materials Ratio on Hydration.....	11
2.2 Steel Reinforcement in Concrete.....	12
2.2.1 Corrosion by Carbonation.....	12
2.2.2 Corrosion by Chloride Attack.....	13
2.3 Chemistry of the Pore Solution.....	16
2.3.1 Effect of Cement Replacement on Pore Solution Chemistry.....	17
2.5 Concrete Durability.....	18
2.5.1 Effect of Cement Replacements on Compressive Strength.....	18
2.5.2 Effect of Cement Replacements on Electrical Resistivity.....	20
2.5.3 Effect of Cement Replacements on Chloride-Induced Corrosion.....	20
3.0 Experimental Procedure.....	25
3.1 Material Information.....	25
3.1.1 Cementitious Materials.....	25
3.1.2 Carbon (Black) Steel Rebar.....	26
3.2 Pore Solution Expression, Chemical Analysis and Corrosion Tests.....	27
3.2.1 Cement Paste Specimens.....	27
3.2.2 Expression of Pore Solutions.....	29

3.2.3	Chemical Analyses of Expressed Pore Solutions	31
3.2.4	Evapourable Water Measurements	33
3.2.5	Synthetic Pore Solutions	34
3.2.6	Preparation of Rebars for Immersion in Solutions	34
3.2.7	Setup for Corrosion Tests in Synthetic Pore Solutions.....	35
3.2.8	Electrochemical Tests	36
3.2.8.1	Open Circuit Potential (OCP) Measurements.....	37
3.2.8.2	Linear Polarization Resistance (LPR) Technique.....	38
3.2.9	Autopsy of Rebar Specimens.....	40
3.3	Reinforced Concrete Block Specimens	40
3.3.1	Concrete Specimen Preparation.....	40
3.3.2	Concrete Mix Design	41
3.3.3	Concrete Resistivity Tests.....	43
3.3.4	Concrete Compressive Strength Test.....	45
3.3.5	Macrocell Electrochemical Tests.....	45
3.3.6	Microcell Electrochemical Tests – OCP, LPR and GP Tests	46
3.3.7	Autopsy by Visual Inspection and X-Ray Fluorescence (XRF).....	48
4.0	Experimental Results	51
4.1	Tests on the Cement Paste Specimens	51
4.1.1	Observations	51
4.1.2	Chemical Analyses of Expressed Pore Solutions	52
4.1.3	Bound Chlorides	60
4.1.4	Corrosion Tests on Rebar in Synthetic Pore Solution	61
4.1.5	Observations from Synthetic Pore Solution Tests	62
4.2	Tests on Concrete Cylinders and Block Specimens	64
4.2.1	Test Results of the Concrete Cylinders.....	64
4.2.2	Macrocell Corrosion Results of the Reinforcement in the Concrete Block Specimens	66
4.2.3	Microcell Corrosion Results of the Reinforcement in the Concrete Block Specimens.....	73
4.2.4	XRF Scans on Autopsied Reinforced Concrete Specimens	83

5.0	Analysis and Discussion of Results	86
5.1	Visible Effect of Cement Replacement on Cement Pastes	86
5.2	Effect of Using PLC Instead of OPC on the Corrosion Behaviour of Rebar	87
5.3	Effect of GBFS Replacement of Cement on the Corrosion Behaviour of Rebar	95
5.4	Interpretation of the Macrocell Corrosion Measurements	99
5.5	Effect of Rebar Condition on Corrosion Performance	101
6.0	Summary, Conclusions and Recommendations.....	104
6.1	Consideration of the Implications of the Experimental Results	104
6.2	Summary of Results	105
6.3	Conclusions.....	107
6.4	Considerations for Future Application of this Research.....	108
6.5	Recommendations for Future Works	109
	References.....	111
	Appendices.....	120
	Appendix A - Material Information.....	120
	Appendix B - Extra Information on Tests based on Expressed Pore Solutions.....	122
	B.1 Sample Calculations for Interpreting Titration Results as pH for Pore Solutions	122
	B.2 Sample Calculations for Determining Bound Chlorides from Evapourable Water	122
	B.3 Averaged Evapourable Water Measurements and Titration Alkalinities.....	123
	B.4 Major Chemical Concentrations of Expressed Pore Solutions, by the ICP/IC Analyses	124
	B.5 Mass Proportions of Laboratory-Grade Chemical Agents for Synthetic Solutions	125
	B.6 Corrosion Measurements and Autopsy of Rebar Specimens in Synthetic Solution	127
	Appendix C - Extra Information on Tests based on Concrete Specimens.....	139
	C.1 Electrochemical Test Measurements and XRF Data for Major Elements for Bars in Individual Autopsied Specimens	139
	C.2 Sketch of Layout of Concrete Specimens in Monitoring Room	180

List of Figures

Figure 1.1 Trends in global CO ₂ emissions, between 1960 and 2020, measured as GtCO ₂ and GtC	2
Figure 1.2 Timeline of changes in limestone limits in European and North American standards	3
Figure 2.1 The average energy consumption and CO ₂ footprint of the main manufacturing segments of the cement production ^[19]	6
Figure 2.2 Development of the major hydration products with age of the cement paste ^[25]	9
Figure 2.3 Schematic representation of the hydration of the clinker without and with GBFS	10
Figure 2.4 Simplified potential-pH diagram for iron at 25°C ^[62] , adapted from Pourbaix ^[48]	14
Figure 2.5 Microcell circuit (Left) versus the macrocell circuit (Right) for steel reinforcement embedded in concrete ^[47]	15
Figure 2.6 Mechanisms of general corrosion and pitting corrosion in concrete ^[94]	16
Figure 2.7 Influence of environment and concrete properties on the critical chloride content ^[94]	22
Figure 2.8 Range of (Cl ⁻ /OH ⁻) ratios as CCT for active corrosion to initiate in OPC pore solutions, mortars and concrete ^[A= 91]	22
Figure 3.1 Longitudinal and sectional photographs at time of testing. (Left) Ha rebar after more than 3 years in the laboratory; (Right) MA rebar few months after dispatch from rolling mill ...	26
Figure 3.2 (Left) Hobart mixer used to blend the cement paste mixes; (Right) Hotdog rolling machine used for continuous rolling of cement paste cylinders	28
Figure 3.3 (Left) Pore solution equipment setup; (Right) Specimen holder and base with collection syringe.....	29
Figure 3.4 Pre- and post- compressed conditions typical of the cement paste cylinders.....	30
Figure 3.5 (Left) Setup for removal of compressed cylinder and disks; (Right) Loading elements	31
Figure 3.6 Tools and chemicals used for titration (Left); Colour changes of diluted sample with 3-4 drops of bromocresol green-methyl red indicator (Right)	32
Figure 3.7 (Left) Tools used for powdering the cement paste cylinders; (Right) Ground samples, three for each cement paste cylinder specimen, in oven.....	34
Figure 3.8 Randles circuit for the steel in synthetic pore solution ^[97]	37
Figure 3.9 Randles circuits for steel reinforcement in (a) passive state (no corrosion) and (b) active corrosion state ^[98]	37
Figure 3.10 Three-electrode system for electrochemical test setup for pore solution	39
Figure 3.11 (Left) Formwork dimensions; (Middle) Polystyrene ponding-well form; (Right) Schematic representation of reinforced concrete block specimen	41
Figure 3.12 Schematic of closed circuit established by Wenner Probe for surface resistivity ^[103]	44
Figure 3.13 Test setup for measuring bulk resistivity of a concrete cylinder	44
Figure 3.14 Cylinder compression strength test setup	45
Figure 3.15 Schematic of typical circuit of concrete block specimen with Keithley device	46
Figure 3.16 Typical potential response to a galvanostatic pulse ^[107]	47

Figure 3.17 Clamping system for concrete saw table	48
Figure 3.18 Schematic of cut of concrete block specimens (Left) and XRF scan-gridlines on interior cut faces (Right)	49
Figure 3.19 Diagrammatic summary of the function of XRF device ^[113]	50
Figure 4.1 Dark blue-greenish discolouration of the cement pastes with and without GBFS replacement and admixed chloride	52
Figure 4.2 pH of expressed pore solutions, measured using an Orion pH meter	53
Figure 4.3 Estimated pH values by method of titration	54
Figure 4.4 Estimated pH values by method of stoichiometry.....	55
Figure 4.5 Molar concentrations of sodium ions measured as a function of admixed chlorides..	56
Figure 4.6 Molar concentrations of potassium ions measured as a function of admixed chlorides	56
Figure 4.7 Sulphate concentrations of the expressed solutions, as a function of admixed chlorides	57
Figure 4.8 Chloride concentrations of the expressed solutions, as a function of admixed chlorides	58
Figure 4.9 Sulphur concentrations of the expressed solutions, as a function of admixed chlorides	59
Figure 4.10 Thiosulphates found in the cement mixes containing GBFS	59
Figure 4.11 The bound chlorides as a function of the admixed chloride concentrations	60
Figure 4.12 Averages of the corrosion current densities recorded for each mix type	61
Figure 4.13 Averaged open circuit potentials recorded, at time of LPR tests, for each mix type	62
Figure 4.14 Discolouration of the 0FSGU test solution at start of day 1 (Left) and after removal of specimens (after day 250)	63
Figure 4.15 Adsorbed white precipitate coating a specimen from 0BFSGUL test solution.....	63
Figure 4.16 Surface resistivities, measured by Wenner probe, on aged concrete cylinders for the different mix types	64
Figure 4.17 Bulk resistivities, calculated from total resistance measurements by Wenner probe, of aged concrete cylinders of the varied mixes	65
Figure 4.18 Compressive strengths of aged concrete cylinders of the various mix types	65
Figure 4.19 Ambient temperature and relative humidity of room of the concrete block specimens	66
Figure 4.20 Current densities varied along with the age of the 0BFSGUL Ha and MA specimens	68
Figure 4.21 Current densities varied along with the age of the 0BFSGU Ha and MA specimens	69
Figure 4.22 Current densities varied along with the age of the 25BFSGUL specimens	70
Figure 4.23 Current densities varied along with the age of the 25BFSGU specimens.....	70
Figure 4.24 Current densities varied along with the age of the 35BFSGUL specimens	71
Figure 4.25 Current densities varied along with the age of the 35BFSGU specimens.....	71
Figure 4.26 Current densities varied along with the age of the 50BFSGUL specimens	72

Figure 4.27 Current densities varied along with the age of the 50BFSGU specimens.....	72
Figure 4.28 Corrosion current densities of the top bars of the 0BFSGUL specimens	74
Figure 4.29 Open circuit potentials of the top bars of the 0BFSGUL specimens	74
Figure 4.30 Corrosion current densities of the top bars of the 0BFSGU specimens	75
Figure 4.31 Open circuit potentials of the top bars of the 0BFSGU specimens.....	75
Figure 4.32 Corrosion current densities of the top bars of the 25BFSGUL specimens	76
Figure 4.33 Open circuit potentials of the top bars of the 25BFSGUL specimens	76
Figure 4.34 Corrosion current densities of the top bars of the 25BFSGU specimens	77
Figure 4.35 Open circuit potentials of the top bars of the 25BFSGU specimens.....	77
Figure 4.36 Corrosion current densities of the top bars of the 35BFSGUL specimens	78
Figure 4.37 Open circuit potentials of the top bars of the 35BFSGUL specimens	78
Figure 4.38 Corrosion current densities of the top bars of the 35BFSGU specimens.....	79
Figure 4.39 Open circuit potentials of the top bars of the 35BFSGU specimens.....	79
Figure 4.40 Corrosion current densities of the top bars of the 50BFSGUL specimens	80
Figure 4.41 Open circuit potentials of the top bars of the 50BFSGUL specimens	80
Figure 4.42 Corrosion current densities of the top bars of the 50BFSGU specimens.....	81
Figure 4.43 Open circuit potentials of the top bars of the 50BFSGU specimens.....	81
Figure 4.44 Corrosion products present on the top rebar of the respective concrete mix types...	83
Figure 4.45 Averaged chloride content, as % by wt. of concrete, analyzed by XRF device.....	84
Figure 5.1 Surface Resistivities of GUL- versus GU-based concrete	90
Figure 5.2 Bulk Resistivities of GUL- versus GU-based concrete.....	90
Figure 5.3 Compressive Strengths of GUL- versus GU-based concrete	91
Figure 5.4 Average concrete resistance, estimated by GP, of the concrete specimens	93
Figure 5.5 Expanded view of the chlorides, detected by XRF, on gridline 2, averaged from two autopsied concrete of each mix.....	94
Figure 5.6 (Top) Averages of the (Bottom) Individual Chloride XRF Datapoints of the Concrete Specimens, along Gridline 2 of Figure 3.18	98
Figure 5.7 Average current densities measured for the Ha- and MA- rebar in 0BFS test solutions	102
Figure 5.8 Average OCP measured for the Ha- and MA- rebar in 0BFS test solutions.....	102

List of Tables

Table 3.1 Chemical compositions of GU and GUL cements and GBFS, per mill certificates.....	25
Table 3.2 Nomenclature of the mix designs for the cement paste mixes	27
Table 3.3 Proportions of the materials for the respective mix designs for the cement paste mixes	28
Table 3.4 Configuration of rebar types in the respective test containers.....	35
Table 3.5 Duration of incremental chloride chemicals to the synthetic pore solutions.....	36
Table 3.6 Corrosion risks of carbon steel embedded in concrete per measured OCP ^[95]	38
Table 3.7 Concrete mix designs for reinforced concrete block specimens.....	42
Table 5.1 Observed corrosion initiations of the reinforcement in the concrete block specimens	97

List of Abbreviations

ASTM – American Society for Testing and Materials

cm – cementitious materials

CE – Counter Electrode

CSA – Canadian Standards Association

GBFS – Ground/Granulated Blast Furnace Slag

GP – Galvanostatic Pulse

GU – General Use; used interchangeably with OPC – Ordinary Portland Cement

GUL – General Use Limestone; used interchangeably with PLC – Portland Limestone Cement

Ha – experimental abbreviation for HarrisRebar Specimens

IC – Ion Chromatography/Ion Exchange Chromatography

ICP-MS - Inductively Coupled Plasma-Mass Spectrometry

ICP-OES – Inductively Coupled Plasma-Optical Emission Spectrometry

MA – experimental abbreviation for MANA Bar Mill Specimens

OCP – Open Circuit Potential

OPSS – Ontario Provincial Standard Specification

LPR – Linear Polarization Resistance

RE – Reference Electrode

SCE – Saturated Calomel Electrode

SCM – Supplementary Cementitious Material

WE – Working Electrode

XRF – X-ray Fluorescence

1.0 Introduction

The innovation, goals and scope of the research study are discussed in this section.

1.1 Background

The production of concrete is a major contributor to the accelerating global warming. The mining of its constituents (basically, limestone, clay, gravel and sand) has a huge impact on the environment. Equally important is the calcining of cement which produces approximately 0.5-1 tonne of carbon dioxide (CO₂) for every tonne of cement ^[9] and requires a huge amount of thermal energy for the chemical reaction at ~1500°C. Naturally, the longer the life of the concrete structure, the better. Therefore, durability is a major factor in sustainability and the predominant limit to durability in this part of the world, where cold climates prolong for over half of each year, is corrosion of reinforcement steel (rebar) ^{[15], [71]}. The purpose of the current research is to investigate the impact on rebar corrosion of reducing the cement content of concrete by partial replacements with limestone and ground-granulated blast furnace slag.

The recent years have recorded a formidable rise in unprecedented phenomena, predominantly cases of climate change, across the North American continent. In just the year of 2021, which is noted in history as one of the warmest years ^[1], the province of British Columbia, Canada succumbed to a lasting heat wave of temperatures in the high 30's-40's in degrees Celsius ^[2], while snow clouds loomed over the state of Texas, United States of America, causing record-breaking low temperatures below 0 degrees Celsius ^[3]. Despite the evolution of technologies introduced in industries for improving sustainability and for reducing the carbon footprint, the numbers are still high above 10 gigatonnes of CO₂ emissions (10GtC/year ≈ 37Gt CO₂/year) in the year of 2021 ^[4], ^[5]. The numbers charted in the graphs in Figure 1.1 were estimated from emissions generated from burning of fossil fuels for transportation, heating treatments and other industrial processes, as categorized in the right graph in Figure 1.1, which excluded agricultural and naval emissions. The industries considered in the estimates included the cement production, and oil and gas industries ^{[5], [19]}. The left graph in Figure 1.1 displayed the global emission counts with a dark-greyish shadow indicating the statistical uncertainty of the estimates. North America was shown to contribute to about 17.5% of the global emissions, with Canada contributing 9% of the North American emissions, as charted by statistics ^[19].

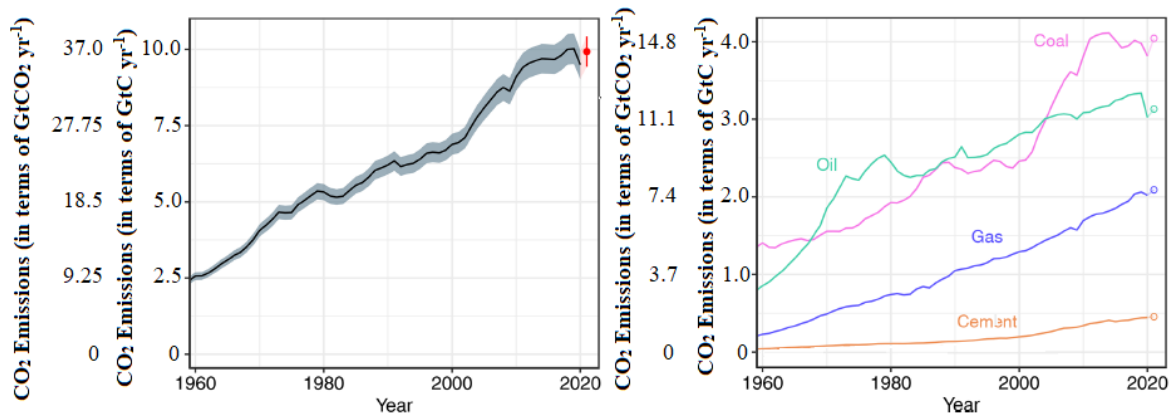


Figure 1.1 Trends in global CO₂ emissions, between 1960 and 2020, measured as GtCO₂ and GtC based on an estimated conversion of 3.7GtCO₂ = 1GtC (adapted from [5])

The topic of global warming has been on the agenda of many conferences and research plans, but it is often overlooked due to the differences in societal values, influence of politics and public opinion, economic considerations, conflicts of interests and other priorities. The concern is most evident, and then only temporary in the surrounding period of an event of an environmental crisis. Many new technologies for sustainability have been researched and developed but the energy consumption for the research tasks, available manpower and resources seem to curtail the progress in mitigating the contributing factors of global warming. Therefore, the more popular alternative includes recycling or using the by-products or wastes from the existing manufacturing processes because, while their effects in mitigating the problem may seem minor, the cumulative outcome will eventually reap the intended goals. With increasing population, construction is never-ending thereby creating a booming cement industry. The statistical figures associated with the cement, namely Portland cement (PC), production, as shown in Figure 1.1, accounted for 5-8% of the global CO₂ emissions [5], [6], [19]. The partial replacement of the cement, with non-CO₂ emitting materials, has grown as a popular alternative in the construction industry as a method to mitigate CO₂ emissions. The replacements have included several supplementary cementitious materials (SCMs) and fillers, such as ground limestone.

The current Canadian standards allow the “General Use (GU)” Ordinary Portland Cement (OPC), to include up to 5% limestone replacement of the cement. Portland Limestone Cement (PLC or GUL) is allowed to contain up to 15% limestone replacement, which is a limit imposed by the North American standards ASTM C595^[24] and CSA A3001^[27]. This is considerably more conservative than the upper limit of 35% limestone replacement adopted since 2000 by European

countries, per EN197-1 standards. The timeline of changes on the allowed limestone replacement of the PC is diagrammatically summarized in Figure 1.2. It was estimated that with the adoption of 20-35% limestone replacement of the cement, the CO₂ emissions estimated by cement production can potentially be halved [8]. For replacement of cement by SCMs, EN197-1 allows for up to 35% replacement while ASTM C595^[24] and CSA A3001^[27] allow for only 20-25% replacement of cement by granulated-ground blast furnace slag (GBFS).

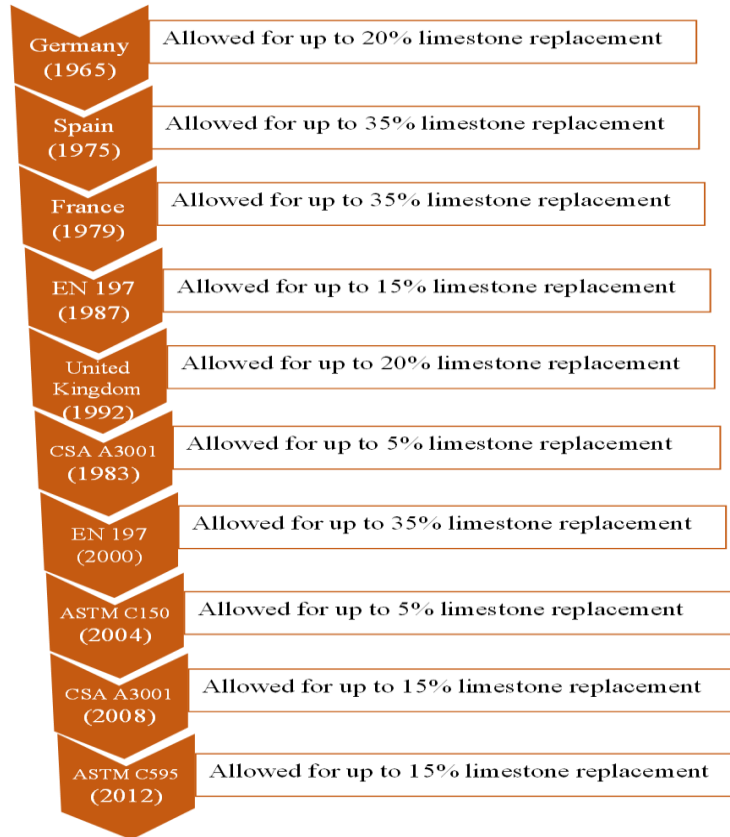


Figure 1.2 Timeline of changes in limestone limits in European and North American standards (adapted from [8], [20])

Based on the statistics of global cement production, 0.5-1 tonne of CO₂ (tCO₂) are released per tonne of cement produced [9]. In a hypothetical scenario, the supply for constructing the concrete foundation slabs of 200,000 homes amounted to approximately 8.5 megatons of cement. From just this one project, the amount of CO₂, between 4.25-8.5 megatons of CO₂, produced can fill a massive sphere with a diameter of 1,443 m (4,710 ft) [4]. This demonstrates that replacements of cement can contribute to substantial carbon savings on a large scale of construction projects, in which the main construction material used is concrete [12].

Concrete, which is based on a mix of cement, water, sand and stones, is one of the most sought construction materials and is typically reinforced with steel rebar to provide tensile strength ^[19]. The inherent properties of concrete, including the natural high alkalinity of the pore solution, allow for long service life predictions, such as 75 years for highway bridges by Canadian standards ^[10]. The high pH promotes the development of a protective passive film on the steel reinforcement in salt-free environments. However, maintaining a salt-free environment is impossible in coastal regions and highly unlikely in northern areas due to the use of de-icing salts on highways to mitigate vehicular collisions in cold climates. De-icing salts reduce the freezing point of snow and ice such that melting is facilitated.

Corrosion of the embedded steel reinforcement is, therefore, one of the most detrimental and contributing factors to the degradation functionality of reinforced concrete elements ^[13]. De-icing salts contain chlorides which penetrate concrete and ingress to attack the protective passive film on embedded rebar to promote corrosion. In addition to the de-icing salts used in the cold weather, concrete elements can be exposed to salts when in proximity to soils, marine environments and industrial effluents. Global warming disturbs the equilibria between the earth's surfaces and atmosphere, altering warm and cold cycles. The unprecedented extension of warm periods can contribute to the increase of salt concentrations of soil and seawater sources due to evaporation and more rapid diffusion ^[79]. While the external environmental conditions significantly influence the rate of chloride attack on concrete, the properties of the concrete also play important roles. These properties include permeability and porosity defined by the pore size distribution and connectivity of the pores ^[117].

Over the years, laboratory techniques have been introduced to monitor and assess the degree of effects on the corrosion of reinforcement in concrete elements, including electrochemical techniques which can be used to estimate corrosion rates based on electrical measurements ^[46]. Despite the differences between the synthesized environments in laboratory simulations and real situations onsite of the concrete elements, the methods were found to produce laboratory results which coincide with field tests with equivalent parametric controls ^[15].

Concrete structures must meet structural expectations during service life to ensure optimum safety and functionality. The durability of concrete is commonly measured by quantitative mechanical properties, including early age and mature strength, and physical properties, such as electrical

conductivity and permeability ^{[11],[88]}. These properties depend on the development of the concrete, which is affected by the composition of the concrete mix and curing conditions. Based on these measures, different concrete mixes can be compared and their influence on corrosion behaviour can be compared. The use of GBFS in OPC mixes has been in practice many years earlier than considerations of PLC. This is reflected in the limited research on PLC mixes and even more so on PLC-GBFS interblended mixes which are incomparable to the broader range of available literature on OPC and OPC-GBFS mixes, some of which are discussed in this document.

1.2 Research Objectives

The goal of this study was to investigate the effects of using PLC instead of OPC in concrete mixes, with and without GBFS replacements of 25%, 35% and 50%. In the perspective of sustainability, the use of PLC and decreased cement amounts reduce the carbon footprint contributed by cement production and so, the study assessed the degree to which the durability of the concrete, most predominantly corrosion resistance of rebar, was compromised for cement mixes aimed for reduced carbon dioxide emissions. The most basic type of reinforcement, which is carbon (black) steel, was used in the experiments to emphasize the influence of the cement replacements on the investigated concrete properties.

The project was divided into two major groups of testing. The first involved investigating the chemical changes of the pore solution due to admixture of chlorides. The major components of the pore solution were used to create synthetic solutions in which carbon steel reinforcement bars were immersed for electrochemical testing. The second group of tests involved monitoring the electrochemical responses of steel reinforcement embedded in concrete and exposed to chloride solutions. The research aimed to address the following questions:

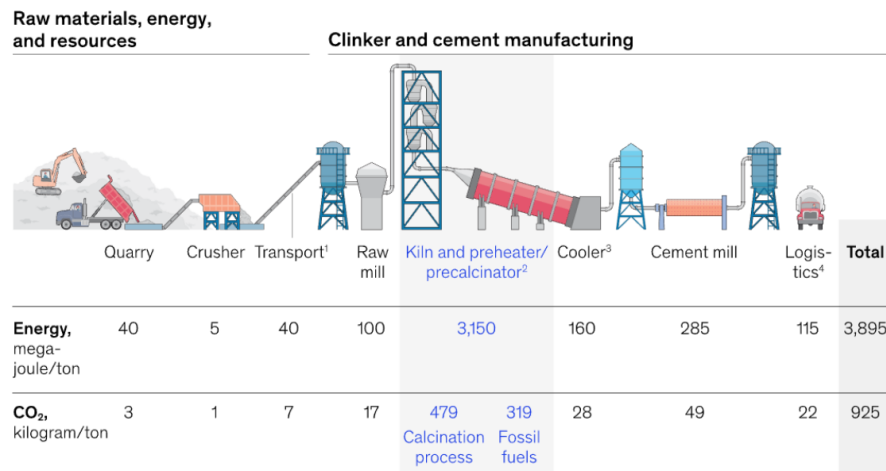
- Do the properties of the concretes made of OPC and PLC (with more limestone, i.e. 15% limestone by mass of cement) differ significantly?
- How is the chemistry of the pore solution affected by GBFS replacement levels, above the standard 25%, in PLC compared to OPC-based concretes?
- How is the corrosion resistance of steel reinforcement in concrete affected by increasing the replacement levels of GBFS in PLC, compared to OPC equivalents?

2.0 Literature Review

This section provides an overview of relevant findings of past research on the properties of ordinary Portland cement and Portland limestone cement specimens without and with varying GBFS concentrations.

2.1 Cement Production

Cement, which was patented as ‘Portland Cement (PC)’ in the 1800’s and named based on its appearance ^[16], is one of the most used ingredients for producing a variety of construction materials including concrete, mortar and masonry grout. PC is produced from quarried raw materials, primarily limestone and clay, which provide the base elements of calcium, silicon, aluminium and iron ^[17]. The raw materials first undergo a series of crushing and then pass through a rotary kiln, of about 1,480°C (2,700°F), to produce clinker. The clinker is then ground and combined with gypsum for controlled setting to produce what is known as PC ^[21]. The general cement manufacturing process is shown schematically in Figure 2.1, along with the average energy required and the CO₂ produced by the respective major components.



¹Assumed with 1kWh/t/100m.

²Assumed global average, data from the Global Cement and Concrete Association, Getting the Numbers Right 2017.

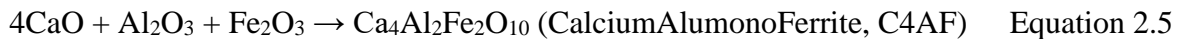
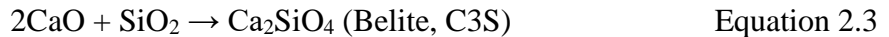
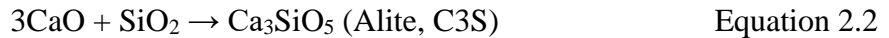
³Assumed reciprocating grate cooler with 5kWh/t clinker.

⁴Assumed lorry transportation for average 200km.

Figure 2.1 The average energy consumption and CO₂ footprint of the main manufacturing segments of the cement production ^[19]

Figure 2.1 demonstrates the carbon dioxide (CO₂) footprint of the processes that occur within the vicinity of the cement mills. It is important to note that the numerical figure for the acquisition of the raw materials may differ depending on the access-point of the quarry and difficulty of the

mining tasks. It is important to also acknowledge that distance between extraction sites and quarries for the raw materials and the cement production site and distance between the cement production site and the destination for use or commercial/industrial distribution of the cement product may greatly increase the CO₂ contribution by transportation. However, considering the quarries and the cement mills are in proximity, the highest consumption of energy and largest CO₂ footprint is associated with the rotary kiln process, typically rounding to about 85%-90% of the total carbon footprint per tonne of cement, according to Figure 2.1. The second contributing process is the milling processes, which involve the grinding to finer particles, contributing to about 5% of the total emissions. The kiln process releases CO₂ both through the burning of fossil fuels and the calcination of cement. The calcination process, by itself, contributes to about 50% of the total CO₂ released per tonne of cement produced. Calcination refers to the breakdown of limestone (CaCO₃) into lime (CaO) and CO₂, as presented in the chemical equation 2.1. The lime then further reacts with the oxides of the base elements at varying temperatures along the kiln. These reactions are shown in chemical equations 2.2-2.5 and form the components which are most commonly identified to characterize the clinker^{[19], [20]}.

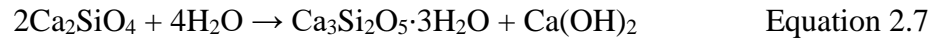
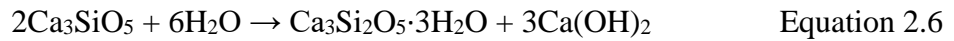


2.1.1 Hardened Cement Paste and Concrete

Concrete is the hardened product of combining cement, water, sand (fine aggregates) and stones (coarse aggregates) and other chemicals, including air entraining agents and plasticizers, for targeted optimization of the properties or performance of the hardened concrete. Cement pastes are combinations of cement and water and their role is to bind the aggregates in the concrete matrix. Mortar is the hardened product of combined cement, water and sand, and it can be used as a paste in masonry and tiling works or it can be moulded into various hardened forms. Greener approaches for promoting sustainability and decreased carbon footprint of cement production have been introduced over the years with partial replacement of the cement by supplementary cementitious

materials (SCMs), which include natural pozzolans and by-products of other manufacturing processes ^[116].

The calcium silicates, C3S and C2S, are the predominant components, which collectively make up about 65%-75% of the clinker, and they are responsible for the heat of hydration, hardening and strength development ^[21]. C3S and C2S react with water, which are chemically represented in Equations 2.6 and 2.7, to form calcium silicate hydrates (abbreviated as C-S-H), which is the primary binding agent in the cement paste comprising about 50%-60% of volume of the concrete matrix ^{[21], [22]}.



The product of the hydration reactions is calcium hydroxide ($\text{Ca}(\text{OH})_2$), alternatively termed as portlandite, which contributes to the high alkaline property of the hardened paste, typically resulting in a minimum pH of 12.5. The minor components of clinker, C3A and C4AF, are responsible for controlling the time to set, which increases stiffness and reduces workability. The addition of gypsum ($\text{CaSO}_4 \cdot 2\text{H}_2\text{O}$) controls the tendency of these components to quickly react with water, resulting in flash-set ^[21]. This is because, when mixed with water, they instead react with the dissolved sulphate in gypsum to form ettringite ($\text{Ca}_3\text{Al}_2\text{O}_6 \cdot 3\text{CaSO}_4 \cdot 32\text{H}_2\text{O}$; alumina-ferric oxide trisulphate, AFt) which controls the setting of the paste ^[23]. Alternatively, they can react with the dissolved hydroxides (OH^-) to form the hydroxy-alumina-ferric oxide monosulphate (hydroxy AFm) ^[98]. Locher et al. (1976) ^[25] mapped the development of the major components of hardened cement paste up to an age of 90 days, as presented in Figure 2.2. They found that the hydration of the clinker components began within hours upon mixture of the cement with water, with the ettringite formation starting almost immediately and being complete by about the age of 7 days, when it decomposes to form the monosulphate. The hydration of C3S and C2S occurs later and the formation of the C-S-H is considered approximately 90% complete by the 28th day. The ettringite is represented as the needle-like particles and the white hexagonal particles represent the $\text{Ca}(\text{OH})_2$ which sit along the C-S-H plates.

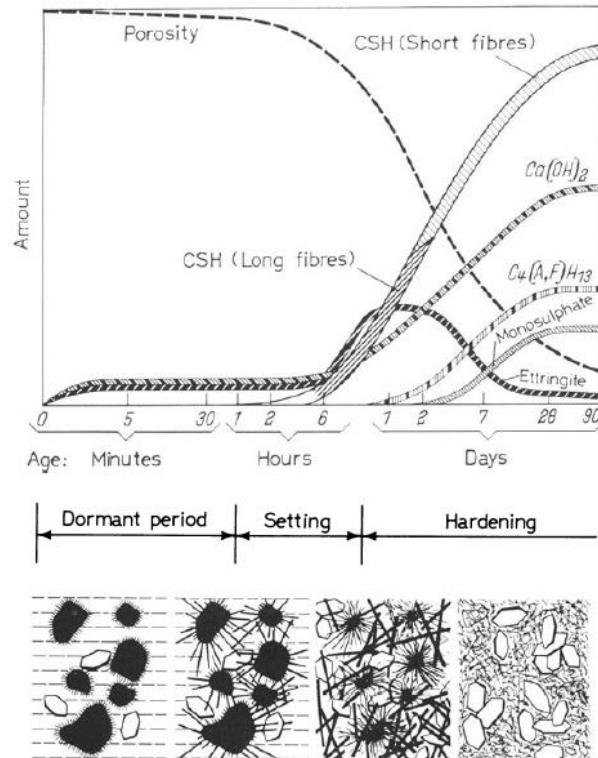


Figure 2.2 Development of the major hydration products with age of the cement paste [25]

2.1.1 Effect of Cement Replacement on Hydration

The degree of cement hydration significantly influences the development of strength and other mechanical, chemical and physical properties of the hardened concrete. Hydration rate is, however, also affected by the type of cement and the composition of the mix to be used for the cement paste, mortar or concrete. Therefore, it is essential to understand the effects of SCMs and fillers on the hydration of cement mixtures with partial replacements.

The limestone content of Portland limestone cement (PLC) typically is limited to 10%-15% [27] and 35% [28], by mass of cement, in North America and Europe, respectively. A small amount of limestone, up to 5% by mass of cement, is permitted in Ordinary Portland cement (OPC). The limestone is commonly assumed to be an inert filler [70], thereby having no significant influence on the properties of the hardened product of cement paste, mortar or concrete but more so on the hydration reactions of the cement composites. PLC certificates typically report a higher Blaine fineness, which is a measurement of surface area per mass for cements' fineness. This is because of the soft nature of ground limestone which requires a greater packing density in order for the limestone to match the physical properties of cement clinker [26].

The water demand for PLC to reach the same level of hydration was found to be lower than that for PC particles [26], [29]. This was well presented by the microscopic study on the time-dependent growth of the hydration products for PC, sand and limestone by Ouyang et al. [83]. It was postulated that the acceleration in the hydration reactions in limestone was due to the increased presence of CaCO_3 in the PLC, as well as the increased nucleation sites provided by the finely ground limestone particles. It was reported that an amount as low as 10% of limestone replacement of the cement was sufficient to accelerate the hydration by 50% compared to that of the control OPC [30]. This is due to the filler or dilution effect, which is attributed to the increased surface area and the increased effective water to cement ratio due to the reduced cement content in PLC [84].

One of the most common SCMs in the construction industry is the granulated-ground blast furnace slag (GBFS), which is a by-product of iron production. The allowable replacement of cement by GBFS is greater than that of the limestone in PLC, as OPSS 1350 allows up to 25% [35] while ASTM C989 allows up to 50% [36]. In the left image in Figure 2.3, the Ca(OH)_2 formed by the hydration of the clinker components in OPC does not undergo any further reaction but on the right image, the slag reacts with the Ca(OH)_2 to form more C-S-H products. Therefore, the hydration occurs slowly because of the need for the production of Ca(OH)_2 in the clinker reactions before the slag can react. Consequently, the beneficial effects of GBFS on the cement paste come later in age, depending on factors, such as the composition, fineness of the slag particles and replacement amounts [37].

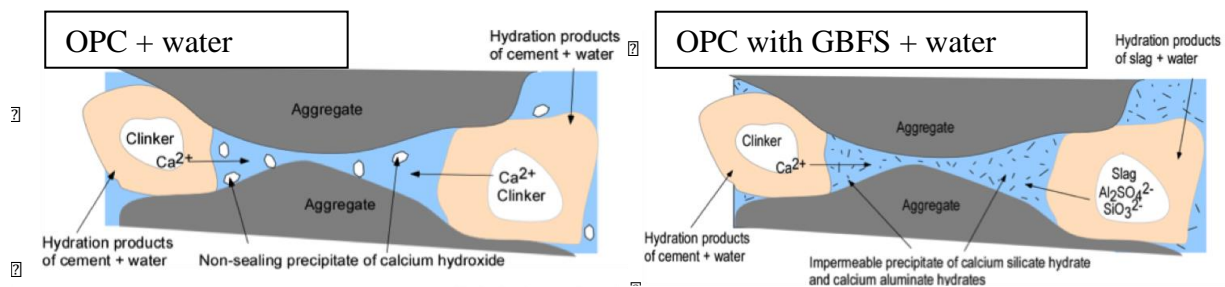


Figure 2.3 Schematic representation of the hydration of the clinker without and with GBFS [courtesy of modification of a figure from Bakker R. M. [116] by Hansson C. M.]

As the cement paste ages and more Ca(OH)_2 is produced to increase the alkalinity, the rate of reaction between the GBFS and water is increased to produce more C-S-H. With more CSH and reduced Ca(OH)_2 particles, the pore structure is more refined with abundant small pores [37]. A

common method for rectifying the issue of the delayed hydraulic activity of GBFS as replacement of cement is including alkali activators in the mix but large quantities can cause flash setting ^[87].

The filler and nucleation effects of the finely ground limestone in ternary mixes of PC with limestone and GBFS were found to mitigate the delayed hydration of the slag ^{[31], [39]}. This is because the increased early hydration of the clinker components in the presence of limestone creates the $\text{Ca}(\text{OH})_2$ required for the hydration of the slag ^[34]. However, another study showed that the improvements in hydration of GBFS cement blends by the increased limestone were not noted until later age, comparably to no limestone additions ^[69].

2.1.2 Effect of Water-to-Cementitious Materials Ratio on Hydration

The effects of water-to-cementitious materials (w/cm) ratio on the hydration of cement are often measured by evaluating the degree of hydration and microscopic observations of the pore structures ^{[92], [93]}. The w/cm ratio is the ratio of the mass of water to the total mass of cement plus SCMs replacements. Despite the limestone being considered as filler, the w/cm ratio can be determined normally as the mass of water to mass of the PLC cement, regardless of the limestone % content ^[81]. Studies have reported 0.23 as the absolute minimum w/cm ratio, in the absence of SCMs, for hydration of the clinker components in a mix without any added agents, such as water reducing agents ^[40]. However, at least 0.38 w/cm ratio is required for efficient binding effect of the hydration products and for workability of the concrete. The additional 15% water partake in the formation of voids in the cement paste ^[40]. While an increase in the w/cm ratio was found to increase the rate of early hydration, the durability performance of the hardened product at later age, was found to be poor because of increased porosity due to the excessive water contributing to formation of capillary pores ^[93].

The concrete mixture contains water required for hydration of the cement components, bound water for the molecular bonds of the hydration products and “free” water. The latter remains stored in the pores of the cement paste and determines the pore solution chemistry. There is no universally accepted optimum w/cm ratio because the required water content differs according to targeted performance, including desired degree of workability (measured by the slump). The w/cm ratio also varies with the mix design, such as the cement type, the inclusion of SCMs, or any included chemical admixtures, which include water-reducing agents, superplasticizers, retarding or accelerating agents and corrosion inhibitors.

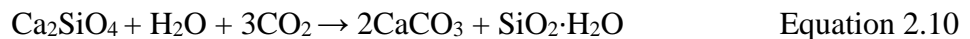
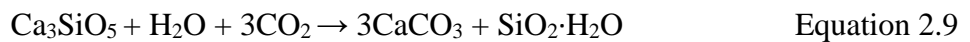
2.2 Steel Reinforcement in Concrete

Concrete is vulnerable to cracking under stress and deterioration by various mechanisms, such as freeze-thaw effects, chemical attack and corrosion of reinforcement over the service life. Steel reinforcement bar (or rebar), one type of which is carbon (black) steel, is used primarily for improvements in the resistance of concrete to tensile stresses.

As mentioned in Section 2.1.1, the cement paste is highly alkaline with $\text{pH} > 12.5$ due to the abundance of Ca(OH)_2 , KOH and NaOH produced by the hydration reactions. This highly alkaline environment is favourable for the steel rebar to form a self-protective passive oxide film in addition to the mill scale, which is an oxide film formed during the manufacturing process of the rebar^[43].^[44] Therefore, without the influence of external environmental factors, reinforced concrete can persevere over long service life without severe deficiencies. However, this ideal environment is unlikely to exist and the reinforced concrete is susceptible to degradation by carbonation and ingress of salts, such as chlorides, resulting in corrosion of the reinforcement.

2.2.1 Corrosion by Carbonation

Carbonation occurs in the hardened cement paste matrix when CO_2 infiltrates the concrete and the Ca(OH)_2 is consumed in reaction to form CaCO_3 precipitates, as shown in Equation 2.8, thereby reducing the alkalinity to below $\text{pH} 9.0$ ^[45]. Eventually, once all the Ca(OH)_2 is consumed, the cement composition is altered as the C_3S and C_2S react with the CO_2 , as shown in Equations 2.9 and 2.10, respectively, precipitating CaCO_3 in the pores of the hardened cement paste^[45].



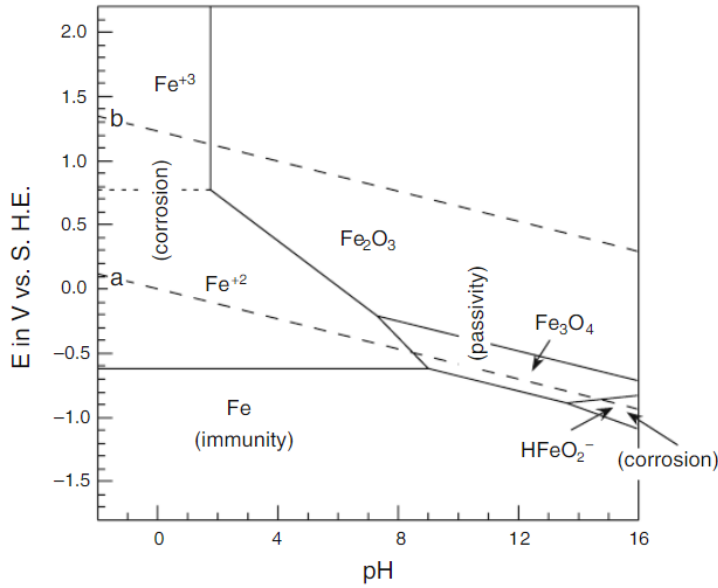
The precipitates occupy the voids of the concrete matrix and decreases the ductility of the concrete. If the depth of carbonation meets the steel/concrete interface, the reduced pH (to below $\text{pH} 11$) around the steel reinforcement causes breakdown of the passive film and initiates active corrosion of the rebar^[79]. The reactions between the CO_2 and the hydrates, in Equations 2.9 and 2.10, are rarely observed because the concrete cover would have been destroyed by cracking or spalling by the effects of carbonation.

2.2.2 Corrosion by Chloride Attack

Chloride contamination can occur through various means, such as location-specific cases where the concrete is near or immersed in marine environments or contact with de-icing salts which are more common in countries with winter climates. On the other hand, chloride can also be introduced into the hardened product matrix by the mix components, such as the aggregates, cement and/or water. To address the possibility, North American standards ^[42] have imposed limits on the allowable degree of the chloride contamination in the mix ingredients.

Whether incorporated in the mix or penetrated into the concrete from the environment, chlorides can react with C3A and C4AF to form the complex Friedel salts, which bind chlorides ^[61]. The unbound or free chlorides are those that remain in the pores and are responsible for the attack on the embedded steel ^[99].

If sufficient levels of chloride are present in the pore solution (if they exceed the chloride threshold level), active corrosion can occur. However, a universally accepted quantity for this limit is still in debate as it depends on various factors, such as the composition of the mix components and the steel reinforcement, the type of salt and the exposure conditions of the steel. Depending on the pH and the potential difference between the anodic region (where oxidation or the dissolution into the respective ions occurs) and the cathodic region (where reduction of the ions occurs), several reactions, which is further dependent on the availability of oxygen, can occur ^[43]. Figure 2.4 depicts the corresponding potentials and pH conditions for the most probable iron phases where corrosive activity does not occur (immunity), where stable and insoluble iron oxides are formed (passivity) and where soluble phases (corrosion) ^[48].



Note:

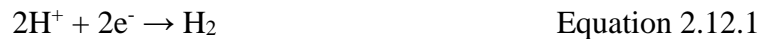
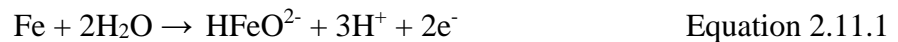
Conversion from V vs S.H.E to V vs S.C.E

$$[V \text{ vs S.C.E.}] = [V \text{ vs S.H.E.}] - 0.24$$

S.C.E. is saturated calomel electrode which was used for measurements in this research

Figure 2.4 Simplified potential-pH diagram for iron at 25°C [62], adapted from Pourbaix [48]
 (Note: the potential measurements, E were measured against a standard hydrogen electrode)

For steel reinforcement, the most common anodic reactions, resulting in the dissolution of the iron in the steel reinforcement, are summarized in Equations 2.11 and 2.11.1 [43], [45]. These must be balanced by reduction (cathodic) reactions, as presented in Equations 2.12 and 2.12.1, the latter of which occurs when there is a low availability of oxygen [43], [45].



As the iron ions diffuse from the metal, they react with the chlorides, which is simplified in Equation 2.13 [45]. The unstable FeCl₂ molecules dissolve and the Cl₂ continue the attack on the reinforcement. The Fe⁺ ions produced at the anodic regions and by dissociation of FeCl₂ further react to form insoluble iron oxides or iron hydroxides, some of which may inhibit further corrosion while some may form solids which are expansive in nature [50]. These expansive products can cause cracking and spalling of the concrete.

Corrosion is an electrochemical phenomenon as it involves the movement of electrons and ions released in chemical reactions. The basis of corrosion measurements is that an electrical circuit is

established in the concrete, where the solution in the interconnecting pores of the concrete act as the electrolyte through which ions travel between the anodic and cathodic regions on metals. For embedded steel reinforcement, two typical circuits exist: 1) microcell, which is the case when both the anodic and cathodic regions exist on the same steel reinforcement bar; and 2) macrocell, which is the case when the anodic region exists on one steel reinforcement bar, adjacent and apart from another bar where the cathodic region exists. For macrocell corrosion to occur, an electrical connection must be established between the two bars to accommodate the flow of electrons as the concrete facilitates the ionic movement in the opposite direction, forming a closed-circuit loop. The two circuits are presented in the schematically in Figure 2.5^[47]. Based on these two concepts, many electrochemical testing methods for evaluating corrosion of steel reinforcement were introduced over the years.

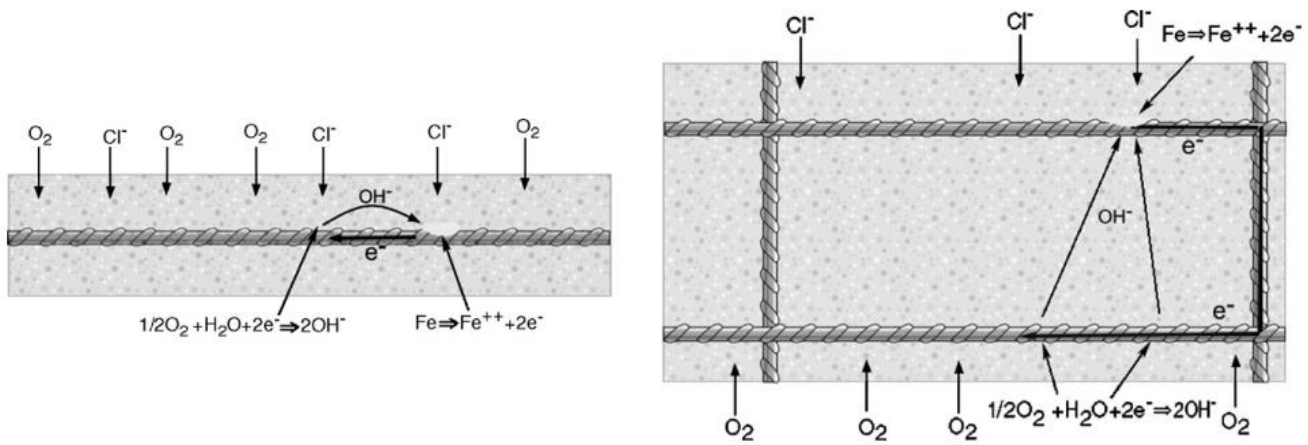


Figure 2.5 Microcell circuit (Left) versus the macrocell circuit (Right) for steel reinforcement embedded in concrete^[47]

Corrosion of metals can exist in various conditional forms. Two of the most known forms associated with embedded steel reinforcement are general corrosion and pitting corrosion, which are well distinguished in Figure 2.6. General corrosion occurs along most of or the entire surface of the reinforcement bar due to absence of a protective film or an unstable protective layer, which has broken down due to corrosive conditions, such as reduced pH from carbonation. On the other hand, pitting corrosion occurs on smaller or localized areas of the bar due to defects in or damage to the protective passive film, as explained earlier. The electrical connection established for a macrocell circuit is also shown in Figure 2.6.

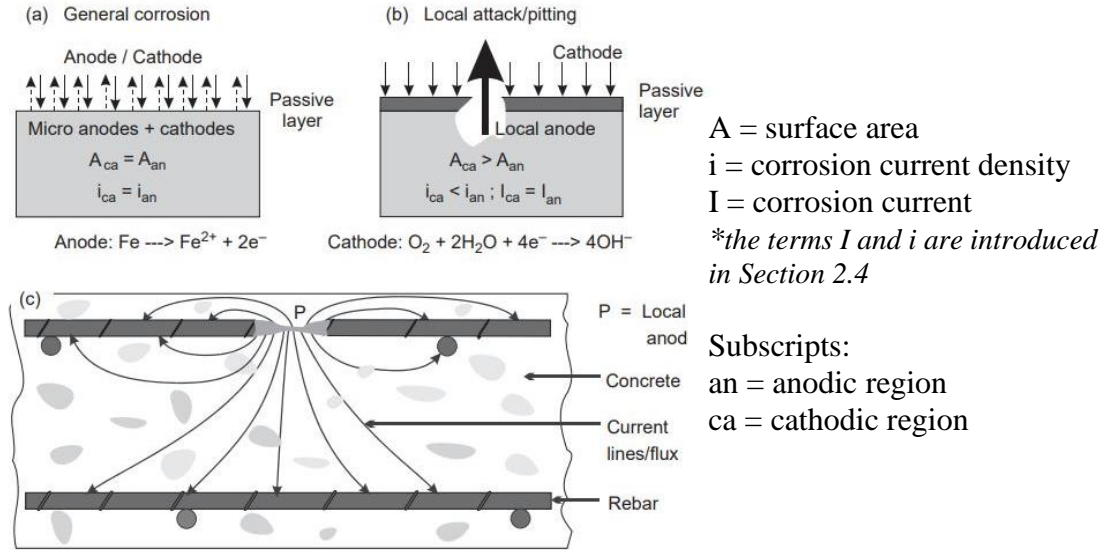


Figure 2.6 Mechanisms of general corrosion and pitting corrosion in concrete [94]

2.3 Chemistry of the Pore Solution

Having discussed the risk of corrosion of the embedded steel reinforcement, it is important to understand the chemical composition of the pore solution, which is in direct contact with the steel, which then affects the development of the passive film, and functions as the medium through which chemicals and ions diffuse. Corrosion tests depend on the diffusivity of the pore solution, the concrete cover and may be affected by external stimulating conditions, such as temperature and relative humidity. A less timely approach is synthesizing pore solutions in which the reinforcement is directly immersed for monitoring. With this approach, the environment is more controlled, observable and unlike concrete, for which the chloride concentration at the steel/concrete interface may be difficult to determine. This approach, however, requires an extra step for determining the chemical composition of pore solution expressed from the specific cement pastes of interest. Barneyback and Diamond [53] developed a high-pressure equipment for expressing the liquids or solution from the pores of hardened products, more commonly cement pastes and mortars.

The method is difficult to apply to concrete and sometimes, mortar specimens, older than 28 days as they would require higher pressures to express the solutions. The differences between the concentrations analysed from pore solutions of OPC mortar and OPC cement pastes were found to be negligible at pressures up to 560 MPa [54], [58]. On the other hand, a study by Vollpracht et al. [56] found that the compositions of the pore solutions of OPC cement pastes of the same mix were comparable up to a pressure of 250 MPa above which the compositions began to change. They

proposed the reason to be the increase in the solubility of the ions with the applied expression pressures thereby increasing the ion concentrations detected in the expressed pore solution. Plusquellec et al. [76] found that no relationship between the expression pressure and the concentration of the pore solutions existed and postulated that changes in the compositions of the pore solutions were mainly due to the heterogenous nature of the cement pastes.

Synthetic pore solutions are made using laboratory-grade chemicals proportioned according to the major components analysed from the expressed pore solution. The main components include Na^+ , K^+ , Ca^{2+} and Cl^- , if chlorides were admixed or exposed to the cement pastes, and sometimes, SO_4^{2-} [53], [97]. Despite the rich source of $\text{Ca}(\text{OH})_2$ produced by the hydration reactions, the Ca^{2+} concentrations recorded extremely low values due to limited solubility of $\text{Ca}(\text{OH})_2$ [54], [56].

To summarize, synthetic pore solutions are widely accepted as a test method for simulating the conditions of the solution in the pores of hardened concrete because (1) the corrosion of the steel is accelerated due to the direct immersion in solution [92]; (2) the ease of observation on the changes in the state and appearance of the steel in solution; and (3) the pH and chloride content can be controlled. Some limitations of the method to consider include

- 1) the kinetics are not representative of the heterogeneity of hardened paste matrix of cement pastes, mortar or concrete, such as the connectivity of pores [76];
- 2) the proportions of the chemicals to match the concentrations analysed from the expressed pore solutions are based on stoichiometric assumptions, for example, if $\text{Ca}(\text{OH})_2$ and CaSO_4 are added for Ca and SO_4 additions, respectively, the Ca^{2+} ions may be an overestimate of the actual pore solution in concrete [77]; and
- 3) the contained synthetic pore solution is subject to changes in chemistry due to interactions with atmospheric contaminants, such as between OH^- and CO_2 [73].

2.3.1 Effect of Cement Replacement on Pore Solution Chemistry

The research on the effects of GBFS on the concentrations of pore solutions are contradictory. Cement pastes and mortar samples made of OPC with 35% replacement by GBFS at were found to have reduced Na^+ and K^+ concentrations compared to samples without GBFS [54]. In contrast, no change in the Na^+ and K^+ concentrations in cement pastes with GBFS was observed even at the expressed age of 28 days, due to the slow hydration reaction of slag, as found by Vollpracht et al. [56]. With admixed sodium chloride in the cement pastes, OPC cement pastes with 25% GBFS

replacement were observed to have lower Na^+ and K^+ concentrations, compared to the OPC without GBFS [60]. Potgieter et al. [61] found that the chloride binding capacity increased with the reduction of the cement in OPC-GBFS samples, up to 30% GBFS replacement, compared to OPC samples without GBFS. Chloride binding is correlated to the corrosion resistance because the bound chlorides would not participate in the progressing the chloride-induced corrosion of the embedded steel reinforcement [37].

The pore solutions for concrete made of (1) OPC, (2) PLC and (3) OPC mixed with 15% limestone powder, each mix type of which was tested with and without 50% GBFS replacement, were investigated by Chopperla et al. [65]. The concrete cylinders were expressed after 28 days of curing and the study found that the mixes (2) and (3) with GBFS had lower alkalinities (both the Na^+ and K^+ concentrations) than the mix (1) with GBFS. They reasoned that the more refined pore structures of the PLC-GBFS samples led to higher resistance to expression of the pore solutions and thus, lower dissolved ion concentrations were detected, compared to the OPC-GBFS equivalents. In general, although there are not many studies on the pore solution chemistry of cement mixes, understanding the chemical compositions can support deductions on the physical and mechanical properties of concrete as well as their effects on corrosion resistance of steel reinforcement.

2.5 Concrete Durability

Durability is the ability of a structural element to function under service conditions, without considerable deficiency. Properties, which are important to consider for measuring the durability of concrete elements, include the development of compressive strength, electrical resistivity and corrosion rates of reinforcement.

2.5.1 Effect of Cement Replacements on Compressive Strength

Compressive strength is undoubtedly the known property whenever concrete is of concern. The gains in compressive strength are progressive with age, provided that the environment is not harmful to the concrete. This is mainly due to the kinetics and products of the hydration reactions, which depend on factors such as the cement type and mix proportions, as well as environmental conditions. The relationship between the compressive strength and w/c ratio is modelled well to

show that a general increase in w/cm ratio leads to decrease in compressive strength, because the excess water contributes to formation of capillary pores which weaken the hardened matrix ^[70].

The research by Volgis et al. ^[26] showed negligible differences between the compressive strengths of OPC and PLC mortars with 0.4 w/cm ratio. As expected, because of expedited early hydration due to the limestone in the PLC, the early age strengths, up to 7 days, were slightly higher than those of the OPC, but the later age strengths of the PLC were slightly lower or equal, even up to 540 days. Garcia et al. ^[69] and Thomas et al. ^[66] concluded similar findings on the comparable strength properties for OPC and PLC concrete specimens at 0.45 w/cm ratio for all ages up to 91 days and 56 days, respectively. Thomas et al. also observed that PLC specimens cured in low temperatures experienced no enhanced early hydration.

Ramezaniapour and Hooton ^[31] tested OPC and PLC, with varied limestone amounts, with and without GBFS, and noted that when the limestone exceeds a limit, which varied with the GBFS content, the compressive strengths decreased with increasing limestone. Their deductions opposed the assumption of limestone being an inert filler, postulating that within a limit, the limestone reacts with the C3A, available from the cement, to form carboaluminates, which would enhance compressive strengths. This reaction increased with the fineness of the interground limestone particles and with the presence of slag. The findings of decreasing compressive strength with increasing limestone amounts and increasing strength with the addition of GBFS were supported by studies on concrete and mortar specimens by Dhir et al. ^[81], Tosun- Felekoğlu ^[72] and Hansen et al. ^[100].

Improvements in strength were observed for increasing GBFS which were prominent at later ages with more GBFS, regardless of PLC or OPC, due to the delayed hydration of the slag, as observed by Thomas et al. ^[71]. Jau et al. ^[80] reported no significant changes in the strength due to the GBFS at 30-50% replacement levels in the cement mixes, even after 1 year of testing. They speculated the cause to be the incomplete hydration of the slag at such high levels in the cement, due to insufficient $\text{Ca}(\text{OH})_2$ produced by the cement hydration reactions. They hypothesized that the optimum slag replacement was 20% for the effect of strength gain to be observed at an age of 28 days. However, Yeau & Kim ^[89] and Pareek et al. ^[90] observed strength gains with 30-40% GBFS replacement of cement at day 90 and day 56, respectively.

In general, studies showed that the compressive strengths of OPC and PLC were comparable [8], [12], [29]. Moreover, with GBFS interblended in the PLC or OPC mixes, depending on the replacement level, the mix composition, and other factors which influence hydration of the cement and slag and curing conditions, the compressive strengths were generally benefitted at later ages [82], [99], [101].

2.5.2 Effect of Cement Replacements on Electrical Resistivity

Electrical resistivity is essential for the resistance to the migration of ions through the pore solution in the cement paste, thereby affecting corrosion activity which is dependent on the transfer of ions between the anodic (oxidation) and cathodic (reduction) regions. Commonly, surface and bulk resistivities are measured for concrete as these parameters relate to the ease with which chemicals can penetrate the surface and ingress through the matrix, respectively. However, the measurements are influenced by factors such as the testing conditions, including the degree of saturation of the specimen and connectivity between the probes and the specimen, the properties of the mix components and mixing methods [96].

If the pore structure lacks continuity, resistivity is increased as the transfer of ions is inhibited. As mentioned before, GBFS replacements resulted in hardened products with a more refined pore structure with limited connectivity, and thus, GBFS generally increases electrical resistivity [37], [38], [45], [87]. The study by Garcia et al. [69] on OPC and PLC concrete concluded that the resistivity decreased with increasing limestone amounts. Hansen et al. [100] found that the increase in resistivity was independent on the presence of limestone but was a result of the replacement of cement by 20-30% GBFS. Their study also showed that the electrical resistivity increased with a decrease in w/cm ratio. Chopperla et al. [65] observed, however, that the presence of limestone did increase the resistivity, at early ages, due to the accelerated early hydration which reduced capillary porosity.

2.5.3 Effect of Cement Replacements on Chloride-Induced Corrosion

Corrosion behaviour of concrete can be estimated by various parameters, such as critical chloride thresholds (CCT) and corrosion rates, which are determined from electrochemical measurements. The CCT is the minimum chloride content required for active corrosion to initiate. The use of the CCT is very limited as it is influenced by interrelated inherent concrete properties, such as the chloride-binding capacity, the pH of the pore solution, the concrete cover for the steel

reinforcement, mix compositions, and external environmental factors such as temperature and relative humidity, and concentrations of chloride and oxygen. CCT can be expressed as a chloride concentration (such as a percentage of cement content) or as Cl^-/OH^- ratio. The reliance of CCT is, however, put into question because of the stochastic nature of corrosion where measurements may exhibit substantial differences when testing concrete, mortar or cement pastes in laboratory conditions compared to field measurements. As corrosion in embedded steel reinforcement is not visible and is usually localised, measurements which are averaged over the entire polarized areas (areas on the rebar subject to changes in electrochemistry) may be misleading.

For carbon steel reinforcement in concrete, Böhni ^[94] presented chloride content limits of 0.2% Cl^- , 0.4% Cl^- and 1.0% Cl^- , by mass of the cement, as the limits for identifying low, medium and high risks of corrosion, respectively. The low corrosion risk limit coincides with the 0.1%-0.2%, by mass of cement, proposed as the CCT for active corrosion by Jau et al. ^[80]. Liu et al. ^[97] suggested that the CCT was 0.05-0.06mol Cl^-/L of pore solution for carbon steel. Moreno et al. ^[79] refuted these singular limits as they presented a range of chloride concentrations which varied according to the pH and chemistry of the pore solution. It is clear that it is impossible to agree upon a universally chloride concentration for the CCT because of the interlapping effects of the environmental factors and properties influences by concrete mix compositions. Figure 2.7 exemplifies the range by which the critical chloride concentrations, as a percentage of the mass of cement, can vary with the environmental conditions in addition to the concrete quality. The quality is expressed as a function for which “good” associates with factors which limit the risk of corrosion, such as pristine steel rebar without superficial deficiencies, large cover depth which greatly limits the time for diffusion of chlorides to reach the embedded rebar, and decreased porosity, while “bad” quality refers to opposite factors which facilitate corrosion, such as contaminations by chlorides in the concrete mix and small concrete cover depths.

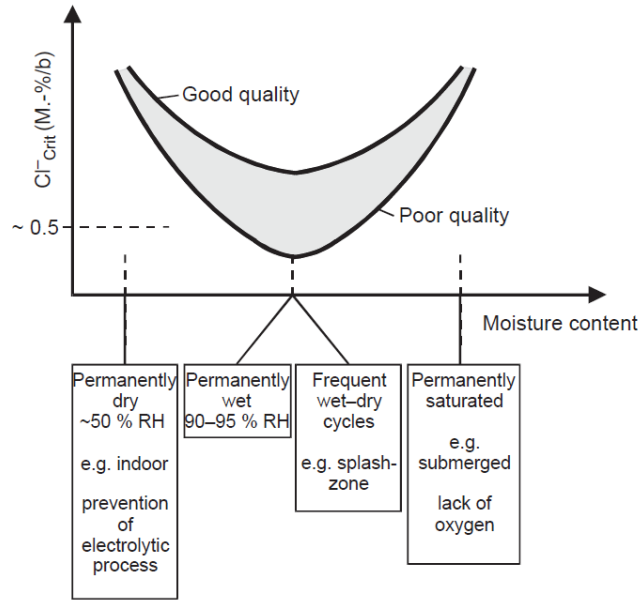


Figure 2.7 Influence of environment and concrete properties on the critical chloride content [94]

The Cl^-/OH^- ratio is one measure of the bulk chemistry of the pore solution to which the steel reinforcement is exposed. Figure 2.8 displays the spread of values proposed for plain OPC mixes, summarized by Alonso et al. [91]. It effectively shows that there is no agreed value or range due to the number of factors which influence CCT.

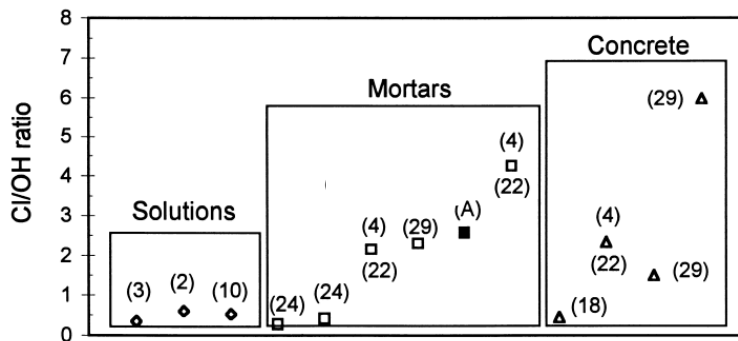


Figure 2.8 Range of $(\text{Cl}^-/\text{OH}^-)$ ratios as CCT for active corrosion to initiate in OPC pore solutions, mortars and concrete [A= 91]

The Cl^-/OH^- ratio is sensitive to change because it relies on interdependent factors such as hydration of the cement, pH and chloride binding capacity. An example of an occurrence in which the limiting Cl^-/OH^- ratio differs by pH of the pore solution is that in an environment with increasing pH above 12.6, the highly alkaline condition (high OH^- ion concentration) is accompanied with reduced chloride binding capacity of the cement paste, thereby increasing the free chlorides in the pores contributing to risk of active corrosion [78].

More common measures of the corrosion behaviour of embedded steel reinforcement are (1) the corrosion potential, which is the measured potential difference between the steel and a reference electrode, and (2) corrosion rates, which are represented as current densities determined from current measurements divided by the polarized areas of the steel. The experimental details are further explained in Section 3.0, which shows the application of Ohm's law and the Stern-Geary^[105] principle.

The steel reinforcement in PLC mortars exhibited better corrosion resistance than those of the OPC specimens in both chloride and chloride-sulphate environments^[74]. It was noted the steel specimens exposed to chloride-sulphate solution showed higher corrosion rates, than those exposed only to chlorides, because of the preferential binding of the sulphates by the Friedel salts, compared to the chlorides^[97]. It was also noted that the corrosion rates increased with increase in w/cm ratio due to increased capillary porosity facilitating ion diffusivity^{[93], [98]}. The enhanced early hydration and lessened porosity associated with steel rebar in PLC contributed to the improved corrosion resistance at early ages, which was said to also benefit with increased fineness of the limestone^[96]. However, this was contradicted by the results of Li et al.^[98] that showed an increase in limestone replacement of the cement led to higher corrosion rates, which were hypothesized to be due to a decrease in the chloride binding capacity of the limestone hydrates of the aluminate phases in the cement, which again refutes the inert filler assumption of limestone. The decrease in the available C3A of the cement limits the Friedel salt formation and thus, reducing the chloride binding effect.

After 1 year of alternating exposure to chloride solutions-and dry cycles, Jau et al.^[80] observed signs of corrosion on the steel embedded in the plain OPC and the OPC with 50% GBFS replacement concrete specimens, while the steel reinforcement in OPC concrete, with 10-30% GBFS replacement, showed better corrosion resistance^[80]. No improvement in corrosion resistance was observed for the OPC-GBFS specimens, with greater than 30% GBFS replacement, because it was speculated that the refinedness of the pore structure was not obtained due to the delayed and incomplete hydration of the slag in the concretes with high GBFS content^[88]. Yeau and Kim^[89] found that with GBFS replacement levels as high as 40-60% in OPC exhibited benefits with reduced risk of corrosion activity, determined by potential measurements, as the concrete matured within 30 weeks of observations. They found that the greater the GBFS replacement, the

later the improvements in corrosion resistance came. Overall, the addition of GBFS improved the chloride-induced corrosion resistance of the OPC specimens with thick concrete cover, but the greater the cement replacement by GBFS, the later the benefits in strength and reduced porosity were observed ^{[38], [61], [80], [89]}.

Improved corrosion resistance, associated with longer incubation period and/or reduced corrosion rates, was accompanied with GBFS replacement in PLC specimens, which observed increased chloride binding capacities ^[74], which opposed the reduced capacities observed with the introduction of limestone by other studies ^[82]. Only a selection of the thousands of research on OPC-GBFS mixes has been mentioned and in contrast, the availability of research on PLC-GBFS mixes is much more limited. Therefore, the lack of research on the effect of cement replacement by limestone and GBFS collectively is concerning to durability aspects of this greener cement mix. The current research therefore intends to fill in the research gap to promote the PLC-GBFS ternary blends as more sustainable alternatives for the cement industry. This research, however, is only a small step to support the industrial use of PLC-GBFS mixes, as the results are specific to the features of the experiments, such as the type, physical properties and composition of the mix components and laboratory conditions, such as type and period of chloride exposure.

3.0 Experimental Procedure

The goal of the project was to determine if replacing cement by both limestone and slag, in amounts exceeding those currently permitted by OPSS 1350 [35], would provide acceptable durability of steel rebar. Four levels of cement replacement by GBFS, 0%, 25%, 35%, 50%, were added to the OPC and PLC (containing 15% limestone by mass of the cement). This section describes the sample preparation and testing procedures, which were focused on evaluating the corrosion behaviour of carbon (black) steel rebar. The project involved two different corrosion tests (1) with the rebar immersed in solutions corresponding to the pore solutions of the cement blends with incrementally added sodium chloride (NaCl); and (2) monitoring embedded steel reinforcement in different OPC-GBFS and PLC-GBFS concrete specimens of the cement blends and exposed to chloride solutions. Various techniques were employed in the experiment, including electrochemical methods, such as linear polarization resistance (LPR) and galvanostatic pulse (GP) techniques, and analytical methods, such as x-ray fluorescence (XRF), ion chromatography (IC), inductively coupled plasma (ICP) and other ASTM/CSA standard methods of testing for cement and concrete samples.

3.1 Material Information

The manufacturers' details of the cements, GBFS and carbon steel rebar used in this experiment are provided in this section.

3.1.1 Cementitious Materials

Herein, OPC specimens were referred to as GU and PLC specimens were referred to as GUL. The main chemical components of the GU and GUL cements and the GBFS are provided in Table 3.1. For further information, the mill certificates for the cements, as provided by the respective suppliers, are provided in Appendix A.

Table 3.1 Chemical compositions of GU and GUL cements and GBFS, per mill certificates

Property	GU/OPC (% wt.)	GUL/PLC (% wt.)	GBFS (% wt.)
SiO ₂	19.8	19.0	38.7
Fe ₂ O ₃	2.62	2.10	0.52
Al ₂ O ₃	4.50	5.10	8.90
CaO	62.5	60.1	38.5
MgO	3.30	2.30	11.32

SO ₃	3.41	3.90	2.75
LOI	2.40	5.00	1.60
Total Alkalies, as Na ₂ O (per ASTM C114 ^[111])	0.58	0.86	0.77
C ₂ S	17	15	-
C ₃ S	52	52	-
C ₃ A	8	10	-
C ₄ AF	8	7	-
Blaine Fineness	386m ² /kg	519m ² /kg	554m ² /kg

3.1.2 Carbon (Black) Steel Rebar

Two carbon (black) steel rebars of the same grade of 400W steel and dimensions of 15M (nominally, 16mm in diameter) were provided by different suppliers, HarrisRebar and MANA bar mill. The main purpose of testing the two rebar types was to investigate the effect on their corrosion performance due to the difference in their initial conditions at the time of testing, as shown in Figure 3.1, where the HarrisRebar specimens (abbreviated as Ha from hereon) were partially rusted due to open exposure to laboratory conditions for at least 3 years, whereas the MANA rebar (abbreviated as MA from hereon) were used shortly after delivery from the rolling mill and thus, were in better conditions.



Figure 3.1 Longitudinal and sectional photographs at time of testing. (Left) Ha rebar after more than 3 years in the laboratory; (Right) MA rebar few months after dispatch from rolling mill

The rebar types were used both in the synthetic pore solution tests and in concrete specimens exposed to chloride solution for macrocell and microcell tests, corresponding to the GU and GUL

cement blends, without GBFS. Only MA bars were used in both tests for cement blends, including GBFS.

3.2 Pore Solution Expression, Chemical Analysis and Corrosion Tests

It is the composition of the aqueous solution in the pores of cement pastes and concrete which is responsible for the development of the passive film formation on the rebar and, when contaminated by chlorides, the breakdown of passivity and onset of active corrosion. This section discusses the methods of the extraction and chemical analyses of the pore solutions compressed out of hardened cement paste specimens of the various mix proportions to allow for preparation of synthetic solutions using laboratory-grade chemicals for corrosion testing.

The procedure involved the extraction of the liquid solutions stored in the pores and voids of hardened cement paste samples, after 28 days of curing in ambient laboratory conditions, and quantitative analyses of the cation and anion constituents, based on which test solutions were synthesized. The outcome of this test was to determine the response of the carbon steel rebar in the aggressive chloride environments.

3.2.1 Cement Paste Specimens

Cement paste cylinders were cast from blended mixtures of the cement, GBFS, distilled water and sodium chloride at varied concentrations, proportioned with a fixed ratio of water to cementitious materials, which summed the mass of GU or GUL cement and any added GBFS, (w/cm) of 0.4. It was estimated that a w/cm ratio of 0.4 would achieve approximately 65-75% hydration, where GUL cement pastes exhibited hydration degrees 5-10% higher than the respective GU cement pastes at day 7^{[108], [84]}. Table 3.2 exemplifies the nomenclature used for the cement paste mix designs, the proportions of which are given in Table 3.3.

Table 33.2 Nomenclature of the mix designs for the cement paste mixes

ID	Description
0BFSGU	GU cement, without any SCMs/GBFS
0BFSGUL	GUL cement, without any SCMs/GBFS
0BFSGU a Cl*	GU cement, without any SCMs/GBFS, admixed with a % Cl-, by wt. of cm
25BFSGU	75% wt. GU cement, with 25% wt. GBFS
25BFSGUL	75% wt. GUL cement, with 25% wt. GBFS
25BFSGUL a Cl*	75% wt. GUL cement, with 25% wt. GBFS, with a % Cl- by wt. of cm
35BFSGU	65% wt. GU cement, with 35% wt. GBFS

35BFSGUL	65% wt. GUL cement, with 35% wt. GBFS
35BFSGU a Cl*	65% wt. GU cement, with 35% wt. GBFS, with a % Cl- by wt. of cm
50BFSGU	50% wt. GU cement, with 50% wt. GBFS
50BFSGUL	50% wt. GUL cement, with 50% wt. GBFS
50BFSGUL a Cl*	50% wt. GUL cement, with 50% wt. GBFS, with a % Cl- by wt. of cm

* a can take either of the following: 0, 0.1, 0.2, 0.5, 0.75, 1.0

Table 3.3 Proportions of the materials for the respective mix designs for the cement paste mixes

Material	Mix Type					
	0BFSGU/GUL	25BFSGU/GUL	35BFSGU/GUL	50BFSGU/GUL...		
GU or GUL Cement	1,500 g	1,125 g	975 g	750 g		
GBFS	0 g	375 g	525 g	750 g		
Distilled Water (0.4 w/cm)	750 g	750 g	750 g	750 g		
... a Cl (by wt. of cm)	...0Cl	...0.1Cl	...0.2Cl	...0.5Cl	...0.75Cl	...1.0Cl
NaCl granules	0 g	2.45 g	4.95 g	12.35 g	18.55 g	24.70 g

Using a flat beater paddle attachment of the Legacy® countertop Hobart mixer (Figure 3.2), the pre-weighed dry materials, including the GU or GUL cement and GBFS, were stirred for 30 seconds prior to the addition of the water, in which reagent grade NaCl crystals were dissolved according to the mix type, and mixed for 2 minutes. After a rest period of 2 minutes to allow for relief of air bubbles introduced by the mixing action, it was mixed for another 1 minute before casting into 50.8 mm (2 inch) diameter by 101.6 mm (4 inch) long cylindrical plastic moulds.



Figure 33.2 (Left) Hobart mixer used to blend the cement paste mixes; (Right) Hotdog rolling machine used for continuous rolling of cement paste cylinders

Five replicates were cast for each of the varied chloride contents of 0%, 0.1%, 0.2%, 0.5%, 0.75% and 1.0% Cl⁻ by mass of cementitious materials (cm). The cylinders were capped and sealed with

electrical tape to prevent leaking of the water or migration of air through the interfacial gap between the cap and the mould body. As shown in Figure 3.2, the cylinders were rolled continuously for 24 ± 1 hours (average speed of 1 revolution per 2.5 seconds) to mitigate uneven distribution of the water due to bleeding and sedimentation. The cylinders were then cured at ambient laboratory conditions for 27 more days.

3.2.2 Expression of Pore Solutions

At age of 28 days, three of the five hardened cement paste cylinders were removed from the moulds for pore solution expression using the setup, shown in Figure 3.3. A 2 mm rubber O-ring was used to prevent leaking of the expressed solution from the base (bottom of Figure 3.3, right image). The inner 1 mm deep-circular indentation functioned to guide the liquids to an outlet channel, to which a $0.45 \mu\text{m}$ filter was attached to a syringe for collection.

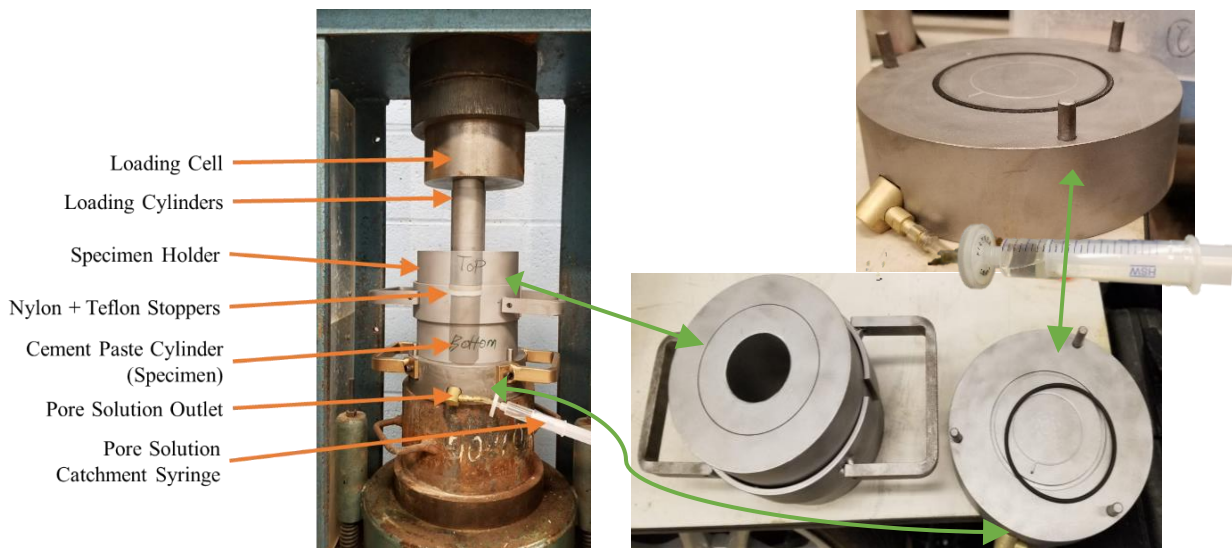


Figure 3.3 (Left) Pore solution equipment setup; (Right) Specimen holder and base with collection syringe

A Teflon disk rested just on the top surface of the cement paste specimen to prevent upflow of extracted liquids. A harder nylon disk was placed between the Teflon disk and loading cylinder to minimize the recovery response, by elongation or expansion, of the specimen at any point of slight unloading during the compression. These disks were replaced if they showed signs of allowing movement or when their deformations reached the point where they were no longer well-fitted to perform their respective functions.

An initial force of about 30-40 kN (approx. 15-20 MPa) was found to be the minimum required for the compressed solutions to begin to flow to the collection syringe. This force was held for about 20-30 minutes depending on the outflow rate of the expressed liquids. The force was increased in increments of 10 kN (5 MPa), each lasting for about 20-30 minutes, up to a maximum of 60-70 kN (30-35 MPa), depending on the volume of expressed solution. Each cement paste cylinder was compressed to about 80-85% of its original length (Figure 3.4) at the end of each expression with the target volume of 5-8 mL of expressed solution.

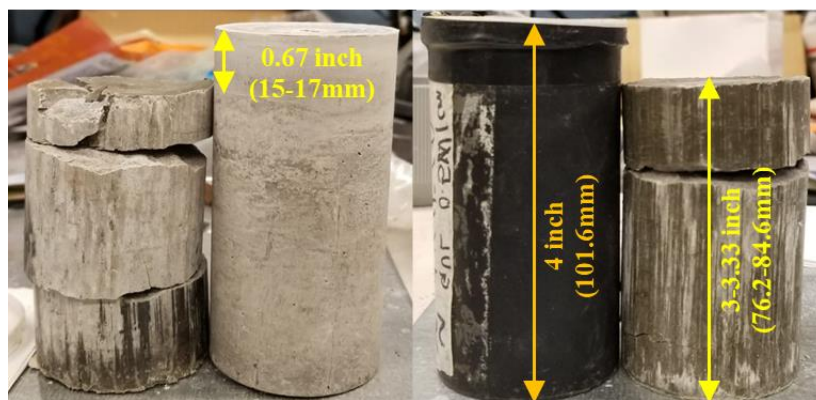


Figure 3.4 Pre- and post- compressed conditions typical of the cement paste cylinders

Some specimens produced just enough (about 4-5 mL) for the chemical analyses and pH tests, due to errors, such as (1) slight displacement of the O-ring during the assemblage of the setup resulting in the loss of expressed liquids; (2) gaps between deformed cement paste cylinders and the inner walls of the high-pressure device, allowing upflow of expressed liquids and loss of the vacuum effect (formed under compressive pressures) required for the downward pull of the extracted liquids; and (3) leaking of the expressed liquids along the external surface of the outlet spout, to which the collection syringe was attached. The lost liquids, which were not guided into the collection syringe, were discarded due to possible chemical changes on reaction with the atmosphere, such as by oxidation, and therefore, deviating from their true chemical nature.

At the end of each expression, the collection syringe was immediately sealed with a sterile cap to prevent atmospheric interference and stored in a box at ambient conditions, away from light, until transfer for chemical analyses. After a series of loading and unloading cycles, the compressed cement paste cylinder and Teflon/nylon disks were removed (Figure 3.5). The outlet channel on the base piece was rinsed with isopropanol before consecutive expression activities.



Figure 3.5 (Left) Setup for removal of compressed cylinder and disks; (Right) Loading elements. After expression of cylinders of the same mix, the inner walls of the specimen holder were sandblasted, blown with compressed air to remove residual debris, wiped with isopropanol and air blown again to minimize risk of cross-contamination. The base piece was sandblasted at the end of each major mix type category, for example, after the successive expressions of the 25SGU specimens of all the various Cl^- concentrations, because excessive sandblasting would lead to pitting on the bevelled surface leading to the outlet hole and difficulty in guaranteeing no residual debris of the sandblasting material on the walls of the small channel to the outlet spout.

3.2.3 Chemical Analyses of Expressed Pore Solutions

2.0-2.5mL of each of the expressed pore solution samples were separated into sealable centrifuge tubes for pH measurement using a portable Orion 290A+ pH meter. For every set of pH measurements, the meter was pre-calibrated using standard buffer solutions of pH 7, pH 10 and pH 12.45. After each successive use, the meter's pH and temperature probes were rinsed with distilled water to mitigate cross-contamination. The centrifuge tubes were then stored in a refrigerator to minimize oxidation or any reactions with atmospheric contaminants.

However, due to the instability of the glass probes of the pH meter due to exposure to the highly alkaline pore solution samples, ranging from 13.0 to 13.9, an alternative method involving titration with 0.02N sulphuric acid (H_2SO_4) solution was incorporated to validate pH measurements. The method was destructive as it required diluting 1 mL of the expressed pore solution sample to 50 mL with distilled water. To ensure precision of measurement, a 1000 μL precision micropipette with a disposable plastic tip and 50 mL volumetric flask were used. It is important to note that while pH meters are influenced by ionic activities, titrations can overestimate pH parameters as

they depend on ionic strength, which would sometimes take into account the “free” ions and some bound in complex molecular structures. However, for more stable pH measurements for comparison, the method was incorporated for comparing the effects of the cement replacement across the various cement blends.

The 50mL diluted sample was then transferred to a ceramic crucible, to which 3-4 drops of bromocresol green-methyl red indicator (with an endpoint pH range of 4.3 to 4.9 ^[33]) were added incrementally to the magnetically stirred mixture. The volume of titrant was recorded when a stable greyish colour was attained, as the colour changed from the initial blue colour, just before a pinkish hue was obtained (Figure 3.6).

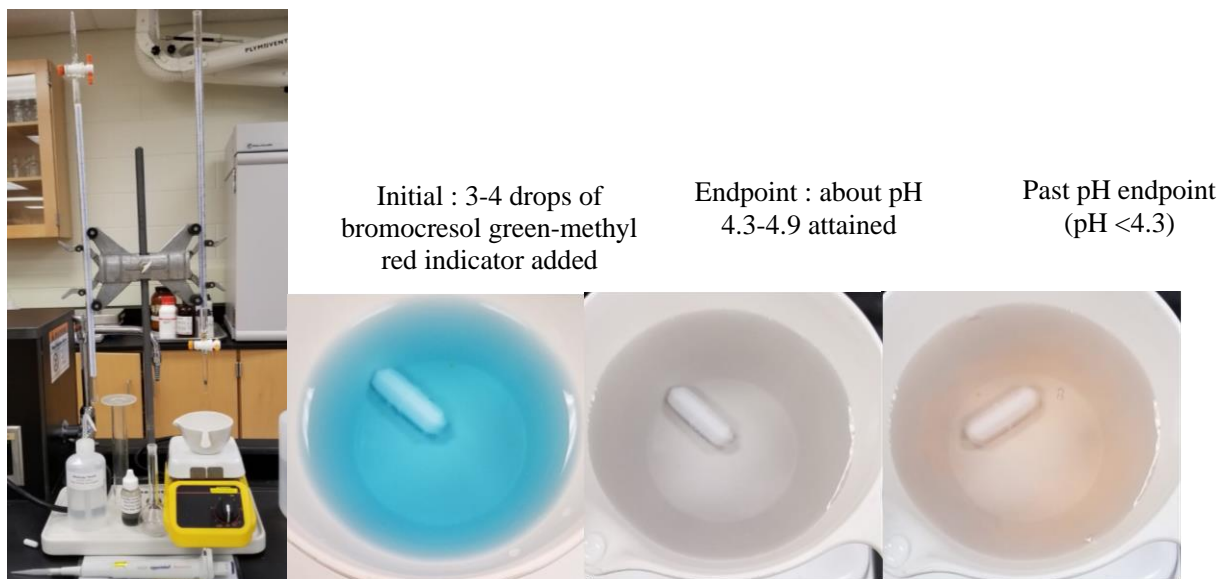


Figure 3.6 Tools and chemicals used for titration (Left); Colour changes of diluted sample with 3-4 drops of bromocresol green-methyl red indicator (Right)

The remaining pore solution samples contained in the sealed syringes were then transferred to the University of Waterloo’s Groundwater Geochemistry and Remediation Group for chemical analyses by technician Joy Hu.

For quantifying the concentrations of the major inorganic anions and some carboxylic acids, the suppressed ion exchange chromatography (IC or IEC) method was performed. The IC method used eluents, which are selective chemicals responsible for removing the analysed ions using highly conductive species, such as NaOH and Na₂CO₃. The eluents are passed through a membrane or immersed in a resin, which contains H⁺ ions, thus displacing the Na⁺ ions and bonding with the

OH^- and CO_3^{2-} ions of the eluents. This exchange in ions between the membrane/resin and the eluents result in the formation of low reactive H_2O and H_2CO_3 molecules. Therefore, the displaced Na^+ ions create a net positive field which would attract the more conductive anions in the analyzed sample ^{[63], [64]} .

The determination of the cation concentrations is performed using the inductively coupled plasma (ICP-) optical emission spectroscopy (-OES) and mass spectroscopy (-MS) methods for higher concentrations, measurable in mg/L, and lower concentrations, measured in $\mu\text{g/L}$, respectively. The ICP methods generally involve the nebulization of the liquid sample, or in other words, the conversion of the liquid sample into a fine spray or aerosol, which is passed through a high-temperature plasma and ionized. In the ICP-OES method, the ionized spray passes through a coil, which is electrically charged where the induced magnetic field excites the ions. The excited ions of higher energy then reach the cooler end of the plasma chamber, where they return to their lower stable energy state, and the energy loss is released as light of various wavelengths which are then interpreted by the spectrometer ^[63]. However, a notable disadvantage of the ICP-OES method is the relatively high detection limit and, therefore, elements of lower concentrations are quantified alternatively using the ICP-MS method. For this method, an optic lens concentrates the ions into a mass analyzer or spectrometer, which simultaneously identifies multiple elements based on the ratio of mass to charge ^[64].

3.2.4 Evapourable Water Measurements

The remaining two of the five hardened cement paste cylinders were prepared for evapourable water measurements, using the tools in Figure 3.7. Each cylinder was sectioned into approximate thirds (denoting the top, middle and bottom portions) and each third hammered in a felt/cotton cloth into finer particles passable through a 1.18mm mesh. The particles were then further ground, using a mortar and pestle, until at least 20g were passable through a 425 μm mesh, which were then stored in individual capped petri dishes.

10 \pm 0.5 g of each of the powdered sample were weighed and transferred onto pre-weighed ceramic crucibles for 24 \pm 1 hours of heating in a preheated oven at 105 \pm 5 °C (Figure 3.7, right image). Upon removal of the heated samples from the oven, they were allowed 5 minutes of cooling in an enclosed desiccator, to prevent absorption of moisture due to the hygroscopic nature of the cement mix on exposure to the atmosphere, before re-weighing. The loss in mass was determined for

calculations of the mass of evaporable water, W_e , as a percentage of the post-heated mass of the ground sample ^[11].



Figure 3.7 (Left) Tools used for powdering the cement paste cylinders; (Right) Ground samples, three for each cement paste cylinder specimen, in oven

3.2.5 Synthetic Pore Solutions

Based on the ICP and IC results for the mix types, the synthetic pore solutions were made with laboratory-grade chemicals of NaOH, $\text{Ca}(\text{OH})_2$, KOH, $\text{CaSO}_4 \cdot 2\text{H}_2\text{O}$ and NaCl, proportioned according to the averaged concentrations of the cations Na^+ , Ca^{2+} , K^+ and anions SO_4^{2-} , Cl^- , respectively. The calculations assumed that the major compounds of the cations were their respective bonded OH^- forms, while for the major compound associated with Cl^- was NaCl and that of SO_4^{2-} was CaSO_4 .

3.2.6 Preparation of Rebars for Immersion in Solutions

The Ha and MA rebar were cut into (203.2 mm) (8 inch) and using a brush with soft bristles, they were lightly brushed with tap water followed by isopropanol and air-blown to remove any residual coolant from the bandsaw cutting machine. The cut ends of rebar specimens were then filed to remove any loosely attached or residual metal shavings or sharp hooks, that may puncture the applied epoxy coating or form crevices. The Ha rebars required gentle wire brushing to remove the visible rust, as shown in Figure 3.1.

Using a 4.75 mm (3/16 inch) diameter drill bit, 12.7 mm (1/2 inch) deep holes were drilled on one end of the rebar for soldering copper wires, with lead solder. The soldering methods used either a blowtorch or the combined method of soldering iron and soldering flux paste. Contact between the stripped copper wire end and rebar was essential for electrochemical measurements. Each mix type was assigned a copper wire colour and marked line stripes to identify the replica ID. The rebar,

particularly the ends, were brushed lightly with tap water followed by isopropanol, rinsed in distilled water and air-blown, to remove any grease or debris prior to coating with electroplating stop-off lacquer. Three coating layers were applied for each end, with at least 12 hours of air-drying time between each application. The exposed lengths of the rebar were measured. Five to six replicas were prepared for each cement mix.

3.2.7 Setup for Corrosion Tests in Synthetic Pore Solutions

Using a hot glue gun, the rebars were mounted vertically in the plastic containers, shown in Figure 3.8. Using translucent containers allowed for visual observation of any changes in the appearance of the rebar or discolouration of the solution, which would indicate the dispersion of corrosion products. The exposed surfaced of the rebar specimens were cleansed of grease and other surface contaminants, following the same process described in Section 3.2.6 within 1 hour prior to immersion in the prepared synthetic pore solutions. Each container held the same number of specimens for each of the rebar types, which meant 3 Ha, 3 MA in one and 2Ha, 2MA in another, for the each of the GU and GUL mixes without GBFS. This arrangement was set to facilitate the comparison between the results of the Ha and MA rebar exposed to the same environment. Likewise, for the mixes with GBFS, each container held all six MA bars assigned for the respective mix type. This is better described in Table 3.4.

Table 3.4 Configuration of rebar types in the respective test containers

Mix Type	Method	Container ID	No. of Ha Rebars	No. of MA Rebars
0BFSGU	M1	A-01	3	3
0BFSGU	M1	A-02	2	2
0BFSGUL	M1	A-03	3	3
0BFSGUL	M1	A-04	3	3
0BFSGU	M2	A-05	3	3
0BFSGUL	M2	A-06	3	3
25BFSGU	M1	B-01	0	6
35BFSGU	M1	B-02	0	6
50BFSGU	M1	B-03	0	6
25BFSGUL	M1	B-04	0	6
35BFSGU1	M1	B-05	0	6
50BFSGUL	M1	B-06	0	6

Note: Mixes without GBFS were tested first using the six test containers. After the end of testing and removal of the specimens, the mixes with GBFS were tested with the test containers after thorough cleaning.

Note: Method M1 involved adding NaOH, Ca(OH)₂, KOH and Ca(SO)₄ only at the start for 0% Cl⁻ conditions, followed by the incremental additions of NaCl. Method M2 followed M1, except that for every incremental increase in NaCl, the other chemicals were also added, where necessary.

The duration of the conditions of the solutions for each chloride concentration varied accordingly to Table 3.5. It was ensured that Ca(OH)₂ was added to excess, till precipitation, to maintain the high alkaline Ca(OH)₂-rich environment typical of concrete due to the hydration reactions.

Table 3.5 Duration of incremental chloride chemicals to the synthetic pore solutions

Chloride Concentration (% Cl ⁻ by mass of cm)	Duration of chloride level (days)	Test Days
0%	28	1, 3, 7, 10, 14, 17, 21, 24, 28
0.10%	7	1, 3, 7
0.20%	7	1, 3, 7
0.35%	7	1, 3, 7
0.50%	7	1, 3, 7
0.60%	7	1, 3, 7
0.75%	≥ 28	1, 3, 7, 10, 14, 17, 21, 24, 28...
1.00%	≥ 28	1, 3, 7, 10, 14, 17, 21, 24, 28...

Note: The test days represent the number of days after addition of chemicals to match the respective chloride concentration

3.2.8 Electrochemical Tests

Corrosion can be assessed by a multitude of methods based on electrical circuits. Figures 3.8 and 3.9 show simplified Randles circuits for steel directly immersed in synthetic pore solution and embedded in concrete, respectively. The main components of the circuits are as follows:

(1) R_s and R_c represent the resistance of the electrolytic solution and, for the case of embedded steel, of the concrete, respectively. They are affected by impurities and temperature.

(2) CPE (Constant Phase Element is an electrical element that may act as a capacitor) or C_{dl}, which is the capacitance of the Helmholtz double layer^[46]. The double ionic layer is analogous to the dielectric plates of a capacitor of opposite charges. It is formed when the metal is immersed in solution and an inner layer is formed at the steel/solution interface due to the adsorption of water molecules to the charged metal. The oppositely charged side of the polar water molecules then form another outer layer with the ions in the solution.

(3) R_{ct} or R_p is the resistance to charge transfer or to polarization of the metal. This is the resistance of the metal to be dissolved into its respective ions by loss of electrons.

(4) W is Warburg impedance. This is related to the diffusivity in concrete, which affects the rate of the redox reactions required for the electric flow. Therefore, in the case for the lower bar and upper bar in Figure 2.4, this parameter is dependent on the movement of the oxygen and metal ions, respectively.

(5) R_f is, like R_{ct} , the resistance of the resistance of charge transfer through the passive film

(6) C_f is the capacitance of the passive film.

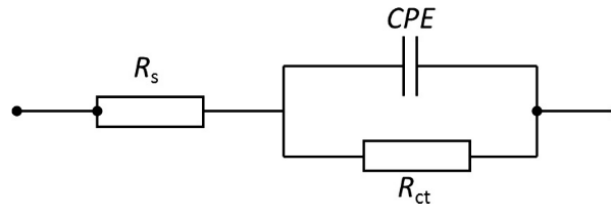


Figure 3.8 Randles circuit for the steel in synthetic pore solution ^[97]

The Figure 3.9 circuits can be simplified to Figure 3.8 with the Warburg impedance element in series with R_{ct} .

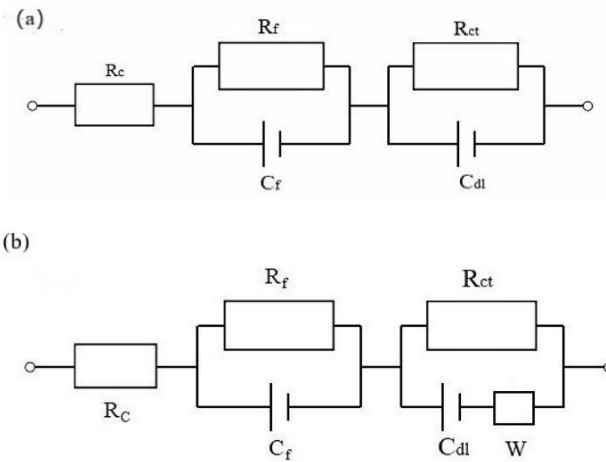


Figure 3.9 Randles circuits for steel reinforcement in (a) passive state (no corrosion) and (b) active corrosion state ^[98]

3.2.8.1 Open Circuit Potential (OCP) Measurements

Electrochemical testing involves applying either a current to flow through or potential across two electrodes and measuring the other parameter which is not applied. The open circuit potential (OCP) is the natural potential of the metal against a reference electrode when no current or potential is applied. From the OCP measurements, the probable state of the metal can be deduced. A commonly adopted evaluation system follows ASTM C876 ^[95], as shown in Table 3.6.

Table 3.6 Corrosion risks of carbon steel embedded in concrete per measured OCP [95]

OCP [mV versus SCE]	Condition of Embedded Steel
More positive than -120mV	>90% probability for no corrosion
Between -120mV and -270mV	Uncertain
More negative than -270mV	>90% probability for active corrosion

Note: SCE is Saturated Calomel Electrode

There are limitations to the OCP method as the measurements do not conclude on the type of corrosion and can be affected by various factors, such as oxygen availability and the resistance of the electrolytic solution. However, the method is used for its simplicity [78].

3.2.8.2 Linear Polarization Resistance (LPR) Technique

The technique used involves charging or polarizing the metal in solution by an applied potential while the induced flow of current is measured. The applied potential and measured currents are then plotted as polarization curves. Following Stern & Geary's findings on the linearity in the polarization plots, within ± 5 -20mV of the OCP, a Stern-Geary's constant, B, was established for determining the corrosion current, I_{corr} , as shown in Equation 3.2 [105]. In Equation 3.1, R_p , which was described previously as the polarization resistance of the metal, represented that linear relationship between the measured current, I, and the applied potential, E. R_p is alternatively known as the linear polarization resistance (LPR).

$$R_p = \frac{\Delta E_{applied}}{\Delta I_{measured}} \quad \text{Equation 3.1}$$

$$I_{corr} = \frac{B}{R_p} \quad \text{Equation 3.2}$$

$$i = \frac{I_{corr}}{A} \quad \text{Equation 3.3}$$

For steel reinforcement in concrete, B is commonly assumed to be 26mV for actively corroding steel or 52mV for passive steel [79], [98]. To effectively account for the degree of the corrosion of steel, the corrosion current represented as corrosion current density, i_{corr} , based on the surface area of steel exposed to the corrosive environment, A, as shown in Equation 3.3. Broomfield presented interpretations of corrosion rates which relate to different levels of risk of corrosion activity [75]. For reference, 0.001 A/m² is equivalent to approximately 1 μ m/year of iron metal loss, as the

minimum indication for active corrosion [78], [97]. This conversion from current density to physical metal loss is based on Faraday's Law [15].

Limitations to the LPR technique are similar to those mentioned for OCP, whereby it does not explicitly provide information on the type of corrosion and the effects of the electrical resistance of the solution or concrete and may fluctuate due to instability of the passive film and changes in concrete, temperature, relative humidity, etc. [78], [98].

Figure 3.10 shows a schematic representation of the three-electrode system for the pore solution test. The main components of the system include:

- (1) the respective Ha/MA rebar as the working electrode (WE). It is the electrode on which the chemical reactions would occur due to the movement to and from this WE and the electrolytic solution (synthetic pore solution);
- (2) titanium-titanium oxide mesh strip as the counter electrode (CE), which is typically made of a highly inert and unreactive metal and carries the current flows through the WE; and
- (3) a saturated calomel electrode (SCE) as the reference electrode (RE), against which the WE potential is controlled or measured. The type of SCE used was one with a plastic body as glass is soluble in highly alkaline solutions.

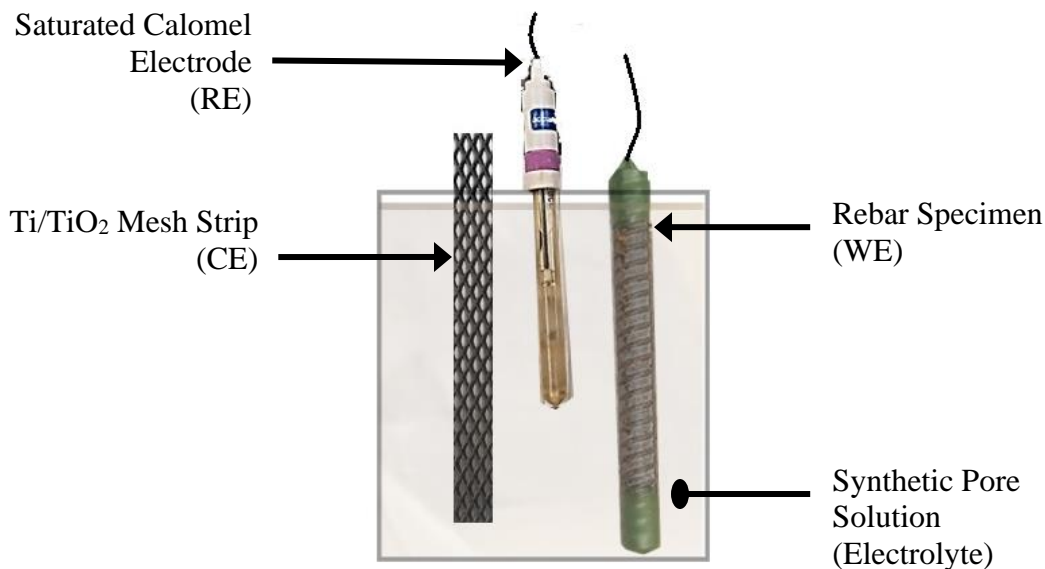


Figure 3.10 Three-electrode system for electrochemical test setup for pore solution

An individual mesh CE was used for each rebar specimen ensuring that the WE and CE were not in contact throughout the tests to prevent electrical interference. The electrochemical

measurements were performed by a Biologic potentiostat which functions to input the programmed electrical signals and measure the response.

The test solutions in the containers were stirred for at least one minute using a magnetic stirrer and allowed to rest for 5-10 minutes before testing to allow for any small electrical charge by the magnetic field to disperse. The OCP was measured for three minutes, at the end of which the final reading was noted as the reference potential. The potential of the rebar was scanned at a rate of 10mV/minute, from the reference OCP to 30 mV more negative than the reference OCP, and then held for 1 minute. Then, the potential was scanned at the same rate in the anodic direction to 30 mV more positive than the reference OCP. The last step was for the system to return the WE to the reference OCP before ending the test program. These steps were adapted from the potentiodynamic ASTM G59 test ^[67]. The current response was recorded during the entirety of the test run.

3.2.9 Autopsy of Rebar Specimens

When the monitoring period for the pore solution tests ended, the specimens were removed from test containers for autopsying by visual inspection and photographed for comparison with pre-test conditions.

3.3 Reinforced Concrete Block Specimens

Four to five concrete specimens of the varied GU and GUL cement blends, with and without GBFS, were made based on changes to the ASTM G109 standards ^[68].

3.3.1 Concrete Specimen Preparation

To assess the corrosion behaviours of the different concrete mixes, the standard ASTM G109 test specimen was adopted with some modifications:

- To maintain 1 inch (0.025 m) concrete cover on all sides of the rebar, the dimensions for specimens are detailed in Figure 3.11. It is expected that the reduction reactions would be more prominent at the two bottom bars, assuming the cathodic role, while the top bar would be responsible for the oxidation reactions, assuming the role of the WE and the anodic electrode.
- The ponding well was cast-in using polystyrene/Styrofoam insulation board cutouts, which were bevelled along the edges with sandpaper to ensure smooth finish and ease of removal

when demoulding. The specimens were cast inverted such that the ponding well cutout sat at the bottom.

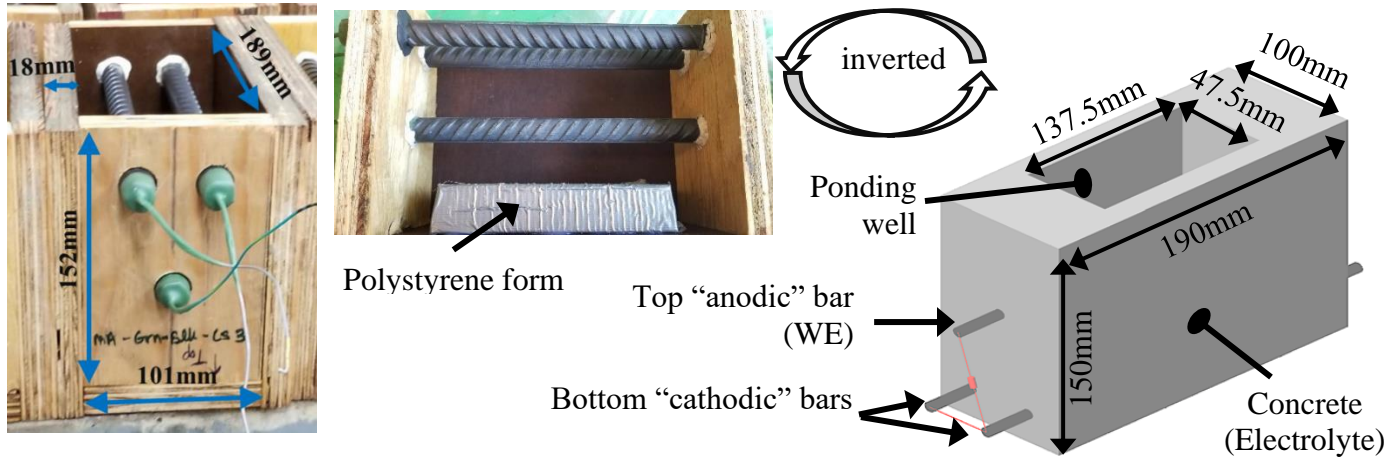


Figure 3.11 (Left) Formwork dimensions; (Middle) Polystyrene ponding-well form; (Right) Schematic representation of reinforced concrete block specimen

Note : The concrete block specimens were cast inverted with the ponding well form at the bottom

- Plywood formwork walls were left attached at the opposite ends holding the rebars in place.
- The exposed sides of the concrete specimens were not coated with epoxy as recommended by ASTM G109 standards.

For the 0BFSGU and 0BFSGUL specimens, both the Ha and MA rebar specimens were cast as top bars, while for all specimens, the bottom bars were MA bars. This was arranged to avoid the pre-rusted conditions of the Ha bars from causing premature corrosion of the bottom bars.

The specimens were prepared similarly to the steps explained in Section 3.2.6. The bars were cleaned prior to placement and after the assembly of the formwork. Minor gaps existed between the walls of the drilled holes in the formwork and the rebar were plugged with plasticine.

3.3.2 Concrete Mix Design

A generic Ontario highway bridge concrete mix design, with a targeted 28-day compressive strength of 35 MPa for the OPC mix, was adopted as the baseline concrete mix design. The mix design complied with the OPSS 1002 ^[18] and OPSS 1350 ^[35] standards, except that the nominal maximum coarse aggregate size of 12.5 mm was used and greater replacements by GBFS exceeded the 25% maximum allowable limit. Table 3.7 summarizes the proportions of the raw materials used for each design mix and the measured slump. An air entraining agent is normally required in

Ontario but it was not included in these mixes since the specimens were not subjected to freeze-thaw cycles.

Table 3.7 Concrete mix designs for reinforced concrete block specimens

Constituent	Amount (per m ³)	Visual Observation Comments
Coarse Aggregate (max 12.5mm)	1,045 kg	
Fine Aggregate / Sand	705 kg	
Water	158 L	
w/cm Ratio	0.4	
Water-Reducing Agent	900 -1100 mL	
<u>GU and GUL Mixes (0BFS / no SCM)</u>		
Cement	395 kg	
Blast Furnace Slag	0 kg	
Slump	GU: 220mm GUL: 152mm	
<u>GU and GUL Mixes (25BFS)</u>		
Cement	296 kg	
Blast Furnace Slag	99 L	
Slump	GU: 190-195mm GUL: 200mm	"wet slurry-like mix" "more workable than GU, not too stiff and not too flowy"
<u>GU and GUL Mixes (35BFS)</u>		
Cement	257 kg	
Blast Furnace Slag	138 L	
Slump	GU: 205mm GUL: 200mm	"wet but not very slurry" "stiffish but fairly workable"
<u>GU and GUL Mixes (50BFS)</u>		
Cement	198 kg	
Blast Furnace Slag	198 L	
Slump	GU: 160-165mm GUL: 180-185mm	"stiffish but workable" "wetter than GU equivalent but not very slurry"

Additional water, equivalent to 3% of the mass of coarse aggregates, was also added for “wetting” or saturating the dry aggregates in the hopper prior to mixing for 1 minute, followed by another 2 minutes of mixing after adding the cement, during which the mixing water was slowly poured to ensure even distributed. The workability was checked by the slump and Master Glenium® water reducing agent was added as needed to obtain a desirable consistency. The concrete block specimens were cast in two lifts on a vibrating table, with 20-25 seconds of vibration and slight

tapping off the sides, when necessary, after each lift. The top of each specimen was then smoothed with a trowel to ensure it would sit level when inverted to its correct orientation, as shown in the schematic diagram in Figure 3.11. The specimens were then covered with a pre-soaked hessian or burlap to retain water for the ‘wet’ curing and topped with a plastic covering to reduce the drying rate of the fabric.

For each design mix, 20-25 concrete cylinders were cast in 101.6 mm (4 inch) diameter by 203.2 mm (8 inch) long cylindrical moulds. After four days of curing in ambient laboratory conditions, the reinforced concrete block specimens were demoulded and transferred to the testing room, the temperature and relative humidity conditions of which were monitored using a HOBO UX100 digital data logger. These measurements were used to determine their effects on any electrochemical test results. On contrary, the cylinder specimens were demoulded and transferred for storage in a fog room.

3.3.3 Concrete Resistivity Tests

The Wenner probe is commonly used to measure concrete resistivity, as a resistance corrected to consider the path of flow of charge, which is typically in $k\Omega\text{cm}$.

For surface resistivity (ρ_s) measurements, electrical contact between the probes and the concrete surface is ensured by soaking the specimen in water for wetting the surface or soaking till saturation of the pores for more stable and accurate readings. The latter eliminates the influence of moisture content ^[102]. As shown in Figure 3.12 ^[103], the device outputs an a/c current through the outer two probes and the inner two probes measure the potential. The device then ultimately outputs the surface resistivity, which is the resistance corrected to the travel lines of current flow.

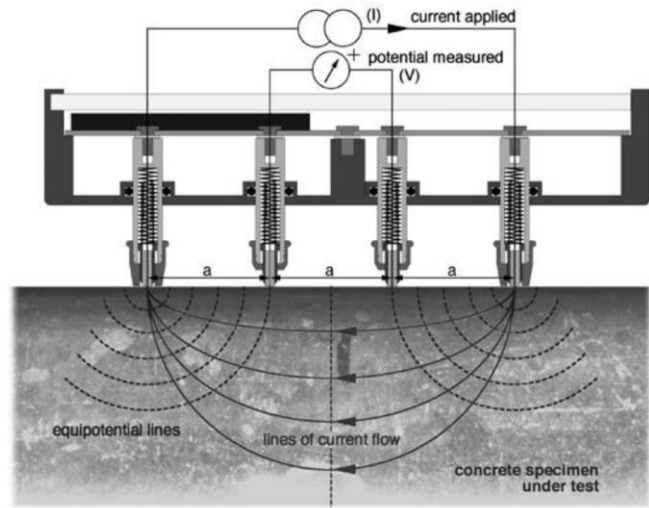


Figure 3.12 Schematic of closed circuit established by Wenner Probe for surface resistivity [103]

Bulk resistivity (ρ_b) measurements require two metallic electrodes placed at the opposite ends of the concrete specimen. Wet porous media, such as sponge or foam, are placed between the concrete and the plates/electrodes to maintain electrolytic contact. Similar to the above concept, a potential is applied between the electrodes and the current measured. The Wenner device then outputs the resistance of the concrete specimen (R_c). The setup is shown in Figure 3.13. To estimate the bulk resistivity (ρ_b), R_c must be factor in the distance of flow, as shown in Equation 3.4 [103], which is dependent on the spacing of the equidistant probes, a , the surface area of the contact surface of the concrete specimen, A , and the distance between the electrodes or depth of the specimen, L .

$$\rho_b = \frac{R_c}{2\pi a} * \frac{A}{L} \quad \text{Equation 3.4}$$

To ensure electrolytic connectivity, the cylinder specimens were fully immersed in water for about 1 hour prior to tests using the Wenner probe.



Figure 3.13 Test setup for measuring bulk resistivity of a concrete cylinder

3.3.4 Concrete Compressive Strength Test

An open-air drying period of 1-2 hours between the resistivity and compression tests was allowed. The compressive tests were conducted following the test setup shown in Figure 3.14. The rate of the force application was maintained in the recommended range of 1.6-2.4 kN/s and the peak force was noted.



Figure 3.14 Cylinder compression strength test setup

3.3.5 Macrocell Electrochemical Tests

After 28 days of curing at ambient room conditions, the two interconnected bottom bars and the top bar of the reinforced concrete block specimens were wired across a 100-ohm resistor to their designated channels to a Keithley 2700 Digital Multimeter and Data Acquisition (DMDAQ) device, as shown in Figure 3.15. The Keithley device was programmed to store recorded measurement of the potential drop across the resistor every four hours.

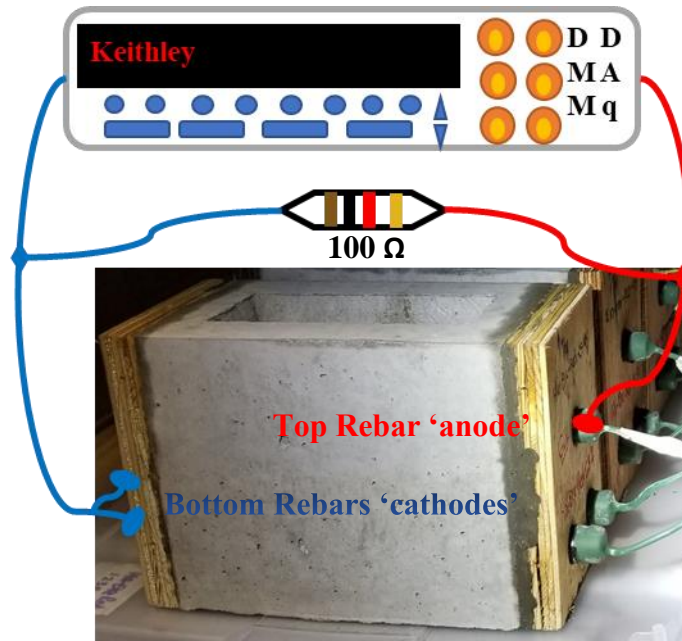


Figure 3.15 Schematic of typical circuit of concrete block specimen with Keithley device

ASTM G109 recommends two-week wet period, during which the ponding well is filled with 3%, by weight, NaCl solution, cycled with a consecutive two-week dry period with the specimens held at 38°C to enhance the salt ingress, by absorption, for the following wet periods. However, this experiment adopted a three-week periodic wet-dry cycle. That meant that after three weeks of the wet period, the solution was syphoned off to allow the cover of the ponding well to dry for three weeks, without heating. One replica of each mix was kept as a control specimen, in which only distilled water was added to the ponds. Initially, the 3% wt. NaCl solution, as recommended by ASTM G109, was followed for the chloride-exposed specimens, but the concentration was increased to 5.75% wt. NaCl by the 210th day to increase the probability of corrosion activity.

3.3.6 Microcell Electrochemical Tests – OCP, LPR and GP Tests

The galvanostatic pulse (GP) technique involves applying an instantaneous current signal or pulse, which can range from 5-400 μA for a duration of 10-200 seconds ^{[104], [106]}, and measuring the potential response, which ideally appears as shown in Figure 3.16 ^[107].

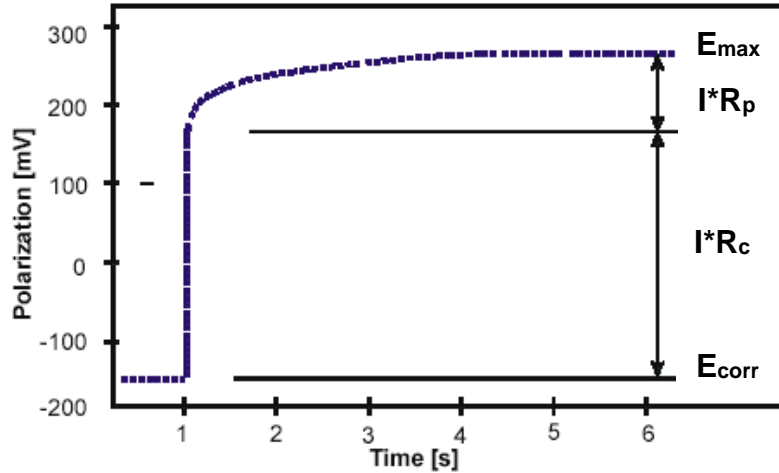


Figure 3.16 Typical potential response to a galvanostatic pulse ^[107]

The corrosion potential of the embedded steel, E_{corr} , represents the OCP value. The advantage of the GP technique is that from the distinctive shape of the response time plot, when steady state is achieved as indicated by the plateau at the maximum potential reached, E_{max} , the following can be easily interpreted: (1) the potential change due to the resistance of the concrete or electrolytic solution, represented by IR_c which is also known as the IR drop; (2) the potential change due to the polarization resistance R_p . From (1), the effect of the resistance of the electrolytic solution or concrete can be accounted for in LPR measurements to correct the R_p , calculated using Equation 3.2, before substitution in Equation 3.3.

During the three weeks of wet period, weekly microcell electrochemical tests were conducted. The top and bottom bars were disconnected at least 2 hours in advance of conducting the respective microcell electrochemical test. For the microcell measurements, a Ti/TiO₂ mesh CE and an SCE RE were placed in the ponding well solution to establish the three-electrode system for the OCP measurements, LPR and Galvanostatic Pulse (GP) techniques (discussed in Section 3.3.7).

Within an hour after disconnection, the OCP was measured for each bar, using a Fluke digital multimeter. This is measured against the SCE RE, immersed in the ponding well. By measuring the OCP just after disconnection, the discharge state of each rebar was assessed and by means of comparing the potential values with those measured at the time of microcell testing, any significant changes were noted.

The LPR test followed the same procedure described in Section 3.2.8.2. The GP test involved monitoring the zero-current OCP for 3 minutes before an input pulse of 10 μA is applied for 3

minutes. The duration of the applied current signal was determined based on the length of time required for the ± 30 mV polarization in the LPR test. The GP test was used to evaluate the concrete resistance.

3.3.7 Autopsy by Visual Inspection and X-Ray Fluorescence (XRF)

After 280 days of monitoring, two concrete specimens, with chloride-contaminated ponding solutions, of each concrete mix type were cut, using a water concrete saw table as shown in Figure 3.17.



Figure 3.17 Clamping system for concrete saw table

Following the schematic of the cutlines shown in Figure 3.18, each specimen was cut along the horizontal lines such that the slab piece, centered between the top and bottom cut pieces, was separable. The bottom left cut piece was separated from the bottom right piece by a cut through the centreline. Then, for each cut piece containing a rebar, a shallow cut was made to a depth of at least 15mm away from the longitudinal edge of the bar. This was to prevent water from altering the diluting the concrete immediately surrounding the rebar. The steel/concrete interfacial surfaces surrounding the top and bottom bars were photographed and chemically analysed using a Thermo Fisher Scientific X-Ray Fluorescence (XRF) device. At least two arbitrary points along each of the gridlines 1-6, as annotated in the right diagram of Figure 3.18, were scanned.

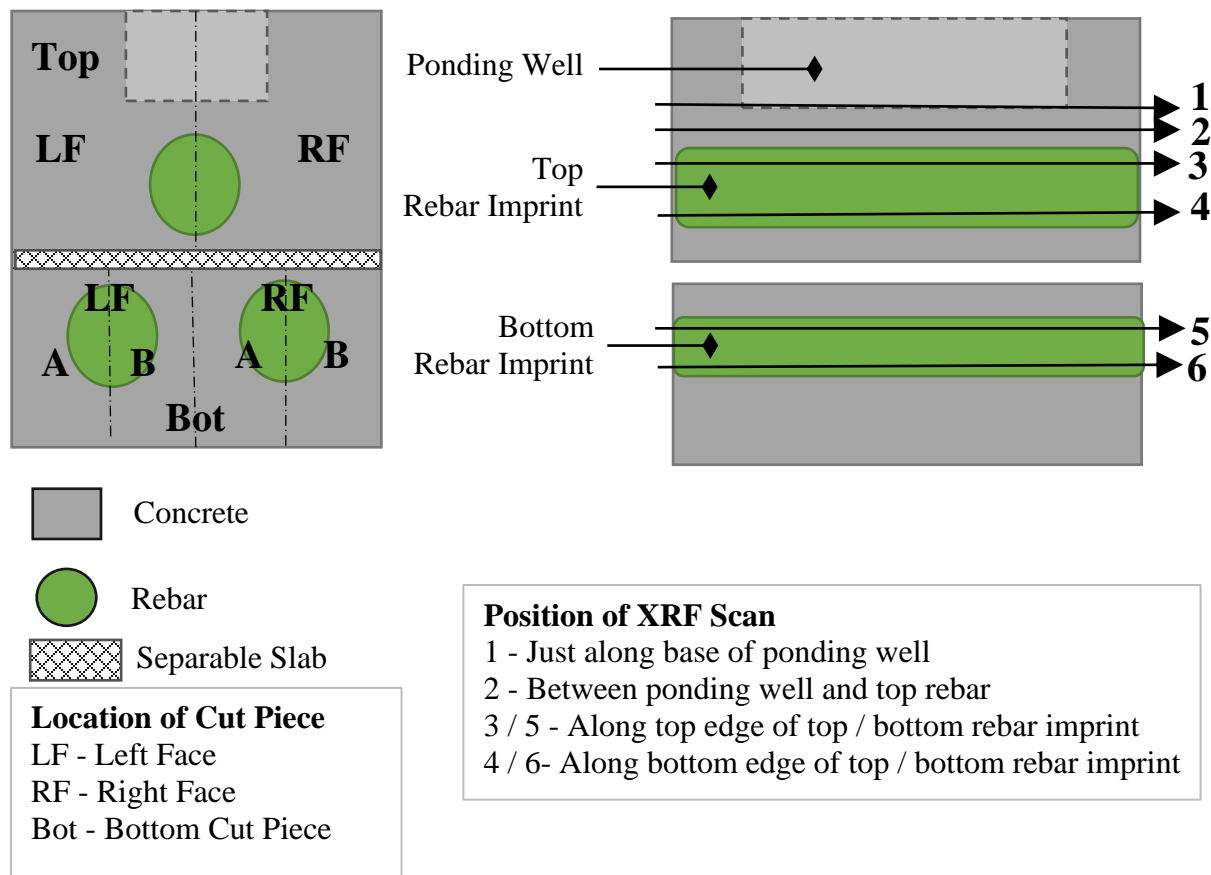


Figure 3.18 Schematic of cut of concrete block specimens (Left) and XRF scan-gridlines on interior cut faces (Right)

The XRF analysis is based on the concept of the release of energy, in the form of X-rays, as electrons move from a higher state to a lower state of energy ^[108]. The detected wavelengths are then interpreted by referencing the intensity spectra, above detection limits of aluminium. The analyses were executed within a short period after cutting to mitigate the chemical changes brought about by exposure to the atmosphere, such as the carbonation of the concrete. It is to be noted that the use of the device is not destructive to the subject of analysis, but its danger comes mainly from the use of X-rays and exposure to the users. A simplified schematic of a handheld XRF device is shown in Figure 3.19. The device typically scans a 1-2 mm diameter area of the sample's surface, at an unknown depth of detection which varies on user application, such as the distance between the XRF device point scanner and the surface of the investigated specimen ^[113].

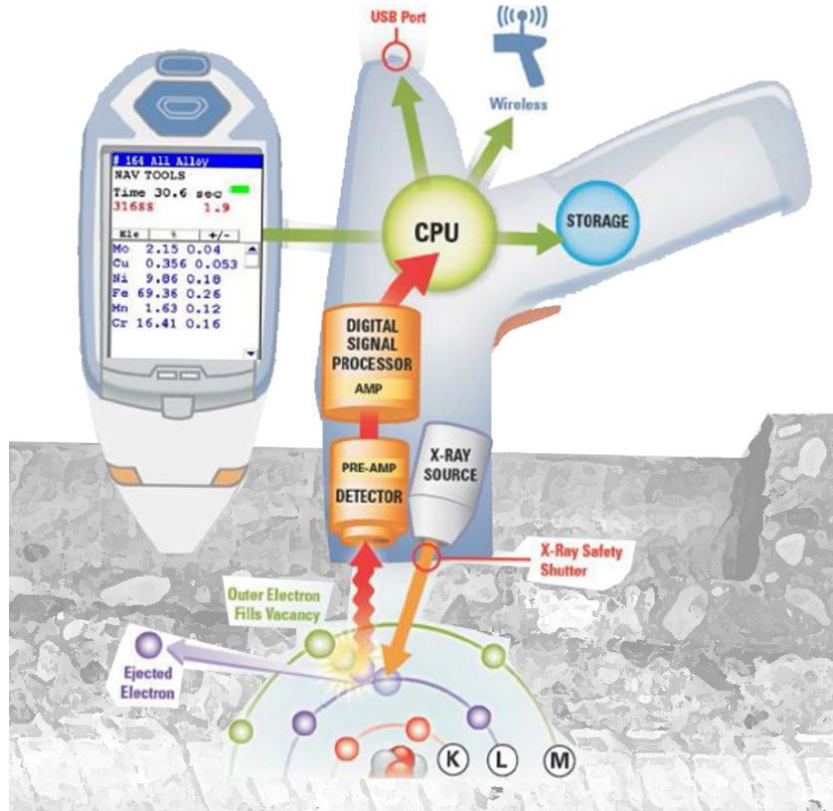


Figure 3.19 Diagrammatic summary of the function of XRF device ^[113]

4.0 Experimental Results

This section discusses the results of the tests performed on the cement pastes and concrete specimens. It is to be noted that the main intent of these two groups of tests was to identify the effect of increased limestone replacement in the cement, i.e. GU versus GUL, as well as the effect of increasing levels of GBFS on both cement types.

4.1 Tests on the Cement Paste Specimens

For the cement pastes, the decision to proceed with a relatively high w/cm ratio of 0.50 was to increase the porosity, thereby facilitating the ease with which the liquids can be expressed. This mitigates the need to apply excessively high pressures for the expression, possibly resulting in a liquid sample that is unrepresentative of the true solution in the cement paste cylinder.

4.1.1 Observations

A distinct dark blue-greenish discolouration was observed in the paste cylinders of cement mixes containing GBFS. The discolouration was accompanied by a pungent odour on exposure to the interior of these cement pastes, which was presumed to be due to the abundance of sulphur ions [109]. The cross-sections of the internal fracture surfaces of the cement paste specimens were photographed immediately after expression, at age of 28 days, and presented in Figure 4.1. The fractured pieces obtained after expression were shown in Figure 3.4. The colour intensified with the increase in the GBFS replacement levels while its appearance faded with the addition of chlorides and thus, it can be assumed to be a physical indication of the degree of the hydration reactions of slag at the age of 28 days. In addition, an increased resistance to the expression of the pore liquids was experienced for the cement paste cylinders, with increasing GBFS content. To obtain the target volume of solution, the application pressure had to either be increased and run at a specific pressure for lengthened time. Moreover, a light-coloured rim is observed along the circumference of each of the cement pastes. The rim appeared to be consistent in thickness on each of the specimens, regardless of the GBFS content.

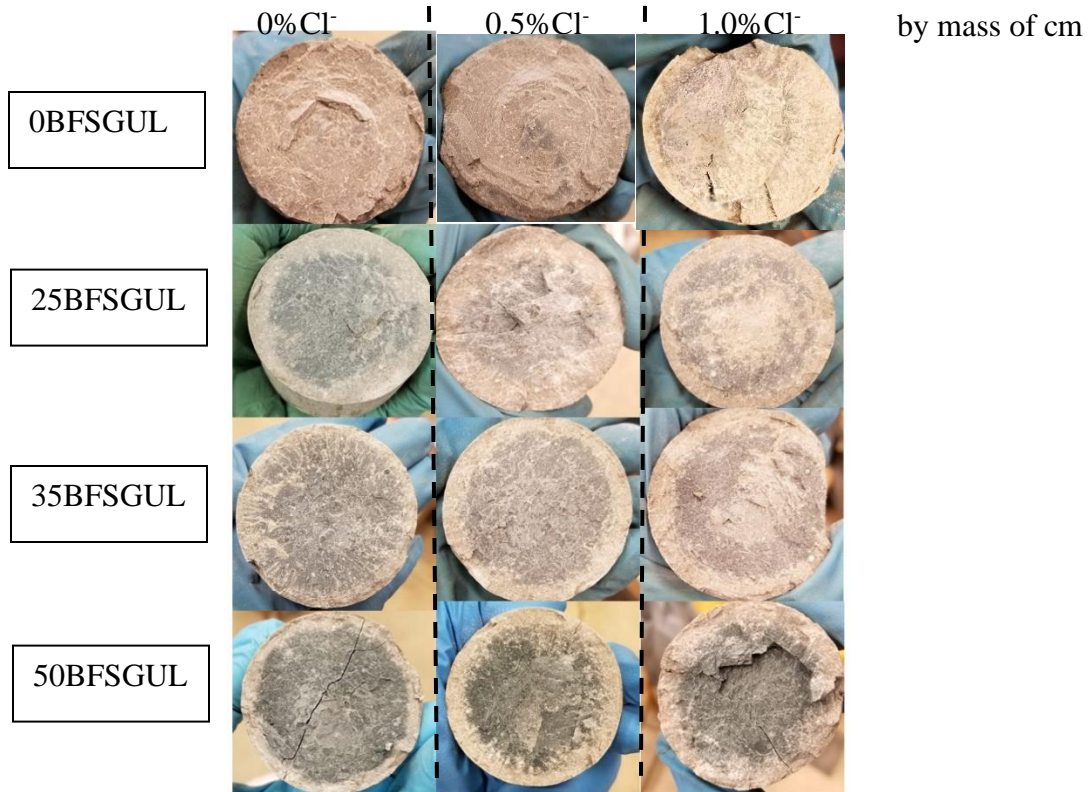


Figure 4.1 Dark blue-greenish discolouration of the cement pastes with and without GBFS replacement and admixed chloride

4.1.2 Chemical Analyses of Expressed Pore Solutions

The pH of the 1-2mL of the expressed pore solutions was measured and then, the remainder stored for later analyses by Joy Hu of the Water and Remediation Group at the University of Waterloo. More details on the chemical analyses are provided in Appendix B.

pH is an important measure as it can affect the kinetics of corrosion reactions as well as influence the development of the hardened cement paste responsible for binding the aggregates in concrete. pH values are significantly influenced by ion activity and so, it was important that the pH of the expressed pore solution was measured soon after the sample was obtained to eliminate risk of interaction with the atmosphere. However, error is inevitable for high-pH measurements because there are no available stable buffers of pH 13 and higher for efficient calibration of the meters, but it is also very likely for the meter to misread interactions between the H⁺ and alkali ions [76]. These errors can cause over- or under-estimations in measurements [56], such as observed in the variable range of pH measurements obtained using a pH meter, presented in Figure 4.2. The pH meter was calibrated using standard buffer solutions of pH 4, 7, 10 and 12.5.

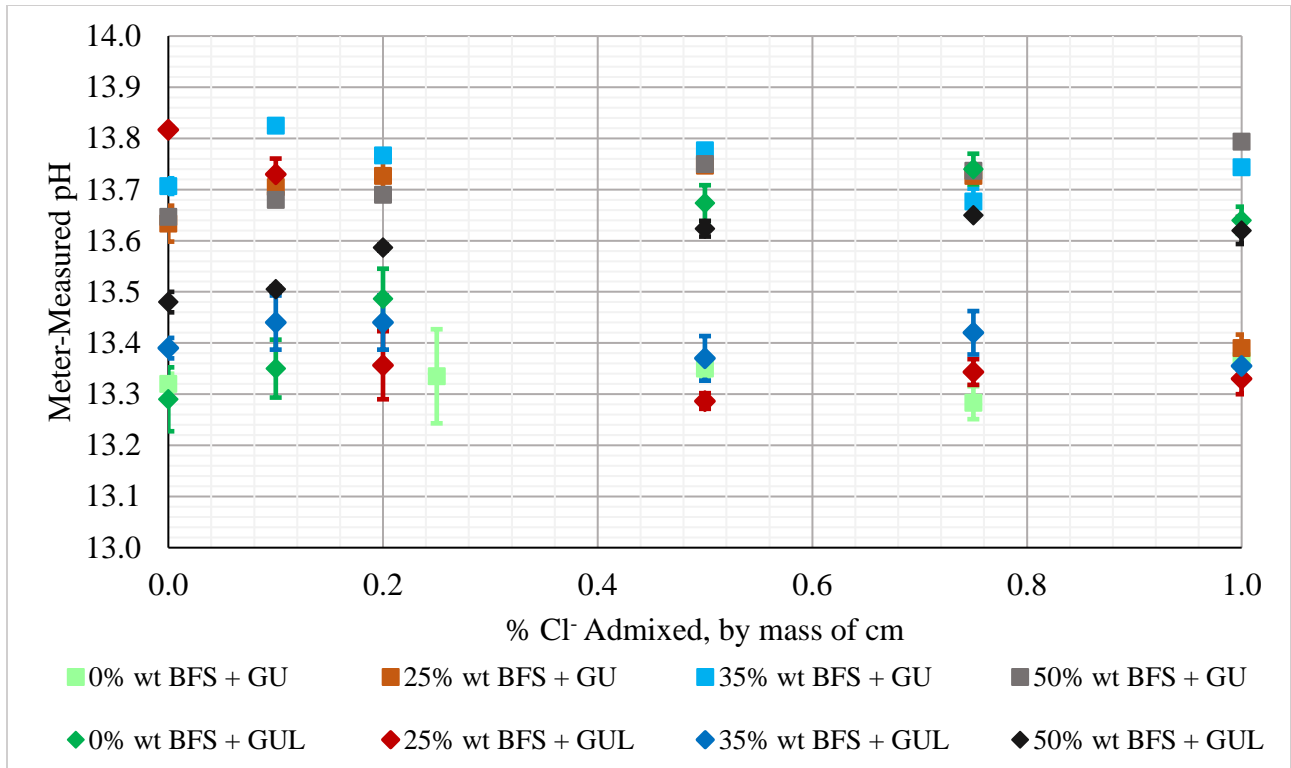


Figure 4.2 pH of expressed pore solutions, measured using an Orion pH meter

Note : the pH values for the 0% GBFS GU mix were obtained from literature ^[110]

The most notable difference in the meter-pH measurements is the decrease in pH of the 25BFSGUL mix, as the admixed chloride concentration increased from 0.1% to 0.2% wt. Cl⁻ and for the 25BFSGU solution, from 0.75% to 1.0% wt. Cl⁻. Comparing the GU and GUL mixes, with the varied GBFS replacement levels, it is generally observed that the GU-GBFS mixes produce higher pH measurements than the GUL-GBFS mixes. This is favourable for promoting passivity for steel reinforcement. However, the 0% GBFS mixes have shown the GUL to have higher pH than the GU equivalents, at any given chloride concentration.

The pH meter measurements were inconclusive showing indications of increased pH with increase in GBFS from 25% to 50% for the GUL-GBFS mixes but varied among the GU-GBFS mixes. The deficiency of the pH measuring device led to the alternative of method of pH evaluation by titration. It is to be noted that the titration tests were not performed directly after the solutions were expressed and thus, the results may not well be representative of their true nature. The pH computations will, therefore, only be compared relatively to each other. Sample calculations detailing assumptions and steps for the estimation are provided in Appendix B.

Figure 4.3 depicts slightly increasing trends in the titration-calculated pH with increase in admixed chlorides, which were observed to be similar across the various blends. Note that the 0BFSGU specimens were not available for the titration. Considering the similarities in the cement composition of the clinker phases, this was not unpredictable. As mentioned in Section 3.2.3, the titration depends on the “free ions” in solution and thus, the calculated pH values, estimated from the total alkalinity titration, agree with the trends observed for the potassium concentrations.

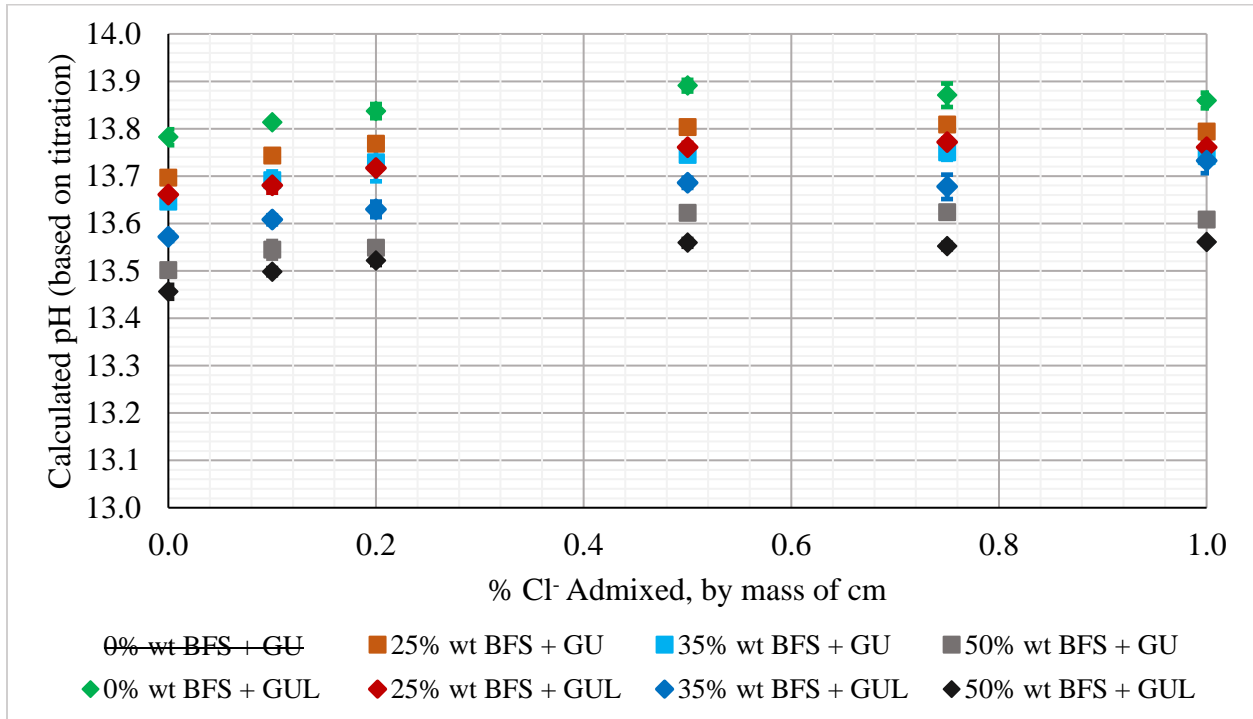


Figure 4.3 Estimated pH values by method of titration

Note : the pore solution data for the 0% GBFS GU mix were obtained from literature ^[110]

This introduces another method of estimating the pH, which relies heavily on stoichiometric assumptions on the alkali ions which would chemically balance the total hydroxide concentration. The calculated hydroxide concentration is then used to determine the pH by the relationship shown in Equation 4.2. The method assumes that the two main contributors to the alkalinity were sodium and potassium, the summed concentrations, in units of mol/L, of which were equated as the hydroxide concentration, following Equation 4.1. The pH values were capped at the absolute maximum of pH 14. As shown in Figure 4.4, as the chloride content increased, which would simultaneously increase sodium concentrations as shown in Figure 4.5, the pH increased. These results differed from the pH values estimated by the titration results which assumed the sodium

ions to be inert. This simple calculation methodology neglected the possibilities of the presence of other forms of the alkali ions, such as sodium carbonate used for accelerating hydration and potassium sulphate used for controlling hardening.

$$[OH^-] = [K^+] + [Na^+] \quad \text{Equation 4.1}$$

$$pH = 14 - \log_{10}[OH^-] \quad \text{Equation 4.2}$$

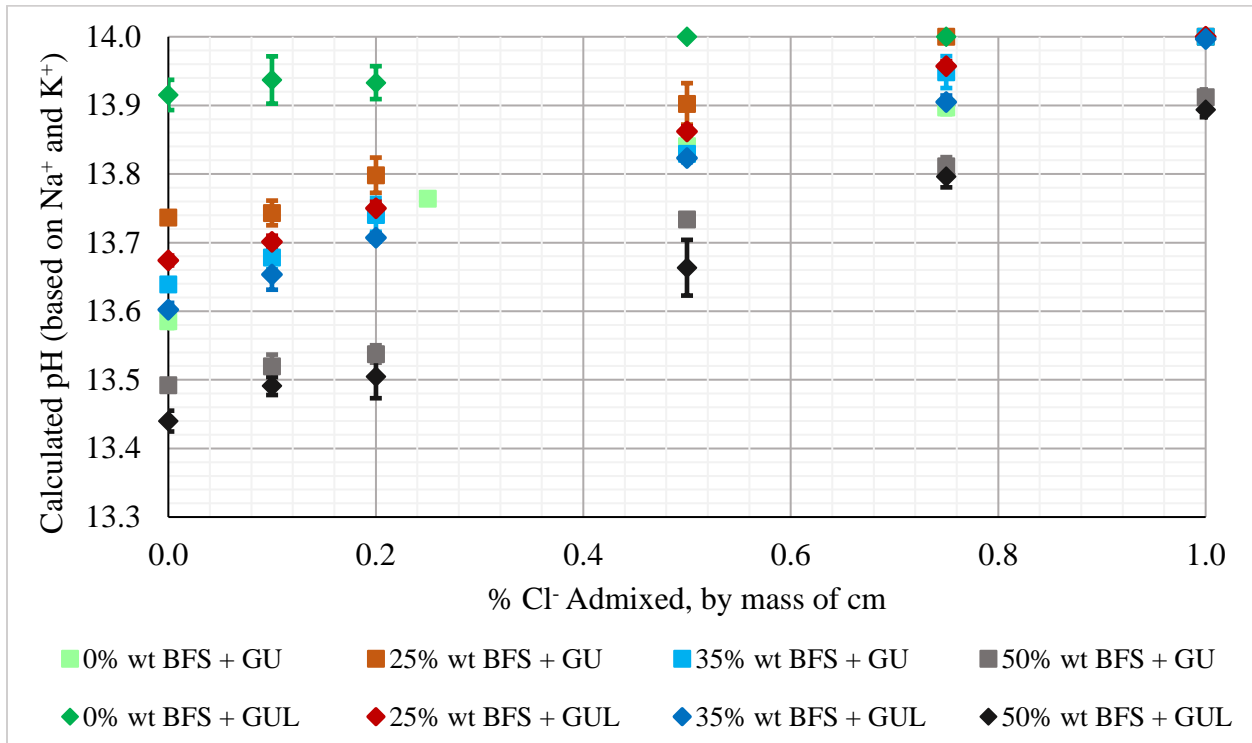


Figure 4.4 Estimated pH values by method of stoichiometry

Note : the pore solution data for the 0% GBFS GU mix were obtained from literature ^[110]

As expected, adding more chloride, as NaCl, proportionally increased the sodium ions detected in the pore solutions. While the chloride ions have interactions with the cement paste, such as binding to form Friedel salts, the sodium ions are left in solution in the pores. Therefore, the concentration increased almost linearly with every addition of chlorides. With the increase in cement replacement by GBFS, the sodium concentrations in pore solution decreased, with little differences between the GU and GUL mixes.

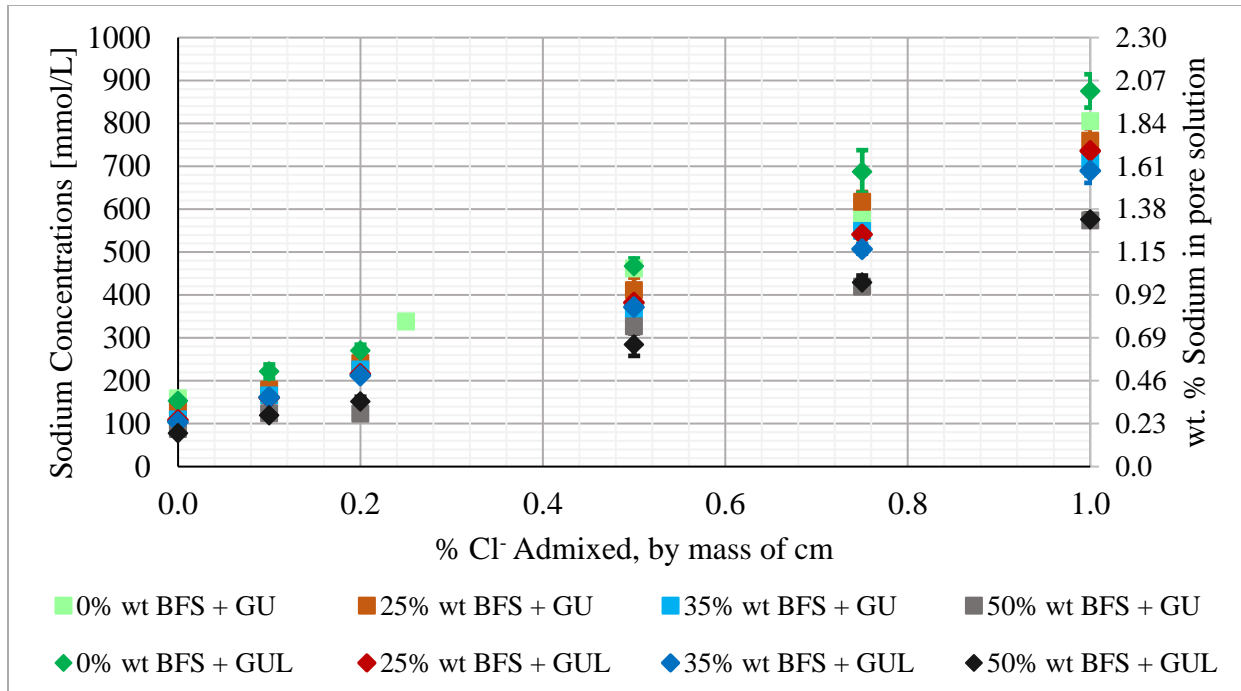


Figure 4.5 Molar concentrations of sodium ions measured as a function of admixed chlorides

Note : the pore solution data for the 0% GBFS GU mix were obtained from literature ^[110]

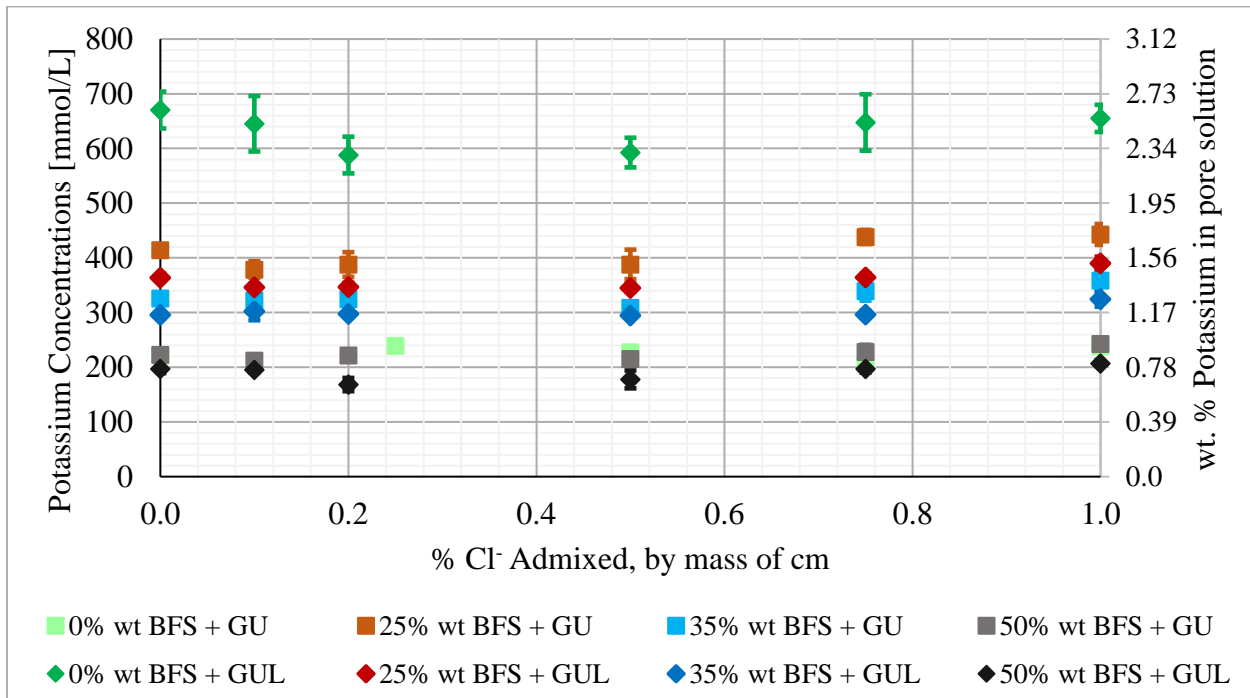


Figure 4.6 Molar concentrations of potassium ions measured as a function of admixed chlorides

Note : the pore solution data for the 0% GBFS GU mix were obtained from literature ^[110]

The alkalinity of pore solutions is dependent on the hydroxides of potassium, sodium and calcium. They are introduced into the pore solutions by dissolution from the ingredients of mixes, including the cement and slag. As shown in Figure 4.6, the potassium concentrations were observed to decrease with increased GBFS and limestone replacements, suggesting that the limestone and GBFS blends would thus exhibit slightly low pH readings. The decreasing alkalinity with increasing GBFS content was, however, not clear in the pH meter-measurements. With the exception of the 0BFSGU mix, the positional differences in the trend lines of the sodium and potassium concentrations were similar with an increase in GBFS replacement leading to reduced Na^+ and K^+ concentrations. This is attributed to the chemical compositions of the cement and slag, the latter of which has lower Ca/Si ratio and thus, enhanced alkali binding capacities [22].

In the absence of chlorides, sulphates dissolving from the gypsum, react with C3A and C4AF to form ettringite. When chlorides are added to the cement mix, the chlorides can preferentially combine with C3A and C4AF to form Friedel salts, thus, leaving the sulphate ions in solution, as shown in Figure 4.7. The amount of chlorides able to be chemically bound is limited and so the concentration of dissolved chlorides also increases as indicated in Figure 4.8.

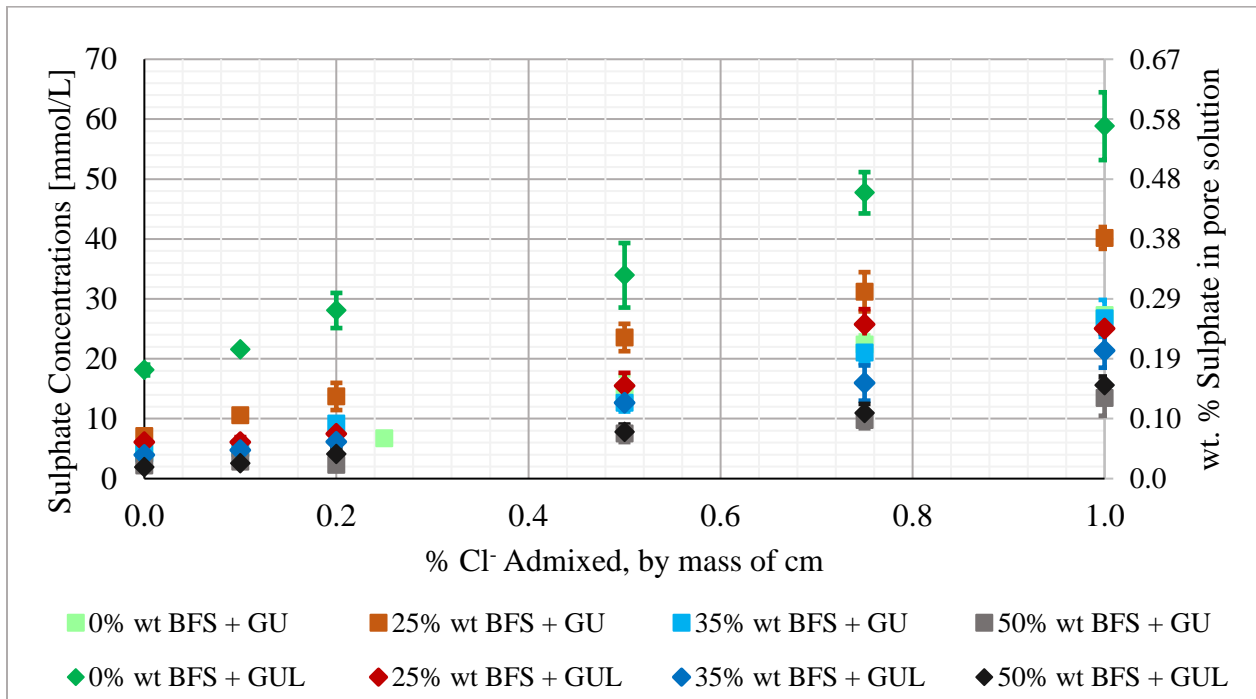


Figure 4.7 Sulphate concentrations of the expressed solutions, as a function of admixed chlorides

Note : the pore solution data for the 0% GBFS GU mix were obtained from literature [110]

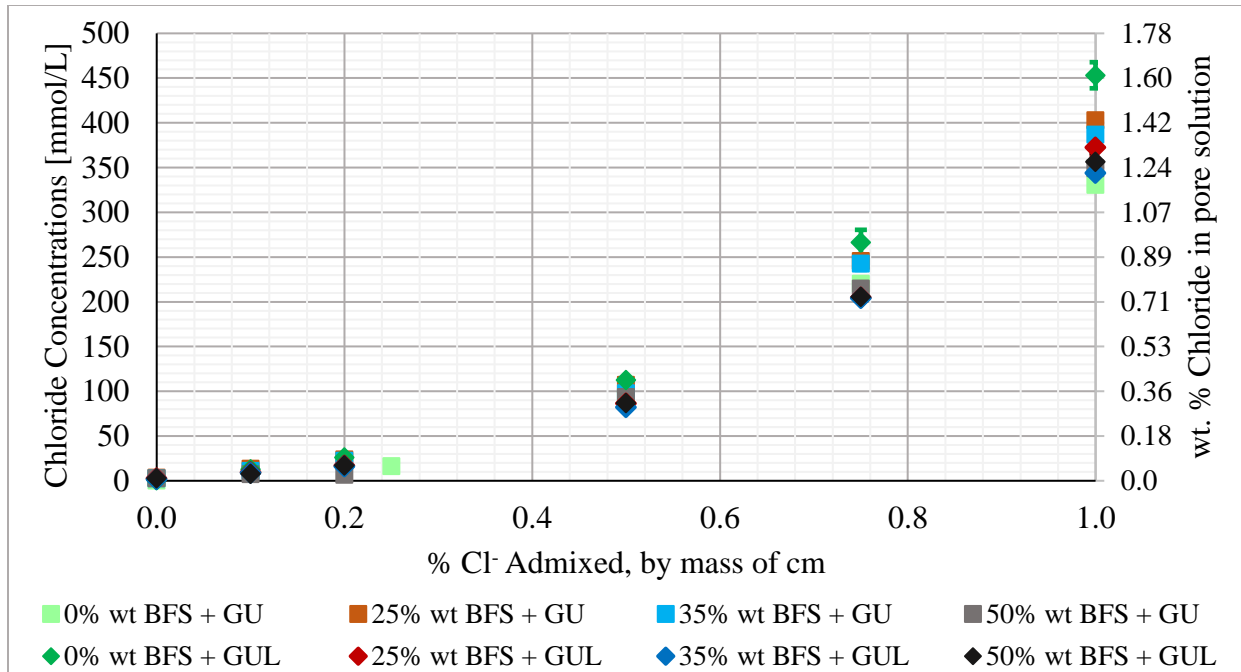


Figure 4.8 Chloride concentrations of the expressed solutions, as a function of admixed chlorides

Note : the pore solution data for the 0% GBFS GU mix were obtained from literature ^[110]

For the GUL mixes, the increase in slag replacement resulted in a decrease in the sulphates detected in the pore solution. This was also observed for the GU-GBFS mixes, apart from the outlier 0BFSGU data values. The greater the GBFS replacement level, the less significant the differences between the GU and GUL equivalents, with similarities observed between 25BFSGU and 35BFSGU, and between 25BFSGUL and 35BFSGUL. However, for the case of 0% GBFS, the GUL mix exhibited higher chloride concentrations compared to the 0BFSGU mix.

The discolouration and odour of the GBFS-contained specimens, discussed earlier, attributed to the presence of sulphur which generally increased with the increase in GBFS replacement, as shown in Figure 4.9. However, the total sulphur ion concentrations detected in the pore solutions were significantly higher than the sulphate concentrations. Therefore, the sulphur would have to be present in other forms, and one such form is thiosulphates. As shown in Figure 4.10, thiosulphates were detected only in cement mixes containing GBFS. This is not surprising for the sulphur-rich material, as thiosulphates can readily oxidize to form sulphates upon the release of sulphur molecules, given the right conditions. Due to the ease with which thiosulphates can easily oxidize in the atmosphere, the increase in the concentration with increasing GBFS content was not consistent in the observed trends.

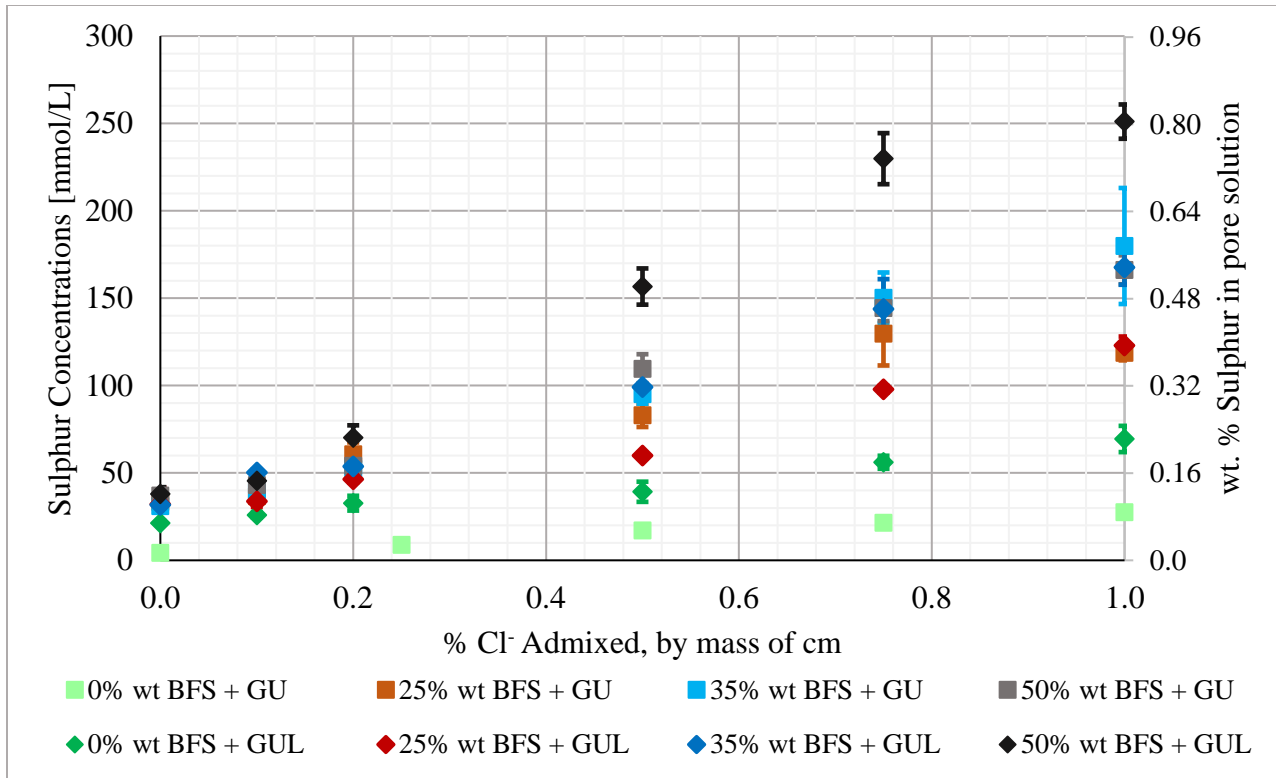


Figure 4.9 Sulphur concentrations of the expressed solutions, as a function of admixed chlorides

Note : the pore solution data for the 0% GBFS GU mix were obtained from literature ^[110]

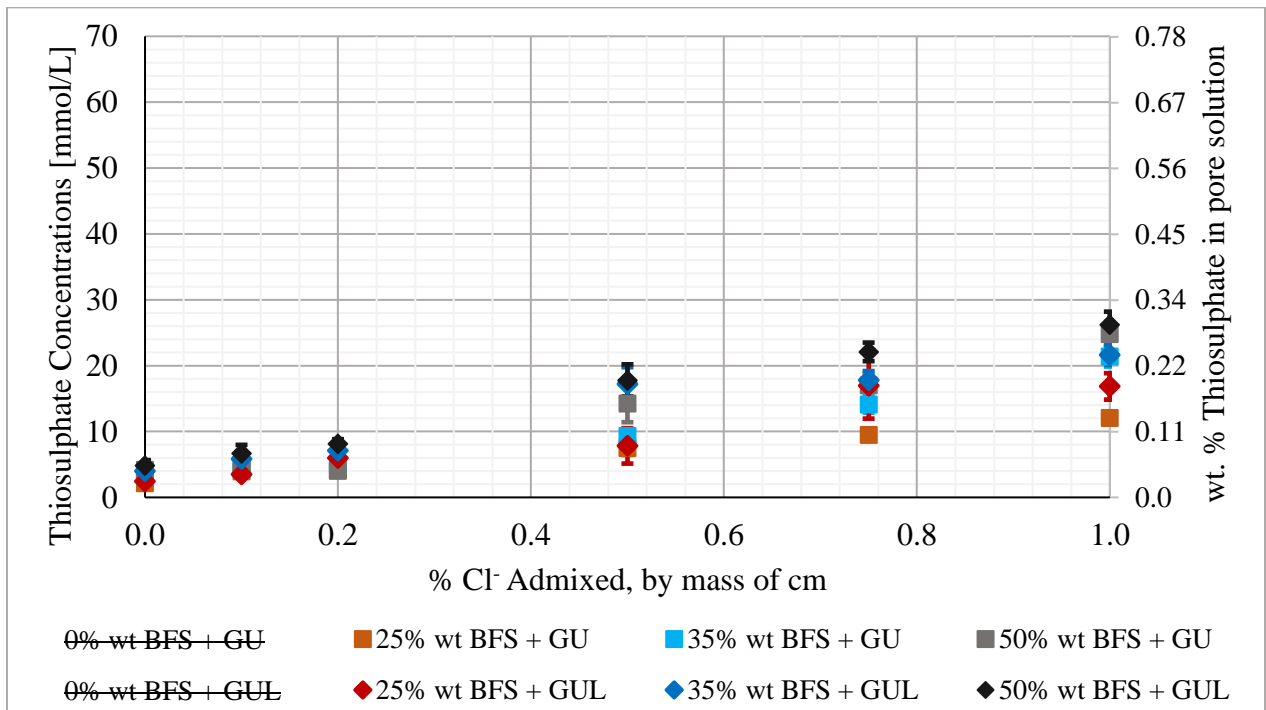


Figure 4.10 Thiosulphates found in the cement mixes containing GBFS

4.1.3 Bound Chlorides

By the method described in Section 3.2.4, the W_e measurements were obtained and summarized in Appendix B. There was no observed trend or significant difference in the W_e measured for the cement pastes of the various mixes. The bound chlorides were calculated (as exemplified in Appendix B following ^[60]) as percentages of the mass of the cementitious materials for the various mixes, and the data are presented in Figure 4.11. These results provided insights on the chloride binding capacities of the GBFS mixes. The differences in the bound chlorides across the various mixes were observed to be negligible. This observation agrees with the chloride concentrations in pore solution, observed in Figure 4.8, where the differences among the various mixes were insignificant. As the admixed chloride concentrations increased, the trendlines began to plateau away from the 1:1 ratio line. This is attributed to the limited chloride binding capacity of the cement paste. It was, however, expected that with the increase in GBFS replacement, chloride binding would increase ^[61]. This was not observed in Figure 4.11, but the differences were more noticeable in the slight reduction in chlorides detected in the pore solutions with increasing GBFS replacement.

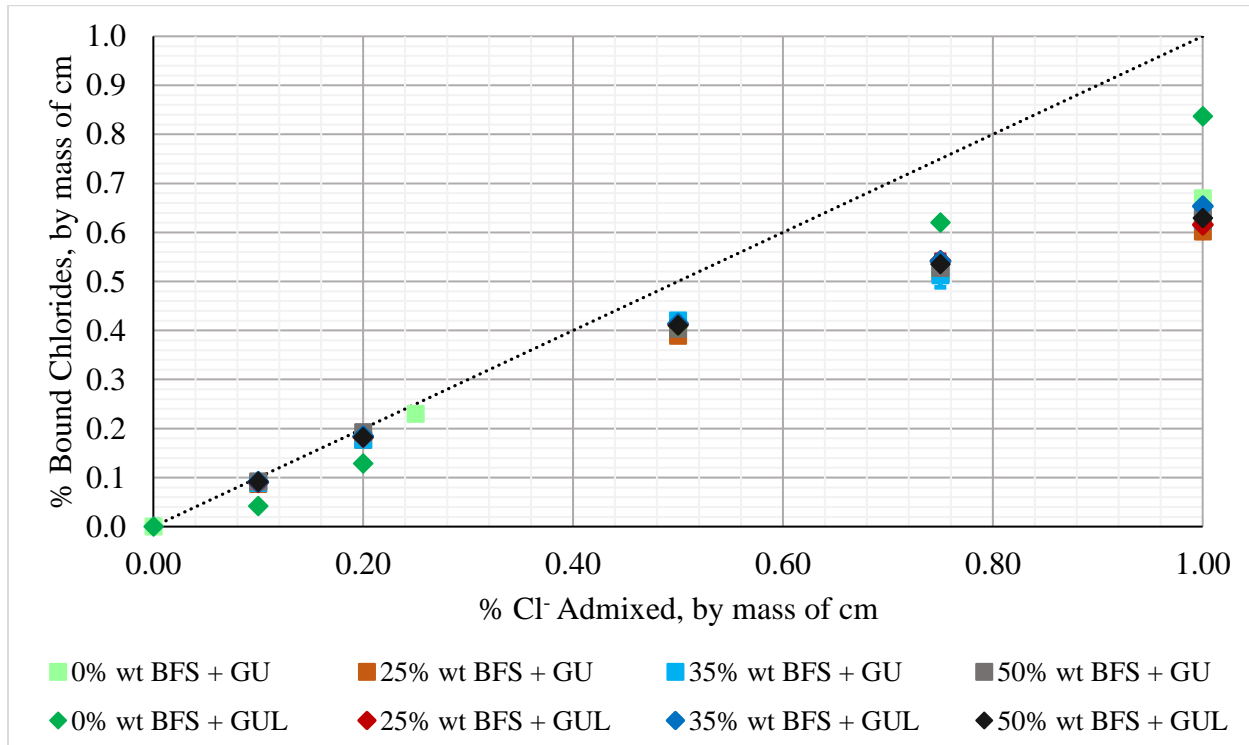


Figure 4.11 The bound chlorides as a function of the admixed chloride concentrations

Note : the pore solution data for the 0% GBFS GU mix were obtained from literature ^[110]

4.1.4 Corrosion Tests on Rebar in Synthetic Pore Solution

The incremental additions of NaCl, LPR tests and OCP measurements followed the schedule summarized in Table 3.5. More details on the proportions of added chemical agents for the synthetic pore solutions are provided in Appendix B. The corrosion current densities, i_{corr} , and OCP are provided in Figures 4.12 and 4.13, respectively. The figures show the averaged results of five to six rebar specimens immersed in solutions of each of the various mixes. The i_{corr} values are plotted in a logarithmic scale on the vertical axis in Figure 4.12, because of the wide range of magnitude varied in the results.

The i_{corr} and OCP results show no changes in the behaviours of the specimens in the synthetic pore solutions of the various mixes, until the chloride concentration reached 0.5% wt. Cl^- by mass of cm. Signs of corrosion activity are depicted by simultaneous stabilized increase in i_{corr} and drop in OCP (i.e. more negative).

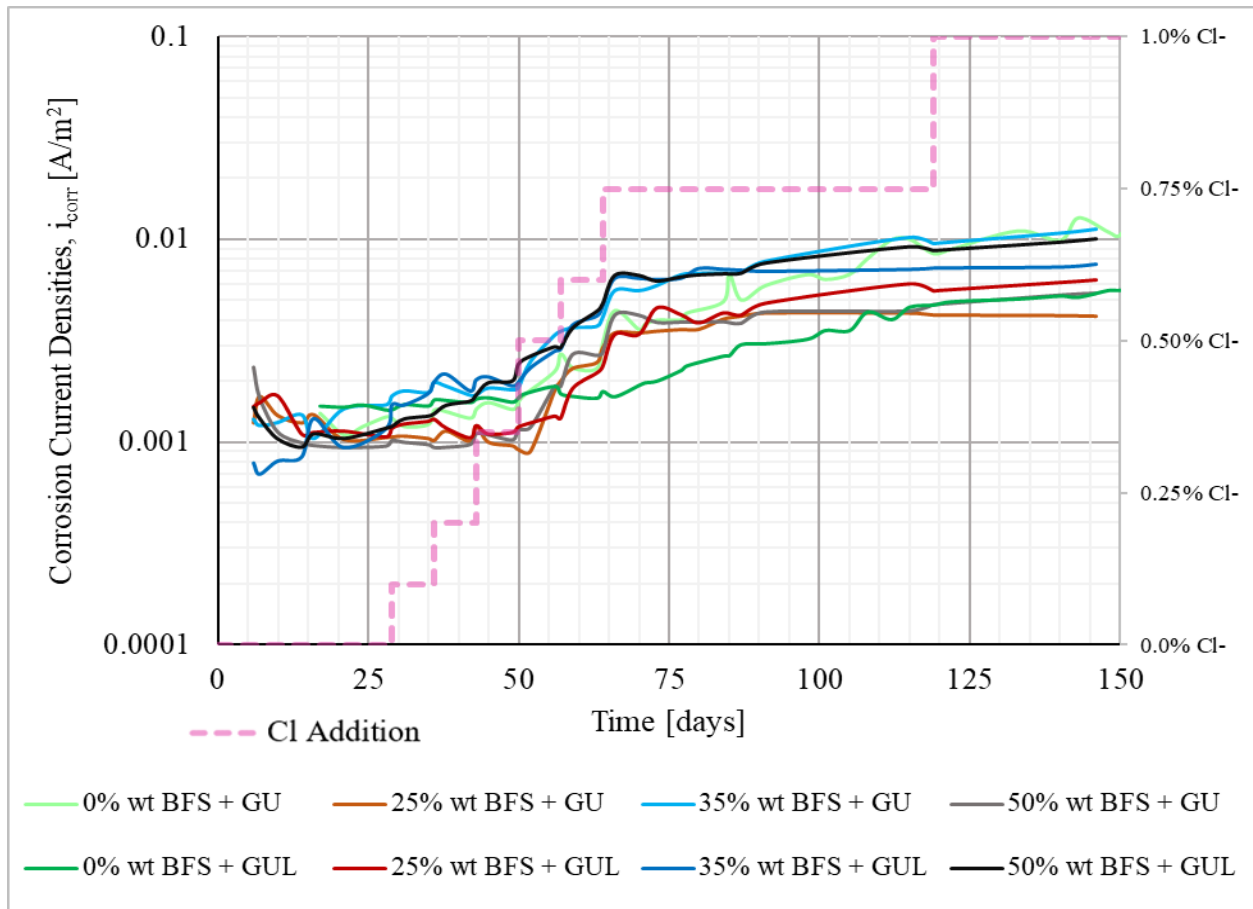


Figure 4.12 Averages of the corrosion current densities recorded for each mix type

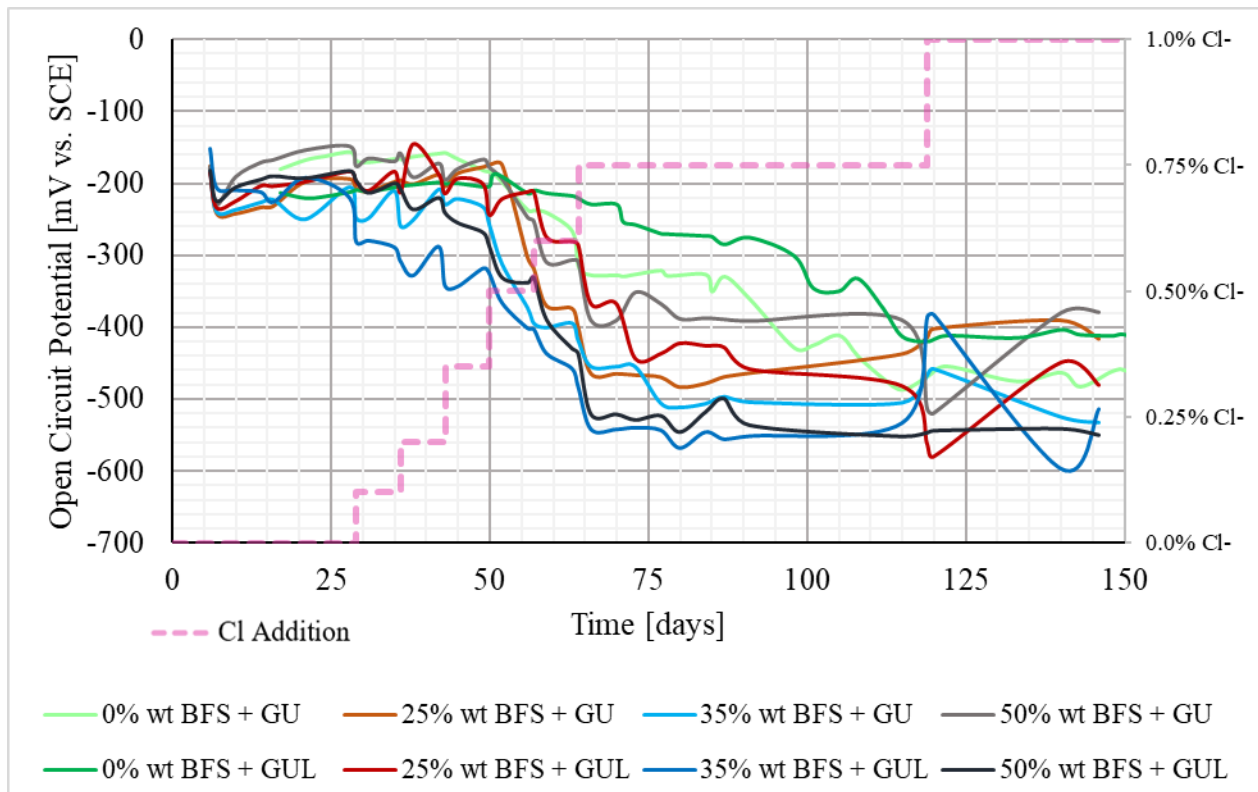


Figure 4.13 Averaged open circuit potentials recorded, at time of LPR tests, for each mix type. The LPR and OCP results agree on the observation that the specimens began to experience some noticeable changes when the chloride concentrations of the solutions were in the range of 0.6-0.75% wt. Cl^- . In the absence of GBFS, the specimens in the GUL synthetic pore solution showed the lowest i_{corr} rates and more positive OCP, than those suspended in the 0BFSGU test solution. The most negative OCP values and the highest corrosion rates were obtained from the synthetic pore solutions of 35BFSGU, 35BFSGUL and 50BFSGUL, identifying them as the most corrosive environments, while the least corrosive solution was shown to be the 0BFSGUL. The specimens exposed to the test solutions for the 0BFSGU, 25BFSGU, 25BFSGUL and 50BFSGU mixes showed comparable results.

4.1.5 Observations from Synthetic Pore Solution Tests

On visual observation of the rebar specimens, no visible signs of severe corrosion were noted on the exposed surfaces, apart from some specimens showing signs of crevice corrosion under the lacquer/steel interface at the ends of the bar. The lack of visible corrosion products adhering to the exposed surface of the rebar specimens is because the corrosion products were susceptible to

removal during stirring of the test solutions prior to electrochemical tests and on addition for altering chloride concentration. The products were dissolved into the test solutions, as observed in the visible browning of the solutions, exemplified by a 0BFSGU test container in Figure 4.14.

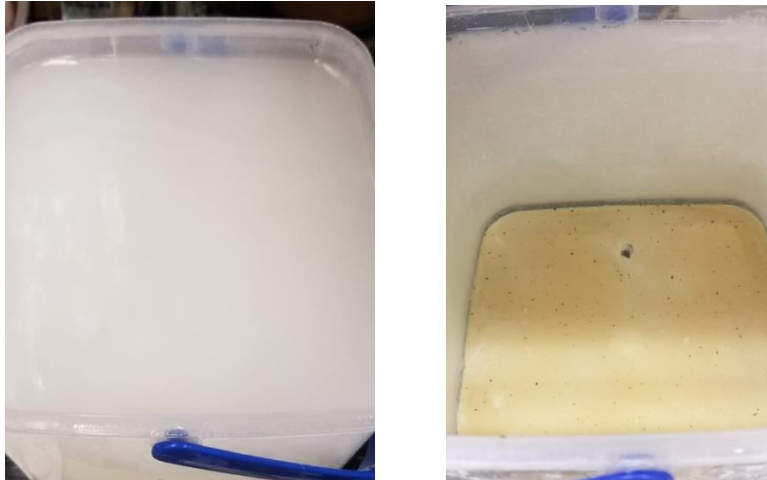


Figure 4.14 Discolouration of the 0BFSGU test solution at start of day 1 (Left) and after removal of specimens (after day 250)

If pitting occurs on a rebar specimen, the electrochemical measurements would show instantaneous peaks in the i_{corr} and drops in the negative OCP measurements which would increase the statistical deviations of the averages in the Figures 4.12 and 4.13. These peaks are better captured in the data for the individual specimens provided in Appendix B. Most of the 0BFSGUL test specimens exhibited notable adherence of a white coating, presumably due to the excess calcium hydroxides in solution, which could have attributed to a protective make-shift coating. This is shown in the Figure 4.15, in which there are signs of rust discolouration on the white coating but no stable change in the electrochemical measurements indicating active corrosion on the specimen was noted.



Figure 4.15 Adsorbed white precipitate coating a specimen from 0BFSGUL test solution

4.2 Tests on Concrete Cylinders and Block Specimens

The results of the mechanical, electrochemical and inspection tests performed on the GU and GUL concrete specimens, with different GBFS replacements of the cement, are presented in this section.

4.2.1 Test Results of the Concrete Cylinders

The test results for the surface and bulk resistivities and compressive strengths reported herein are averages of three concrete cylinder replicas for each concrete mix.

Although the extent to which the degree of saturation affects the resistivity of the concrete specimens, is well-acknowledged, for this experiment, to maintain consistency, the specimens were immersed in water for a fixed period of time prior to testing using the Wenner probe-devices. As previously mentioned in Section 3.3.3, the surface resistivity measurements provide indication of the ease of penetration of ions at the surface of the concrete while the bulk resistivity measures the overall resistance to diffusion of ion through the concrete matrix. Therefore, they both play important roles in quantifying the measure of corrosion susceptibility. Figures 4.16 and 4.17 present similar results which show the comparable resistivity properties between the GU and GUL equivalents of each mix type. The figures also support the literature findings on the effect of slag replacement in cement due to the more refined pore structure brought about by the slag hydration.

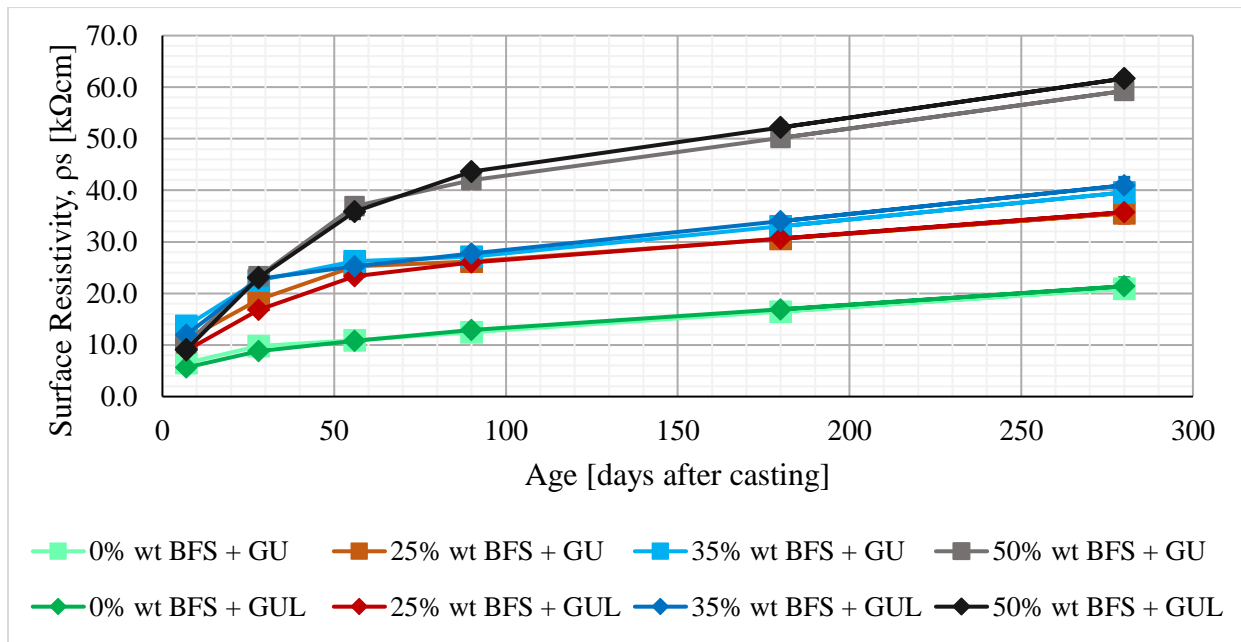


Figure 4.16 Surface resistivities, measured by Wenner probe, on aged concrete cylinders for the different mix types

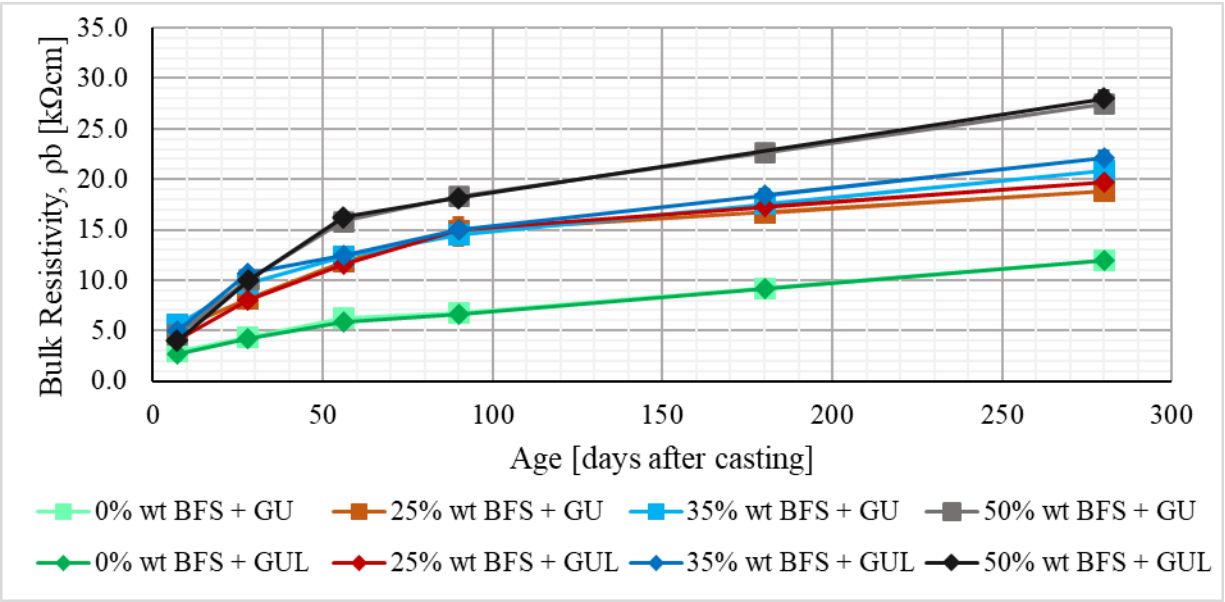


Figure 4.17 Bulk resistivities, calculated from total resistance measurements by Wenner probe, of aged concrete cylinders of the varied mixes

At an age as early as 7 days after casting, the increase in GBFS, up to the 50% replacement, led to higher resistivities than the 0BFS specimens. This indicated the initiated hydration of slag, which occurs at a slower rate than that of cement [88]. The 50BFS specimens outperformed the other mixes from day 28 and onwards, exhibiting increasing resistance to charged ions. After the non-destructive resistivity measurements, the same cylinders were tested for compressive strength, after at least 2 hours of air-drying. The peak strengths are recorded in Figure 4.18.

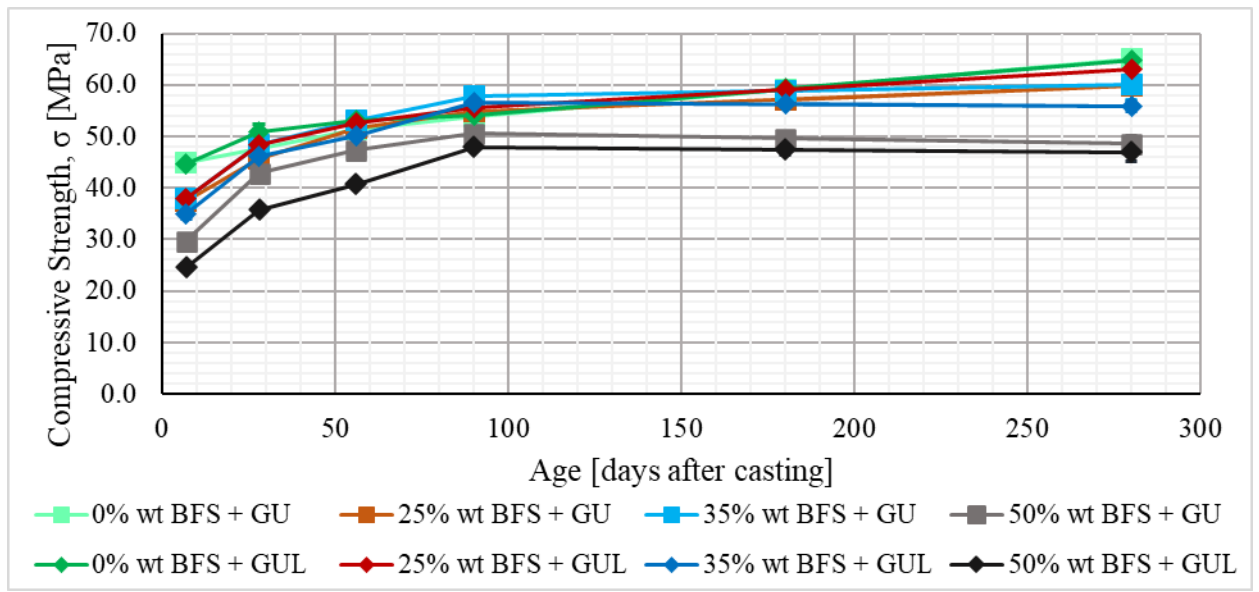


Figure 4.18 Compressive strengths of aged concrete cylinders of the various mix types

Unlike the resistivity results, the replacement of cement by GBFS showed no improvements in the compressive strength relative to the 0BFS-concretes. The strengths of the 25BFS- and 35BFS-concretes caught up to those of the 0BFS- concretes only after day 56, after which they showed less or equal strengths than the 0BFS concretes. The lack of strength development by increasing GBFS replacement was also reported by Yeau and Kim for their OPC-GBFS concretes, up to 50% replacement [89]. The specimens with 50% GBFS replacement exhibited increasing compressive strength development up to the age of 90 days, but the improvements were insufficient to be on par with the specimens of the other mixes as they remained the lowest in ranking of compressive strength. The 50BFS-concrete specimens were observed to decrease slightly thereafter till the age of 280 days. The GU-based specimens showed slightly higher or equal strengths to the GUL equivalents. The difference between the 50BFSGU and 50BFSGUL specimens was more significant at ages earlier than day 90. In all the cylinder test results, the differences, between the specimens with 25% GBFS replacement and those with 35% GBFS replacement, were almost negligible. This shows that the increase of 10% slag replacement, between 25% and 35%, does not significantly affect the tested concrete properties.

4.2.2 Macrocell Corrosion Results of the Reinforcement in the Concrete Block Specimens

Measurements of the potential difference between the top bar and bottom bars across a 100-ohm resistor were recorded every four hours, using the Keithley DMDAq device. The respective current densities were computed by using Ohm’s law to determine the current and averaging the results over the exposed surface area of the top rebar. The temperature and relative humidity conditions of the monitoring room for the concrete block specimens are plotted in Figure 4.19.

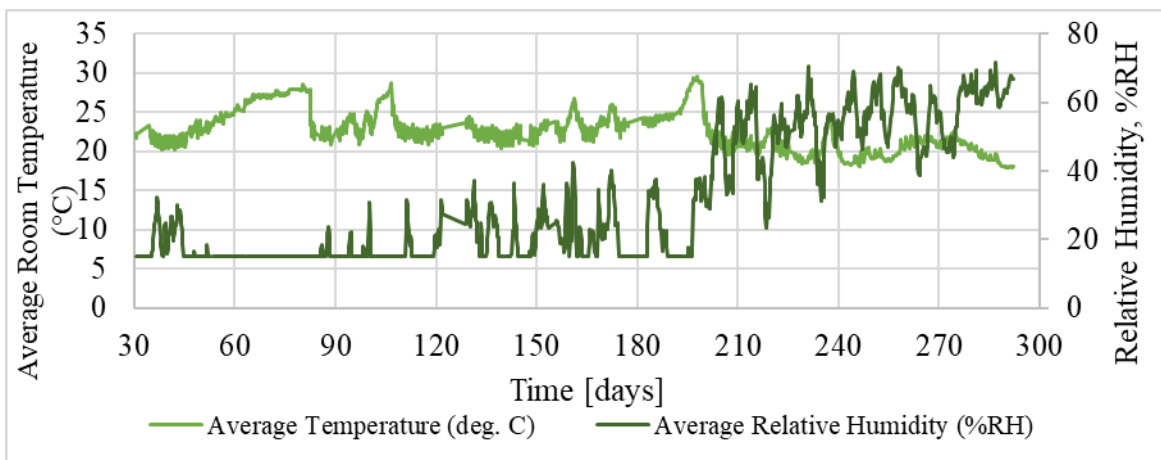


Figure 4.19 Ambient temperature and relative humidity of room of the concrete block specimens

On average, the temperatures ranged between 20 and 27 degrees Celsius, while the relative humidity (RH) dipped to minimum detection limit of the measuring device, (15%). The monitoring period began in the Fall season as indicated by peaks of 25-40% during the first 200 days. The RH then jumped to 50-70% during the latter summer days.

The average daily macrocell corrosion current densities for the 0BFS-GUL and -GU concrete specimens were provided in Figures 4.20 and 4.21, respectively. As noted in Section 3.0, the case in which both Ha and MA rebar were tested applied only to the concretes of the 0BFS mixes. The following figures 4.22 – 4.27 present the macrocell current densities for the GBFS specimens, with 25%, 35% and 50% replacement by mass of the respective GU or GUL cement. On the right secondary axis, the wet period is indicated by a peak value of 1 while the dry periods were represented as 0.

One of the replicas of each mix was designated the “control” specimen, having only chloride-free distilled water in the ponding well. The designated specimen for the 0BFS mixes, are identified as specimen #5. For the mixes containing GBFS, the control specimen was identified as #4. Initially, 3% wt. NaCl solution was added during the wet periods of the wet/dry cycles and then, at the age of 210 days, the ponding well salt solution was increased to 5.75% wt. NaCl to encourage corrosion activities in the rebar.

As noted in Section 3.0, a corrosion current density of 0.001 A/m^2 , approximates a loss of rebar of $1 \mu\text{m}/\text{year}$. For the purpose of this project, active corrosion is defined when the change in the current densities, by at least an order of magnitude, is sustained for some time or continues to increase in magnitude. The erratic fluctuations shown in the figures may be due to changes in the passivity of the top and bottom rebar specimens in the concrete, or contaminations on the exposed wiring causing electrical errors or any considerable environmental changes. While researchers have tried to determine the effect of temperature on macrocell tests, there appears to be no significant relationship between the ambient room conditions and the recorded macrocell measurements.

The peaks observed with quick recovery to the preceding readings may be instances of electrical interference in the connections, while the peaks observed with a slowed recovery could be signs of pitting activity on the rebar, followed by repassivation. The Ha- specimens embedded in the

0BFSGUL and 0BFSGU concretes exhibited periodic fluctuations, which were observed to mostly align with the wet periods. The pre-rusted conditions of the Ha bars, prior to being cast in the concrete, may have contributed to the observed fluctuations in the data. At least two of the top bars in the GBFS concrete specimens showed significant variations in the measurements for the starting 75 days. The sudden introduction of wetting solution to the ponding wells, therefore, appeared to have brought shock to the specimens.

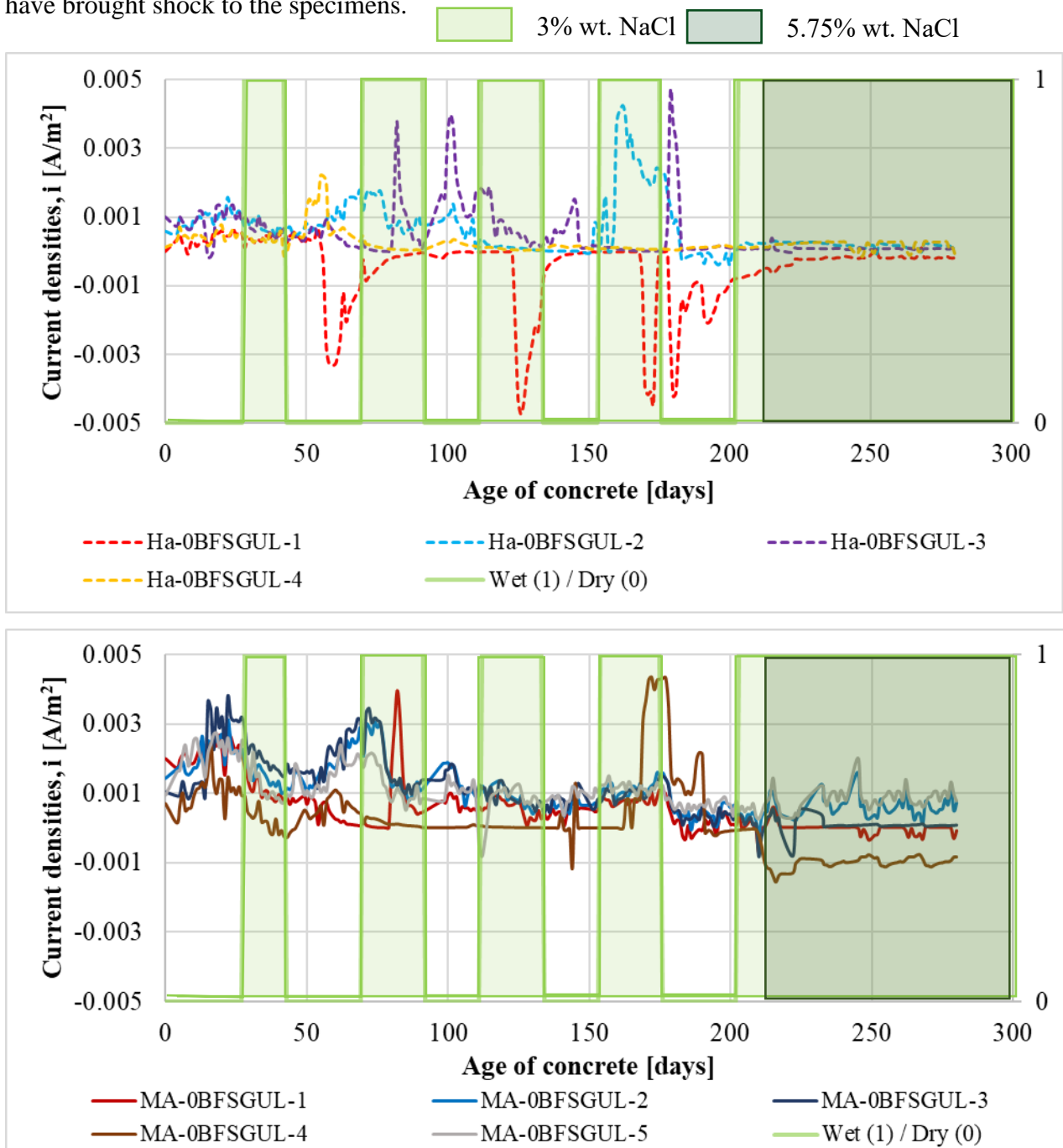


Figure 4.20 Current densities varied along with the age of the 0BFSGUL Ha and MA specimens

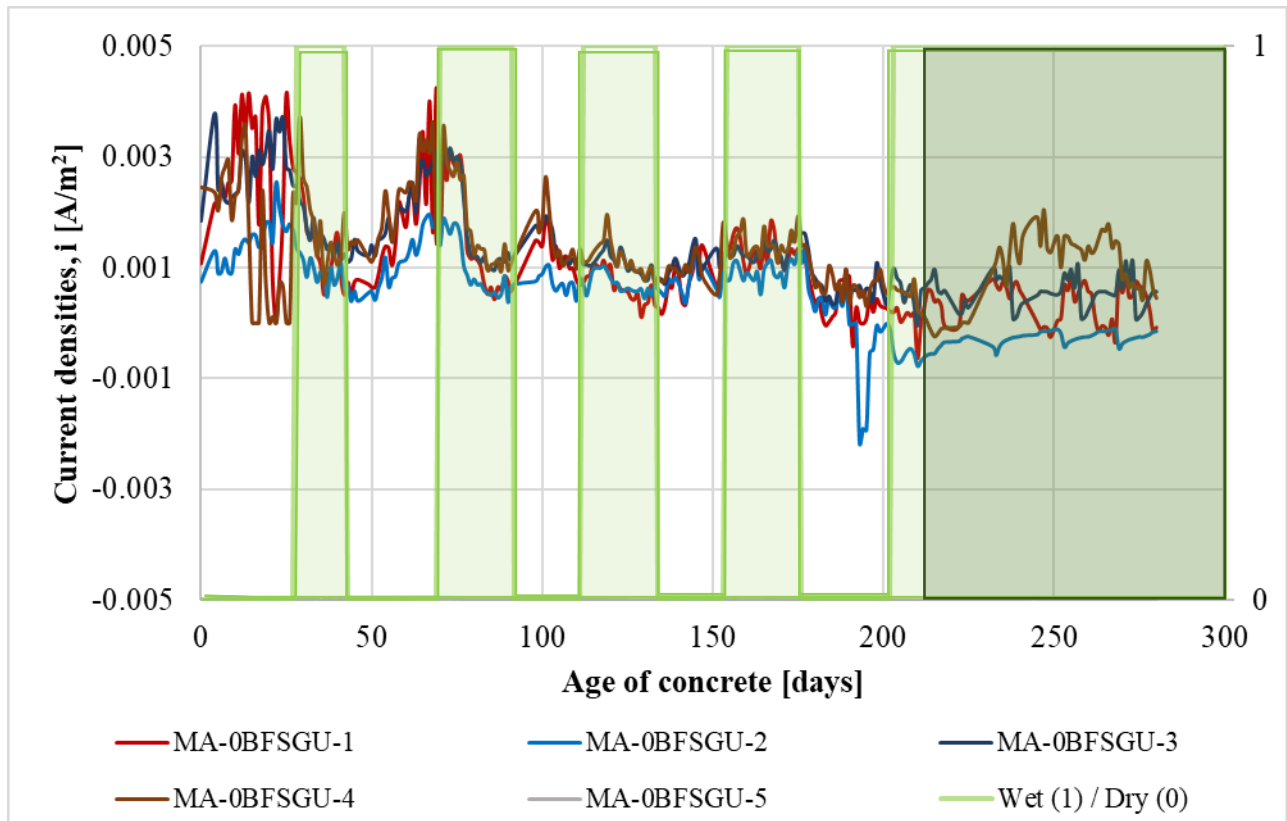
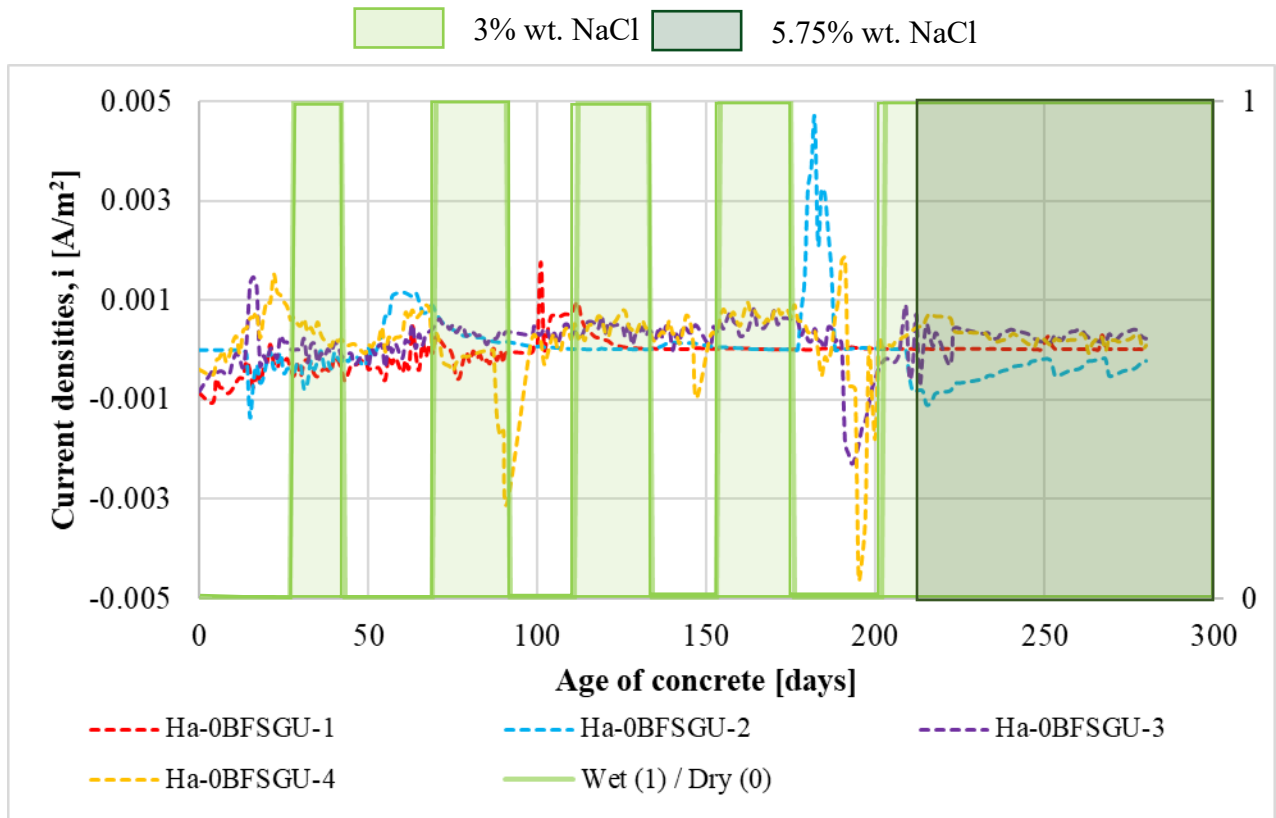


Figure 4.21 Current densities varied along with the age of the 0BFSGU Ha and MA specimens

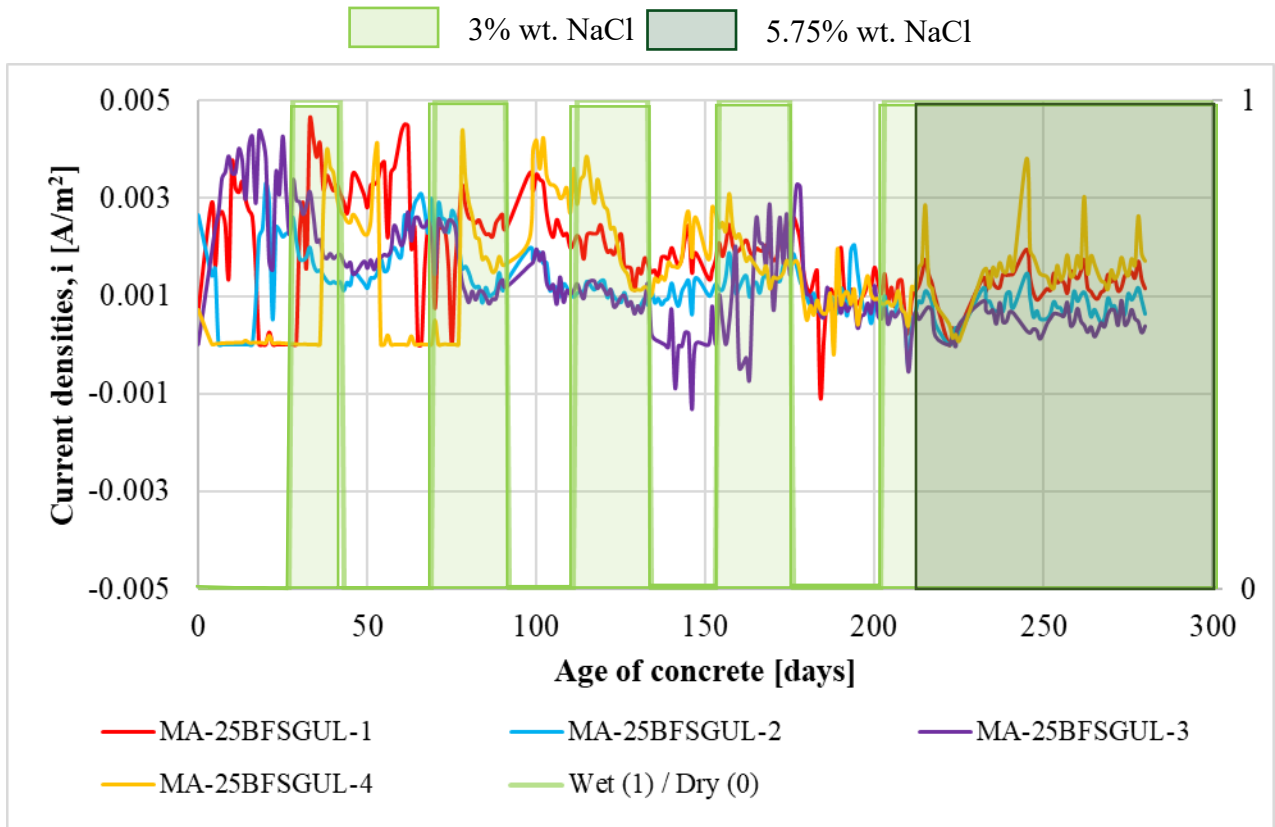


Figure 4.22 Current densities varied along with the age of the 25BFSGUL specimens

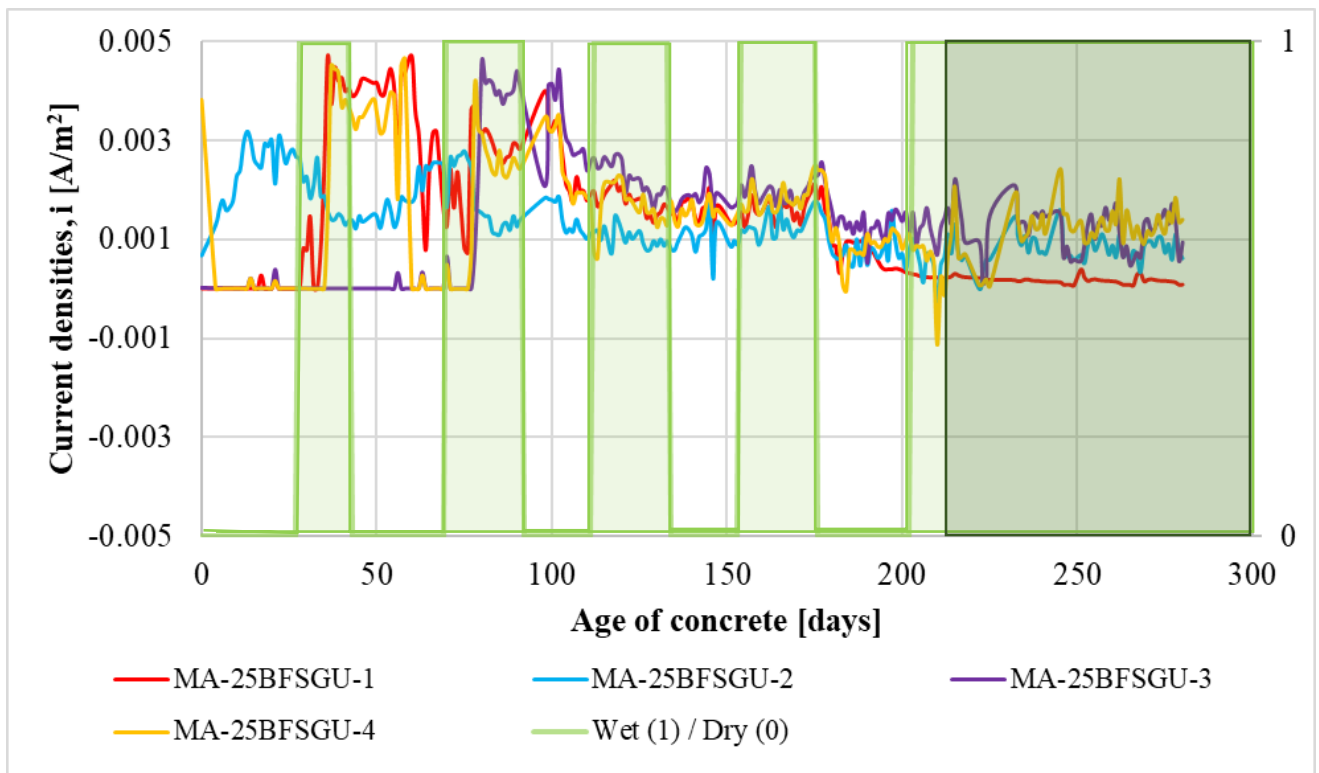


Figure 4.23 Current densities varied along with the age of the 25BFSGU specimens

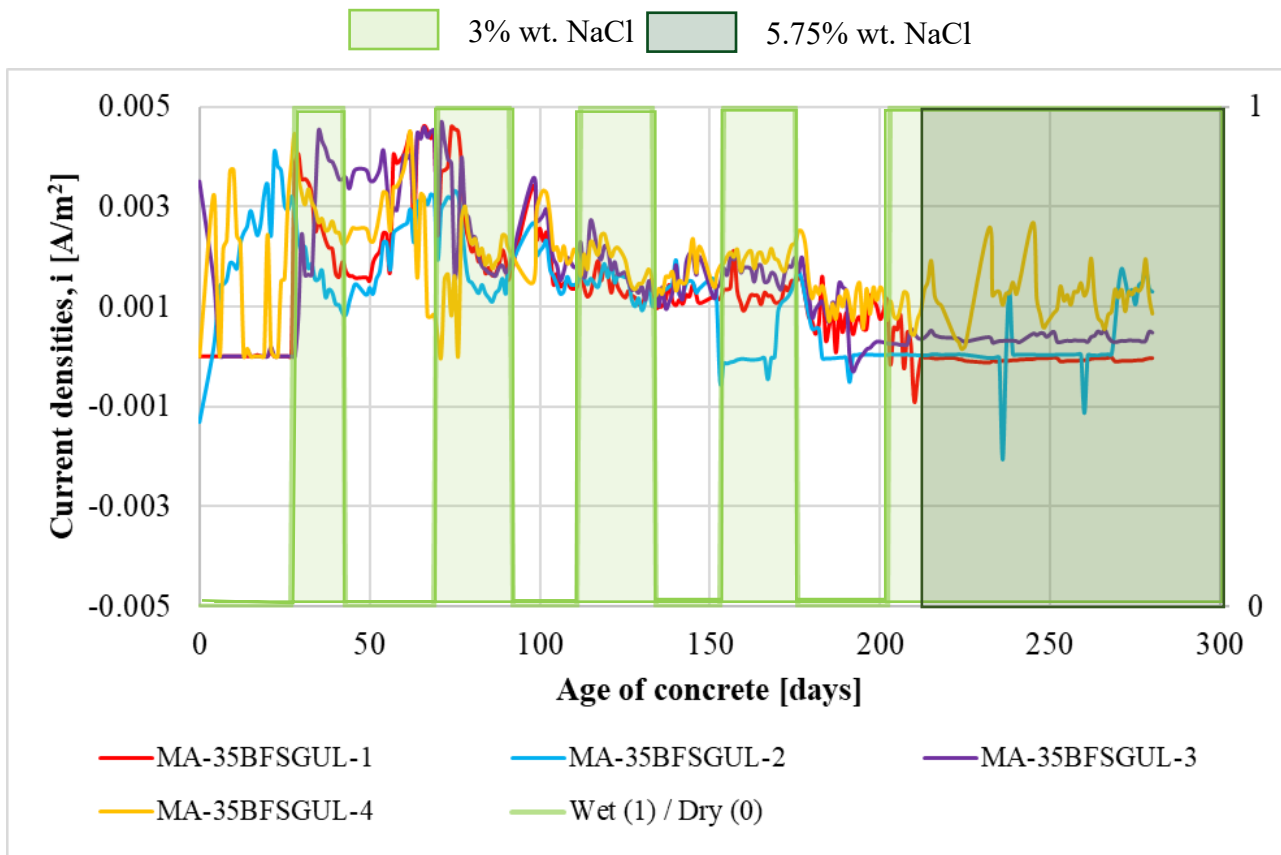


Figure 4.24 Current densities varied along with the age of the 35BFSGUL specimens

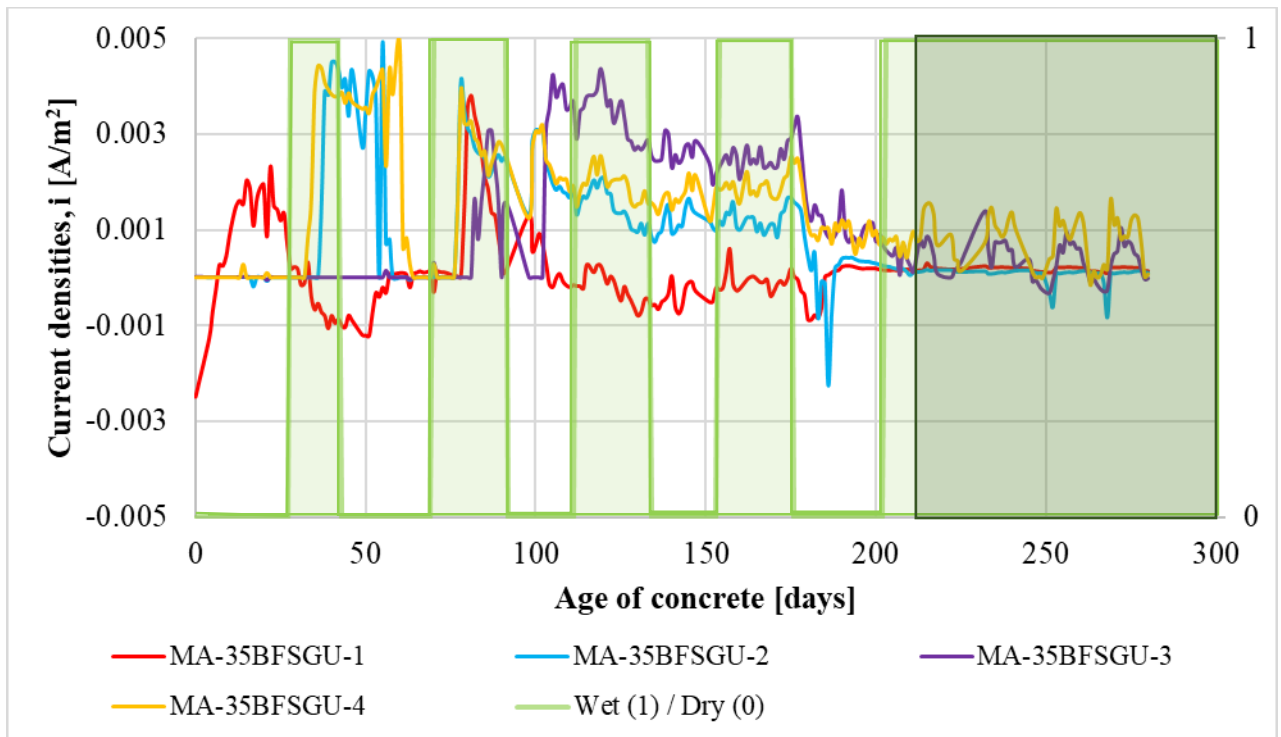


Figure 4.25 Current densities varied along with the age of the 35BFSGU specimens

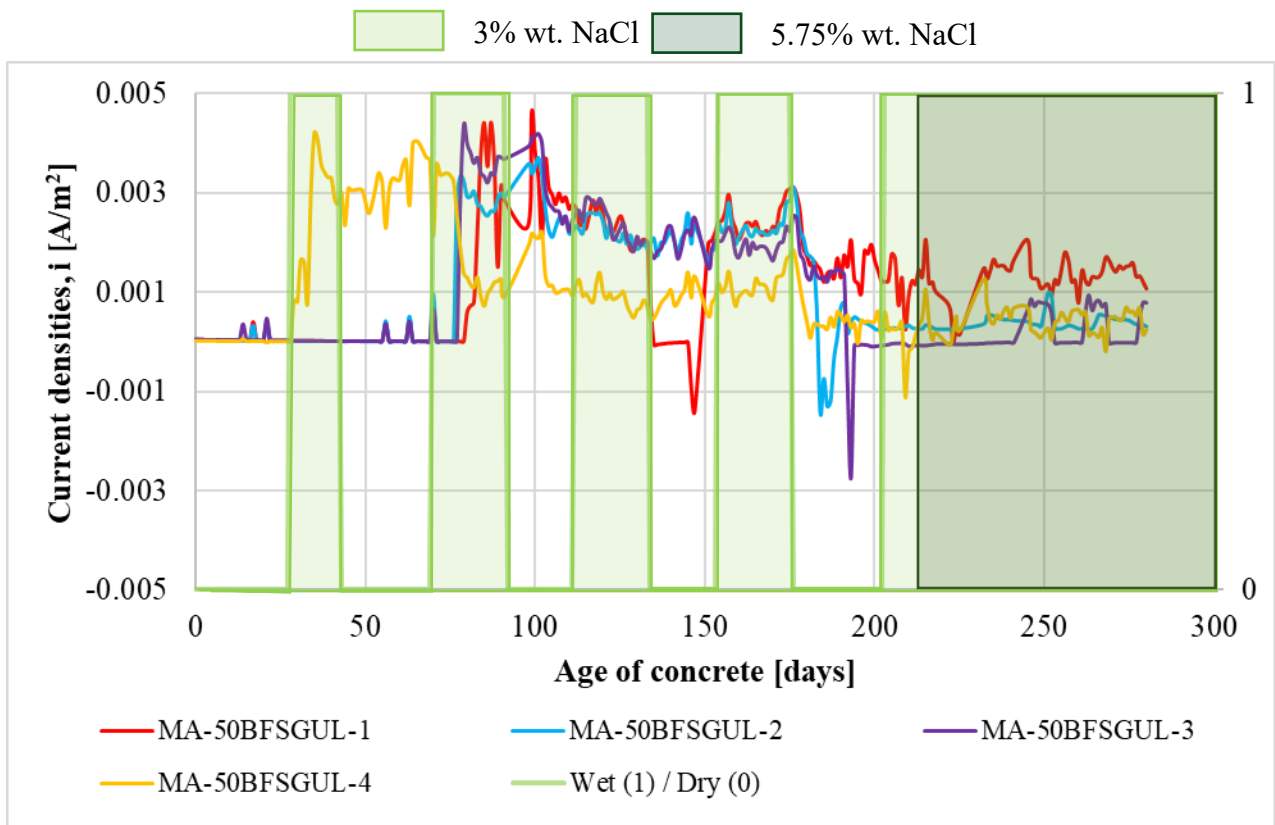


Figure 4.26 Current densities varied along with the age of the 50BFSGUL specimens

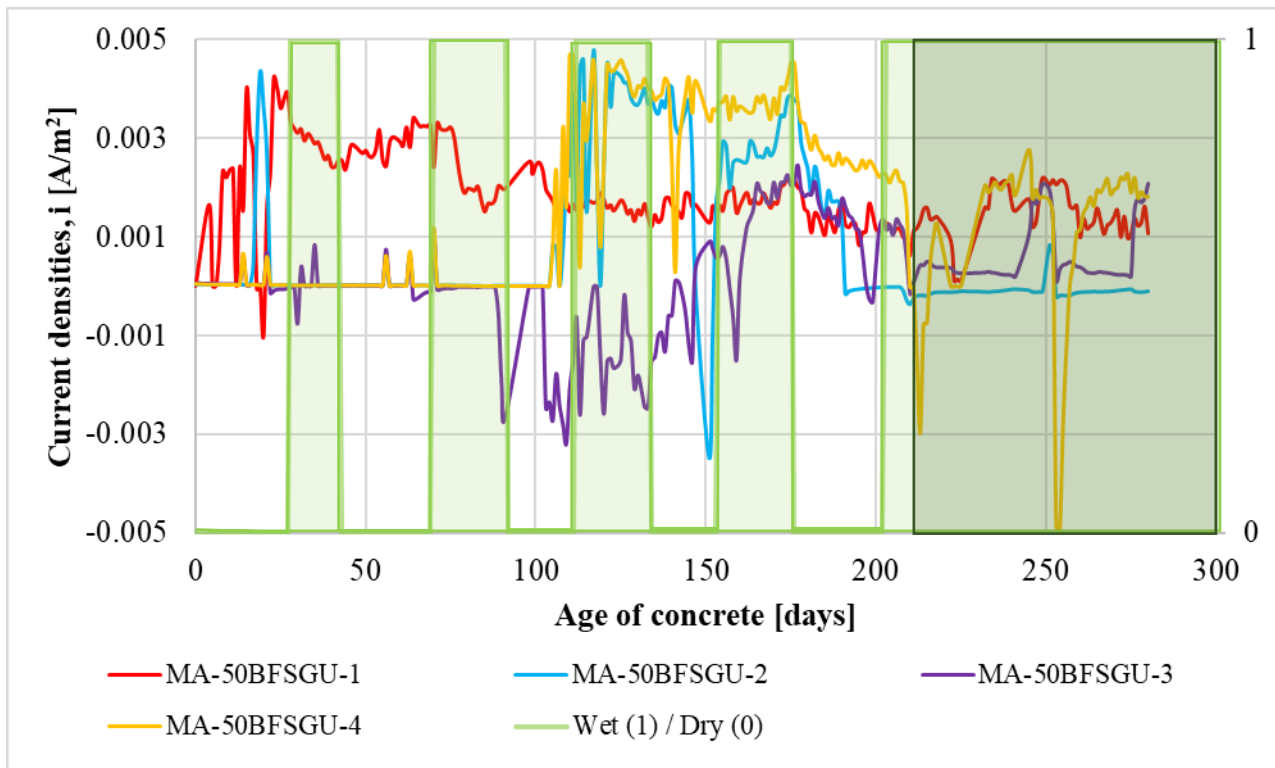


Figure 4.27 Current densities varied along with the age of the 50BFSGU specimens

As mentioned before, the ideal macrocell interaction between the top and bottom twin-bars is such that the bottom bars are to remain in passive state. The specimens were elevated on small wooden pedestals to facilitate the ingress of oxygen to the bottom bars for reduction reactions. Correspondingly, oxidation and corrosion activity are idealized to occur on the top bar, which is closer to the ponding well than the bottom bars. However, the erratic peaks in the negative direction of the vertical scale in the figures indicate a temporary switch of roles of the macrocell system. It is important to note that the wires were connected such that a negative potential difference, resulting in a negative i , would be obtained if the potential of the bottom bars was more negative than that of the top bar.

Interestingly, no obvious distinction in the macrocell behaviours between the salt-free control specimens and the chloride-contaminated specimens were observed. This would imply that the chloride concentrations in the pores of the concrete surrounding the top bars were insufficient to initiate corrosion. This meant that the chlorides had not fully diffused through the depth of concrete cover between the ponding well and top bar. For all mix types, disregarding the occasional peaks, the trend of the responses was generally the same among the specimens of a certain concrete mix type, regardless of the constituents of the ponding well. For the 35BFS and 50BFS mixes, the rebar specimens of the GU-GBFS concretes exhibited more fluctuations in the macrocell test data of greater in magnitude, than those in the the GUL-GBFS equivalents.

4.2.3 Microcell Corrosion Results of the Reinforcement in the Concrete Block Specimens

During the wet periods of the wet-dry cycles, weekly microcell measuring techniques were applied to the top bars. These measurements, however, provide only instantaneous datapoints, as opposed to the continuous monitoring for the macrocell. To allow for the top rebar to stabilize its electrochemical properties, a resting duration of two hours, at minimum, followed the disconnection from the electrical circuit with the resistor and two bottom bars. OCP and LPR measurements are summarized in Figures 4.28-4.43. Note that the numbering ID for the control specimens (i.e. those without chlorides in the ponding well solution) remain the same, i.e. the MA-rebars in the 0BFS specimens ending with “5” and the MA-specimens of the concretes with GBFS ending with “4”.

During the 3% wt. NaCl wet -dry cycles, the corrosion measurements of the rebar in the various GBFS concrete specimens remained relatively stable at OCP values between 0 and -150mV with

i_{corr} values within the range of 0.0001 to 0.0005 A/m². Thus, it can be deduced that they remained in passive state during the cycles with the 3% wt. NaCl environment. However, the change in concentration of the wetting salt solution to 5.75% wt. NaCl, at day 210, influenced at least one non-control MA-specimen of each mix, except for those in the 0BFSGU, 0BFSGUL and 25BFSGUL concretes. These specimens experienced a potential drop of at least 200mV in the negative direction with increased i_{corr} rates of at least 0.0005A/m². Following Table 3.6, for carbon steel in concrete, a potential drop of -270mV associates with 90% probability of active corrosion.

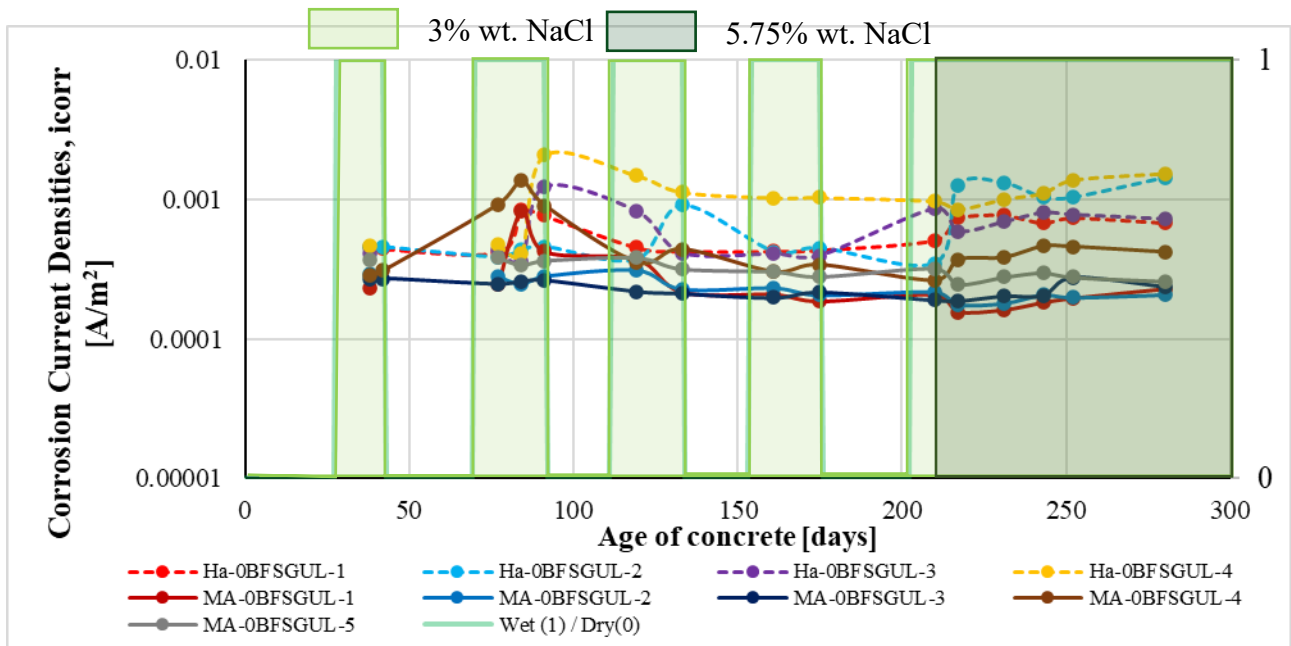


Figure 4.28 Corrosion current densities of the top bars of the 0BFSGUL specimens

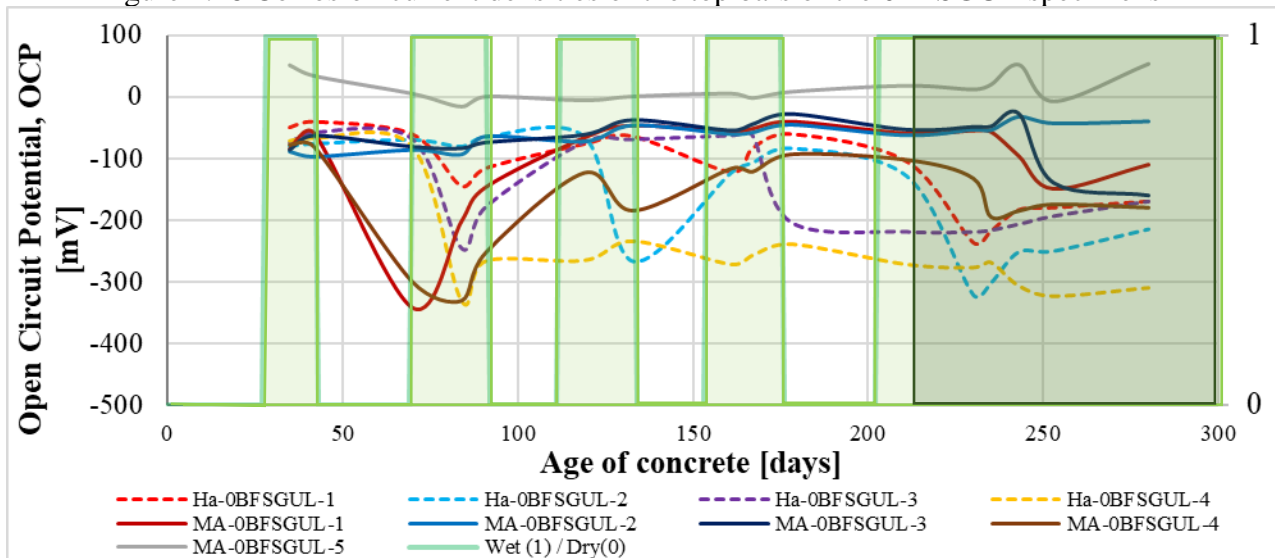


Figure 4.29 Open circuit potentials of the top bars of the 0BFSGUL specimens

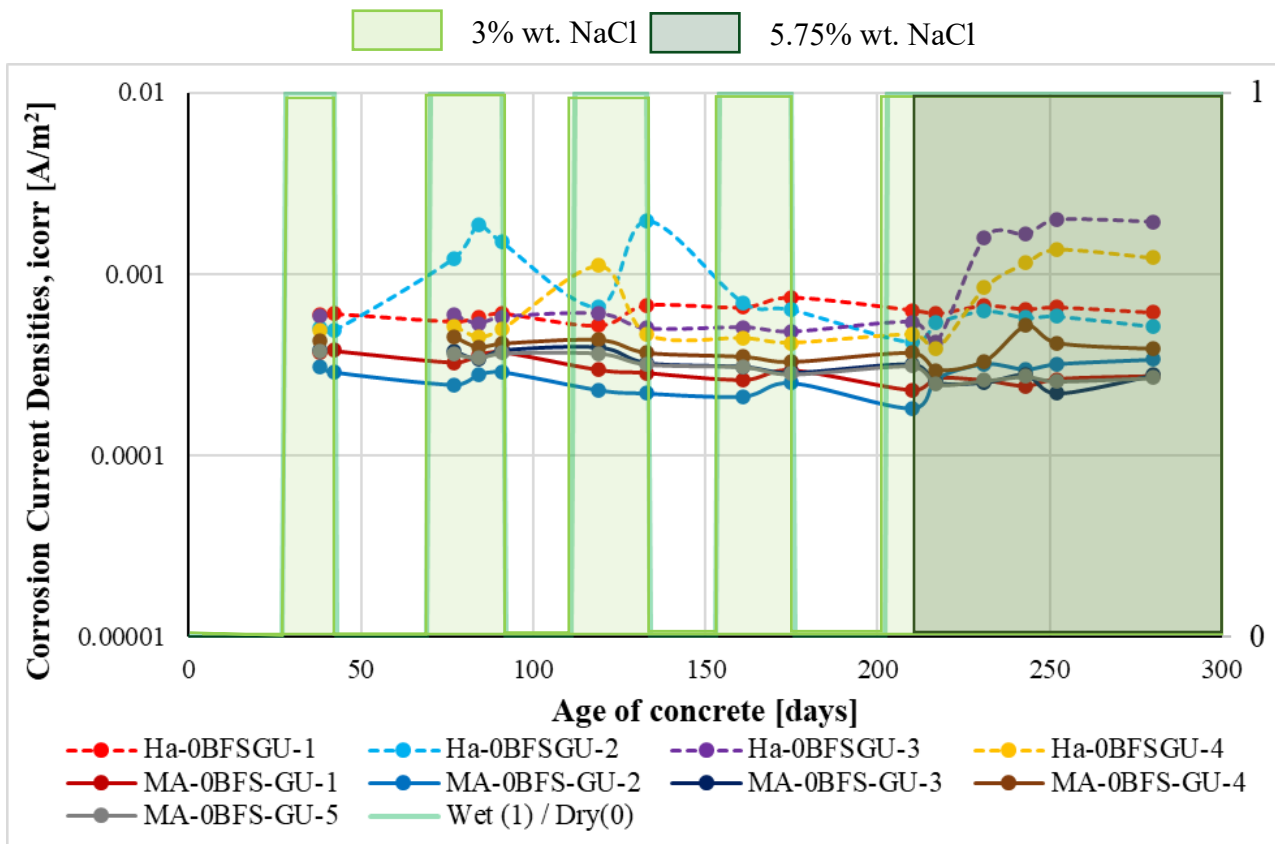


Figure 4.30 Corrosion current densities of the top bars of the 0BFSGU specimens

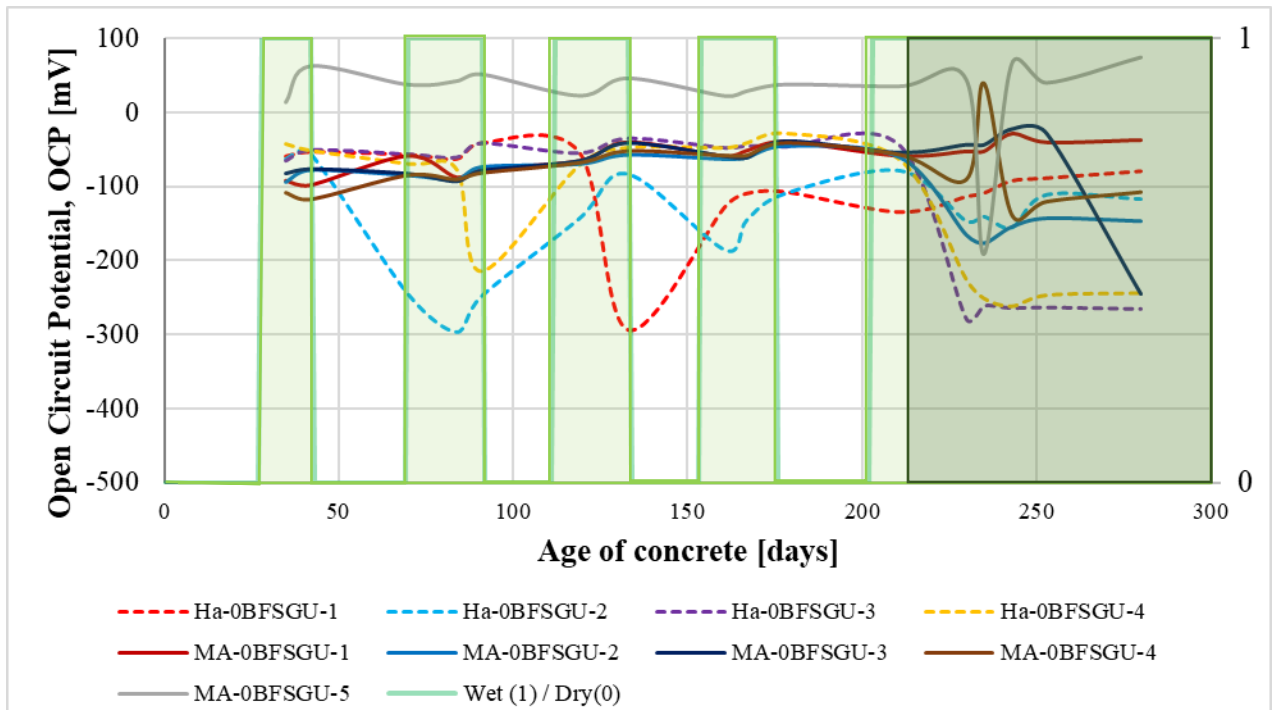


Figure 4.31 Open circuit potentials of the top bars of the 0BFSGU specimens

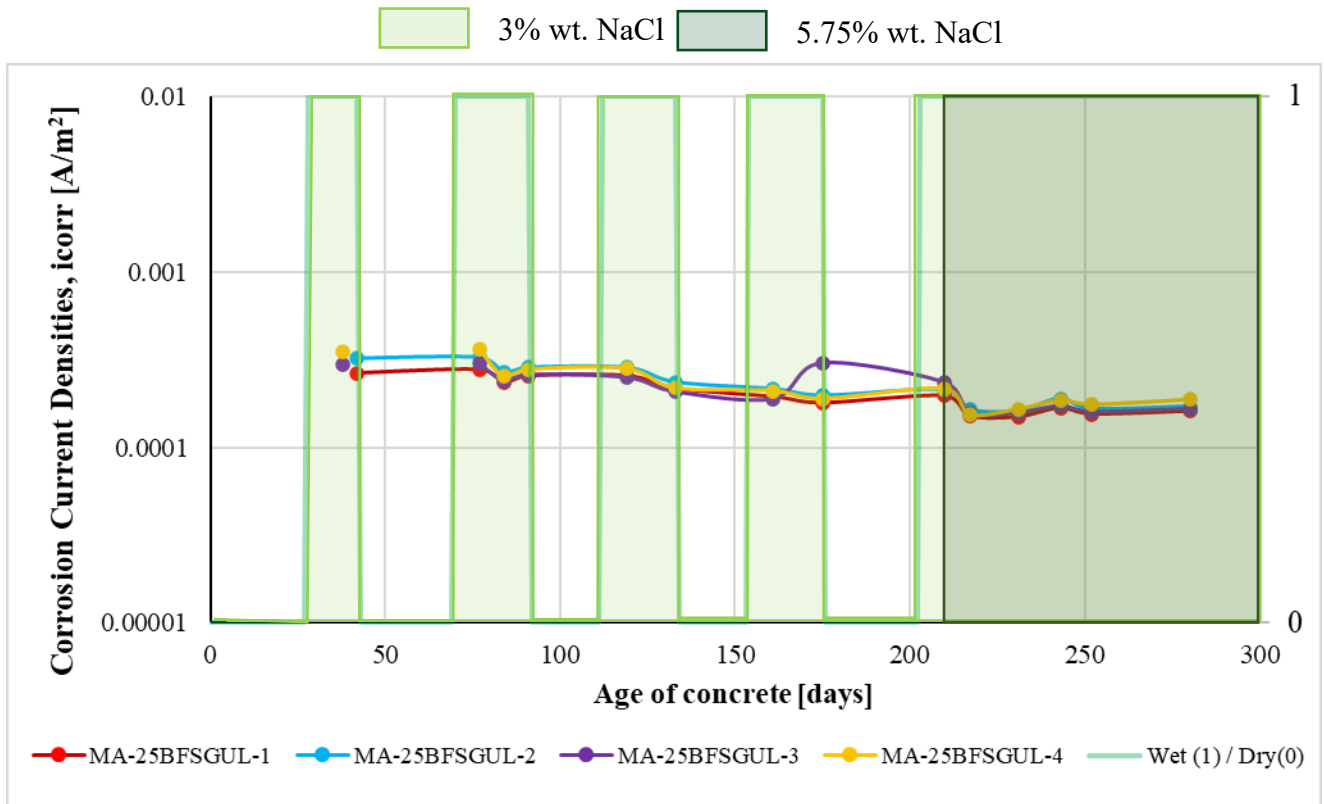


Figure 4.32 Corrosion current densities of the top bars of the 25BFGUL specimens

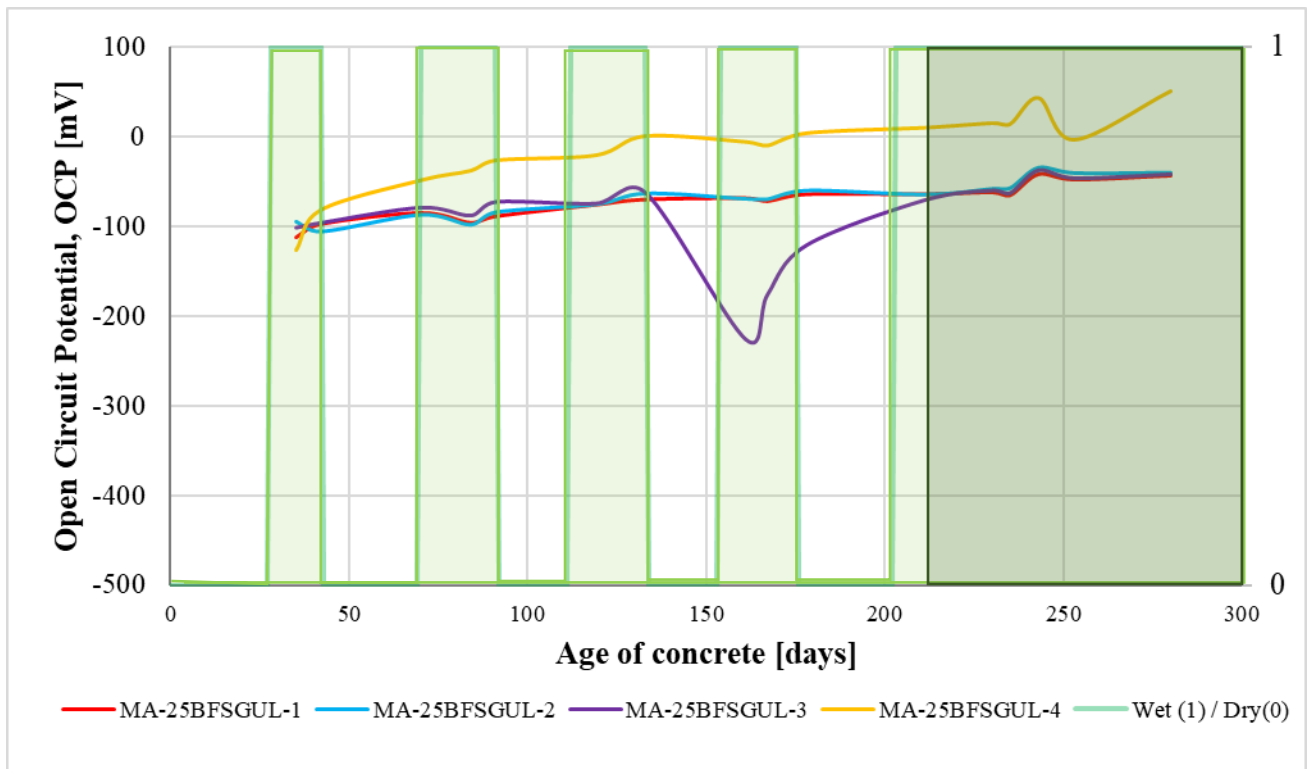


Figure 4.33 Open circuit potentials of the top bars of the 25BFGUL specimens

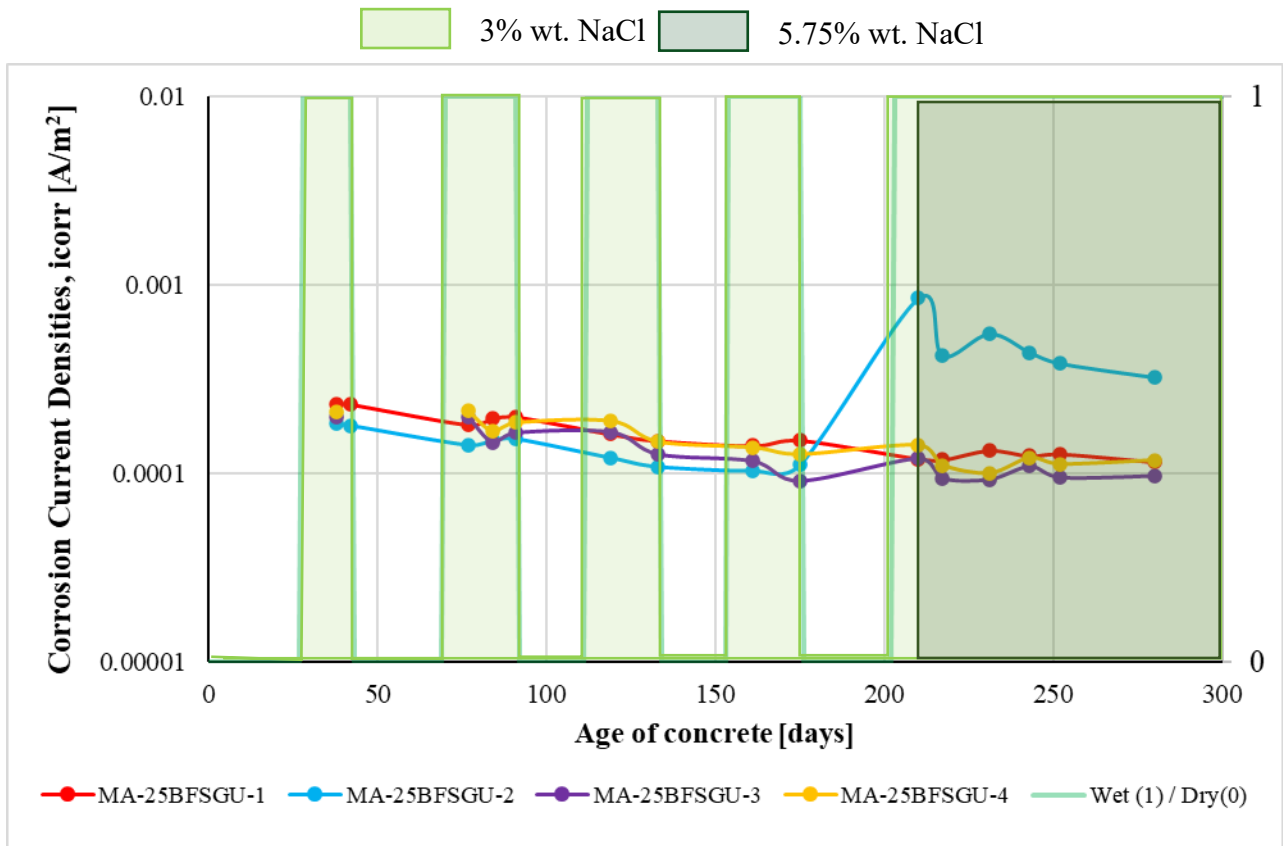


Figure 4.34 Corrosion current densities of the top bars of the 25BFSGU specimens

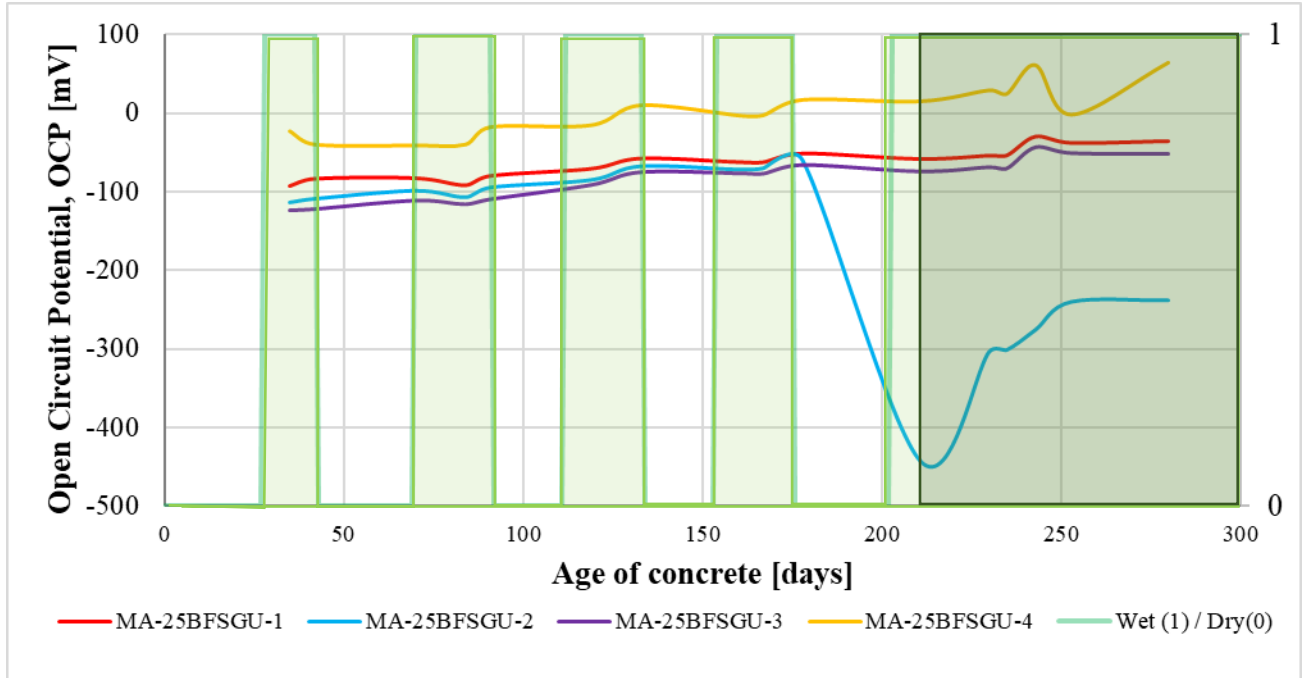


Figure 4.35 Open circuit potentials of the top bars of the 25BFSGU specimens

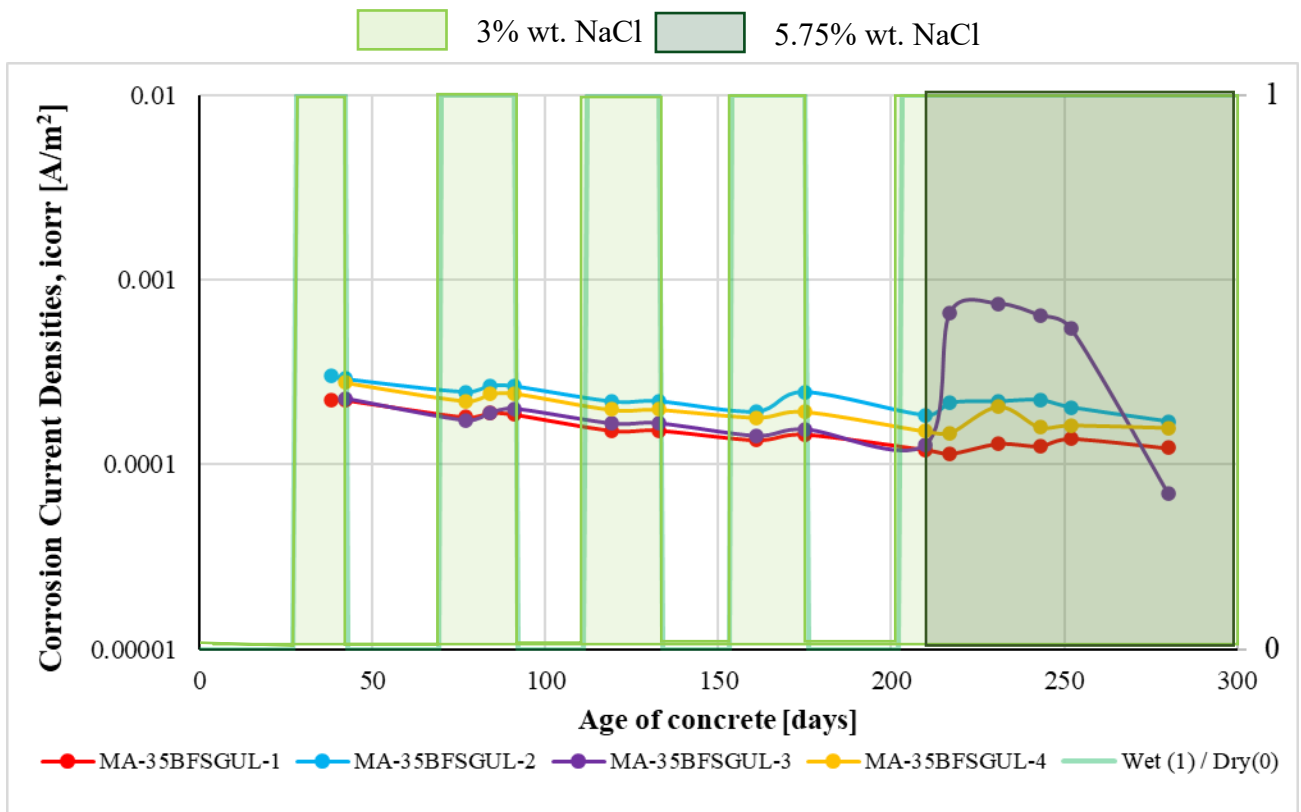


Figure 4.36 Corrosion current densities of the top bars of the 35BFGUL specimens

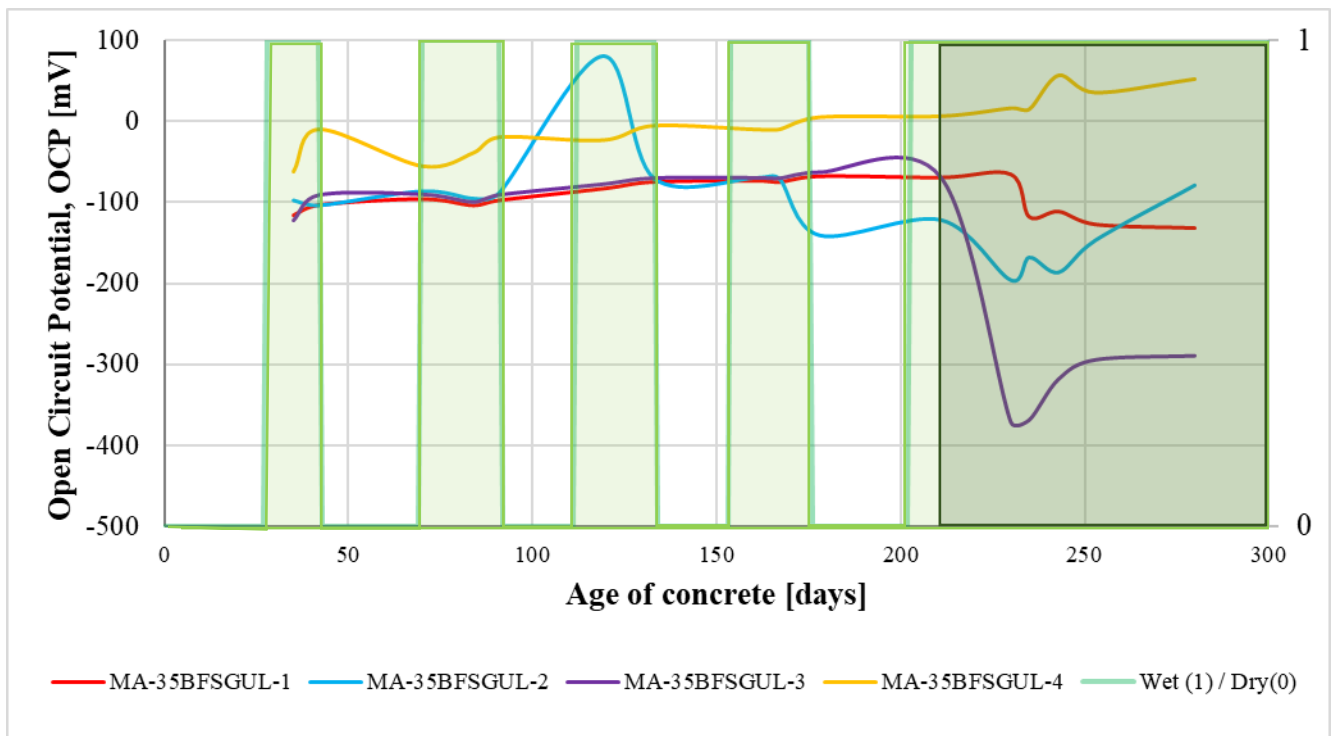


Figure 4.37 Open circuit potentials of the top bars of the 35BFGUL specimens

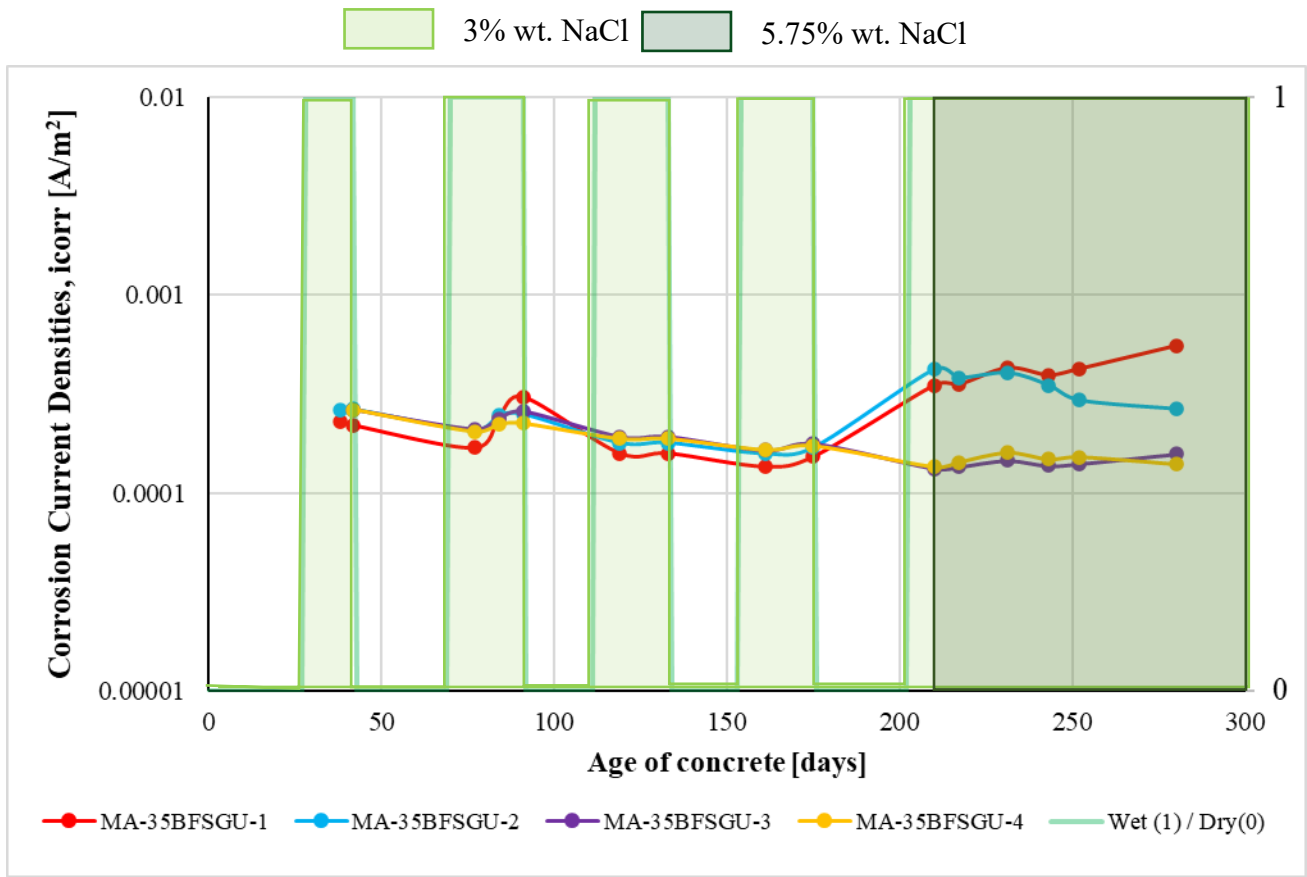


Figure 4.38 Corrosion current densities of the top bars of the 35BFGU specimens

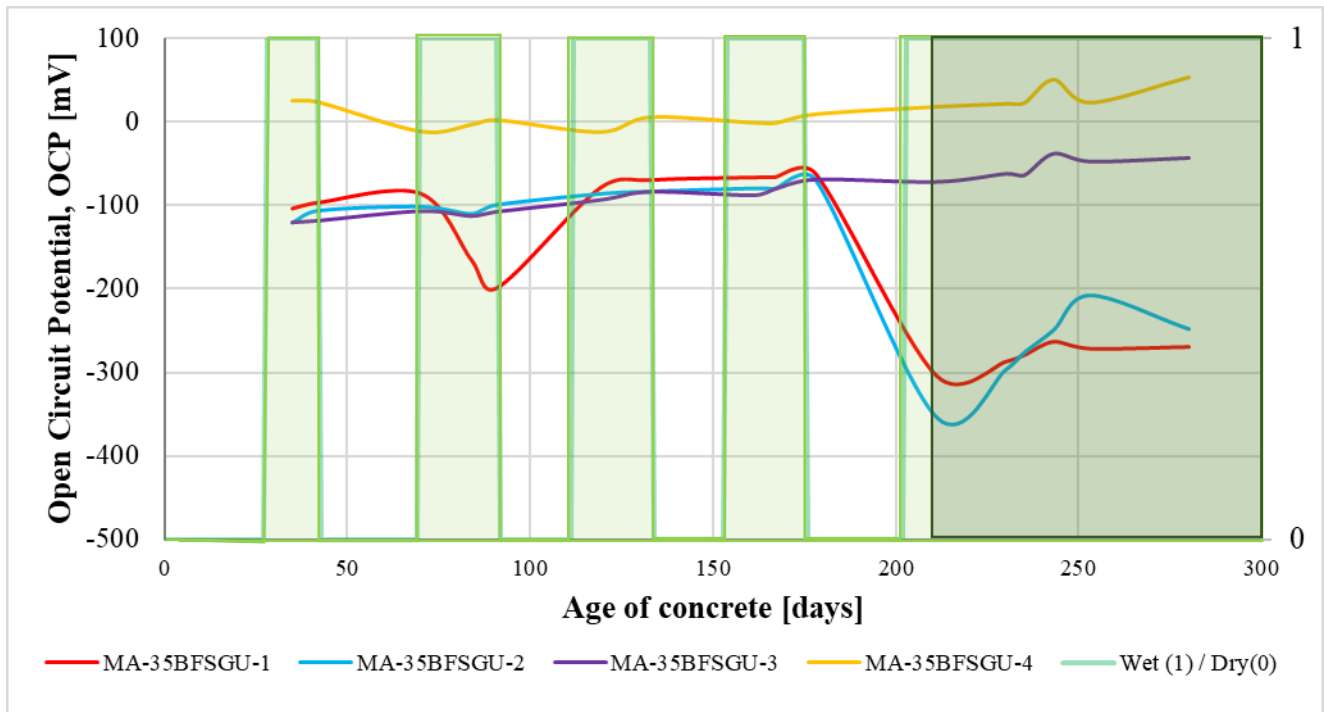


Figure 4.39 Open circuit potentials of the top bars of the 35BFGU specimens

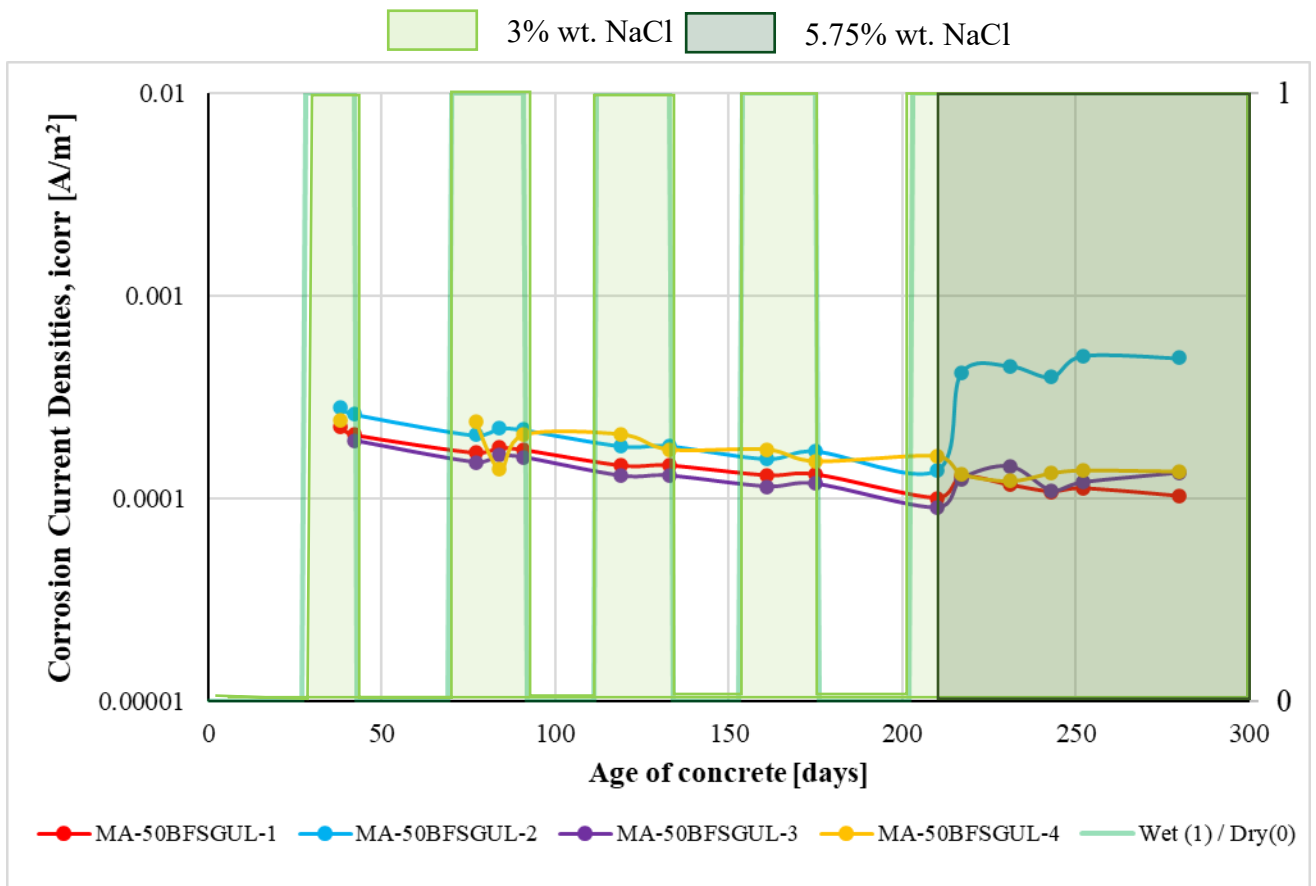


Figure 4.40 Corrosion current densities of the top bars of the 50BFGUL specimens

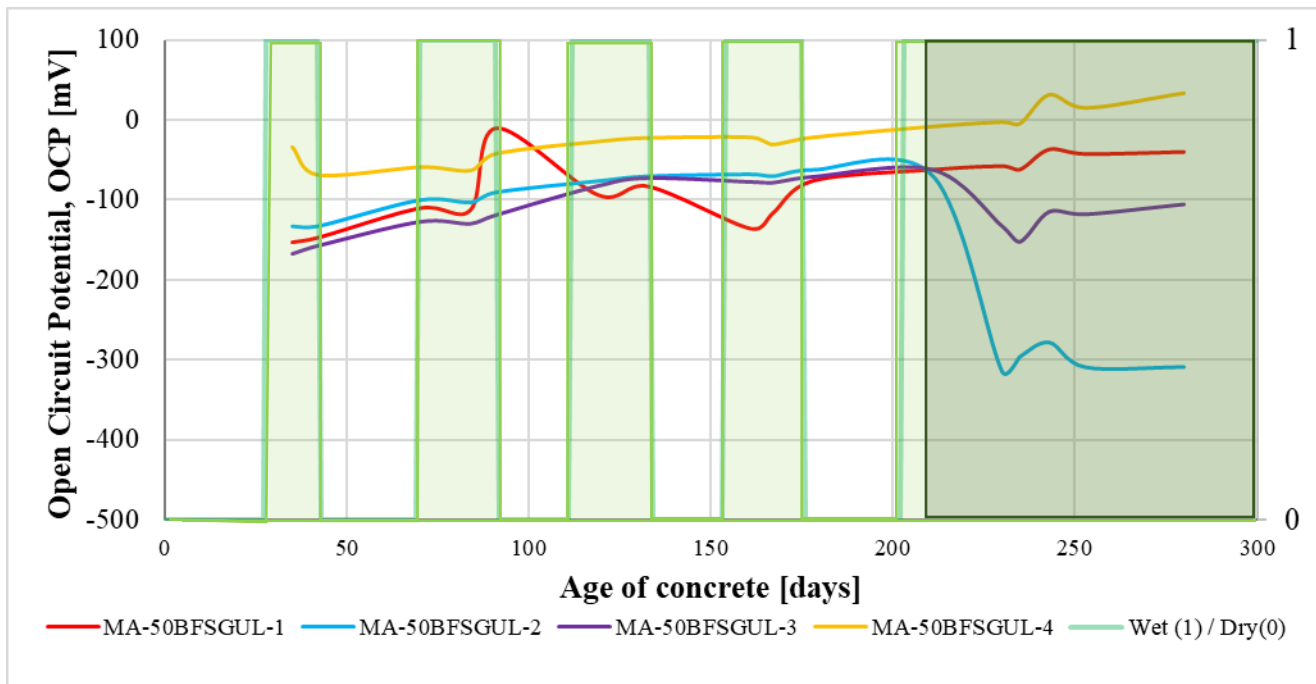


Figure 4.41 Open circuit potentials of the top bars of the 50BFGUL specimens

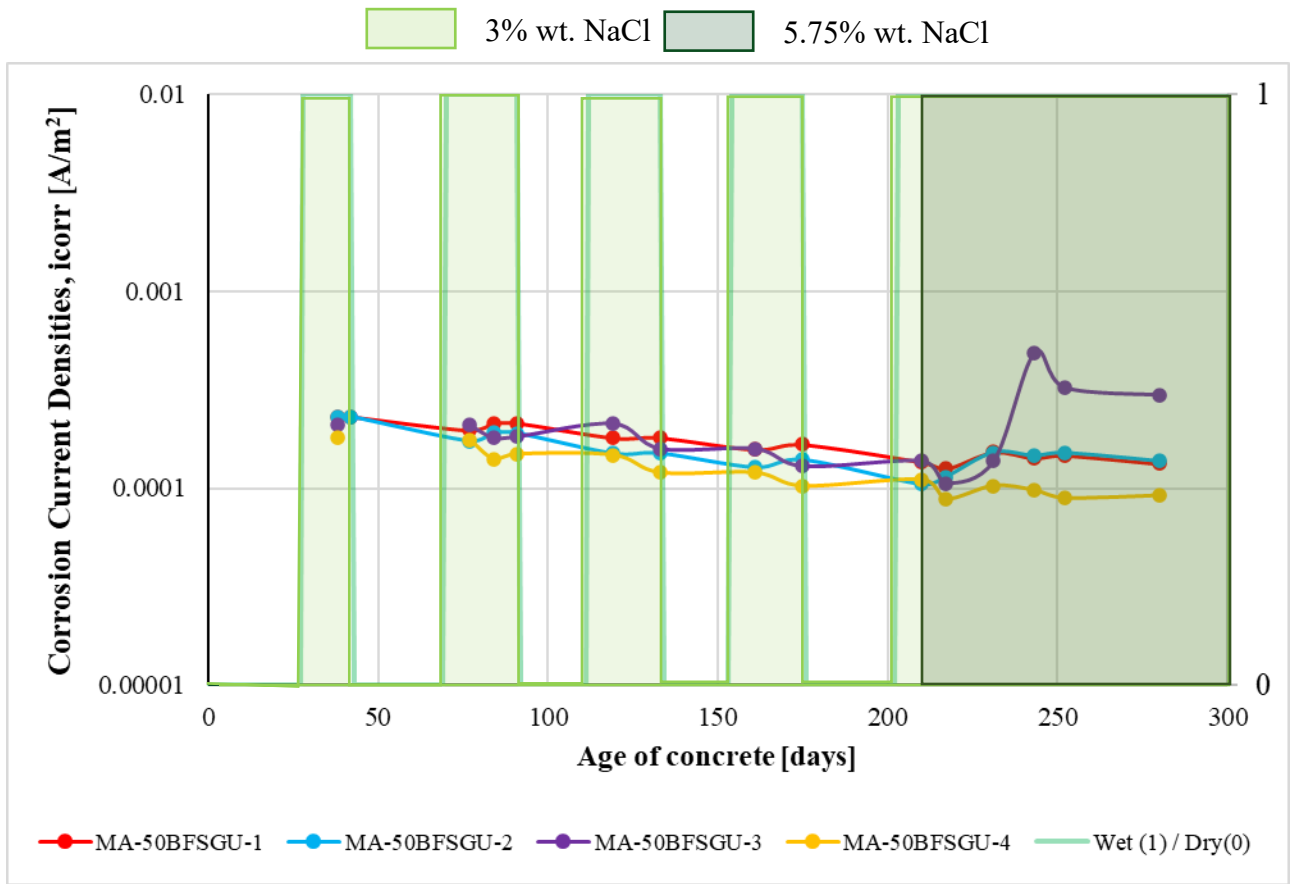


Figure 4.42 Corrosion current densities of the top bars of the 50BFSGU specimens

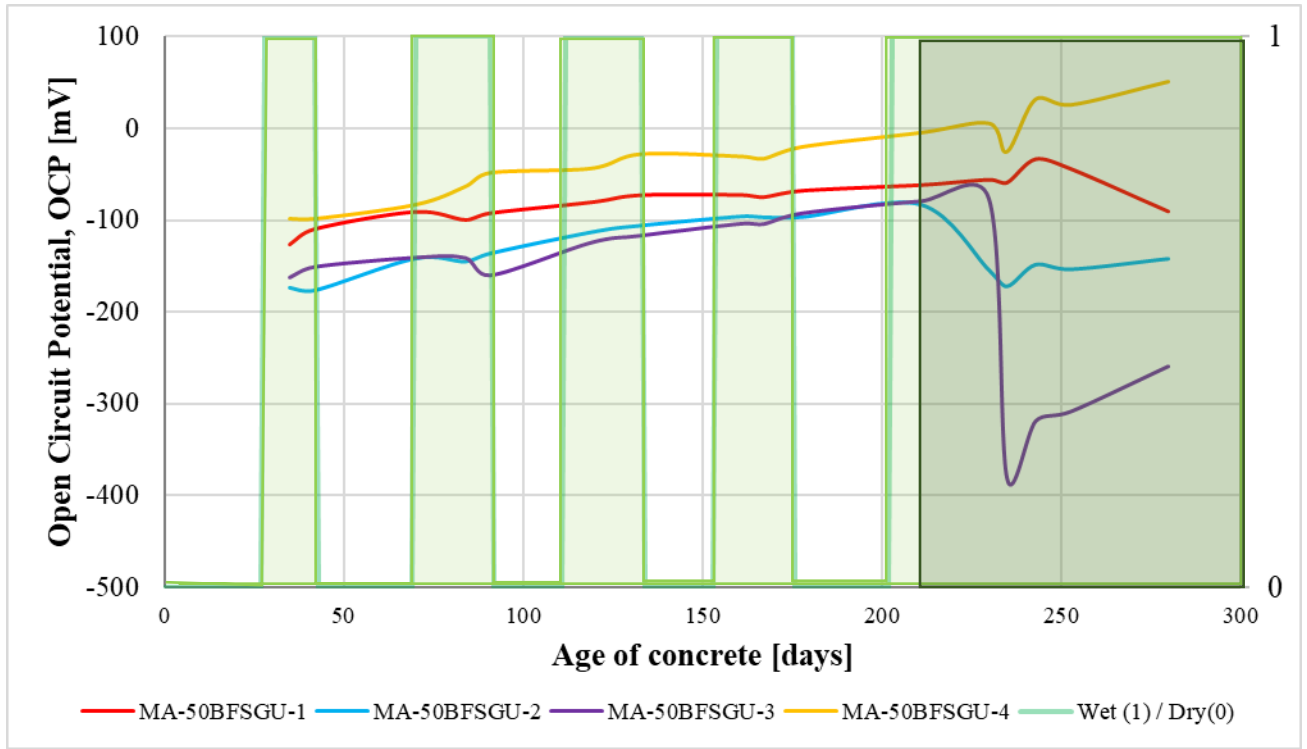


Figure 4.43 Open circuit potentials of the top bars of the 50BFSGU specimens

Both i_{corr} and OCP measurements are easily affected by external factors, such as electrical interference or defects in electrical connectivity between measuring probes and the wire connection to the specimens. The recovery of OCP to preceding stable measurements is slower than the recovery of i_{corr} after an instantaneous peak/drop. Compared to OCP, i_{corr} is more sensitive to changes in the specimens and thus, it can more easily capture pitting on a rebar by a drastic drop or change in magnitude. Recovery in the data could imply repassivation of the steel rebar or removal of corrosion products from the rebar's exposed surface, such as observed in the synthetic pore solution tests. The said quick recovery of the i_{corr} , as opposed to the slower recovery of the OCP, was observed at day 280 for the MA-35BFSGUL-3 specimen, which was the only one among the specimens that peaked at day 210 after the change in chloride concentration of the chloride-contaminated ponding solutions.

The only rebar specimen which showed an early initiation of corrosion activity was the Ha-0BFSGUL-4 at day 90, where the increase in i_{corr} by 0.0005A/m^2 and drop in OCP by at least -200mV (relative to its starting stable OCP) were sustained till day 280. This is a clear indication of active corrosion of the rebar and this deduction was further proven in the autopsy as shown in Figure 4.44. In contrast, the Ha-25BFSGU-2 specimen exhibited an increase in i_{corr} of about $0.0005\text{-}0.0007\text{A/m}^2$, and simultaneous potential drop to -300mV at day 80. The two parameters returned to their preceding stable ranges and then, peaked again at day 170. However, as these changes did not remain with time, they were assumed to be indications of pitting followed by repassivation of the rebar.

In agreement with the macrocell data, the microcell data of the Ha- specimens fluctuated more than the MA rebar of the same 0BFS- concrete mix type. The fluctuations were likely due to the spread of or advanced corrosion facilitated by the pre-test rusted conditions of the Ha bars. The differences between the behaviours of the MA rebar in the control specimen and in the chloride-contaminated specimens are more significant for the 0BFS -GU and -GUL mixes, than for the GBFS-concretes. Elsewise, the chloride-contaminated specimens behaved similarly to the respective non-chloride contaminated specimen of the mix type. There were no significant differences between the i_{corr} and OCP ranges for the rebar of the GU- and GUL-based concrete specimens, apart from 25BFSGUL specimens having exhibited slightly higher i_{corr} values than the 25BFSGU concretes.

4.2.4 XRF Scans on Autopsied Reinforced Concrete Specimens

Two chloride-contaminated concrete specimens of each concrete mix type were cut for autopsy and the bars photographed (photos provided in Appendix C). Figure 4.44 provides photographs of five top bars, on which some corrosion products were evident (as encircled) and which also exhibited signs of some corrosion activity in the i_{corr} and OCP microcell data. Note that the wired ends of the bars rest to the right of the photographs.

Ha-0BFGUL-4



MA-0BFGUL-1



Ha-0BFGU-4



MA-35BFGUL-3



MA-50BFGU-3



Figure 4.44 Corrosion products present on the top rebar of the respective concrete mix types. Apart from MA-50BFGU-3 specimen, the corrosion products appeared at the wired ends of the bars. The formation of the corrosion products is attributed to crevice corrosion at the steel/lacquer interface. However, no signs of severe crevice corrosion were observed under the lacquer at the area of interest.

LPR and OCP measurements do not distinguish localized corrosion activities, but they quantify the corrosion activities as averaged over the entire exposed area of the tested rebar. Therefore, in cases where localized corrosion occurs, the current densities are underestimated because they should be corrected to consider only the corroding area. Therefore, the spikes in the i_{corr} microcell data respective to the specimens, listed in Figure 4.44, would indicate when the corrosion activity initiated or progressed to cover a larger area.

To estimate the degree of chloride ingress in the concrete specimens, the chloride ion concentrations were quantified using an XRF analyser on random points along the defined scan-lines of the cut specimens. It is difficult to distinguish whether the depth of the XRF analysis covers only a volume of the cement paste or the matrix of aggregates and paste and so, the chloride concentrations are expressed as percentages by weight of the concrete at the scanned points. The averages of several points along the respective scan-gridlines are plotted in Figure 4.45, as a function of the vertical depth from the bottom face of the ponding well to the bottom bars.

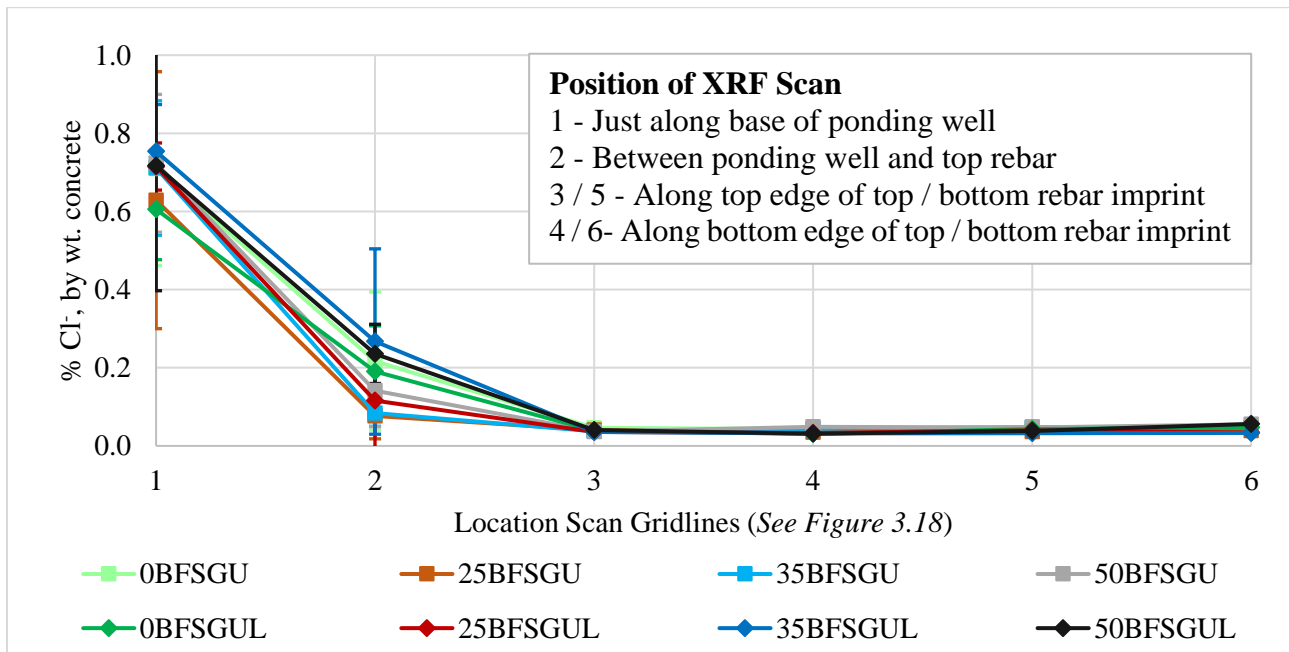


Figure 4.45 Averaged chloride content, as % by wt. of concrete, analyzed by XRF device

Based on the dimensions of the concrete block specimen, as discussed in Section 3.3.1, the distance between the gridlines 1 and 3 is approximately 25mm (1 inch). At gridline 3 or 4, the chloride concentrations did not differ across the various concrete mix specimens. This indicates that the chlorides have not diffused that far into the concrete matrix. Therefore, the focus will be on the

gridline 2 averages to compare the measure of chloride diffusivities of the different concrete mixes. 35BFSGUL was detected with the highest chloride percentage followed by the 50BFSGUL. At any GBFS replacement level, greater than the 0%, the GUL-GBFS concretes had greater chloride concentrations, than the GU-GBFS equivalents. The 25BFS-GU, 35BFSGU and 50BFSGU chloride concentrations did not differ from each other significantly, as compared to the difference between the 25BFSGUL and the 35BFSGUL/50BFSGUL. It is observed that the error bars at gridline 1 have the greatest spread for all mixes and this is because at just at the bottom of the well, due to the 1-2 cm diameter scan area of the XRF device, the scanned pores could have either been saturated with the NaCl salt solid precipitates or diluted by the water from the concrete saw upon cutting the specimens for autopsy. In summary, the GUL-BFS mixes were observed to be the concrete mixes with the lower chloride resistances, compared to the GU-GBFS mixes, but this finding contradicts the bulk resistivity data where the increase in GBFS led to more resistivity.

5.0 Analysis and Discussion of Results

To address the main purpose of this research, which is to investigate whether the replacement of cement by increased limestone (in PLC relative to OPC) and/or partial replacement by high levels of GBFS significantly affects the performance of concrete, discussions on the findings based on the experimental results and the literature are provided herein.

5.1 Visible Effect of Cement Replacement on Cement Pastes

The photographs in Figure 4.1 of the fracture surfaces of the cement paste specimens were taken after most of the free water had been removed by expression and so, the colour is largely reflective of the solid phases of the paste. The dark green/blue discolouration observed in Figure 4.1 for the GUL-GBFS cement paste specimens is assumed to be an indication of the presence of sulphur components of the slag in the solid phases. As the admixed chloride concentrations increased, it was observed that the intensity and spread of the green/blue discolouration decreased. The assumption is supported by the data provided in Figure 4.9, which showed an increase in sulphur ions detected in the pore solutions extracted from the cement pastes with increasing admixed chlorides. Therefore, the fading of the green/blue colour indicates the removal of the sulphur ions from the solid hydrate phases of the cement paste. Also, the green/blue colour fades upon exposure to the atmosphere which induces oxidation ^[37].

It was observed that the light greyish rim along the circumference of each of the cross-sections, shown in Figure 4.1, was consistent in thickness for all cylinders, irrespective of the GBFS or salt contents. The reason could be that during the expression of the cement paste specimens, the extracted pore liquids were channelled more easily along the edges than at the bulky centre of the cylinders. The presence of the light-coloured rims was less likely due to the influence of atmospheric exposure because each specimen was only removed from the cylindrical mould prior to placement in the high-pressure expression equipment and the cross-sections were photographed immediately upon extraction from the equipment and, thus, atmospheric exposure was not prolonged.

5.2 Effect of Using PLC Instead of OPC on the Corrosion Behaviour of Rebar

The chemical and electrochemical measurements have shown the compositions of and influence on corrosion of the GU and GUL cements to be comparable, despite the increase in limestone to 15% in GUL/PLC relative to GU/OPC. The differences in the concrete and cement paste properties were found to be small between GU- and GUL- based concretes, without slag and with 25% GBFS, and even smaller or negligible at the higher GBFS replacement levels at 35% and 50%.

The meter-measured pH values for the 0BFSGUL were higher and accompanied by greater potassium and slightly greater sodium concentrations detected in the pore solutions than those for the 0BFSGU mix. Consequently, the 0BFSGUL solution, with the higher pH, proved to be less corrosive as its rebar specimens exhibited lower corrosion current densities and less negative OCP than the 0BFSGU specimens in the electrochemical data. As noted under multiple figures in Section 4.1.2, the results of the 0BFSGU cement paste specimens were obtained from literature [110], using the same OPC cement. However, the preparation methodologies may have differed from the steps performed in this current studies. Therefore, it is difficult to make accurate assumptions comparing the results of the pore solution analyses of the 0BFSGU and 0BFSGUL mixes. This shows that despite using the same cement mix proportions and components, homogeneity and reproducibility are not guaranteed.

The pH, regardless of the means of quantification, for all the GU-GBFS and GUL-GBFS mixes with varied admixed chlorides from 0% to 1%, by mass of the cm, ranged between 13.3 and 13.9. The meter-measured and titration-estimated pH values of the GUL-GBFS based expressed pore solutions were generally lower than or equal to those of the GU-GBFS based solutions. The slightly lower pH obtained for the GUL-GBFS solutions corresponded to lower concentrations of alkalis (sodium and potassium) in the pore solutions, compared to the respective GU-GBFS mixes. The similarly high pH/ highly alkaline conditions were reflected as similar corrosion behaviours of the rebar specimens immersed in the 35BFS- and 25BFS-mixes, where the corrosion current measurements showed small differences between the GU and GUL equivalents. Despite the similarities in the alkali concentrations and the pH values between the 50BFSGU and 50BFSGUL solutions, the 50BFSGUL rebar specimens showed higher corrosion current densities and more negative OCP than those in the 50BFSGU solution.

The C3A component of cement can interact with the cement paste in the following ways: (1) react with hydroxyl ions to form the hydroxy-AFm, (2) react with the calcium sulphate from gypsum to form ettringite, and (3) react with admixed chlorides to form Friedel salts. As the admixed chlorides increased, the case (3) becomes more likely and the conversion of ettringite to Friedel salts results in increased sulphate concentrations in the pore solution ^[74], as shown in Figure 4.7. This is limited by the chloride binding capacity of the cement paste. For the chlorides to bind with the C3A thereby forming Friedel salts and leaving the sulphates in solution. In addition, as the admixed chlorides increase, the chloride binding as Friedel salts is limited (analogous to the plateauing trends in the bound chlorides in Figure 4.11) and thus, the free chlorides dissolve into the pore solution thereby mapping the increasing trends shown in Figure 4.8. It is important to note the order of magnitude of the difference between the ranges of the vertical axes of the chloride and sulphate concentrations, because while the chlorides were sourced from the added NaCl to the mixing water in making the cement pastes, the sulphates were sourced from the gypsum and elements of cement and slag compositions. The chloride and sulphate in the pore solution of the GUL-based mixes were slightly lower than or equal to those of the GU-based mixes. As a result, it would be expected that from the corrosion measurements of the rebar specimens in the respective solutions, the GUL-based solutions would provide more corrosion protection than those of the GU-based solutions. However, for the case of the 50BFS- mixes, the rebar specimens in the GUL-based solutions showed higher corrosion current densities and more negative OCP than the GU-based mixes. This would be due to the greater presence of sulphur-based chemicals in the mixes with higher GBFS replacement.

The chemical imbalance between the sulphur cation and the detected sulphur-based anions (the sulphates and the thiosulphates) is due to the presence of other auxiliary forms such as sulphides. The detrimental effect of the presence of sulphur-based compounds, such as hydrogen sulphide (which can oxidize to form the sulphuric acid) and the oxidated forms as sulphates and thiosulphates, on the efficiency of the protective passive films of rebar were reported by Ghods et al. ^[55] and Scott & Alexander ^[109]. Although not clear in the sulphate concentrations, the sulphur (Figure 4.9) and thiosulphate (Figure 4.10) concentrations in the pore solutions were generally observed to increase with the cement replacement. However, the difference between GUL- and GU-counterparts was less significant in the 25BFS- and 35BFS- mixes than in the 0BFS- and 50BFS- mixes, where the GUL-based mixes contained more sulphur and thiosulphate than the

GU-based mixes. The presence of more sulphur in the 50GBFSGUL solutions can explain the observed greater corrosion current densities and more negative OCP exhibited by the immersed rebar specimens, than in the 50BFSGU solutions. However, this does not support the greater corrosion susceptibility of the steel observed for the 0BFSGU than the 0BFSGUL specimens. This shows that in addition to the sulphur ions, the corrosion performance of the rebars in the immersed solutions collectively depend on the pH and other ions, such as the alkalis and chlorides, in addition to the saturated conditions in $\text{Ca}(\text{OH})_2$.

The initial 28 days after immersion of the rebar specimens in the test solutions provided a chloride-free environment to promote the passivation of the specimens. Hence, the results were almost levelled, implying no major activity in the rebar at the 0% admixed chloride conditions. Where a higher pH and alkaline environment were characteristic of the pore solution, the lower the passive current densities reported for immersed specimens. Based on the corrosion performance of the rebar in the synthetic pore solutions, the GUL-based mixes were ranked slightly better (based on lower corrosion current densities and lesser negative OCP values) than the GU-based mixes, without and with GBFS, up to 35% replacement. Apart from the discussed differences in the ionic concentrations and chloride binding capacities of the mixes, the observed white coating on the rebar, exposed to the 0BFSGUL test solutions (Figure 4.15), may also explain the results that showed lower current densities than the 0BFSGU specimens. This white coating, which was assumed to be the adsorption of excess calcium hydroxide, was not as visible on the rebar of the GUL-GBFS solutions as on the rebar of the 0BFSGUL mix. This may be because of the higher sulphur content in the mixes with higher GBFS content, thus, promoting the displacement of the hydroxides by sulphates. However, the $\text{Ca}(\text{OH})_2$ was added to saturation and thus, the sulphate and thiosulphate contents were incomparable with the hydroxide content.

The surface and bulk resistivities of the concrete cylinders were observed to be similar for both GU- and GUL-based concrete, without and with GBFS, as shown in Figures 5.1 and 5.2, respectively. Despite the accelerated early hydration brought about by the increased limestone in the GUL as reported in literature ^{[31], [32], [39]}, which would lessen porosity at the early ages, the day 7 resistivities in this current research did not capture any noticeable differences between the GU- and GUL-based concretes. Both GU- and GUL-based concrete specimens continued to experience increases in both surface and bulk resistivities for over almost ten months. The resistivity

parameter is assumed to be proportional to porosity based on decreased pore size distribution and degree of connectivity. Figures 5.1 to 5.3 show that the measured parameters of the GU- and GUL-based concretes were comparable and differed within $\pm 10\%$.

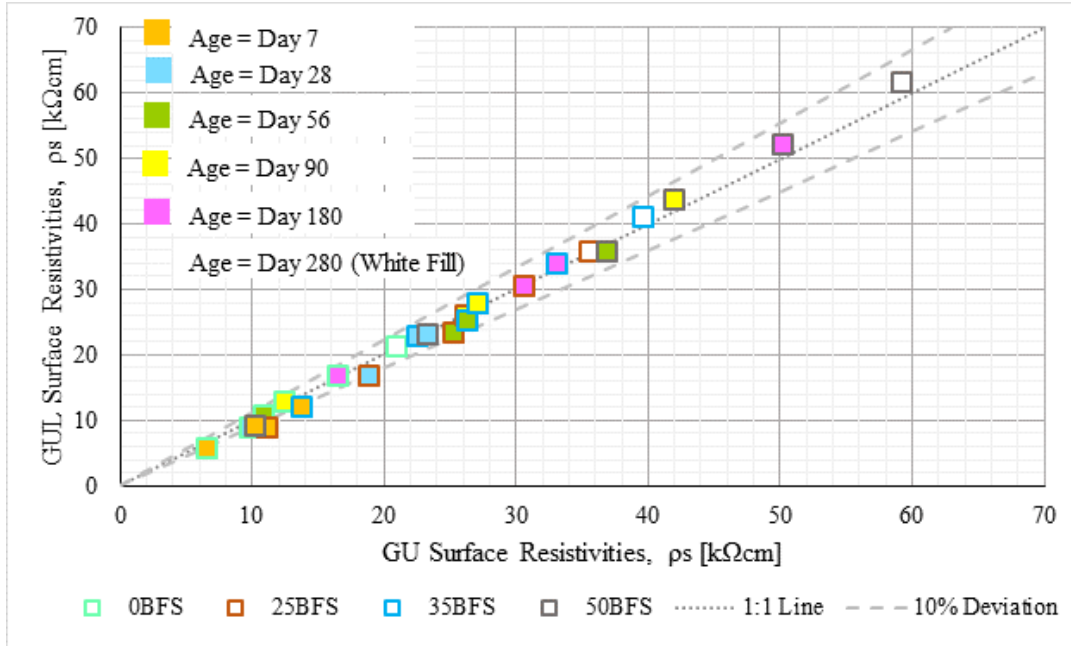


Figure 5.1 Surface Resistivities of GUL- versus GU-based concrete

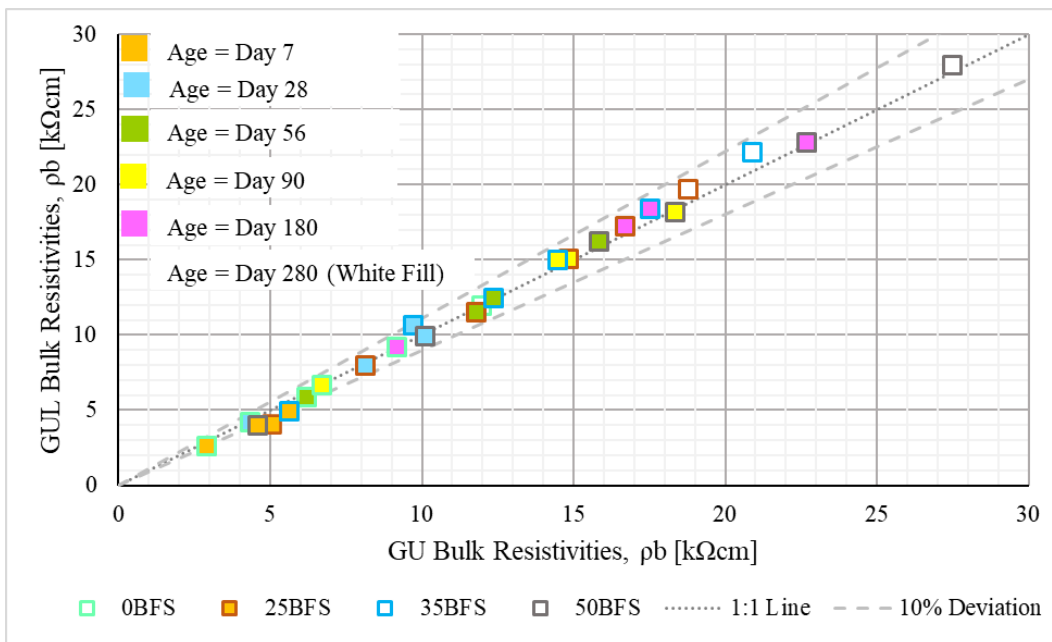


Figure 5.2 Bulk Resistivities of GUL- versus GU-based concrete

In contrast, the compressive strength plateaued after approximately three months for both GU- and GUL-based concrete specimens. The compressive strengths at days 7 to 180 showed comparable results for the GU- and GUL-based concretes, without and with GBFS of up to 35% replacement, as shown in Figure 5.3. After day 180, the compressive strength was slightly greater for the GU-based concretes than the GUL-based concretes, at the various GBFS levels. At 50% GBFS replacement, the 50BFSGU concrete specimens showed greater compressive strengths than the 50BFSGUL concrete, throughout the tested concrete ages.

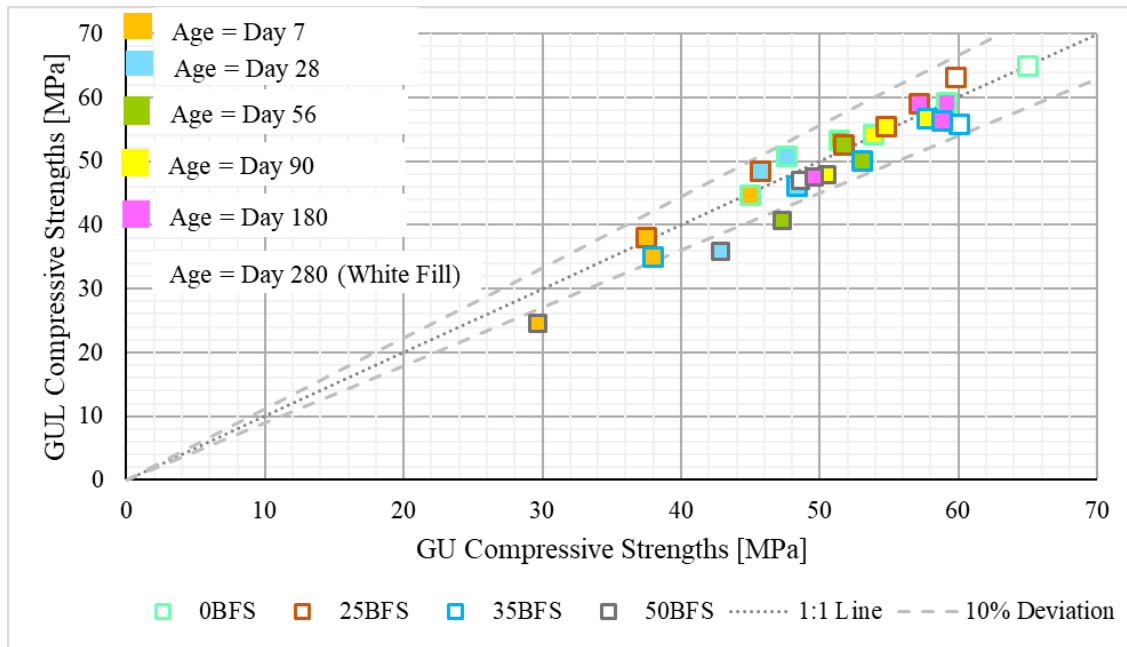


Figure 5.3 Compressive Strengths of GUL- versus GU-based concrete

The slightly lower compressive strengths of the GUL-based concrete compared to the GU-based concrete could be attributed to the high alkali content of the cement clinker [22] and the increase in water absorptivity with the increase in limestone [86]. It is to be noted that the concrete cylinders were demoulded, between days 4 and 7, and then stored in the fog room, at 100% relative humidity. In addition, as mentioned in Section 2.0, the studies on the effect of limestone on water demand for hydration of the cement [8], [82] have shown that the additional limestone and its associated fineness in GUL/PLC cement decreased water demand compared to GU/OPC cements. Therefore, at the fixed w/cm ratio of 0.4 for the concrete mixes, the GUL concrete would have more water in excess which would contribute to increasing the capillary porosity, leading to decreased compressive strengths [30]. However, the resistivity data showed no differences between GU- and GUL-based concrete cylinders. The reason for the contradiction between the resistivity and

strength results may be that, if the additional limestone did result in increased water absorptivity and decreased water demand, the introduced capillary pores were smaller in size with poor connectivity in the pore structure. No notable differences in the fracture surfaces after the compression-to-peak/failure of the concrete cylinders were observed to validate the significance of the role of the pore structure on the strength. The relative strength and resistivity properties of GUL- and GU-based concretes are in agreement with past literature which studied limestone replacement of up to 15% by mass of the cement [26], [85], [101].

Due to similarities in the pore solution compositions and the resistivities of the concrete cylinders, it was expected that the corrosion behaviours of the rebar specimens in GU- and GUL-based concrete would not be significantly different from each other. The macrocell corrosion data generally comprised fluctuations for all of the GU- and GUL-based concrete specimens, but the rebar specimens in the GU-based concrete specimens exhibited slightly more erraticism peaking to higher current density magnitudes than those of the GUL-based specimens. The microcell corrosion measurements of the 0BFSGU and 0BFSGUL specimens showed comparable behaviours throughout the monitoring period, with the exception of one of the eight GUL-based specimens which exhibited signs of active corrosion from day 90 and onwards. The current densities of the rebar in the 25BFSGUL specimens were higher than those of the 25BFSGU specimens with one of the three chloride-contaminated 25BFSGU specimens showing initiated signs of active corrosion at day 210. Compared to one 35BFSGUL specimen, two of the three chloride-contaminated 35BFSGU specimens showed initiated signs of corrosion at day 210. Despite the small differences between the compressive strength development and similarities in the resistivities of the 50BFSGU and 50BFSGUL concrete, their corrosion behaviours were similar. In short, the GUL-based concretes showed competitive corrosion resistance as those of the GU-based concretes, at the respective GBFS replacement levels. This correlated to the expectations based on the pore solution chemistry where the differences between the GU- and GUL-based mixes were small, apart from the 0BFSGU and 0BFSGUL mixes due to the pore solution data of the former being obtained from literature.

The concrete resistance was also measured as part of the galvanostatic polarization (GP) corrosion rate measurements and the data are presented in Figure 5.4. The bulk resistivity is the product of the concrete resistance and geometric factor considerations. Therefore, the bulk resistivity should

be proportional to the GP-estimated concrete resistance, where the latter concerns the concrete immediately surrounding the tested (top) rebar. Each of the concrete resistance datapoints in Figure 5.4 was averaged from the three to four concrete replicas of the various mixes investigated. The influence of the limestone in the GUL appears to be negligible due to the similarities to the respective GU-based specimens, without and with GBFS up to 35% replacement. Considering the error-bar ranges of the 50BFSGUL datapoints and their overlap with those of the 50BFSGU datapoints, it can be concluded that the concrete resistances of the 50BFSGUL concrete specimens were slightly greater or equal to those of the 50BFSGU specimens.

The hydration of the slag reduced pore size distribution, due to the formation of smaller and denser pores, thus, reducing the overall porosity [31]. The increase in the concrete resistance, as shown in Figure 5.4, agrees with the concrete cylinder resistivities (Figures 5.1 and 5.2) with increasing GBFS replacement. Despite the increase in resistivities, the compressive strengths showed no developments with the increase in GBFS in the concrete mix. The significant reduction in compressive strength at the 50% GBFS replacement level is attributed to the decreased Ca/Si ratio of the cement mix [115]. In addition, the decrease in the compressive strength with increasing GBFS content can be explained by the effect of the total alkali content of the cement mix on the delayed hydration [22]. The decrease in compressive strengths observed in the current study agreed with literature studying concrete with high GBFS replacement levels exceeding 35% [29], [80].

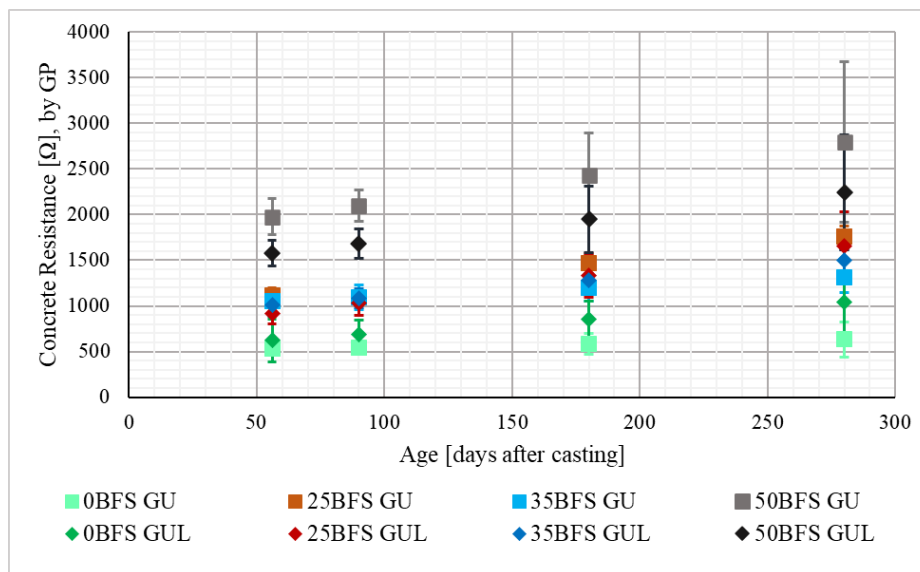


Figure 5.4 Average concrete resistance, estimated by GP, of the concrete specimens

The higher resistance corresponds to lower interconnected porosity and thus, reduced diffusivity of chloride ions in concrete. On this basis, the concrete mixes with the higher resistivity and GP-estimated concrete resistance results should have the lower chloride detection amounts. For the comparison between the GU- and GUL-based specimens on their concrete resistance measurements, it was observed that the GUL-based specimens had slightly higher or equal resistances to their respective GU-based concretes. This is contradicted by the data in Figure 5.5, which show the higher chloride amounts for the GUL-based concretes, compared to the respective GU-based concretes. Figure 5.5. highlights the chlorides detected by XRF at gridline 2, which is the concrete cover just above the top bar and below the base of the ponding well, for the various autopsied concrete block specimens.

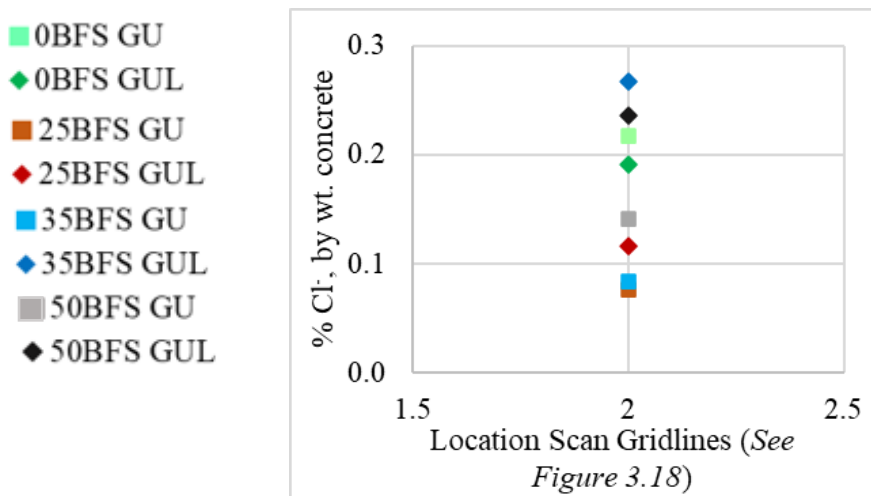


Figure 5.5 Expanded view of the chlorides, detected by XRF, on gridline 2, averaged from two autopsied concrete of each mix (See Figure 4.45 for full plot)

In Figure 5.5, the average chloride content analysed from the 35BFSGUL concrete was shown to be the highest and 3 times higher than the 35BFSGU average. The result appears to deviate from expectations based on the concrete cylinder properties which show both concrete types to be similar in resistivities and strength. This result is due to the influence of the environmental factors on the chloride ingress. The 35BFSGUL and 50BFSGUL specimens were located nearest to the entryway to the monitoring room, as shown in the sketch provided in Appendix C. While it was mentioned that the concrete specimens were loosely covered with plastic sheets, wind drifts and temperature fluctuations can be introduced to the localized atmospheric area surrounding the concrete, as the door to the room was opened and closed regularly on daily basis.

5.3 Effect of GBFS Replacement of Cement on the Corrosion Behaviour of Rebar

This section discusses the effect of the increasing GBFS content on the chemical composition of the pore solution and on the corrosion resistance of rebar subject to such conditions as test solutions and in concrete. The influence of the additional limestone in GUL on the pore solution chemistry and concrete properties was not significant as the GUL-based specimens performed comparably to the GU-based specimens as discussed in Section 5.2. In contrast, the effects of the changes in the GBFS content were more noticeable on the pore solution chemistry, concrete properties and influence on the corrosion resistance of rebar. Based on the observations of the corrosion tests in the test solutions, the increasing GBFS corresponded to increasing risk of corrosion of the rebar, while the corrosion tests on the rebar embedded in the concrete block specimens concluded that the 0BFS concretes showed greater risk of corrosion than the concretes containing GBFS.

The electrochemical results for the rebar suspended in the synthetic pore solutions showed increased risk of corrosion with increasing GBFS replacement which is explained by the expressed pore solution data, which showed decreased alkalinity and increased sulphur content. The difference between the results of the tests in pore solution and those in concrete is due to the chlorides being immediately available at the steel surface in the test solutions and is limited by the migration through the concrete in the reinforced concrete specimens. Thus, for corrosion of rebar in concrete, the probability of the chlorides reaching the rebar is inversely proportional to the resistivity of the concrete.

The pH values, estimated by titration, decreased with increasing GBFS, which followed the concentrations of the sodium and potassium (in Figures 4.3 and 4.4). The concentrations of the sodium and potassium in pore solution decreased with increasing GBFS replacement of the cement, regardless of whether GU or GUL was the base cement. This was not surprising since the titration measurements depended on the ionic strengths of the alkali ions, namely the potassium, sodium and, to a lesser extent, calcium and silicon ions in the pore solutions ^[76]. The reduced alkalinity is attributed to the lower Ca/Si ratio of the cement mix composition, as shown in Table 3.1 (it is estimated that GBFS has Ca/Si ratio of about 1.52 while the GU and GUL cements have similar Ca/Si ratio of about 4.83). Due to reduced positivity of the lowered Ca/Si cation ratio, the alkali ions adsorb more readily to the interfacial surfaces between the interlayers of solid C-S-H phases ^[112]. The reduction in pH with increased cement replacement agrees with literature ^[56].

Sulphur concentrations in pore solution increased with increasing GBFS replacement. The concentration of the oxidated form as thiosulphates were observed to increase slightly with increasing GBFS replacement, while the sulphates were decreased with increasing GBFS replacement. As mentioned previously, the chemical imbalance between the sulphur ions and the sulphate + thiosulphate anions confirms the presence of other forms which were not investigated in the current research, such as sulphides. The chlorides decreased with increasing GBFS replacement of the GU or GUL cement, with the 0BFSGU data trending as outlier to this observation. While the replacement of cements by GBFS, up to 30%, was found to have increased bound chlorides compared to cement mixes without GBFS in a study by Potgieter et al. ^[61], the calculated bound chlorides (in Figure 4.11) did not explicitly show any significant differences in the chloride binding capacities among the mixes, regardless of the cement replacement levels. However, the chloride concentrations in Figure 4.8 did show slight decrease with increasing GBFS replacement of cement, apart from the outlying 0BFSGU trendline. The bound chlorides were estimated from the free “evapourable” water test method which involved series of hammering and grinding the hardened 28-day cement paste specimens to an acceptable powdered form. During these tasks, it is difficult to prevent possible loss by evaporation or adsorption of water to the tools used, and thus, the results may not be representative of the true water contents of the specimens. In addition, the 28 days of curing may not have provided ample time for the significant changes to take into effect in the cement paste samples, brought about by the benefits of the slag hydration, and thus, the differences may not be representative of the true effects of the replacement levels as high as 50%. As indicated by the resistivity data in Figures 5.2 and 5.3, the slag hydration continued for at least 10 months.

A general increase in the corrosion current densities and increased negativity of the OCP data were observed as the GBFS replacement increased, up to the 35% replacement level, as shown in Figures 4.12 and 4.13. The specimens corresponding to the 35% GBFS replacement showed the highest corrosion rates for both GU- and GUL-based test solutions. Based on the sulphur concentrations, which were assumed to relate directly to the presence of sulphides, the greater the GBFS replacement led to higher corrosion risk due to the detrimental effect of the sulphides on the pH and the passivity of the rebar. Based on the titration-estimated pH, corrosion was expected at the corresponding lower pore-solution chloride contents for the higher GBFS levels. Therefore, the chloride concentration threshold for initiating corrosion activity on the rebar is lessened by the

increasing presence of sulphides and reduced pH, with increasing GBFS content ^[109]. This explains why the specimens began exhibiting signs of corrosion activity with increased corrosion current densities and OCP drops at the 0.5%-0.6% admixed chloride condition in the synthetic pore solution tests. Corresponding with the higher sulphur contents in the mixes with higher GBFS replacements, the increased risk of corrosion activity on the rebar exposed to the 35BFS- and 50BFS-solutions started earlier into the change to the 0.5% admixed chloride conditions than the specimens in the 0BFS- and 25BFS-solutions. At the 0.5% admixed chloride level, the differences in the sulphur concentrations among the various mixes became more significant. For example, the sulphur concentration of the 50BFSGUL pore solution increased by 20% to 40% from the 35BFSGUL solution at 0.5% to 1.0% admixed chloride concentrations, respectively.

Based on the concrete cylinder resistivity and GP-estimated concrete resistance measurements, the time to corrosion initiation is expected to prolong with increasing GBFS replacement. With the reduced pH and increased sulphur in the pore solutions of higher GBFS-mixes, active corrosion of the rebar would require lower chloride concentrations for initiation, compared to 0BFS-mixes. On average, the maximum post-initiation current densities decreased with increasing GBFS as shown in Table 5.1. Otherwise, no consistent trends in the corrosion initiation time and probability of rebar corrosion were observed.

Table 5.1 Observed corrosion initiations of the reinforcement in the concrete block specimens

Mix	No. of Bars Showing Signs of Initiated Corrosion		Age at Which First Sign of Initiated Corrosion		Max. Post-Initiation Corrosion Current Density, [mA/m ²] ~approximately
	Ha	MA	Ha	MA	
0BFSGU	1	0	230	-	1.60
0BFSGUL	1	0	90	-	2.08
25BFSGU	-	1	-	210	0.85
25BFSGUL	-	0	-	-	-
35BFSGU	-	2	-	210	0.56
35BFSGUL	-	1	-	217	0.66
50BFSGU	-	1	-	245	0.49
50BFSGUL	-	1	-	220	0.42

The general overview of the microcell corrosion data shows little difference in the passive current densities of the bars, with the values for the bars of both 0BFS-mixes being noticeably higher than those with GBFS, but still within the same order of magnitude. The autopsy on the specimens,

which showed signs of initiated corrosion activity in the microcell corrosion data, did not show significant physical signs of corrosion on the rebar surface and thus, it would have been better if the specimens were monitored longer after day 280. The lack of corrosion activity observed for the embedded rebar in the concrete and the equivalence of the chloride contents analysed at and lower than the top bar imprint for the autopsied concretes (gridlines 3 to 6 in Figure 4.45) are attributed to the slowed chloride ingress in the GBFS-concretes, which were predicted from the resistivity measurements. The averaged chloride percentages, by mass of the concrete, detected by the XRF scans, presented in Figure 5.5 are further examined as a function of the GBFS replacement in the concrete mix in Figure 5.6.

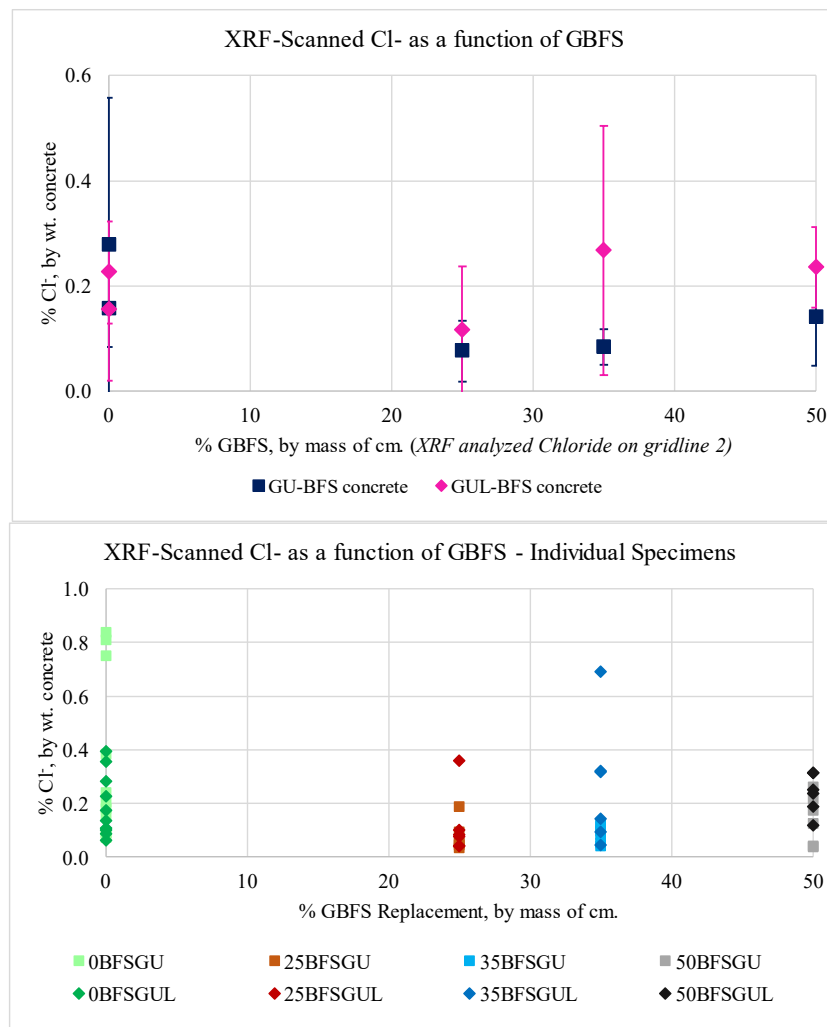


Figure 5.6 (Top) Averages of the (Bottom) Individual Chloride XRF Datapoints of the Concrete Specimens, along Gridline 2 of Figure 3.18
(Note the different scales of the vertical axes of the top and bottom plots)

Similar to the corrosion behaviours of the rebar specimens suspended in the synthetic pore solutions, which showed the highest risk of active corrosion activity from the 35BFSGU, 35BFSGUL and 50BFSGUL specimens, the averaged chloride concentrations in the autopsied 35BFSGUL and 50BFSGUL concrete specimens were highest (as observed in Figure 5.5). The greater the chlorides detected on gridline 2 (located between the bottom of the ponding well and the top bar), the more susceptible the top bar of the concrete specimen is to chloride-induced corrosion. As shown in Figure 5.6, the chloride levels decreased with the inclusion of GBFS, relative to the concrete specimens without slag. In the presence of GBFS, the chloride levels increased with GBFS replacement up to 35% and then decreased from 35% to 50% GBFS. This contradicts the deductions from the concrete cylinder resistivity and concrete resistance results. The variation in the data points, as shown in Figure 5.6, is attributed to difficulty in distinguishing the depth of the analysis of the 1.0-1.5cm diameter scanned area, by the XRF device, based on the bound chlorides in the solid cement paste or the free chlorides that remained in the capillary pores upon evaporation of the moisture. The uncertainty exists in the case of the 35BFSGU concrete, where two of the three chloride-contaminated specimens showed signs of active corrosion (sustained OCP drop and increase in current density) from the day 210, despite the autopsied concretes corresponding to the lowest quantified chloride detection levels.

5.4 Interpretation of the Macrocell Corrosion Measurements

The variations in the room temperature and relative humidity (Figure 4.19) external to the reinforced concrete specimens had no notable influence on the electrochemical measurements. For example, the spike in relative humidity measurements at day 190 and onwards, dictated the start of the summer hot days. A simultaneous drop in temperature, due to influence of the air conditioning in the room, is observed corresponding to no lasting changes in the macrocell corrosion data. These environmental factors can affect the chloride diffusivity and chloride concentrations in the ponding well ^[106]. At high temperature and/or low relative humidity conditions, evaporation of water is enhanced, thus, leaving the salts as solid precipitates at the base of the ponding wells or at the pores near the concrete surface. This causes clogging of the pores thereby reducing further chloride ingress in the concrete matrix. To mitigate unwanted evaporation, the ponding wells were covered with plastic sheets and the solution levels in the

ponding wells were routinely monitored to ensure the wells remained adequately wet during the wet period of the wet-dry cycles.

Macrocell measurements of corrosion current densities are typically expected to be lower in magnitude than those of microcell measurements. This is because the macrocell system collectively concerns the top and bottom bars which are separated across a depth of concrete, through which the ions need to travel. Therefore, the current flow is expected to be less than in a microcell system, where the active and passive areas are interchangeably adjacent to each other on the same metal rebar. However, the macrocell data in this research had recorded peaks of 0.005A/m^2 , which was not near the range of the microcell data. There was also no relationship between the fluctuations and wet-dry cycles. During the wet periods, the solution in the pores facilitates electrolytic movement and so, increases in the macrocell measurements would not have been surprising.

The variations in the macrocell data could be due to various possibilities. One reason for the instantaneous spikes in magnitude of the macrocell current densities is the isolation of actively localized corroding areas or pits. The relativity of the potential of that chloride-concentrated area to the surrounding passive steel areas, in addition to the spatially separated bars, results in high potential differences, which act as driving forces for ionic flow for corrosion activity ^[114]. An example of this possible occurrence is shown for the autopsied bars corresponding to Ha-0BFSGUL-1 in Appendix C, where Figure 4.20 (top) shows the occasional peaks in the current densities, indicating higher risks of corrosion activities on the bars. The top and bottom bars were observed with small signs of corrosion. Note that the microcell measurements were conducted only on the top bars and, thus, the data did not capture the LPR-estimated corrosion rates of either of the bottom bars. Alternatively, the Appendix C provides the OCP measurements for the bottom bars which captured the potentials which influenced the macrocell corrosion data.

The macrocell measurements showed that the rebar in the GBFS concrete, in general, experienced large scatter of data. It was observed that from the data of the 25BFSGU/25BFSGUL blends to the 50BFSGU/50BFSGUL, the fluctuations stabilized more slowly. From Figures 4.22 and 4.23 for 25BFSGUL and 25BFSGU concretes, respectively, the scatter started stabilizing just past day 125 and day 100, respectively. For the 35BFSGUL concretes, the data stabilized at about day 100, while for the 35BFSGU concretes, it was observed at day 150. On the other hand, the 50BFSGUL

and 50BFSGU concretes corresponded to the most scatter which started to smoothen at day 175 and 200, respectively. This is once again attributed to the delayed hydration of the slag and, consequently, the slowed development of the pore structure, as the GBFS replacement levels increased across the various concrete mixes. The large scatter was also observed in a study by Warkus et al. ^[14] on GBFS-specimens compared to the (0BFBS)GU specimens.

The macrocell corrosion measurements showed no significant change to indicate the changed NaCl concentration of the salt solutions of the ponding wells at day 210. In contrast, there were increases in the microcell current densities and drops in the OCP in the negative direction for the top bars of some concrete specimens in response to the increased chloride concentration. The OCP of non-chloride contaminated specimens were clearly passive throughout the monitoring period, as some bars exhibited OCP in the positive potential regions or remained unchanged in the range of the lowest values of negativity.

5.5 Effect of Rebar Condition on Corrosion Performance

The surfaces of the Ha rebar specimens were photographed after the Ha-bars were lightly wire-brushed to remove excessive corrosion products and were shown in Figure 3.1. Despite the brushing, the influence of the corrosion products remaining on the Ha bars affected the corrosion and more so when embedded in concrete than when immersed in the synthetic pore solution tests. The differences between the Ha and MA rebar in the latter tests were not significant because as shown in Figure 4.14, the stirring of the test solutions facilitated the removal of the corrosion products from the exposed surfaces of the rebar into the solution. The averages of the measured corrosion current densities, by LPR, and the OCP for the two rebar types in the synthetic pore solutions tests are shown in Figures 5.7 and 5.8, respectively. Except for the 0BFSGUL-M1 test solutions, the Ha-rebar generally exhibited higher corrosion current densities and more negative OPC values than the MA-rebar. M2 method involved adding all the laboratory grade hydroxide chemicals to account for changes in the auxiliary cations (Na^+ , K^+ , Cl^- and SO_4^{2-}) with the incremental increase in admixed chloride conditions, compared to method M1 which involves adding for only the Cl^- and SO_4^{2-} changes. The concentration of the hydroxyl (OH^-) ions is therefore overestimated in the M2 test solutions, thereby altering the pH, but the difference in corrosion performances was observed to be insignificant between M1 and M2 solution specimens.

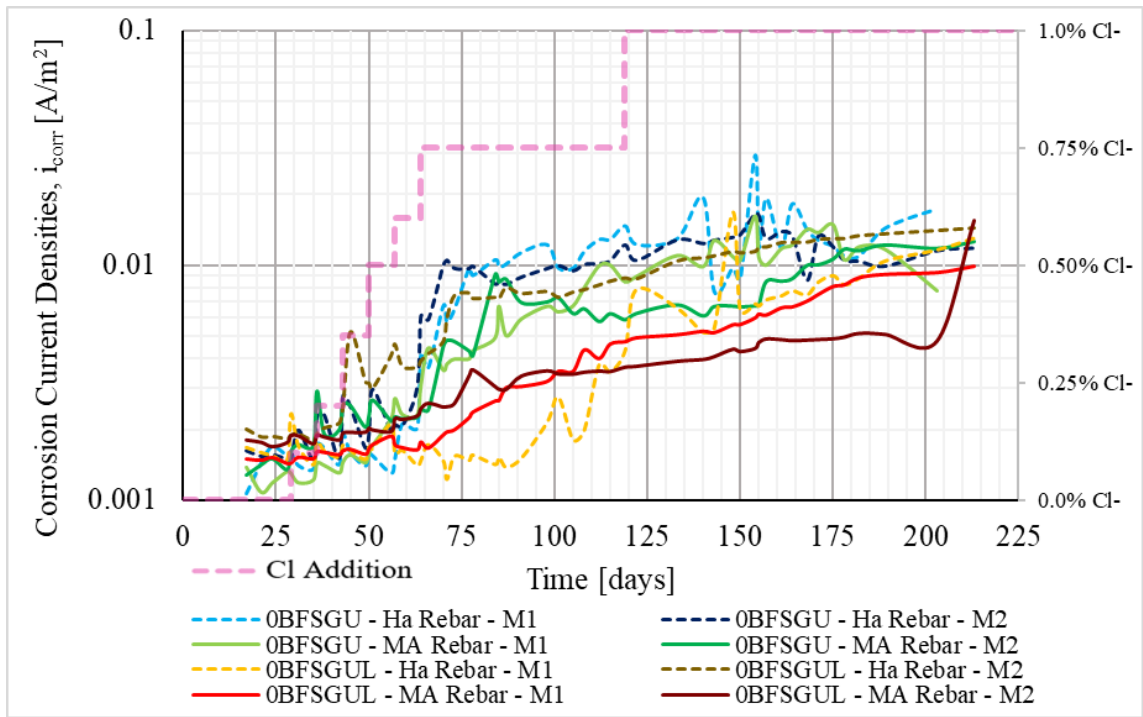


Figure 5.7 Average current densities measured for the Ha- and MA- rebar in 0BFS test solutions

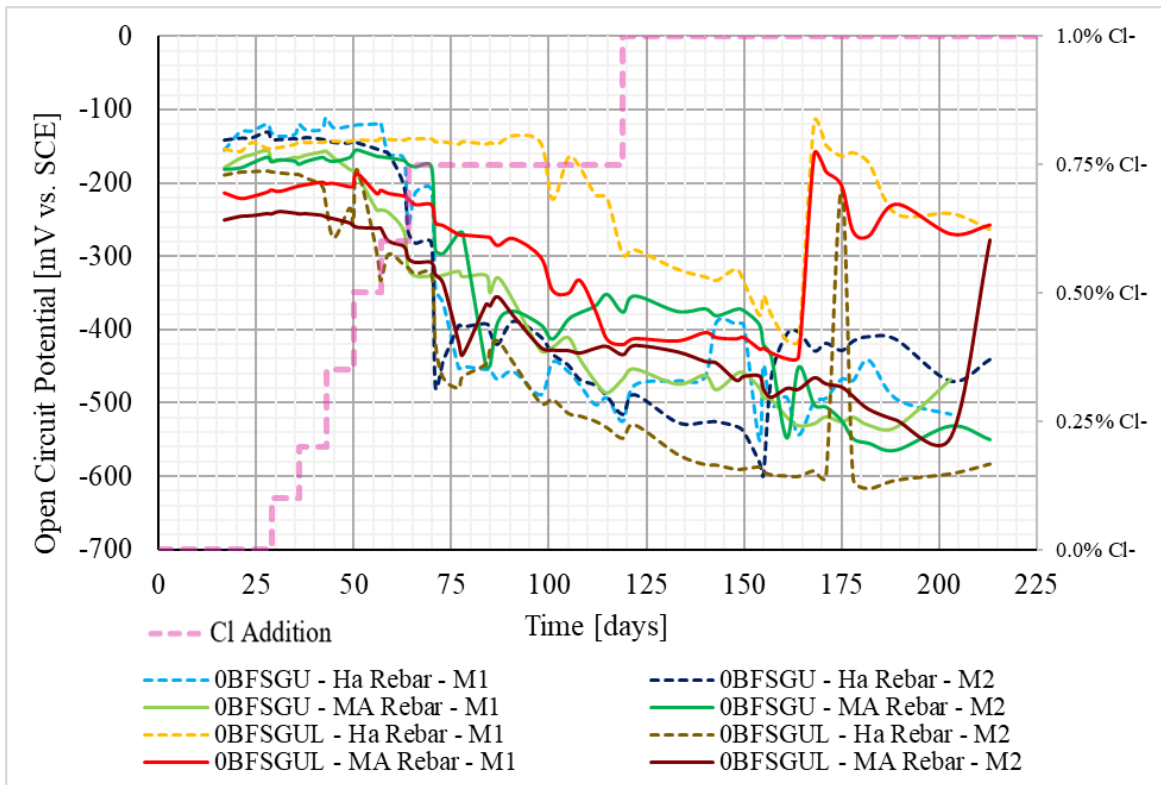


Figure 5.8 Average OCP measured for the Ha- and MA- rebar in 0BFS test solutions

Similarly, the microcell corrosion measurements of the embedded Ha-rebar in the 0BFSGU and 0BFSGUL concretes exhibited higher corrosion current densities than the MA rebar. In addition, all autopsied Ha-rebar showed signs of corrosion on localized areas of the exposed surfaces. It is clear that the rust on the Ha-rebar facilitated further corrosion of the rebar in concrete, but as the XRF-analysed chloride levels were insignificant at the top bar concrete area, chloride-induced corrosion may not have actively occurred. The small amount of corrosion was insufficient to cause cracking to the concrete cover on any of the specimens.

6.0 Summary, Conclusions and Recommendations

To address the pressing concerns of global warming, the current research aimed to promote the movement towards more sustainable cement mixes which adopt PLC/GUL instead of OPC/GU, with cement replacements at greater levels than currently permitted. The objectives were focused on investigating the effects on the corrosion performance of black (carbon) steel rebar in concrete due to the replacement of cement by limestone and/or GBFS. The chemistry of the pore solutions from cement pastes was analysed to gain better understanding of the influence of the mix components on the corrosion behaviours of rebar in chloride-contaminated concrete of equivalent cement mix proportions. The outcomes of the experiments have shown that understanding the pore solution chemistry can influence decisions on concrete compositions and forms. This section summarizes the conclusions based on the research presented herein and recommendations for improvements and future research.

In the perspective of the cement production and its contribution to carbon footprint, the use of PLC instead of OPC with cement replacements by SCMs is recommended for sustainable cement mixes. This is, however, true only in disregard to the contribution by transportation and acquisition of the raw materials for cement production, which is influenced by length and time of travel and location-dependent availability of the cementing materials.

6.1 Consideration of the Implications of the Experimental Results

It is important to note the specifics of the experiments discussed herein and thus, consider with care on adopting the following conclusions. The pore solutions investigated were expressed from 28-day hardened cylindrical cement pastes, cured in ambient laboratory conditions, with a w/cm ratio of 0.5. While the proportions of the OPC or PLC cement and the GBFS were varied accordingly to the various cement mixes studied, the ratio of w/cm ratio for the concrete was kept at 0.4 with added water-reducing agent to obtain the desired workability. Concrete specimens were stored in monitored ambient conditions, while the demoulded concrete cylinders were stored in a fog room (assumably with 100% relative humidity). In this text, the cementitious materials (cm) referred to the cement (either of the two types used) and the GBFS. These conditions are very different from those experienced in the field.

6.2 Summary of Results

- A blue-greenish discolouration, accompanied by a pungent odour, of the cement pastes was observed for the cement mixes with slag and the intensity of the colour decreased with the increase in admixed chlorides in the cement mix, owing to the displacement of the sulphates by the chlorides in the hydrate phases. No distinction in the colour intensity was observed for the variation of GBFS levels in the cement mix.
- The pH of the expressed pore solutions varied between 13.3 and 13.9 for the various cement mixes investigated. No conclusive trend was observed for the pH measurements by meter, which was calibrated using standard buffer solutions of pH 4, 7, 10 and 12.5, which does not capture the pH range of above pH 13 for the highly alkaline expressed solutions. The pH values of the PLC-based mixes were generally lower than the OPC-based equivalents. As the GBFS replacement levels increased, the pH values decreased along with the concentrations of the sodium and potassium ions in the pore solutions.
- Bound chloride estimations, which were dependent on non-evapourable water measurements, did not differ significantly among the various cement mixes. The chloride ion concentrations in the pore solutions of the OPC-based mixes were slightly higher or equal to those of the PLC-based mixes. An increase in the GBFS replacement resulted in a decrease in the detected chloride ion concentrations.
- The sulphur ion concentration increased with increasing GBFS replacement. A decrease in sulphate and slight increase in thiosulphate concentrations was observed for the increase in the GBFS replacement. Decreased sulphur and sulphate ion concentrations were observed for the PLC-based mixes relative to the OPC-based mixes. The chemical imbalance in the sulphur cation and anion concentrations should be further investigated since an effect of the changes to the chemistry by GBFS was observed in the synthetic solution-tests.
- Although no visible signs of severe corrosion were observed on the rebar specimens which were exposed to the synthetic $\text{Ca}(\text{OH})_2$ -saturated chloride-contaminated test solutions after ≥ 150 days of testing, the general observation was made: the increase in GBFS replacement led to higher risks of corrosion, determined by greater current densities and more negative OCP. In addition to the decrease in solution alkalinity for increasing GBFS replacement,

the increase in sulphur ions was reasoned to be one of the primary causes of the increased risk of corrosion. However, similarities in the behaviours were observed for the 35% and 50% levels. Except for 0% GBFS level, the rebar specimens in the PLC-based solutions showed slightly greater risk of corrosion than those in the OPC-based solutions.

- The electrical resistivities of the concrete cylinders were observed to increase with age with increasing GBFS replacement. The concrete specimens with 25% and 35% GBFS replacement showed similar results, surpassing the 0% GBFS-concretes at day 28, along with the 50% GBFS replacement which exceeded all other mixes at day 56. The use of PLC instead of OPC saw no significant changes to the electrical resistivities.
- The compressive strengths of the concrete cylinders were observed to decrease with increasing GBFS replacement, with comparable results among the concretes with 0%, 25% and 35% GBFS after day 56. The use of PLC instead of OPC saw no significant changes to the compressive strengths of the concrete. After day 90, the compressive strengths saw little to no improvements.
- With a concrete cover of 25mm (1 inch), the concretes exposed to the 3% NaCl solution were found to act similarly to the concrete specimen, that was not exposed to chlorides, over 210 days. Therefore, it was concluded that either the chlorides had not yet diffused to reach the reinforcement bar or the diffused chloride concentration surrounding the rebar was insufficient to induce any corrosion activity. Then, a change to 5.75% NaCl solution saw some response in the electrochemical data for at least one specimen of each concrete mix type after ≥ 70 days after increasing the chloride concentration, while the other specimens aligned with the behaviours of the non-chloride contaminated specimen. While the increase in GBFS replacement level was observed with a slight decrease in the risk of corrosion of the embedded rebar (as determined by decreased current densities and decreased negativity of OCP), there was no consistency in the results observed. Therefore, further investigation on the remaining specimens is required to conclude on the corrosion performance of the rebar in the different concrete mixes.
- The surface conditions of the rebar used as reinforcement to the concrete structure do affect the rebar corrosion. As observed in the electrochemical tests on the reinforced concrete

specimens, the Harris rebar, which were rusted prior to testing period, exhibited higher levels of corrosion activity than the MANA rebar. Also, as evident from the autopsied reinforced concrete specimens, the affected area on the Ha-rebar, which had corrosion products on the exposed surface, was greater than those of the MA-rebar which were observed with corrosion signs. This is not an evaluation of the two bar sources but an observation of the importance of the suitable storage for maintaining the conditions of the bars prior to placement in concrete.

6.3 Conclusions

The following answers to the questions presented by the research objectives are based on the above summaries of the research.

- Despite the small differences in the chemistry of the expressed pore solutions of the OPC- and PLC-based cement pastes, the corrosion performance in the synthetic solutions of the respective cement types was not significantly different from each other, at the respective GBFS replacement levels. Moreover, the concrete properties of OPC- and PLC-based mixes were observed to show competitive results. Thus, it is concluded that using PLC instead of OPC would not cause any detrimental effects on the physical and mechanical properties of the concrete or the corrosion performance of reinforced concrete.
- There were significant changes to the chemistry of the pore solutions due to the GBFS replacement of the cement above the standard 25%. These changes include decreases in alkalinity and pH and increase in sulphur content but little to no changes in the chloride concentrations of the pore solutions with increasing GBFS. The effects of the changes in the pore solution chemistry were observed in the synthetic solution-corrosion tests, where increasing the GBFS content saw reduced corrosion resistance of the rebar.
- The higher the GBFS content of the concrete, the higher the electrical resistivities but the lower the compressive strength. It is concluded that the benefits to corrosion performance of reinforced concretes is improved with GBFS replacement as the increased resistance to chloride ingress outweighs the slight decreases in corrosion resistance once sufficient levels of chlorides reach the rebar. Therefore, with good planning and design, reinforced

concretes with high GBFS content, as high as 50%, can be used for their improved corrosion resistance.

- Based on considerations from the combined results of the tests on the concrete properties and pore solution chemistry, it is concluded that concrete mixes with GBFS replacement up to 35% can compare with the performance of the concrete mixes without GBFS, but that the additional GBFS to 50% only serves to reduce the CO₂ emitting cement.

6.4 Considerations for Future Application of this Research

The following presents some recommendations on future applications of the research.

- Comparing the chemical compositions of the cements as shown in Table 3.1, apart from the difference in the fineness and content of the limestone, the OPC/GU and PLC/GUL cements appear to be very similar. However, PLC/GUL cements sourced from other regions may differ significantly in the phase compositions, compared to the OPC/GU, and thus, it is important to note that the general conclusions of this research should be adopted with such considerations in mind.
- It is not recommended to depend on the 0BFSGU pore solution data, which were obtained from literature ^[110]. However, the 0BFSGU concrete and synthetic pore solution corrosion tests were specific to this research and thus, those results could be adopted for comparison with the other mixes.
- As reported in the literature, the findings on the effect of limestone in the PLC/GUL cement is primarily on the early hydration of the cement phases. The results of the various experiments in this research have shown that the PLC-based specimens behaved comparably to the OPC-based specimens and therefore, the limestone is inert in the chemistry and concreting properties. The tests in this research were conducted at later ages, exceeding 7 days after mixing. Therefore, to better investigate the effect of the limestone on the pore solution chemistry, it is recommended to analyse the pore solutions of the cement pastes at various times from as early as day 1 after casting. This may impose issues such as expressing from the early aged cement paste and so, other techniques that were common in literature can be adopted, such as XRD and thermogravimetric techniques.

- The amount of water-reducing agent was not kept consistent among the various concrete mixes, but the effect of the different volumes used was neglected in this research. However, it is known that the concrete properties, such as the pore structure, can be affected by use of the agent and thus, it is recommended that the amounts be restricted to within a certain range to determine the true effects of the GBFS replacement amounts on the concrete.
- It was mentioned multiple times that the pH meter readings varied significantly and thus, definite conclusions on the pH of the pore solutions, measured directly after the expression, were difficult to make. It is to be noted that the pH meter was calibrated using buffers of lower pH range and thus, for future works, it is recommended that a buffer with pH closer to the pH 13.3-14 range (expected for the cement paste pore solutions) be used. It is difficult to prepare a stable high pH solution and so, alternatives like the titration method can be adopted for day-of expression tests. However, in this research, the titration tests were not performed the day-of the expressions and so, the chemistry of the pore solutions may have changed during the time of storage.
- It was observed that 280 days were insufficient for the chlorides in the ponding wells of the concrete specimens of 0.4 w/cm ratio to ingress in the concrete cover of 25mm (1 inch). Therefore, further investigation is recommended for conclusive results on the corrosion performance of the rebar in the concretes of the various mixes. However, for future works with time restrictions, the concrete mix can be modified to allow for quicker chloride diffusion by increasing the permeability, such as by increasing the w/cm ratio, or decreasing the concrete cover. The increase of the chloride solution from 3% NaCl to 5.75% NaCl was intended to accelerate the chloride diffusion, but if time is not too restrained, the 3% NaCl solution can be kept throughout the testing for the carbon steel reinforced concrete specimens, as the concentration simulates conditions closest to sea water^[117].

6.5 Recommendations for Future Works

While the current research focused on the corrosion behaviour of carbon steel rebar, the motivation of the research is promoting the use of greener cement mixes for sustainability without

compromising the durability of the reinforced concrete. Therefore, the current research is but a small step in encouraging the bigger picture of global carbon savings by promoting the industrial use of PLC with high levels of GBFS, in North American countries, as alternatives to reducing the carbon footprint of cement production. While the PLC was found to produce comparable results with the OPC, the findings were specific to the materials used in this study and thus, it is recommended to repeat the experiments on PLC based on different national standards, such as the equivalent EN 197 Type CEM II PLC which allows for up to 35% limestone replacement by mass of the cement. Although the high GBFS was found to have direct detriment on the rebar corrosion due to its pore solution chemistry, the cement mixes with GBFS replacements as high as 50% can be adopted with ample concrete cover depths and/or the use of more corrosion resistant reinforcement options. In addition, with the declining availability of the most common SCMs, such as fly ash due to the abandonment of coal fired power plants for sustainability perspectives and GBFS due to the increasing use of steel arc furnaces instead of the blast furnace in iron production plants, future research on even greener cement alternatives is recommended. One such alternative comprises agricultural wastes, such as the rice husks, corn cobs and bamboo leaves. To obtain the powdered ash forms for replacement of cement, heating processes are inevitable, but the process may not be as intensive as the kiln process at 1500°C for cement production.

The experiments in the current research were run for durations which were short-term in comparison to the service lives of reinforced concrete structures. Therefore, it is recommended to consider performing life cycle assessments to better evaluate the time-dependent changes in the concrete properties and conditions for the different concrete mixes.

References

- [1] Greene T., Jacobs P. (Jan. 2021). 2021 Tied for 6th Warmest Year in Continued Trend, NASA Analysis Shows. National Aeronautics and Space Administration (NASA) Climate News. Retrieved from : <https://climate.nasa.gov/news/3140/2021-tied-for-6th-warmest-year-in-continued-trend-nasa-analysis-shows/>
- [2] Schmunk R. (Nov. 2021). 595 people were killed by heat in B.C. this summer, new figures from coroner show. CBC News, Canada. Retrieved from : <https://www.cbc.ca/news/canada/british-columbia/bc-heat-dome-sudden-deaths-revised-2021-1.6232758>
- [3] Taylor A. (Feb. 2021). Texas's cold-weather catastrophe is a global warning. The Washington Post, United States of America. Retrieved from : <https://www.washingtonpost.com/world/2021/02/18/texas-cold-global-climate-change/>
- [4] Conlen M. (Jul. 2021). How Much Carbon Dioxide Are We Emitting? – Visualizing the Quantities of Climate Change. National Aeronautics and Space Administration (NASA) Climate News. Retrieved from : <https://climate.nasa.gov/news/3020/how-much-carbon-dioxide-are-we-emitting/>
- [5] Friedlingstein, P., Jones, M. et al. (2021). Global Carbon Budget 2021. DOI : 10.5194/essd-2021-386
- [6] Rodgers L. (Dec. 2018). Climate change: The massive CO2 emitter you may not know about. BBC News Science. Retrieved from : <https://www.bbc.com/news/science-environment-46455844#:~:text='Clinker'%20%2D%20the%20big%20polluter&text=In%202016%2C%20world%20cement%20production,to%20the%20production%20of%20clinker.>
- [7] Innis A. et al. (Oct. 2018). Portland-Limestone Cement after 10 Years in the Field. CP Road Map – Track 6: Moving Advancements into Practice. Retrieved from : <https://intrans.iastate.edu/app/uploads/2019/10/MAPbriefOctober2018.pdf>
- [8] Gupta, S., Mohapatra, B. N., & Bansal, M. (2020). A review on development of Portland limestone cement: A step towards low carbon economy for Indian cement industry. Current Research in Green and Sustainable Chemistry, 3(September), 100019. <https://doi.org/10.1016/j.crgsc.2020.100019>
- [9] IEA (2021). Cement, IEA, Paris. Retrieved from : <https://www.iea.org/reports/cement>
- [10] Canadian Standards Association (2019). CSA S6-2019 : Canadian Highway Bridge Design Code.
- [11] Kropp J. (1999). Permeability of Concrete as a Criterion of its Durability. Materials and Structures/Matériaux et Constructions, 32(April), 5.
- [12] Prokopy S. (Feb. 2012). Low-CO2 Portland Limestone Cement for Canadian Pavement Construction. Retrieved from : <https://cementproducts.com/2012/02/09/low-co2-portland-limestone-cement-for-canadian-pavement-construction/>

- [13] Poudyal, L., Adhikari, K., & Won, M. (2021). Mechanical and durability properties of portland limestone cement (PLC) incorporated with nano calcium carbonate (CaCO₃). *Materials*, 14(4), 1–19. <https://doi.org/10.3390/ma14040905>
- [14] Warkus J., & Raupach M. (2010). Modelling of reinforcement corrosion – geometrical effects on macrocell corrosion. 6, 494–504. <https://doi.org/10.1002/maco.200905437>
- [15] Daniyal, M., & Akhtar, S. (2020). Corrosion assessment and control techniques for reinforced concrete structures: a review. *Journal of Building Pathology and Rehabilitation*, 5(1), 1–20. <https://doi.org/10.1007/s41024-019-0067-3>
- [16] Abrams, D. A. (1925). The Contribution of Scientific Research to the Development of the Portland Cement Industry in the United States. *The ANNALS of the American Academy of Political and Social Science*, 119(1), 40–47. <https://doi.org/10.1177/000271622511900107>
- [17] Rahman F. U. (2009). Manufacture of Cement – Materials and Manufacturing Process of Portland Cement. *The Constructor – Building Technology Guide*. Retrieved from : <https://theconstructor.org/building/manufacture-of-cement/13709/>
- [18] Ontario Provincial Standard Specification (2018). OPSS 1002 – 2018 : Material Specification for Aggregates – Concrete
- [19] Hanley S. (2020). Reducing Emissions From Cement & Steel Production. *CleanTechnica*. Retrieved from : <https://cleantechnica.com/2020/09/14/reducing-emissions-from-cement-and-steel-production/>
- [20] Moir, G. (2003). Cements. In *Advanced Concrete Technology* (pp. 3–45). Elsevier. <https://doi.org/10.1016/B978-075065686-3/50277-9>
- [21] Soroka, I. (1979). *Portland Cement Paste & Concrete*. The Macmillan Press Ltd.
- [22] Huang L., & Yan P. (2019). Effect of alkali content in cement on its hydration kinetics and mechanical properties. *Construction and Building Materials*, 228, 116833. <https://doi.org/10.1016/j.conbuildmat.2019.116833>
- [23] Portland Cement Association (2001). *Ettringite Formation and the Performance of Concrete*, IS417.
- [24] American Society for Testing and Materials (2016). *ASTM C595 – 16 : Standard Specification for Blended Hydraulic Cements*
- [25] Locher F. W., Richartz W., & Sprung S. (1976). Setting of cement, Part I. Reaction and development of structure, *Zement-Kalk-Gips*, 29, pp. 435–442.
- [26] Voglis, N., Kakali, G., Chaniotakis, E., & Tsvivilis, S. (2005). Portland-Limestone Cements. Their Properties and Hydration Compared to Those of Other Composite Cements. *Cement and Concrete Composites*, 27(2), 191–196. doi:10.1016/j.cemconcomp.2004.02.006
- [27] Canadian Standards Association (2018). *CSA A3001 : Cementitious Materials for Use in Concrete*
- [28] European Standards (2011). *BS EN197-2:2011 : Cement Compositions, Specifications and Conformity Criteria for Common Cements*

- [29] Livesey, P. (1991). Strength characteristics of Portland-limestone cements. *Construction and Building Materials*, 5(3), 147–150. [https://doi.org/10.1016/0950-0618\(91\)90065-S](https://doi.org/10.1016/0950-0618(91)90065-S)
- [30] Wang X. Y. (2017). Modeling of Hydration, Compressive Strength, and Carbonation of Portland-Limestone Cement (PLC) Concrete. *Materials (Basel, Switzerland)*, 10(2), 115. <https://doi.org/10.3390/ma10020115>
- [31] Ramezani-pour, A. M., & Hooton, R. D. (2014). A study on hydration, compressive strength, and porosity of Portland-limestone cement mixes containing SCMs. *Cement and Concrete Composites*, 51, 1–13. <https://doi.org/10.1016/j.cemconcomp.2014.03.006>
- [32] Péra, J., Husson, S., & Guilhot, B. (1999). Influence of finely ground limestone on cement hydration. *Cement and Concrete Composites*, 21(2), 99–105. [https://doi.org/10.1016/S0958-9465\(98\)00020-1](https://doi.org/10.1016/S0958-9465(98)00020-1)
- [33] HDS IP Holding LLC (2022). Hach Company Bromcresol Green-Methyl Red Indicator Solution, 500mL. USABlueBook. Retrieved from : <https://www.usabluebook.com/p-312284-or-hach-bromcresol-green-methyl-red-indicatorsbquo-500mlsbquo-2329249.aspx>
- [34] Berodier E., & Scrivener K. (2014). Understanding the Filler Effect on the Nucleation and Growth of C-S-H. *Journal of the American Ceramic Society*. 97(12):3764-3773. doi:10.1111/jace.13177
- [35] Ontario Provincial Standard Specification (2019). OPSS 1350 – 2019 : Material Specification for Concrete – Materials and Production
- [36] American Society for Testing and Materials (2014). ASTM C989 – 14 : Standard Specification for Slag Cement for Use in Concrete and Mortars
- [37] Sun J., Kong K. H., Lye C. Q., & Quek S. T (2021). Effect of ground granulated blast furnace slag on cement hydration and autogenous healing of concrete. *Construction & building materials*. 2022;315:125365-. doi:10.1016/j.conbuildmat.2021.125365
- [38] Cahyani, R. A. T., & Rusdianto, Y. (2021). An Overview of Behaviour of Concrete with Granulated Blast Furnace Slag as Partial Cement Replacement. *IOP Conference Series: Earth and Environmental Science*, 933(1). <https://doi.org/10.1088/1755-1315/933/1/012006>
- [39] Heikal, M., Morsy, M. & Eldidamony, H. (2001). Effect of limestone on the hydration characteristics of Portland slag cement. 71. 350-351+422.
- [40] Neville A. M. (2011). *Properties of Concrete*. Pearson Education Ltd. pp. 120-145
- [41] Locher F. W. (2013). *Cement : Principles of Production and Use*. Verlag Bau+Technik.
- [42] American Concrete Institute (2014). *ACI 318-14 : Building Code Requirements for Structural Concrete*.
- [43] Ghods P, Isgor O., McRae G., Li J., & Gu G. (2011). Microscopic investigation of mill scale and its proposed effect on the variability of chloride-induced depassivation of carbon steel rebar. *Corrosion science*. 53(3):946-954. doi:10.1016/j.corsci.2010.11.025

- [44] Karadakis K., Azad V. J., Ghods P., & Isgor O. B. (2016). Numerical Investigation of the Role of Mill Scale Crevices on the Corrosion Initiation of Carbon Steel Reinforcement in Concrete. *Journal of the Electrochemical Society*. 163(6):C306-C315. doi:10.1149/2.0731606jes
- [45] Zhou Y., Gencturk B., Willam K., & Attar A. (2015). Carbonation-Induced and Chloride-Induced Corrosion in Reinforced Concrete Structures. *Journal of materials in civil engineering*. 27(9):1-. doi:10.1061/(ASCE)MT.1943-5533.0001209
- [46] Poursaei, A., & Hansson, C. M. (2009). Potential pitfalls in assessing chloride-induced corrosion of steel in concrete. *Cement and Concrete Research*, 39(5), 391–400. <https://doi.org/10.1016/j.cemconres.2009.01.015>
- [47] Hansson C., Poursaei A., & Laurent A. (2006). Macrocell and microcell corrosion of steel in ordinary Portland cement and high performance concretes. *Cement and concrete research*. 36(11):2098-2102. doi:10.1016/j.cemconres.2006.07.005
- [48] Pourbaix M. (1974). *Atlas of Electrochemical Equilibria in Aqueous Solutions*. National Association of Corrosion Engineers.
- [49] DorMohammadi H., Pang Q., Murkute P. et. al. (2019). Investigation of chloride-induced depassivation of iron in alkaline media by reactive force field molecular dynamics. *npj Mater Degrad* 3, 19. <https://doi.org/10.1038/s41529-019-0081-6>
- [50] Jaffer S. J., & Hansson C.M. (2009). Chloride-induced corrosion products of steel in cracked-concrete subjected to different loading conditions. *Cement and concrete research*. 39(2):116-125. doi:10.1016/j.cemconres.2008.11.001
- [51] Lawrence C. D. (1990). Sulphate attack on concrete. *Magazine of concrete Research*, 42(153), 249-264.
- [52] Hou X., Powers L., Lawler J., & Koray T. (2015). Thaumassite Sulfate Attack: Case Studies and Implications. *ICMA Proceedings*, October 2016.
- [53] Barneyback R., & Diamond S. (1981). Expression and analysis of pore fluids from hardened cement pastes and mortars. *Cement and concrete research*. 11(2):279-285. doi:10.1016/0008-8846(81)90069-7
- [54] Duchesne J., Bérubé M. (1994). Evaluation of the validity of the pore solution expression method from hardened cement pastes and mortars. *Cement and concrete research*. 24(3):456-462. doi:10.1016/0008-8846(94)90132-5
- [55] Ghods P., Isgor O. B., McRae G., & Miller T. (2009). The Effect of Concrete Pore Solution Composition on The Quality of Passive Oxide Films on Black Steel Reinforcement. *Cement and Concrete Composites*, 31(1), 2–11. <https://doi.org/10.1016/j.cemconcomp.2008.10.003>
- [56] Vollpracht A., Lothenbach B., Snellings R. et al. (2016). The pore solution of blended cements: a review. *Mater Struct* 49, 3341–3367. <https://doi.org/10.1617/s11527-015-0724-1>
- [57] Andersson K., Allard B., Bengtsson M., & Magnusson B. (1989). Chemical Composition of Cement Pore Solutions. *Cement and Concrete Research*, 19(3), 327–332. [https://doi.org/10.1016/0008-8846\(89\)90022-7](https://doi.org/10.1016/0008-8846(89)90022-7)

- [58] Tritthart J. (1989). Chloride binding in cement I. Investigations to determine the composition of porewater in hardened cement. *Cement and concrete research*, 19(4):586-594. doi:10.1016/0008-8846(89)90010-0
- [59] Lothenbach B., Winnefeld F., Alder C., Wieland E., Lunk P. (2007). Effect of temperature on the pore solution, microstructure and hydration products of Portland cement pastes. *Cement and concrete research*, 37(4):483-491. doi:10.1016/j.cemconres.2006.11.016
- [60] Van Niejenhuis C. B., Ogunsanya I. G., & Hansson C. M. (2020). Analysis of pore solution of different cements with and without admixed chlorides. *ACI Materials Journal*, 117(3), 21–28. <https://doi.org/10.14359/51724590>
- [61] Potgieter J. H., Delport D. J., Verryn S., & Potgieter-Vermaak S. S. (2011). Chloride-binding effect of blast furnace slag in cement pastes containing added chlorides. *South African Journal of Chemistry*, 64, 108–114.
- [62] McCafferty E. (2010). *Introduction to Corrosion Science*. Springer Science & Business Media.
- [63] United States Environmental Protection Agency (2017). EPA Method 6010C: Inductively Coupled Plasma-Atomic Emission Spectrometry. United States of America, 2017.
- [64] United States Environmental Protection Agency (2017). EPA Method 6020A: Inductively Coupled Plasma - Mass Spectrometry. United States of America, 2017.
- [65] Chopperla K. S. T., Smith J. A., & Ideker J. H. (2021). The efficacy of portland-limestone cements with supplementary cementitious materials to prevent alkali-silica reaction. *Cement*, Volume 8, 100031, ISSN 2666-5492. <https://doi.org/10.1016/j.cement.2022.100031>
- [66] Thomas M. D., Hooton D., Cail K., Smith B. A., de Wal J., & Kazanis K. G. (2010). Field trials of concrete produced with Portland limestone cement. *Concrete international*, 32(1), 35-41.
- [67] American Society for Testing and Materials (2014). ASTM G59 – 97 (Reapproved 2014) : Standard Test Method for Conducting Potentiodynamic Polarization Resistance Measurements.
- [68] American Society for Testing and Materials (2013). ASTM G109 – 07 (Reapproved 2013) : Standard Test Method for Determining Effects of Chemical Admixtures on Corrosion of Embedded Steel Reinforcement in Concrete Exposed to Chloride Environments.
- [69] Garcia J. E., Tiburzi N. B., Folliard K. J., & Drimalas T. (2022). Mechanical properties and electrical resistivity of portland limestone cement concrete systems containing greater than 15% limestone and supplementary cementitious materials. *Cement*, Volume 8, 100026. <https://doi.org/10.1016/j.cement.2022.100026>
- [70] Bharadwaj K., Isgor O. B., & Weiss W. J. (2022). Supplementary Cementitious Materials in Portland-Limestone Cements. *ACI Materials Journal*, 119(2), 141+.
- [71] Thomas M. D. A., Cail K., Blair B., Delagrave A., Masson P., & Kazanis K. (2010). Use of low-CO₂ Portland limestone cement for pavement construction in Canada. *International Journal of Pavement Research and Technology*, 3(5), 228.

- [72] Tosun-Felekoğlu K. (2012). The effect of C3A content on sulfate durability of Portland limestone cement mortars. *Construction and Building Materials* (36), p437-447. <https://doi.org/10.1016/j.conbuildmat.2012.04.091>
- [73] Goñi S., & Andrade C. (1990). Synthetic concrete pore solution chemistry and rebar corrosion rate in the presence of chlorides. *Cement and Concrete Research*, 20(4), 525–539. [https://doi.org/10.1016/0008-8846\(90\)90097-H](https://doi.org/10.1016/0008-8846(90)90097-H)
- [74] Sotiriadis K., Rakanta E., Mitzithra M. E., Batis G., & Tsivilis S. (2019). Chloride-Related Phenomena in Limestone Cement Materials: Effect of Mineral Admixtures and Sulfates. *ACI Materials Journal*, 116(6), 19–30. <https://doi.org/10.14359/51716820>
- [75] Broomfield J. P. (2006). *Corrosion of Steel in Concrete: Understanding, Investigation and Repair*, Second edition. CRC Press, Boca Raton, Florida.
- [76] Plusquellec G., Geiker M. R., Duchesne J., Lindgård J., & De Weerd K. (2016). Review of methods to determine the pH and the free alkali content of the pore solution in concrete. 15th International Conference on Alkali-Aggregate Reactions (ICAAR)
- [77] Moragues A., Macias A., & Andrade C. (1986). Equilibria of the Chemical Composition of the Concrete Pore Solution. Part I : Comparative Study of Synthetic and Extracted Solutions. *Equilibria, Pore Solutions, Theory*. Volume 17, p.173-182
- [78] Yu, Chiang K.-T. K., & Yang L. (2012). Threshold chloride level and characteristics of reinforcement corrosion initiation in simulated concrete pore solutions. *Construction & Building Materials*, 26(1), 723–729. <https://doi.org/10.1016/j.conbuildmat.2011.06.079>
- [79] Moreno, Morris, W., Alvarez M., & Duffó, G. (2004). Corrosion of reinforcing steel in simulated concrete pore solutions: Effect of carbonation and chloride content. *Corrosion Science*, 46(11), 2681–2699. <https://doi.org/10.1016/j.corsci.2004.03.013>
- [80] Jau, & Tsay D. S. (1998). A study of the basic engineering properties of slag cement concrete and its resistance to seawater corrosion. *Cement and Concrete Research*, 28(10), 1363–1371. [https://doi.org/10.1016/S0008-8846\(98\)00117-3](https://doi.org/10.1016/S0008-8846(98)00117-3)
- [81] Dhir R. K., Limbachiya M. C., McCarthy M. J., & Chaipanich A. (2007). Evaluation of Portland Limestone Cements for Use in Concrete Construction. *Materials and Structures*, 40(5), 459–473. <https://doi.org/10.1617/s11527-006-9143-7>
- [82] Courard L., Herfort D., & Villagran Y. (2016). Performances of Limestone Modified Portland Cement and Concrete. In *University of Liège ULiège (Vol. 1, Issue 2001)*. [https://orbi.uliege.be/bitstream/2268/200184/1/Report on the performance of Portland limestone cements in concrete_20160401.pdf](https://orbi.uliege.be/bitstream/2268/200184/1/Report%20on%20the%20performance%20of%20Portland%20limestone%20cements%20in%20concrete_20160401.pdf)
- [83] Ouyang X., Koleva D. A., Ye G., & van Breugel K. (2017). Insights into the mechanisms of nucleation and growth of C–S–H on fillers. *Materials and Structures/Materiaux et Constructions*, 50(5), 1–13. <https://doi.org/10.1617/s11527-017-1082-y>
- [84] Nadelman E. I., & Kurtis K. E. (2017). Application of Powers’ model to modern portland and portland limestone cement pastes. *Journal of the American Ceramic Society*, 100(9), 4219–4231. <https://doi.org/10.1111/jace.14913>


- [85] Vuk Tinta V., Gabrovšek R., & Kaučič V. (2001). The effects of limestone addition, clinker type and fineness on properties of Portland cement. *Cement and Concrete Research*, 31(1), 135–139. [https://doi.org/10.1016/S0008-8846\(00\)00427-0](https://doi.org/10.1016/S0008-8846(00)00427-0)
- [86] Tosun K., Felekoğlu B., Baradan B., & Altun I. A. (2009). Portland Limestone Cement Part 1 - Preparation of Cements. *Teknik Dergi/Technical Journal of Turkish Chamber of Civil Engineers*, 20(3), 4717–4736. <https://doi.org/10.18400/td.17436>
- [87] Hwang C-L., & Lin C.-Y. (1986). Strength development of blended blast-furnace slag-cement mortars. *Journal of the Chinese Institute of Engineers*, 9(3), 233–239. <https://doi.org/10.1080/02533839.1986.9676884>
- [88] Hogan F., & Meusel J. (1981). Evaluation for Durability and Strength Development of a Ground Granulated Blast Furnace Slag. *Cement, Concrete, and Aggregates*, 3(1), 40–52. <https://doi.org/10.1520/CCA10201J>
- [89] Yeau K. Y., & Kim E. K. (2005). An experimental study on corrosion resistance of concrete with ground granulate blast-furnace slag. *Cement and Concrete Research*, 35(7), 1391–1399. <https://doi.org/10.1016/j.cemconres.2004.11.010>
- [90] Pareek R. K., & Singh V. (2015). Utilization of Ground Granulated Blast Furnace Slag to Improve Properties of Concrete. *International Journal on Emerging Technologies*, 6(2), 72–79.
- [91] Alonso C., Andrade C., Castellote M., & Castro P. (2000). Chloride threshold values to depassivate reinforcing bars embedded in a standardized OPC mortar. *Cement and Concrete Research*, 30(7), 1047–1055. [https://doi.org/10.1016/S0008-8846\(00\)00265-9](https://doi.org/10.1016/S0008-8846(00)00265-9)
- [92] Bentz D. P. (2006). Influence of water-to-cement ratio on hydration kinetics: Simple models based on spatial considerations. *Cement and Concrete Research*, 36(2), 238–244.
- [93] Slamečka T., & Škvára F. (2002). The effect of water ratio on microstructure and composition of the hydration products of portland cement pastes. *Ceramics (Praha)*, 46(4), 152–158
- [94] Böhni H. (2005). *Corrosion in reinforced concrete structures*. Woodhead Publishing Ltd. and CRC Press LLC, 1-45.
- [94] Böhni H. (2005). *Corrosion in reinforced concrete structures*. Woodhead Publishing Ltd. and CRC Press LLC, 1-45.
- [96] Diab A. M., Aliabdo A. A., & Mohamed I. A. (2015). Corrosion Behaviour of Reinforced Steel in Concrete with Ground Limestone Partial Cement Replacement. *Magazine of Concrete Research*, 67(14), 747–761. <https://doi.org/10.1680/macr.14.00156>
- [97] Liu G., Zhang Y., Ni Z., & Huang R. (2016). Corrosion Behaviour of Steel Submitted to Chloride and Sulphate Ions in Simulated Concrete Pore Solution. *Construction and Building Materials*, 115, 1–5. <https://doi.org/10.1016/j.conbuildmat.2016.03.213>
- [98] Li C., Jiang L., & Li S. (2020). Effect of Limestone Powder Addition on Threshold Chloride Concentration for Steel Corrosion in Reinforced Concrete. *Cement and Concrete Research*, 131(March), 106018. <https://doi.org/10.1016/j.cemconres.2020.106018>

- [99] Panesar D. K., & Zhang R. (2020). Performance Comparison of Cement Replacing Materials In Concrete: Limestone Fillers And Supplementary Cementing Materials – A Review. *Construction and Building Materials*, 251, 118866.
- [100] Hansen B. S., Howard I. L., Shannon J., Cost T., & Wilson W. M. (2020). Portland-limestone cement fineness effects on concrete properties. *ACI Materials Journal*, 117(2), 157–168. <https://doi.org/10.14359/51720301>
- [101] Proske T., Rezvani M., Palm S., Müller C., & Graubner C. A. (2018). Concretes made of efficient multi-composite cements with slag and limestone. *Cement and Concrete Composites*, 89, 107–119. <https://doi.org/10.1016/j.cemconcomp.2018.02.012>
- [102] Cheytani M., & Chan S. L. I. (2021). The applicability of the Wenner method for resistivity measurement of concrete in atmospheric conditions. *Case Studies in Construction Materials*, 15(June), e00663. <https://doi.org/10.1016/j.cscm.2021.e00663>
- [103] proceq (2017). Operating Instructions – Concrete Durability Testing. resipod family Product ID 82038104E
- [104] Newton C. J., & Sykes J. M. (1988). A galvanostatic pulse technique for investigation of steel corrosion in concrete. *Corrosion Science*. 28(11): pp. 1051-1074
- [105] Stern M., & Geary A. L. (1957). Electrochemical Polarization – A Theoretical Analysis of the Shape of Polarization Curves. *Journal of the Electrochemical Society*. 104(1): pp. 56-63.
- [106] Raczkiwicz W., & Wójcicki A. (2021). Using the galvanostatic pulse method to estimate the corrosion of reinforcement in structural elements. *South Florida Journal of Development*, 2(3), 4865–4876. <https://doi.org/10.46932/sfjdv2n3-080>
- [107] Babler R., & Burkert A. (2003). GPM-Portable Equipment For Determination Of Corrosion Stage Of Concrete Structures - Laboratory And On-Site Experiences. *Non-Destructive Testing in Civil Engineering*, Germann Instruments.
- [108] Chen Zewu & Gibson Walter & Huapeng Huang. (2008). High Definition X-Ray Fluorescence: Principles and Techniques. *X-Ray Optics and Instrumentation*. 2008. 10.1155/2008/318171.
- [109] Scott A., & Alexander M. G. (2016). Effect of supplementary cementitious materials (binder type) on the pore solution chemistry and the corrosion of steel in alkaline environments. *Cement and Concrete Research*, 89, 45–55. <https://doi.org/10.1016/j.cemconres.2016.08.007>
- [110] Kristufek L. C. L. (2020). The Effect of De-icing Salts on the Chemistry of the Pore Solution in Cement Pastes and Their Influence on Rebar Corrosion. University of Waterloo, Ontario, Canada.
- [111] American Society for Testing and Materials (20148). ASTM C114 - 18 : Standard Test Methods for Chemical Analysis of Hydraulic Cement.
- [112] Hong S. Y., & Glasser F. P. (1999). Alkali binding in cement pastes : Part I. The C-S-H phase. *Cement and Concrete Research*, 29(12), 1893–1903. [https://doi.org/10.1016/S0008-8846\(99\)00187-8](https://doi.org/10.1016/S0008-8846(99)00187-8)

- [113] Kovac S., & Konopatzki P. (2018). Utilization of Portable X-Ray Fluorescence-Spectrometers for the Registration of Contaminated Sites in Vietnam Utilization of Portable X-Ray Fluorescence- Spectrometers for the Registration of Contaminated Sites in Vietnam Authors : 1–16.
- [114] Gulikers J. J. . (1996). Experimental investigations on macro cell corrosion in chloride-contaminated concrete. Heron.
- [115] Kunther W., Ferreiro S., & Skibsted J. (2017). Influence of the Ca/Si ratio on the compressive strength of cementitious calcium-silicate-hydrate binders. *Journal of Materials Chemistry A*, 5(33), 17401–17412. <https://doi.org/10.1039/c7ta06104h>
- [116] Bakker R.M., (1983) Permeability of Blended Cement Concretes, Proceedings of 1st International Conference on the use of Fly Ash, Silica Fume, Slag and other Mineral By-Products in Concrete., Editor: V. M. Malhotra, Montebello, Canada
- [117] Poursaee A. (2016). Corrosion of Steel in Concrete Structures - Chapter 2 : Corrosion of Steel in Concrete Structures. Ed: A. Poursaee, Woodhead Publishing Series in Civil and Structural Engineering.

Appendices

Appendix A - Material Information



St. Marys Cement

Great Lakes Region
 St Marys Plant
 P.O. Box 1000
 585 Water Street South
 St. Marys, ON
 N4X 1B6
 (519) 284-1020
 (519) 284-4104

Mill Test Report - CSA A3001 Type GU March 01, 2017 to March 31, 2017

Chemical Data		Physical Data	
Loss on Ignition	2.4 %	Fineness	Blaine SA 386 m ² /kg
SiO ₂	19.8 %		Retained 325 4.1 %
Fe ₂ O ₃	2.62 %	Normal Consistency	26.0 %
Al ₂ O ₃	4.5 %	Autoclave Expansion	0.16 %
CaO	62.5 %	Air Content	8 %
Free CaO	1.1 %	Sulphate Expansion	0.010 %
MgO	3.3 %	Vicat	Initial 112 Min.
SO ₃	3.41 %		Final 231 Min.
K ₂ O	0.48 %		
Na ₂ O	0.26 %		
TiO ₂	0.27 %		
Insoluble Residue	0.23 %		
Total Alkali as Na ₂ O	0.58 %		

Calculated Compounds

C ₂ S	17 %
C ₃ S	52 %
C ₃ A	8 %
C ₄ AF	8 %

Compressive Strengths

Age	MPa	PSI
1-Day	13.9	2016
3-Day	23.9	3466
7-Day	32.4	4699
28-Day	44.0	6382

Previous Month's 28 Day Avg

Testing methods and equipment comply with the requirements of the A3000 Compendium Specifications A3003, A3004 and A3005. This Mill Test certifies this product to meet all the Standard Chemical and Physical requirements of CSA A3001 for Type GU Cement.

April 17, 2017
 St. Marys Cement

April Innes
 QC Supervisor

Figure A.1 Manufacturer's mill certificate for GU cement/OPC used in this research



**CERTIFICATE OF ANALYSIS: MISSISSAUGA PLANT
CSA: PORTLAND-LIMESTONE CEMENT GENERAL USE (TYPE GUL)**

		ANALYSIS OF: Jul-2020	
CSA-A3001-18 REQUIREMENTS		LIMITS	RESULTS
			TEST METHOD
PHYSICAL	Fineness 45 µm Sieve (%) Retained	≤ 28	4
	Autoclave % Expansion	≤ 1	0.05
	Sulphate Expansion (%) *	≤ 0.020	0.008
	Initial Time of Set (min)	45 ≤ (min) ≤ 375	143
	Blaine (m ² /kg)		519
	Air Content (%)		8
	Compressive Strengths at 1-day (MPa)		19.3
	Compressive Strengths at 3-day (MPa)	≥ 14.5	29.4
	Compressive Strengths at 7-day (MPa)	≥ 20.0	33.6
	Compressive Strengths at 28-day (MPa) *	≥ 26.5	41.6
CHEMICAL	Loss on Ignition (LOI) (%)	≤ 10.0	5.0
	Sulphur Trioxide (SO ₃) (%) **	≤ 3.0	3.9
	Magnesium Oxide (MgO) (%)		2.3
	Silica Oxide (SiO ₂) (%)		19.0
	Alumina Oxide (Al ₂ O ₃) (%)		5.1
	Iron Oxide (Fe ₂ O ₃) (%)		2.1
	Calcium Oxide (CaO) (%)		60.1
	Total Alkali (%)		0.86
	Free Lime (%)		1.0
	C ₃ S (%)		52
C ₂ S (%)		15	
C ₃ A (%)		10	
C ₄ AF (%)		7	
COMMENTS:			
Parameters with no limit listed are included for information purposes only, and are not requirements of the standards.			
* Indicates result from previous month.			
** Compliant with A3004-C5 Test method for determination of expansion of hydraulic cement mortar bars due to internal cement sulphate attack limit of 0.020%.			
This certifies compliance with CSA-A3001-18 General Use Portland-Limestone Cement.			
The data is typical of product shipped by Ash Grove, a Division of CRH Canada Group Inc.. Individual shipments may vary.			
REPORT PREPARED BY:		PRINT DATE:	
<i>Bruno Morgado</i>			
Bruno Morgado, Quality Manager		August 21, 2020	

Ash Grove Cement Company (a CRH Company), Mississauga Cement Plant, 2391 Lakeshore Road West, Mississauga ON, L5J 1K1

Figure A.2 Manufacturer's mill certificate for GUL cement/PLC used in this research

Appendix B - Extra Information on Tests based on Expressed Pore Solutions

B.1 Sample Calculations for Interpreting Titration Results as pH for Pore Solutions

Re: Sample 25SGUL0Cl (1). Given that 22.5ml of 0.02N H₂SO₄ titrant was used to neutralize 1mL of the expressed pore solution sample (diluted to 50mL):

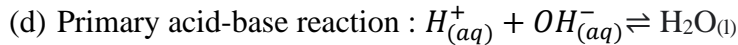
(a) No. of moles of H₂SO₄ used in titration = $22.5\text{mL} * \frac{0.01\text{mol}}{1000\text{mL}} = 0.000225$ moles H₂SO₄

(b) Noting that the titration was performed until the endpoint of the bromocresol green-methyl red indicator (i.e. pH 4.6 to 5.2 ~ taking average as pH 4.9).
0.000225 moles of 0.02N acid reduce pH of 1 ml pore solution from pH *x* to 4.9



Based on 1 H₂SO_{4(aq)} : 2H⁺_(aq), No. of moles of H⁺ introduced by used titrant =
0.00045 moles H⁺

So, 0.00045 moles H⁺ reduce pH of 1 ml pore solution from pH *x* to 4.9



Therefore, 1ml pore solution contains $2*(0.000225 + 10^{-4.9})$ moles OH⁻ =

$$2*(0.000225 + 0.00001259) = 0.00047518 \text{ moles OH}^-$$

So, 0.47518mol/litre = pH (14 - (-log₁₀ (0.47518))) = 14 - 0.3718 = pH **13.677**

B.2 Sample Calculations for Determining Bound Chlorides from Evapourable Water

Re: Sample 25SGUL1.0Cl. Assume negligible water loss from casting, through curing for 28 days, to post-demoulding preparations of the cement paste cylinders for powdering to 10±0.5g for the evapourable water test. Given that after 24 hours of heating at 105°C, the post-heated mass was measured to be an average of 8.18g (m_d):

(a) For the 25BFSGUL1.0Cl mix, the averaged total evapourable water as a mass, W_e = mass before heating – m_d = 2.30g

(b) Evapourable water concentration, as a ratio to the post-heated sample mass, $w_e = \frac{W_e}{m_d} = \frac{2.30}{7.89} = 0.292$

(c) Per chemical IC analysis, 13,203.91 $\frac{\text{mg}}{\text{L}}$ Cl⁻ detected in pore solution sample. To express as % of pore solution (assuming like water, density = 1g/1mL), $Cl_{ps} = \frac{13203.91 * 10^{-3} \text{g}}{10^3 \text{mL}} * \frac{1 \text{mL}}{1 \text{g}} * 100\% = 1.32\%$

(d) To express as wt. % of mass of dry cement Cl_{free} = Cl_{ps} * w_e = 1.32% x 0.292 = 0.385%. Therefore, 0.385% of the chlorides that were added to the cement mix were present as “free” chlorides in the pore solution.

(e) So, bound chlorides, as % of the mass of the cm., $Cl_{\text{bound}} = Cl_{\text{admixed}} - Cl_{\text{free}} = 1.0 - 0.385 = 0.615\%$

B.3 Averaged Evapourable Water Measurements and Titration Alkalinities

Sample Type	Averaged Evapourable Water (fractioned by mass of dry cement)	Averaged Total Alkalinity [g/L CaCO ₃]
0BFSGUL_0Cl	0.27	29.63
0BFSGUL_0.1Cl	0.28	31.90
0BFSGUL_0.2Cl	0.26	33.73
0BFSGUL_0.5Cl	0.28	38.25
0BFSGUL_0.75Cl	0.28	36.48
0BFSGUL_1.0Cl	0.29	35.55
25SGUL_0Cl	0.26	22.25
25SGUL_0.1Cl	0.28	23.30
25SGUL_0.2Cl	0.29	25.42
25SGUL_0.5Cl	0.28	28.20
25SGUL_0.75Cl	0.29	28.90
25SGUL_1.0Cl	0.29	28.20
25SGU_0Cl	0.27	24.22
25SGU_0.1Cl	0.28	27.05
25SGU_0.2Cl	0.27	28.70
25SGU_0.5Cl	0.29	31.17
25SGU_0.75Cl	0.27	31.55
25SGU_1.0Cl	0.28	30.48
35SGUL_0Cl	0.29	18.02
35SGUL_0.1Cl	0.28	19.63
35SGUL_0.2Cl	0.27	20.68
35SGUL_0.5Cl	0.29	23.62
35SGUL_0.75Cl	0.28	23.15
35SGUL_1.0Cl	0.28	26.37
35SGU_0Cl	0.26	21.48
35SGU_0.1Cl	0.29	23.93
35SGU_0.2Cl	0.29	26.13
35SGU_0.5Cl	0.23	27.12
35SGU_0.75Cl	0.27	27.48
35SGU_1.0Cl	0.27	26.93
50SGUL_0Cl	0.30	13.65
50SGUL_0.1Cl	0.30	15.12
50SGUL_0.2Cl	0.30	15.98

50SGUL_0.5Cl	0.29	17.48
50SGUL_0.75Cl	0.29	17.20
50SGUL_1.0Cl	0.29	17.55
50SGU_0Cl	0.29	15.22
50SGU_0.1Cl	0.30	16.88
50SGU_0.2Cl	0.29	17.05
50SGU_0.5Cl	0.29	20.32
50SGU_0.75Cl	0.29	20.37
50SGU_1.0Cl	0.30	19.63

B.4 Major Chemical Concentrations of Expressed Pore Solutions, by the ICP/IC Analyses

Sample Type	Meter	Titration	Ca	K	Na	S	Al	Si	Cl	SO ₄
	pH		mmol/L							
0BFSGUL0.1Cl	13.29	13.78	1.89	670.28	153.04	21.39	0.04	162.74	0.80	18.13
0BFSGUL0.1Cl	13.35	13.81	1.90	645.22	221.57	25.93	0.05	187.91	12.92	21.57
0BFSGUL0.2Cl	13.49	13.84	1.61	588.01	270.18	32.70	0.06	224.02	26.01	28.06
0BFSGUL0.5Cl	13.67	13.89	1.60	592.53	467.01	39.23	0.05	203.59	112.41	33.94
0BFSGUL0.75Cl	13.74	13.87	1.69	647.60	687.69	56.13	0.06	286.77	266.37	47.71
0BFSGUL1.0Cl	13.64	13.86	1.63	655.02	875.60	69.43	0.10	326.14	453.19	58.83
25BFSGUL0Cl	13.82	13.66	2.68	363.87	108.19	32.08	0.11	0.17	2.88	6.09
25BFSGUL0.1Cl	13.73	13.68	2.62	346.22	160.72	33.84	0.06	0.16	9.61	6.05
25BFSGUL0.2Cl	13.36	13.72	2.35	346.82	215.73	46.37	0.07	0.17	17.14	7.46
25BFSGUL0.5Cl	13.29	13.76	2.18	345.46	382.21	59.89	0.07	0.25	86.57	15.48
25BFSGUL0.75Cl	13.34	13.77	2.13	364.55	541.39	97.89	0.05	0.29	204.90	25.75
25BFSGUL1.0Cl	13.33	13.76	2.16	390.13	735.54	122.91	0.06	0.29	372.51	25.04
25BFSGU0Cl	13.63	13.70	2.37	414.17	131.25	33.37	0.06	0.17	3.68	7.11
25BFSGU0.1Cl	13.71	13.74	1.68	378.79	179.64	36.73	0.11	0.26	13.37	10.58
25BFSGU0.2Cl	13.73	13.77	1.72	387.91	241.21	60.62	0.09	0.24	23.87	13.71
25BFSGU0.5Cl	13.75	13.80	1.81	388.08	411.56	82.95	0.09	0.29	107.19	23.55
25BFSGU0.75Cl	13.73	13.81	1.96	438.30	617.51	129.72	0.08	0.30	245.53	31.19
25BFSGU1.0Cl	13.39	13.79	2.29	442.82	759.46	118.70	0.06	0.39	402.98	40.17
35BFSGUL0Cl	13.39	13.57	2.77	295.84	104.36	31.77	0.06	0.12	1.75	3.93
35BFSGUL0.1Cl	13.44	13.61	2.78	302.23	161.71	50.19	0.08	0.18	8.71	4.71
35BFSGUL0.2Cl	13.44	13.63	2.43	297.54	212.25	53.73	0.06	0.18	15.92	6.11
35BFSGUL0.5Cl	13.37	13.69	1.98	294.64	371.47	99.13	0.07	0.24	82.23	12.64
35BFSGUL0.75Cl	13.42	13.68	2.24	296.69	507.03	143.86	0.05	0.32	204.07	15.95
35BFSGUL1.0Cl	13.36	13.73	2.28	324.91	689.58	167.53	0.05	0.34	343.84	21.36

35BFSGU0Cl	13.71	13.65	2.08	325.68	109.96	30.97	0.06	0.17	2.79	4.20
35BFSGU0.1Cl	13.83	13.69	1.99	322.27	165.99	39.19	0.10	0.26	10.95	5.08
35BFSGU0.2Cl	13.77	13.73	2.04	324.57	226.14	52.36	0.12	0.24	22.61	9.15
35BFSGU0.5Cl	13.78	13.74	1.72	308.88	366.30	95.15	0.10	0.25	97.83	12.64
35BFSGU0.75Cl	13.68	13.75	1.83	339.49	549.51	150.26	0.11	0.32	242.88	21.01
35BFSGU1.0Cl	13.74	13.74	1.89	358.67	716.54	179.87	0.10	0.29	386.75	26.75
50BFSGUL0Cl	13.48	13.46	2.14	197.42	78.03	37.92	0.05	0.11	2.78	1.93
50BFSGUL0.1Cl	13.51	13.50	2.12	195.30	119.33	45.53	0.07	0.16	7.77	2.54
50BFSGUL0.2Cl	13.59	13.52	1.62	168.34	151.98	70.12	0.09	0.16	17.16	4.11
50BFSGUL0.5Cl	13.62	13.56	1.61	177.69	284.33	156.67	0.09	0.22	86.90	7.77
50BFSGUL0.75Cl	13.65	13.55	1.71	196.99	429.23	229.84	0.10	0.24	205.73	10.95
50BFSGUL1.0Cl	13.62	13.56	1.67	207.32	576.05	251.05	0.11	0.30	356.62	15.56
50BFSGU0Cl	13.65	13.50	1.97	223.16	87.53	37.02	0.06	0.13	2.89	2.17
50BFSGU0.1Cl	13.68	13.54	1.80	212.29	123.82	43.09	0.08	0.18	7.55	2.79
50BFSGU0.2Cl	13.69	13.55	1.86	221.53	123.46	54.15	0.09	0.16	6.82	2.27
50BFSGU0.5Cl	13.75	13.62	1.56	215.13	326.82	109.64	0.09	0.24	93.72	7.52
50BFSGU0.75Cl	13.74	13.62	1.53	228.29	419.65	144.37	0.08	0.26	214.92	9.73
50BFSGU1.0Cl	13.79	13.61	1.66	242.77	573.58	166.25	0.08	0.28	349.35	13.42

B.5 Mass Proportions of Laboratory-Grade Chemical Agents for Synthetic Solutions

Test Container	Method	Sample Type	Ca(OH) ₂	NaOH	KOH	CaSO ₄ ·2H ₂ O		NaCl
						Added Mass (g/L)		
A-03 or A-04	M1	0BFSGUL0.1Cl	>1	6.12	37.61	3.12	0	
		0BFSGUL0.1Cl	0	0	0	0.60	0.76	
		0BFSGUL0.2Cl	0	0	0	1.11	0.76	
		0BFSGUL0.5Cl	0	0	0	0.54	2.92	
		0BFSGUL0.75Cl	0	0	0	1.56	5.90	
		0BFSGUL1.0Cl	0	0	0	1.91	10.92	
A-06	M2	0BFSGUL0.1Cl	>1	6.13	37.61	3.12	0	
		0BFSGUL0.1Cl	0	2.74	0	0.60	0.76	
		0BFSGUL0.2Cl	0	1.94	0	1.11	0.76	
		0BFSGUL0.5Cl	0	4.18	0	0.54	2.92	
		0BFSGUL0.75Cl	0	5.46	0	1.56	5.90	
		0BFSGUL1.0Cl	0	7.52	0	1.91	10.92	
A-01 or A-02	M1	0BFSGU0.1Cl	>1	6.37	12.45	0.78	0	
		0BFSGU0.1Cl	0	0	0	0.12	0.23	
		0BFSGU0.2Cl	0	0	0	0.10	0.33	
		0BFSGU0.5Cl	0	0	0	0.91	3.03	

		0BFSGU0.75Cl	0	0	0	0.76	4.69
		0BFSGU1.0Cl	0	0	0	0.85	6.45
A-05	M2	0BFSGU0.1Cl	>1	6.37	12.45	0.78	0
		0BFSGU0.1Cl	0	2.98	0.55	0.12	0.23
		0BFSGU0.2Cl	0	2.85	0.40	0.10	0.33
		0BFSGU0.5Cl	0	2.98	0	0.91	3.03
		0BFSGU0.75Cl	0	3.03	0	0.76	4.69
		0BFSGU1.0Cl	0	9.02	0	0.85	6.45
B-04	M1	25BFSGUL0Cl	>1	4.34	20.43	1.06	0
		25BFSGUL0.1Cl	0	0	0	0	0.56
		25BFSGUL0.2Cl	0	0	0	0.22	0.44
		25BFSGUL0.5Cl	0	0	0	0.71	2.26
		25BFSGUL0.75Cl	0	0	0	1.03	4.62
		25BFSGUL1.0Cl	0	0	0	0	9.79
B-01	M1	25BFSGU0Cl	>1	5.26	23.27	1.12	0
		25BFSGU0.1Cl	0	0	0	0.70	0.78
		25BFSGU0.2Cl	0	0	0	0	0.61
		25BFSGU0.5Cl	0	0	0	1.15	2.66
		25BFSGU0.75Cl	0	0	0	0.77	5.35
		25BFSGU1.0Cl	0	0	0	1.55	9.20
B-05	M1	35BFSGUL0Cl	>1	4.18	16.65	0.71	0
		35BFSGUL0.1Cl	0	0	0	0.10	0.51
		35BFSGUL0.2Cl	0	0	0	0.24	0.42
		35BFSGUL0.5Cl	0	0	0	0.53	2.26
		35BFSGUL0.75Cl	0	0	0	0.33	4.63
		35BFSGUL1.0Cl	0	0	0	0.93	8.17
B-02	M1	35BFSGU0Cl	>1	4.42	18.30	0.76	0
		35BFSGU0.1Cl	0	0	0	0.12	0.64
		35BFSGU0.2Cl	0	0	0	0.70	0.68
		35BFSGU0.5Cl	0	0	0	0.33	2.54
		35BFSGU0.75Cl	0	0	0	0.94	5.44
		35BFSGU1.0Cl	0	0	0	0.99	8.41
B-06	M1	50BFSGUL0Cl	>1	3.16	11.10	0.36	0
		50BFSGUL0.1Cl	0	0	0	0.08	0.45
		50BFSGUL0.2Cl	0	0	0	0.27	0.55
		50BFSGUL0.5Cl	0	0	0	0.31	2.30
		50BFSGUL0.75Cl	0	0	0	0.35	4.62
		50BFSGUL1.0Cl	0	0	0	0.80	8.82
B-03	M1	50BFSGU0Cl	>1	3.55	12.53	0.39	0
		50BFSGU0.1Cl	0	0	0	0.09	0.44
		50BFSGU0.2Cl	0	0	0	0	0

50BFSGU0.5Cl	0	0	0	0.45	2.83
50BFSGU0.75Cl	0	0	0	0.21	4.56
50BFSGU1.0Cl	0	0	0	0.63	7.86

B.6 Corrosion Measurements and Autopsy of Rebar Specimens in Synthetic Solution

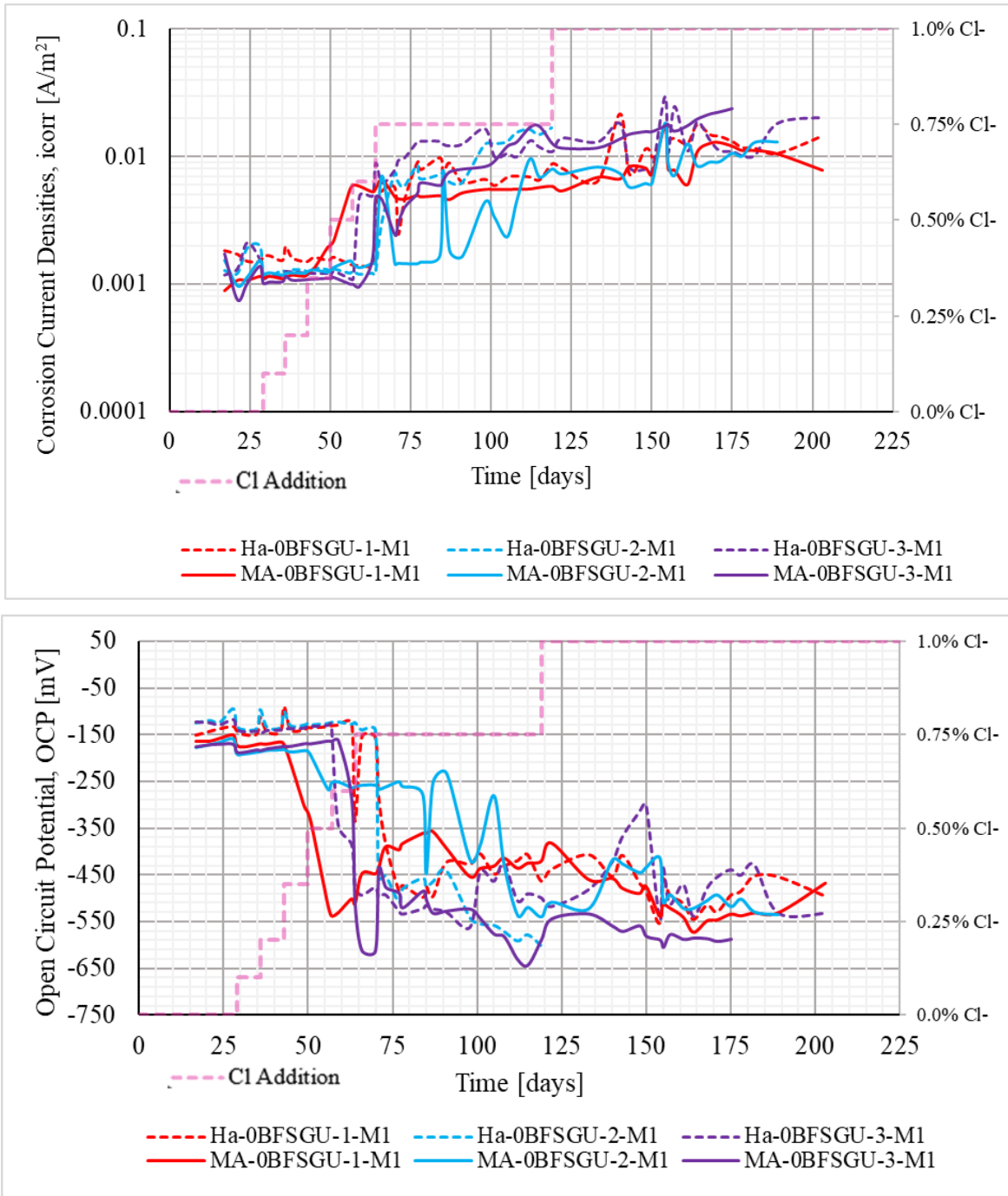


Figure B.1 Current densities, by LPR, and OCP for rebar specimens in 0BFSGU solution A-01

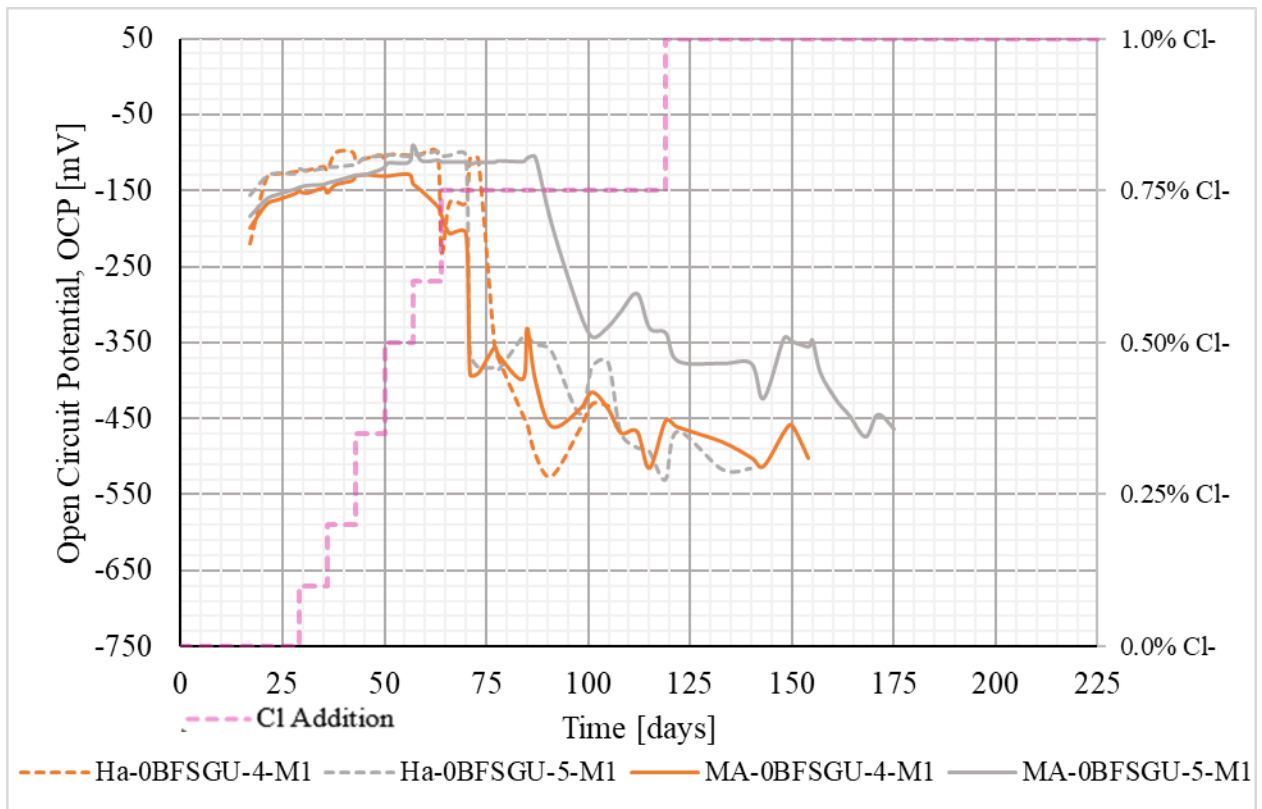
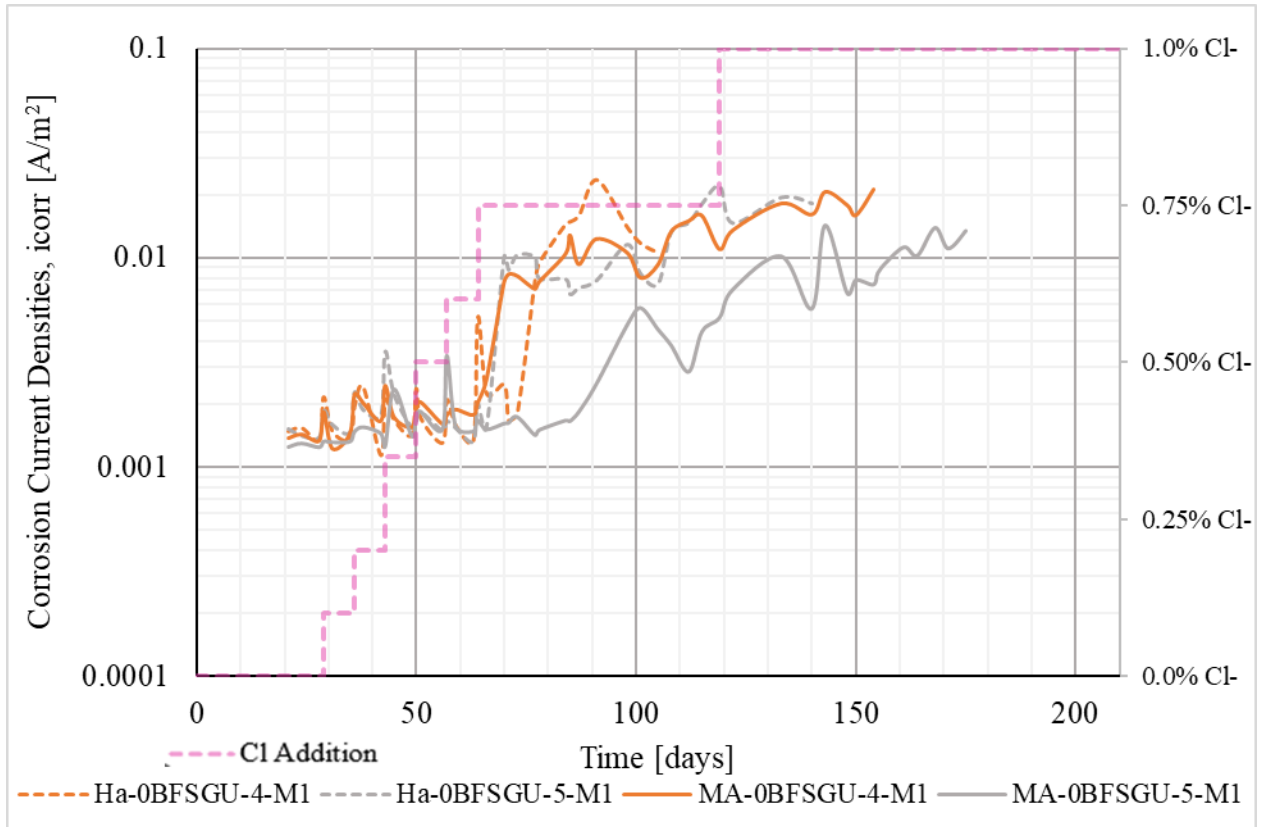


Figure B.2 Current densities, by LPR, and OCP for rebar specimens in 0BFSGU solution A-02

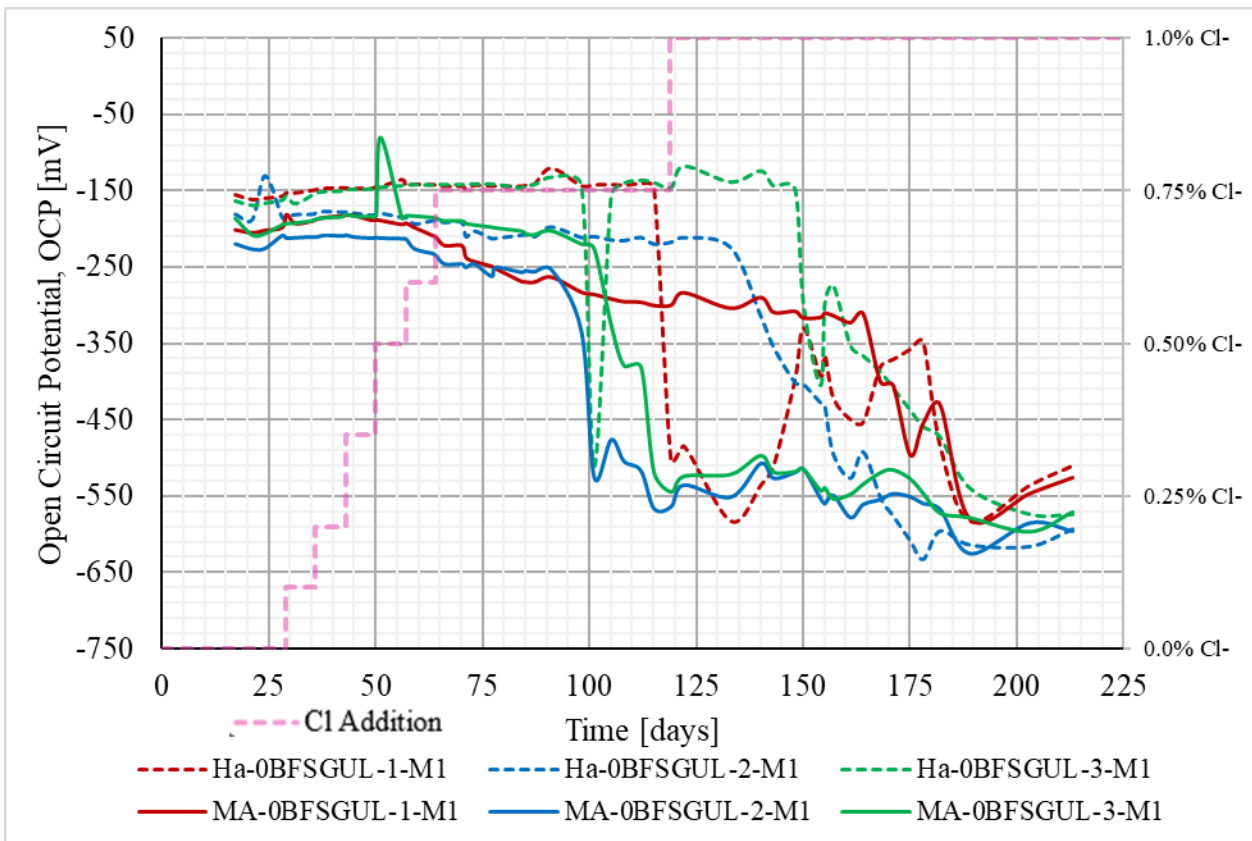
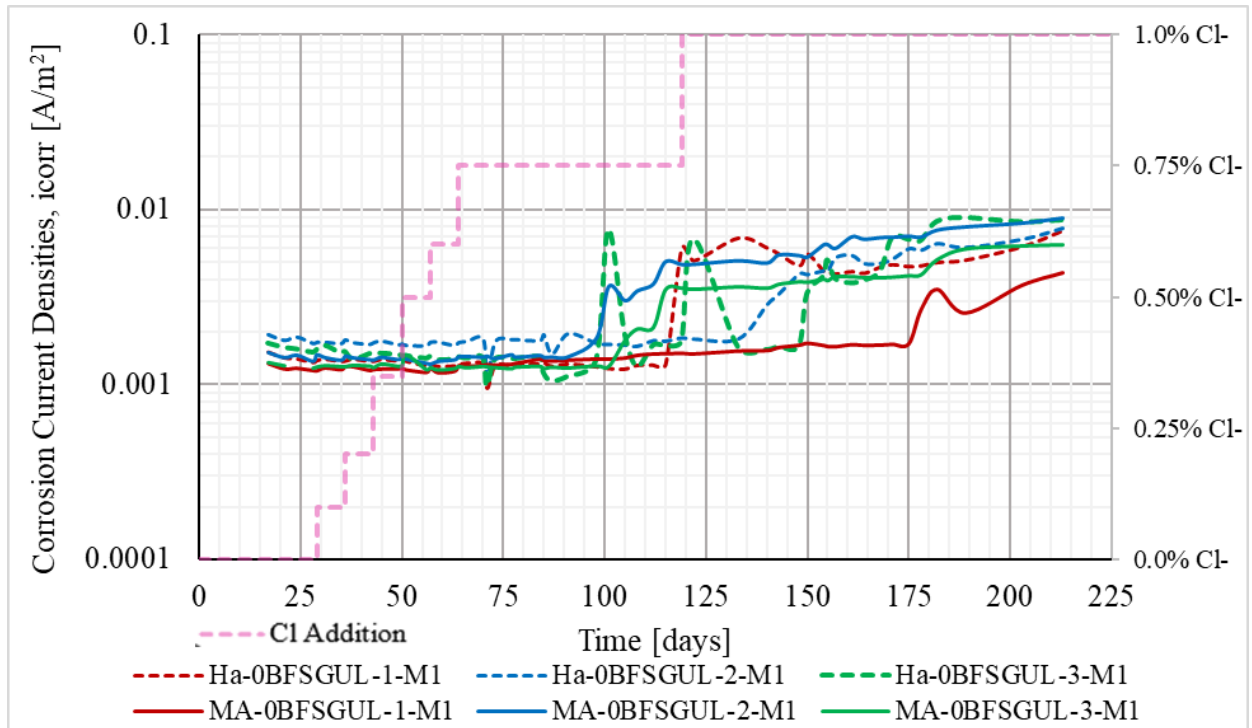


Figure B.3 Current densities, by LPR, and OCP for rebar specimens in 0BFGUL solution A-03

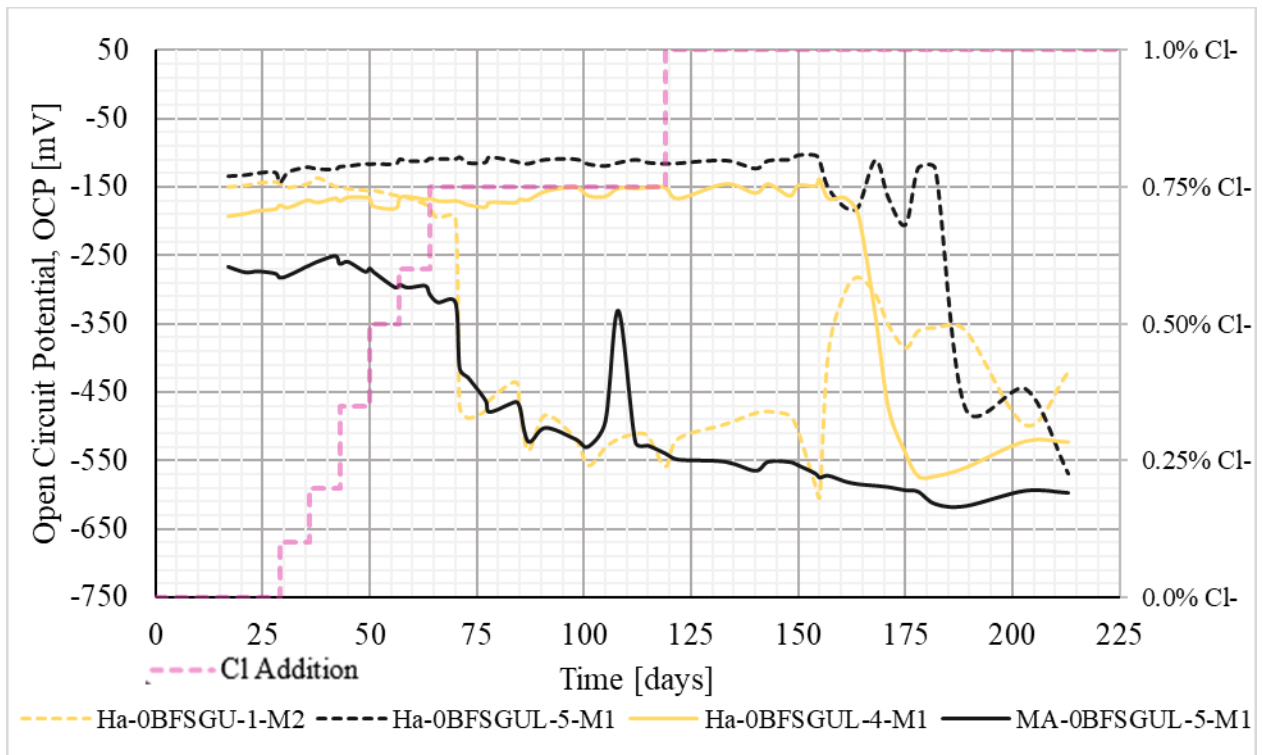
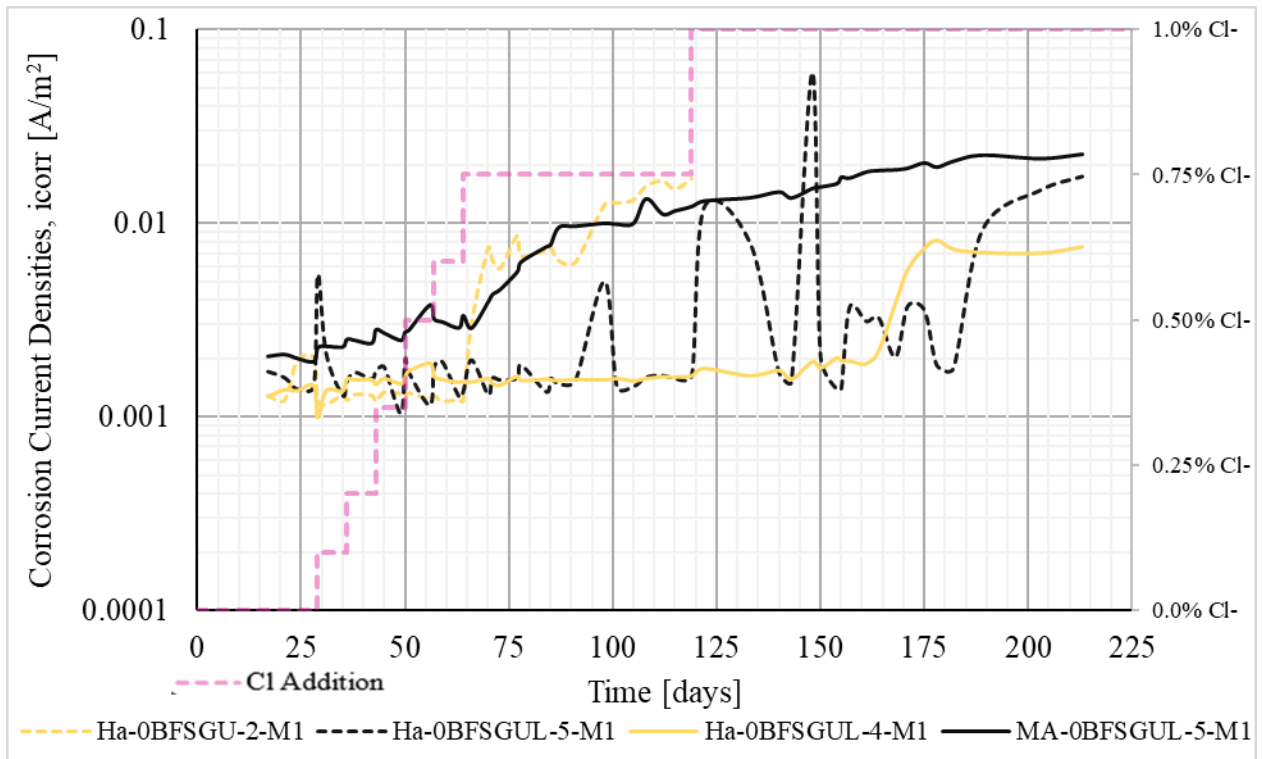


Figure B.4 Current densities, by LPR, and OCP for rebar specimens in 0BFSGUL solution A-04

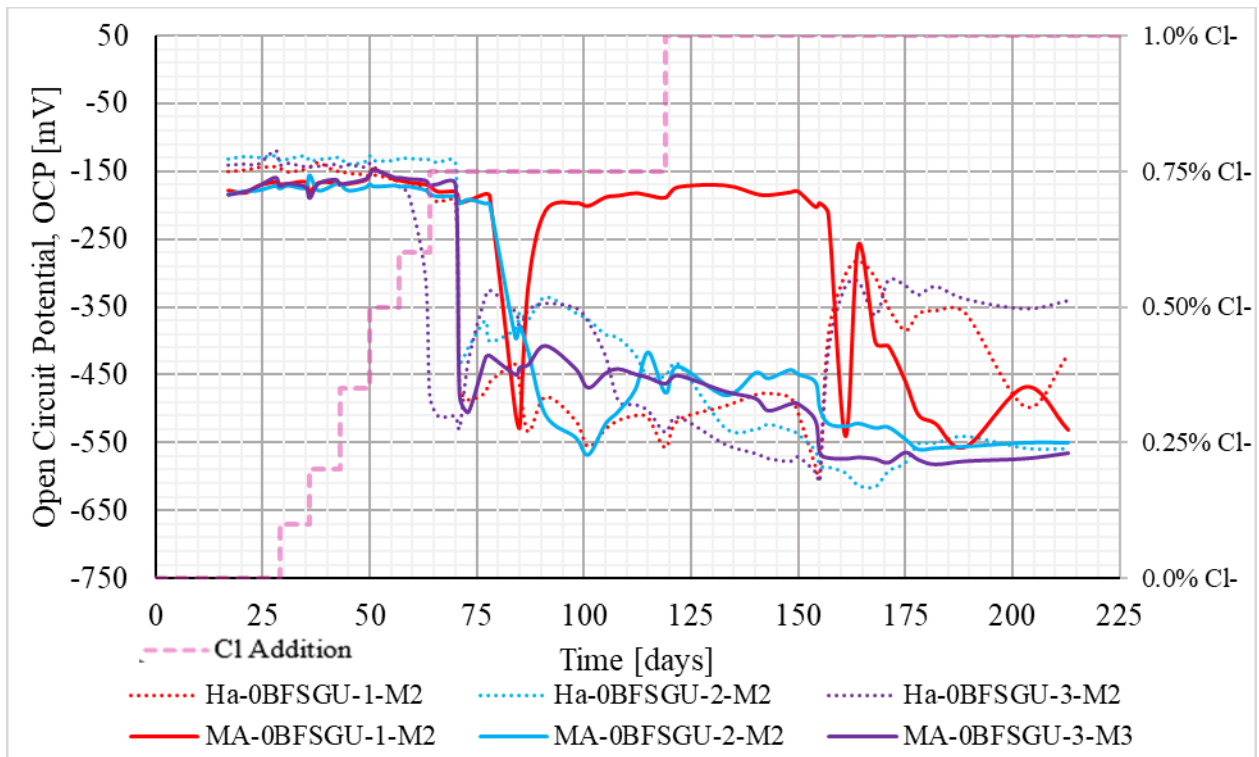
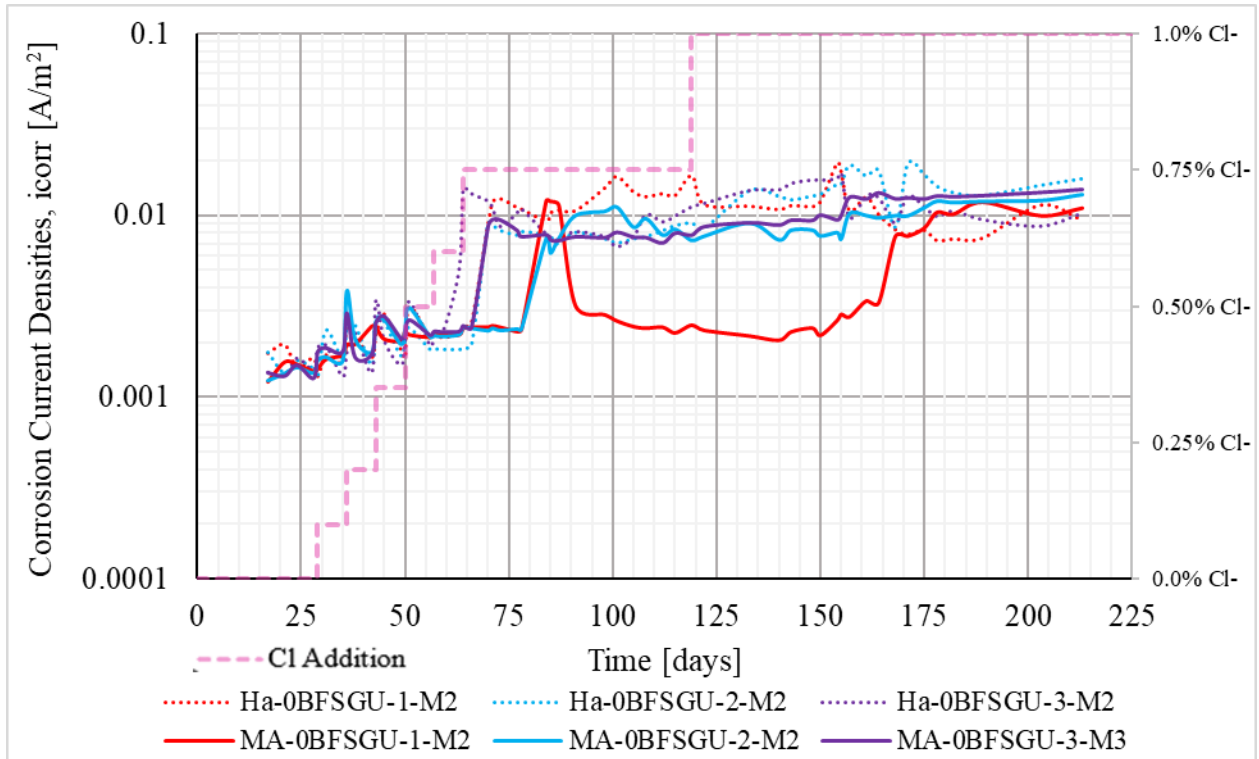


Figure B.5 Current densities, by LPR, and OCP for rebar specimens in 0BFSGU solution A-05

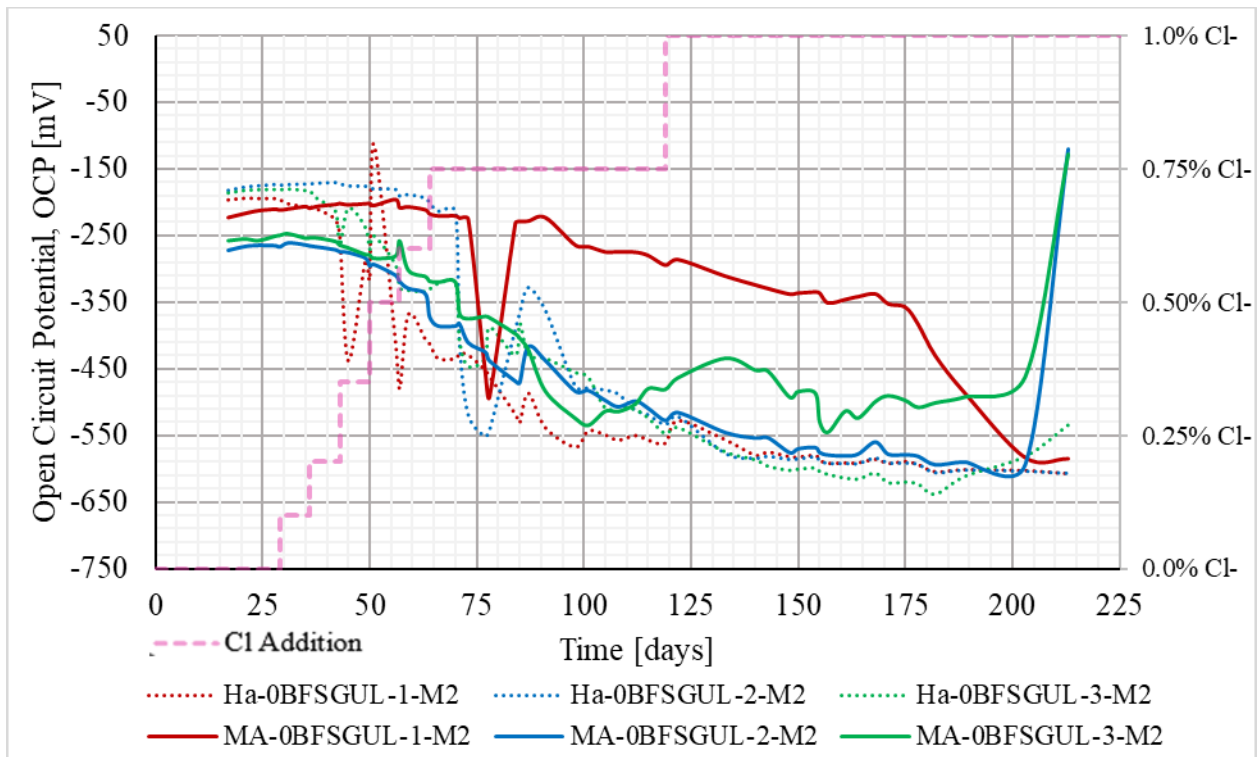
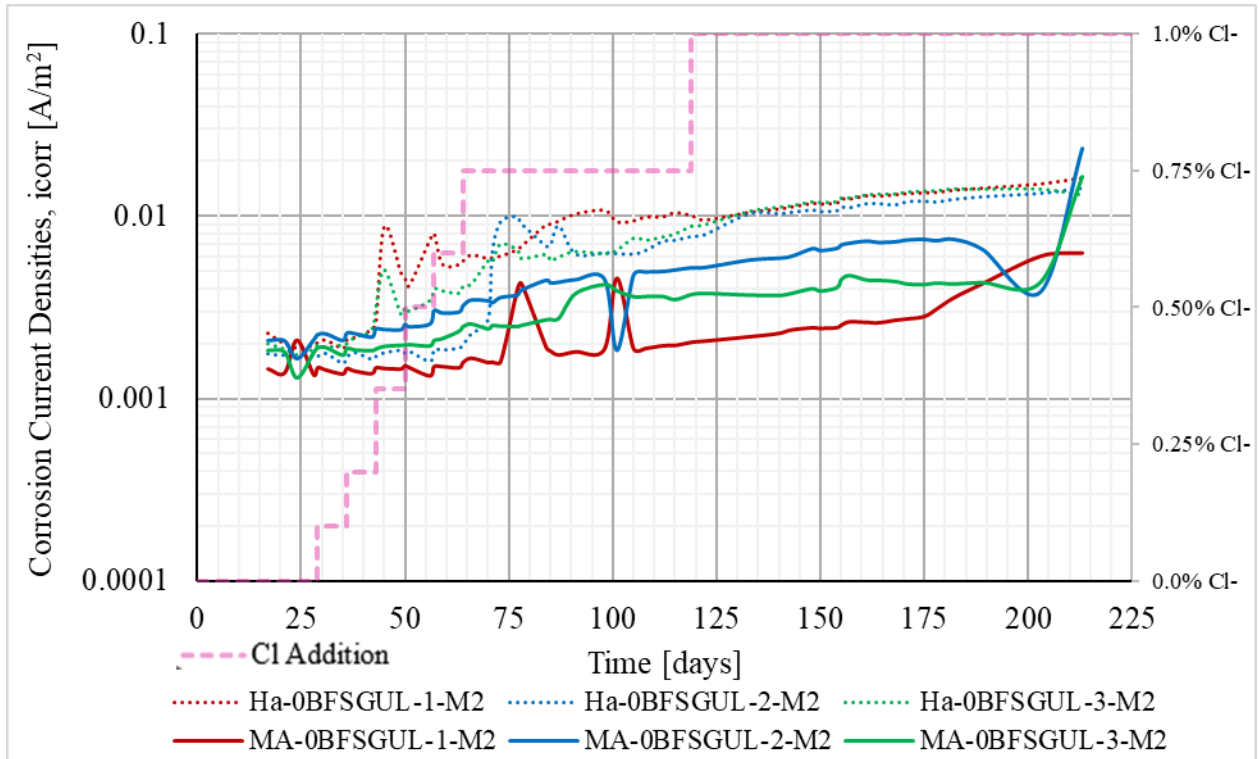


Figure B.6 Current densities, by LPR, and OCP for rebar specimens in 0BFSGUL solution A-06

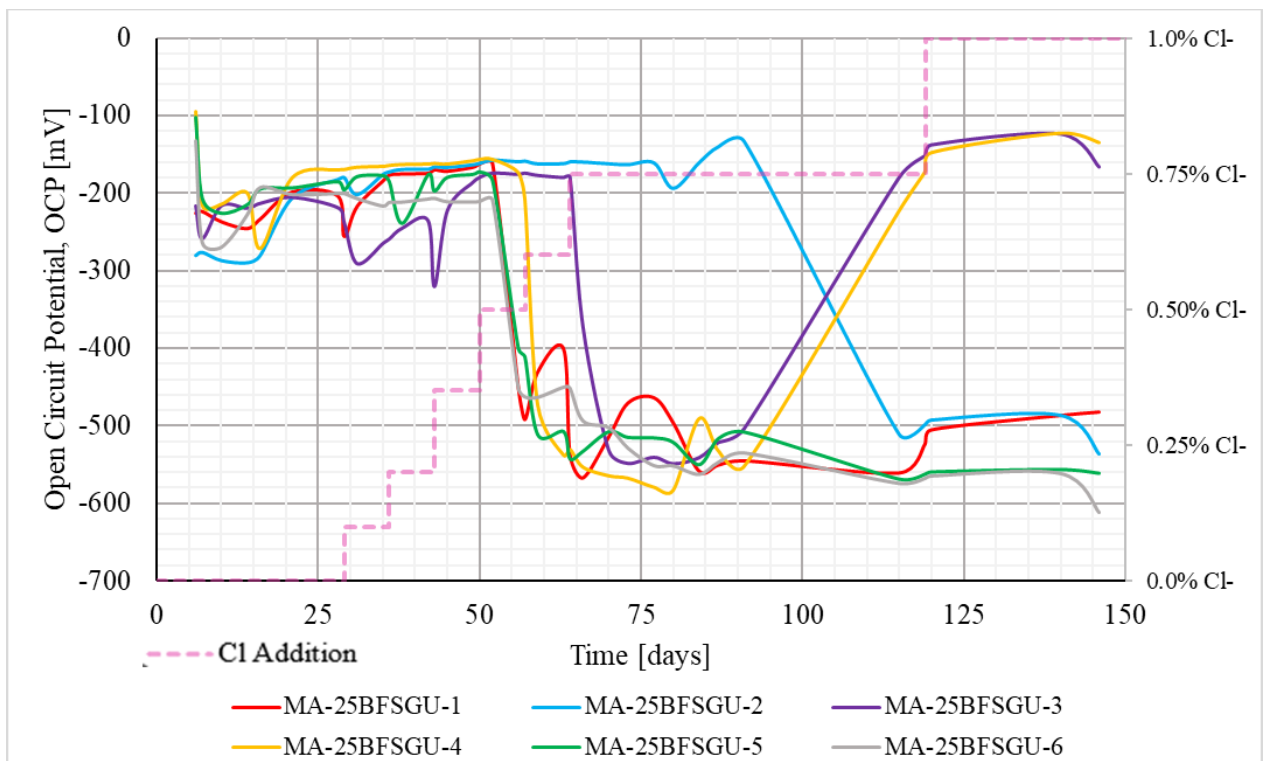
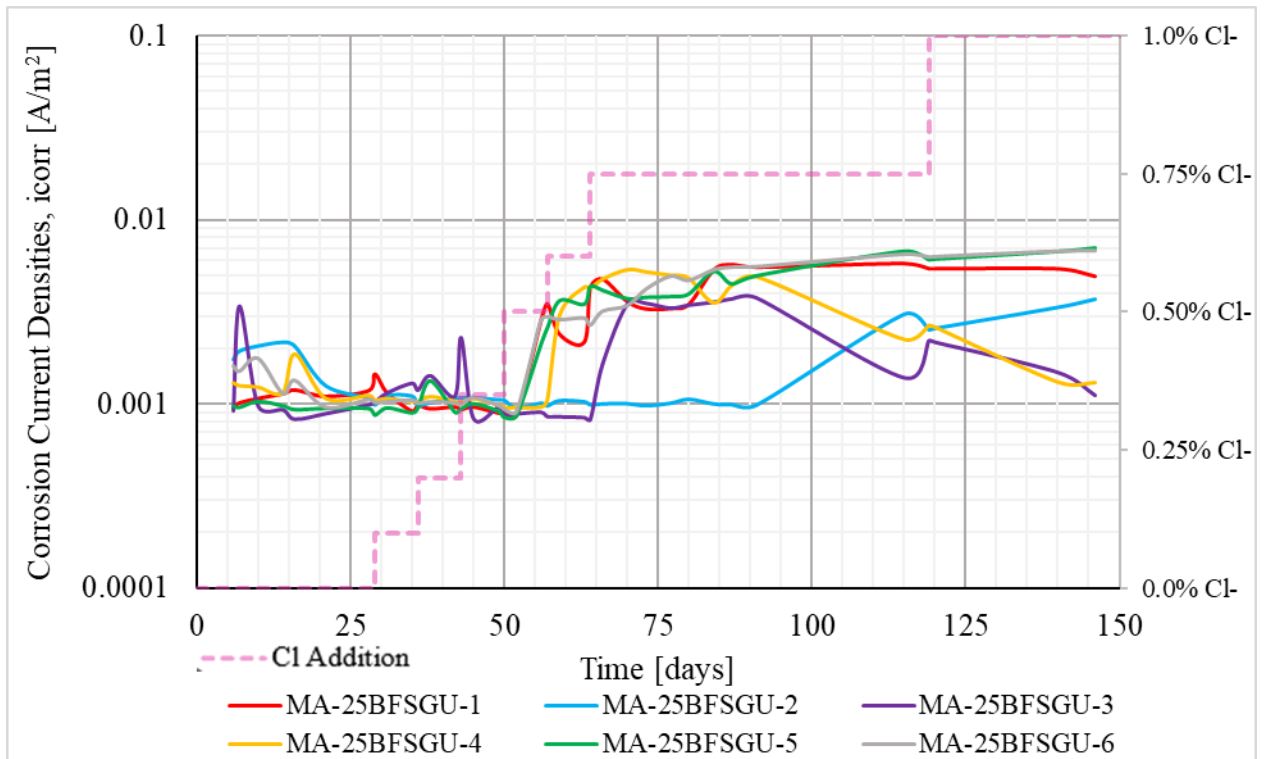


Figure B.7 Current densities, by LPR, and OCP for rebar specimens in 25BFSGU solution B-01

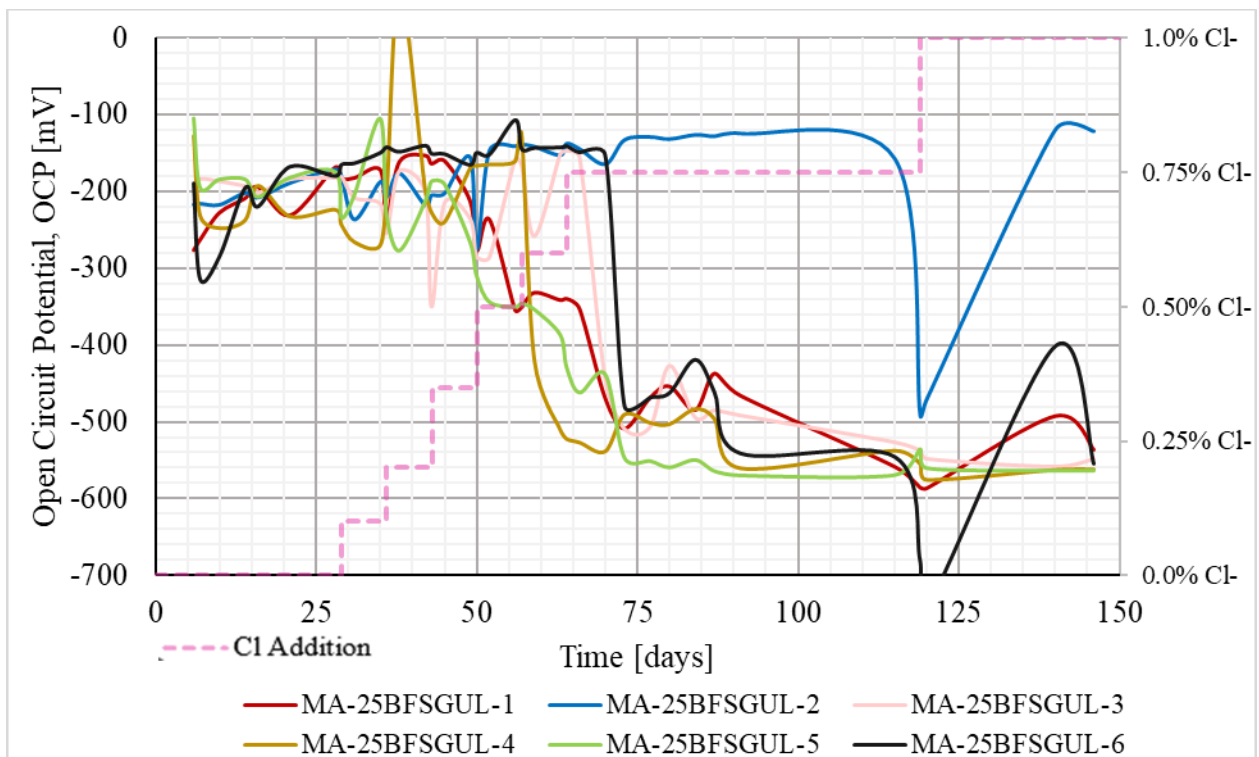
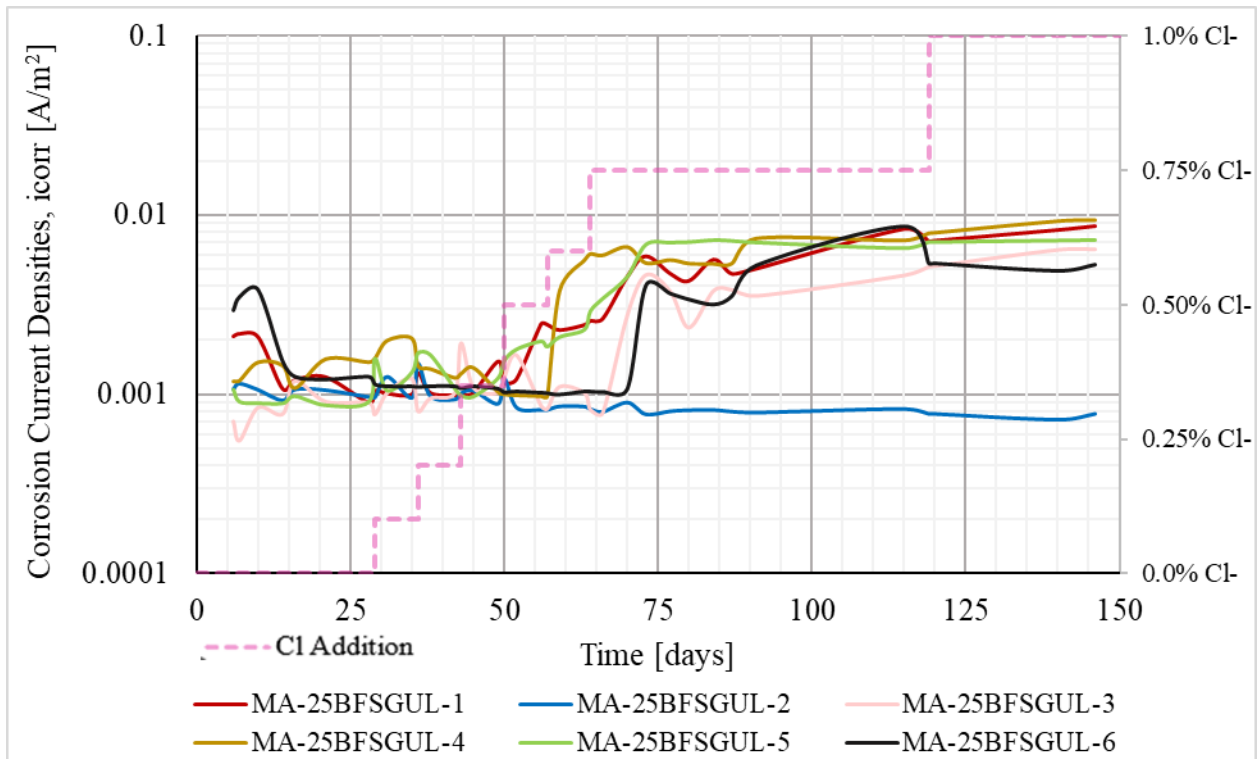


Figure B.8 Current densities, by LPR, and OCP for rebar specimens in 25BFGUL test solution

B-04

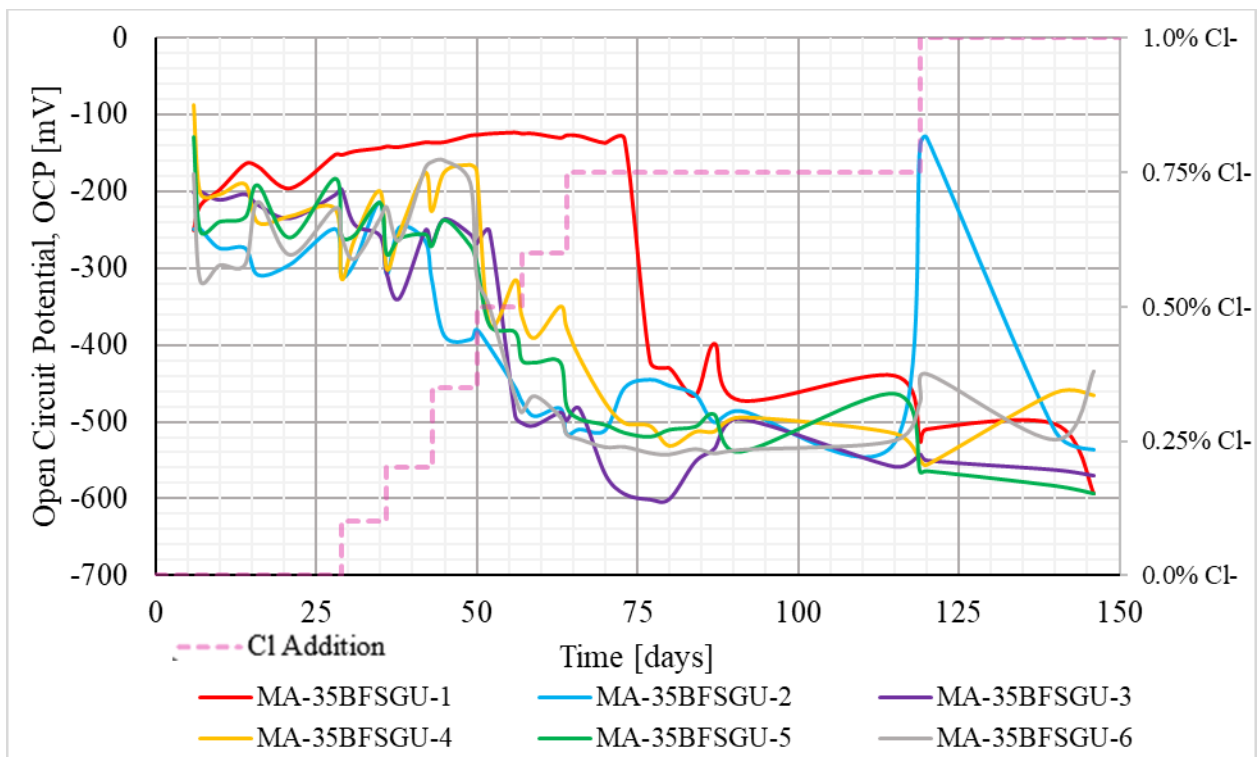
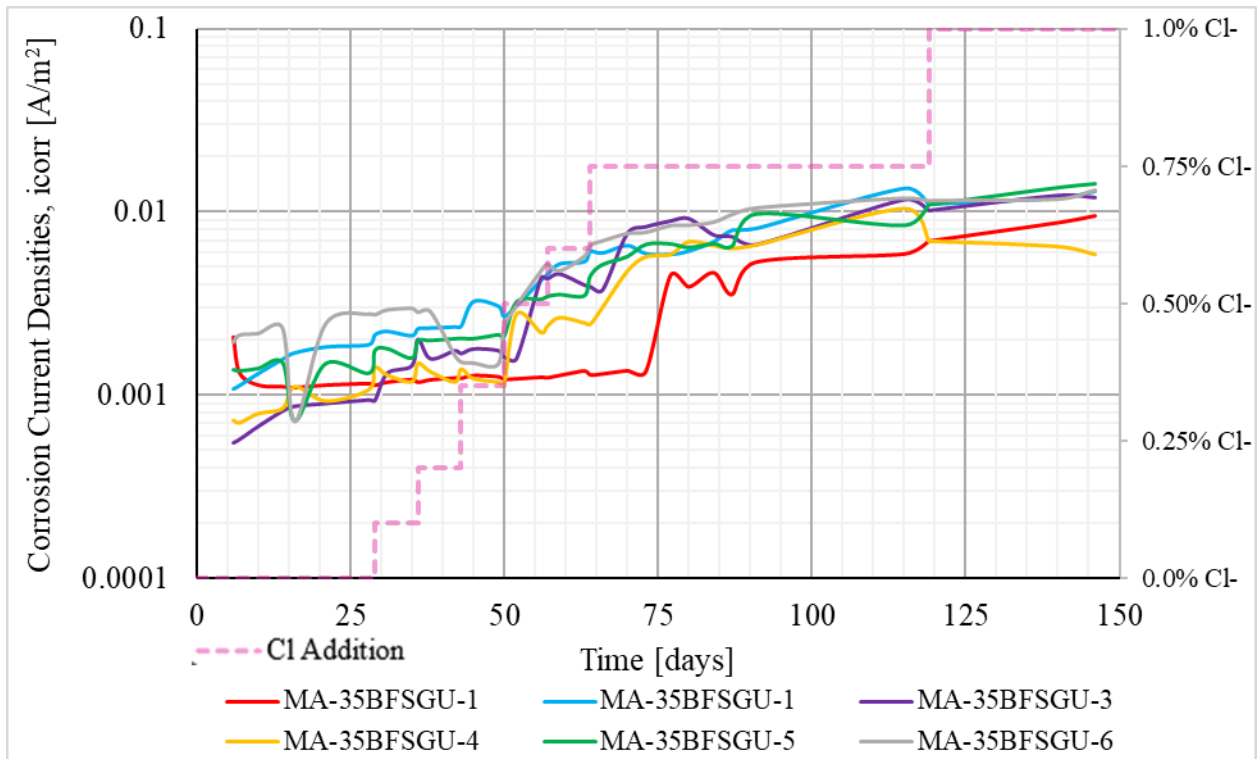


Figure B.9 Current densities, by LPR, and OCP for rebar specimens in 35BFSGU solution B-02

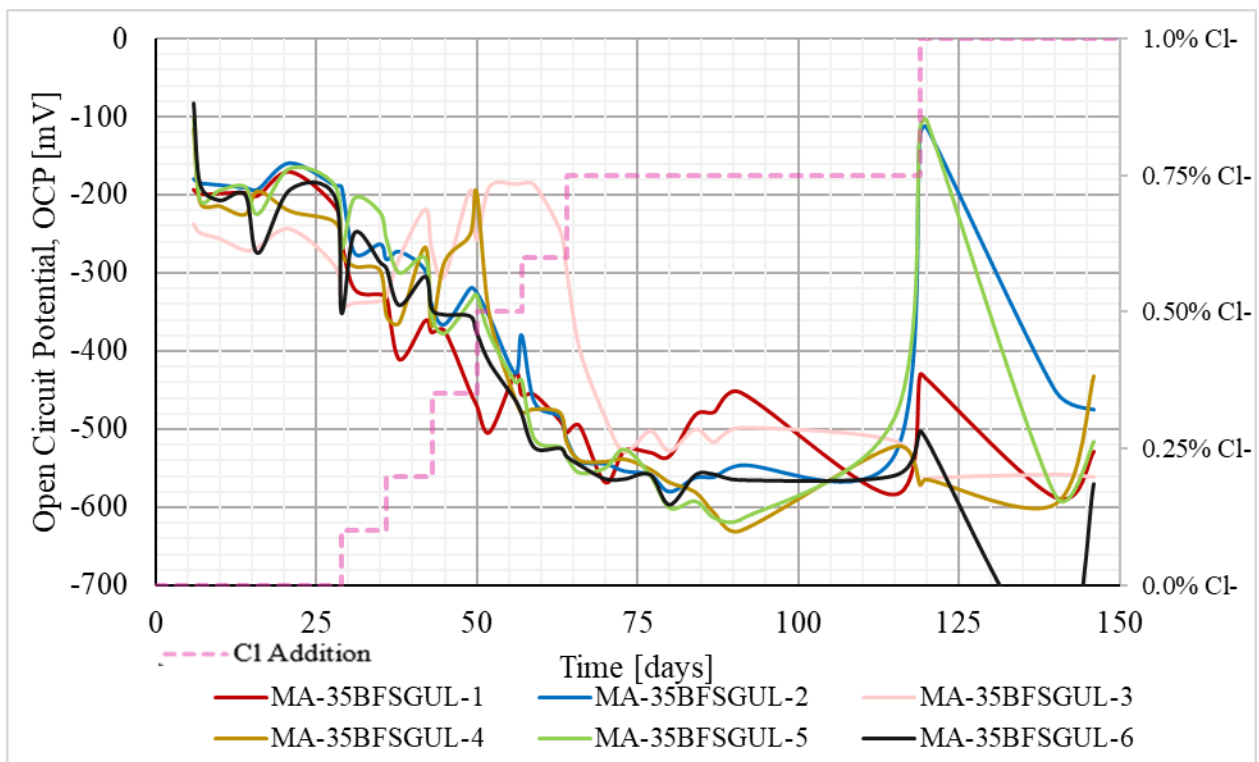
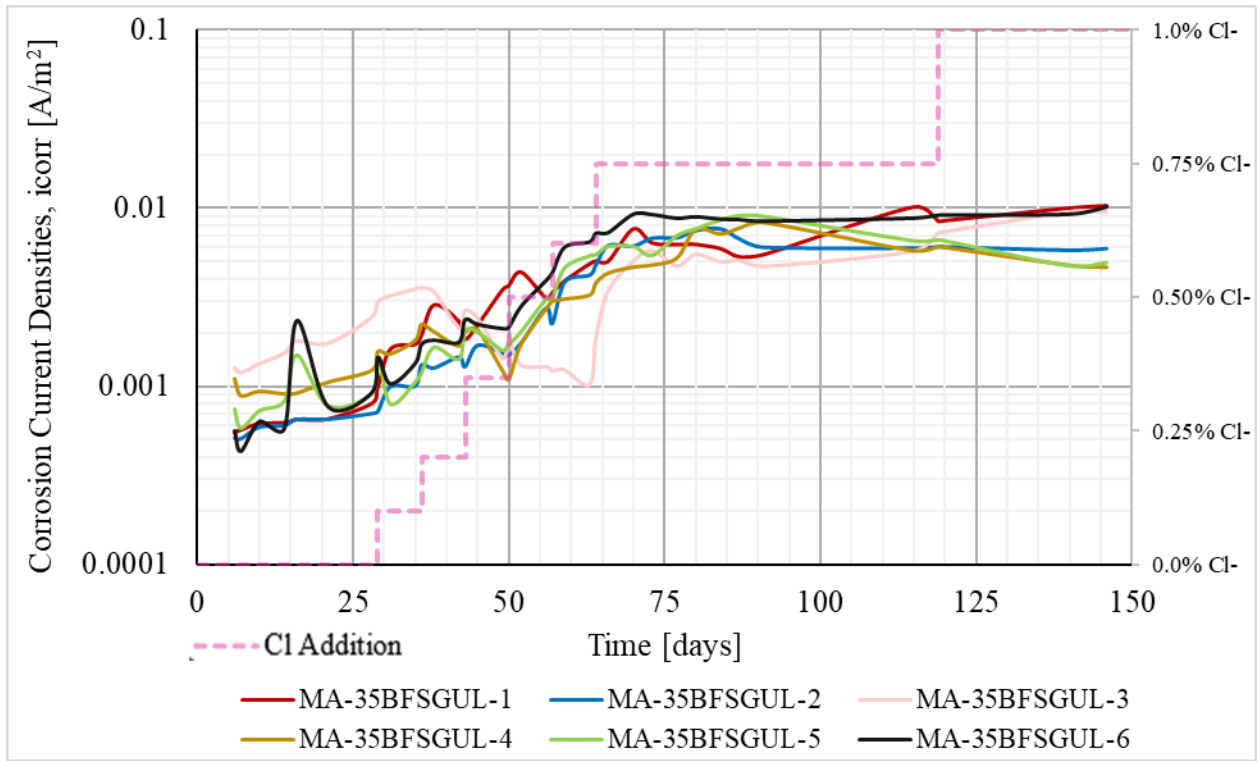


Figure B.10 Current densities, by LPR, and OCP for rebar specimens in 35BFGUL test solution B-05

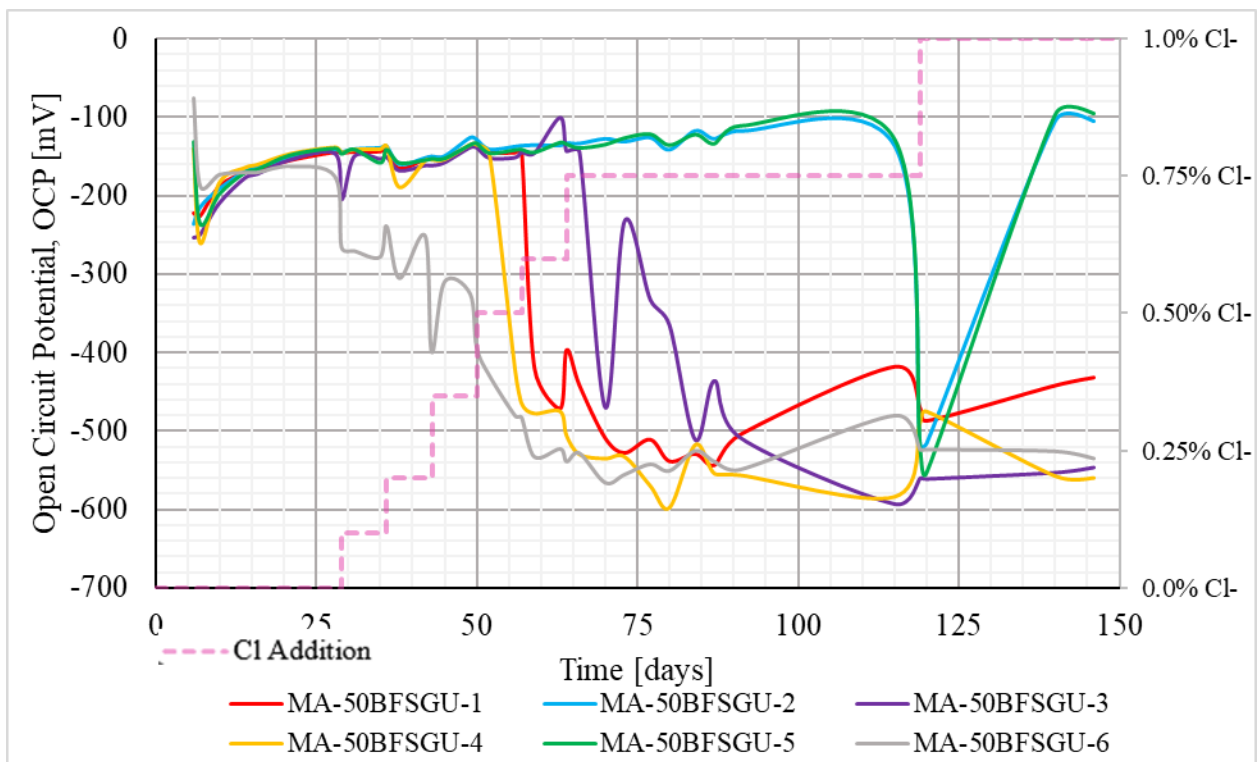
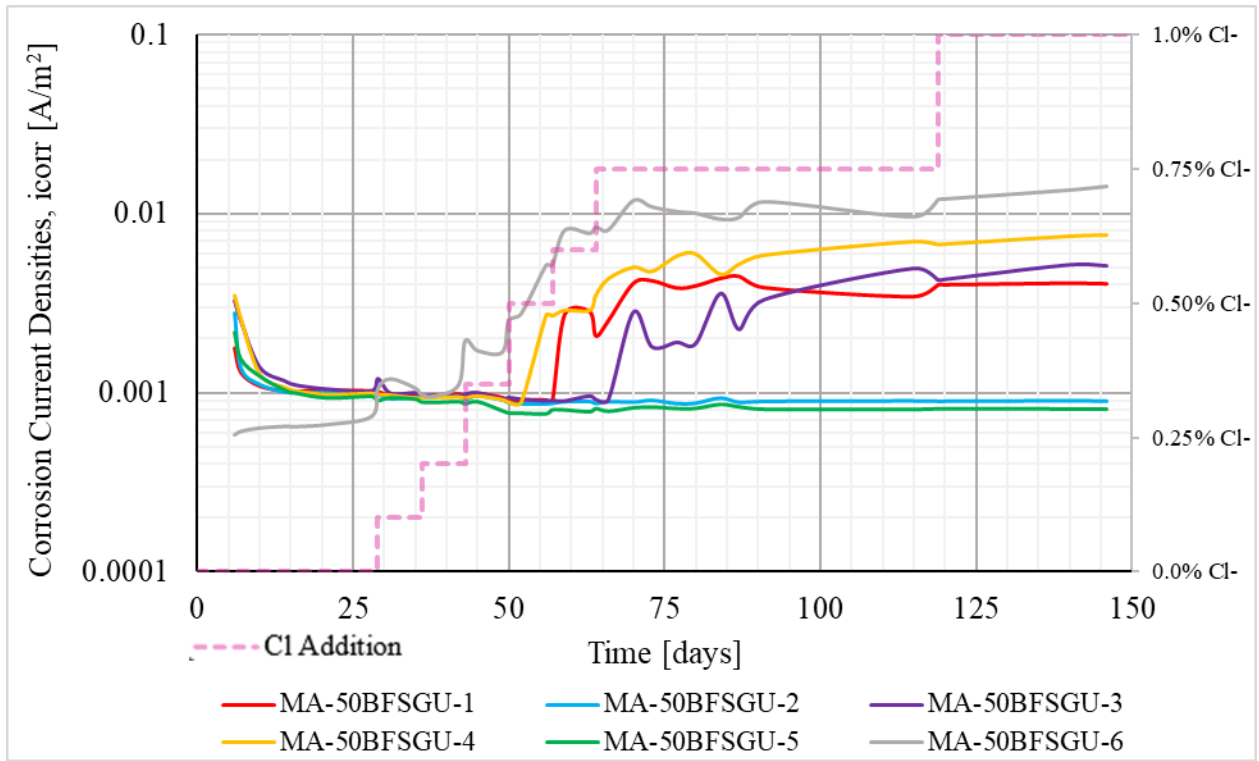


Figure B.11 Current densities, by LPR, and OCP for rebar specimens in 50BFSGU solution B-03

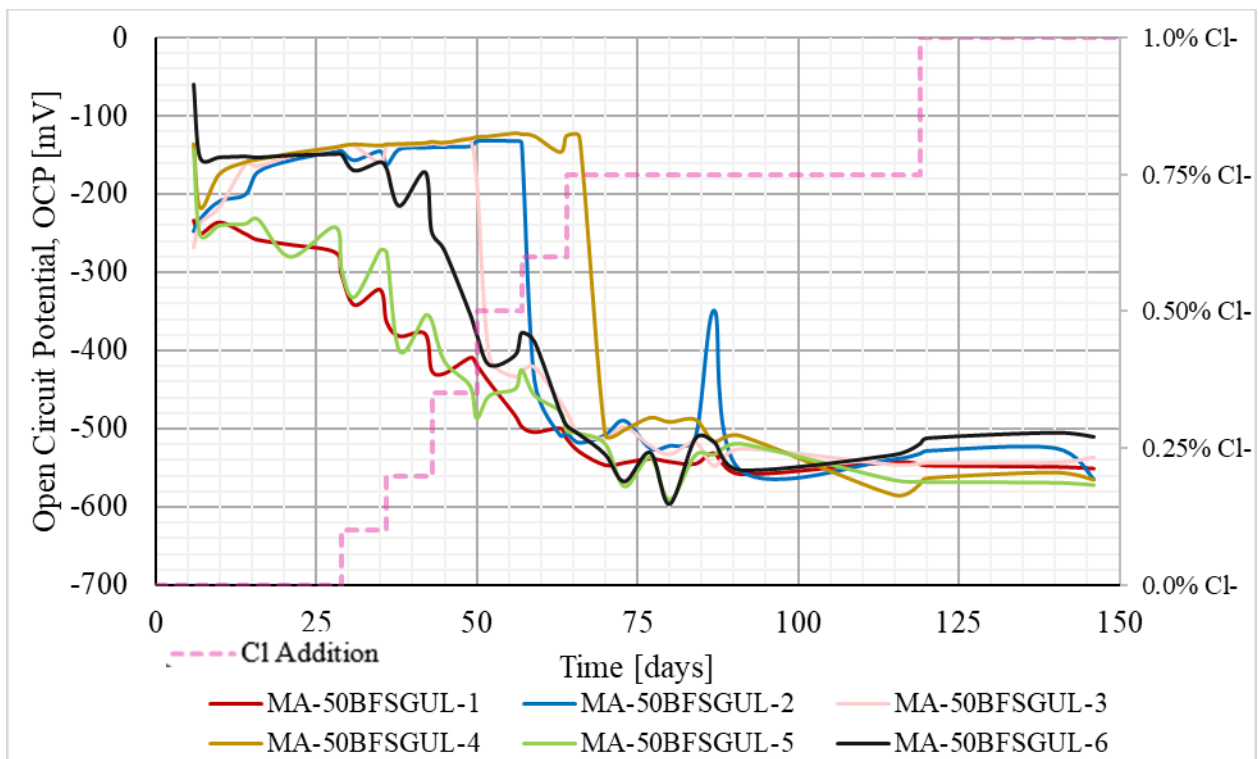
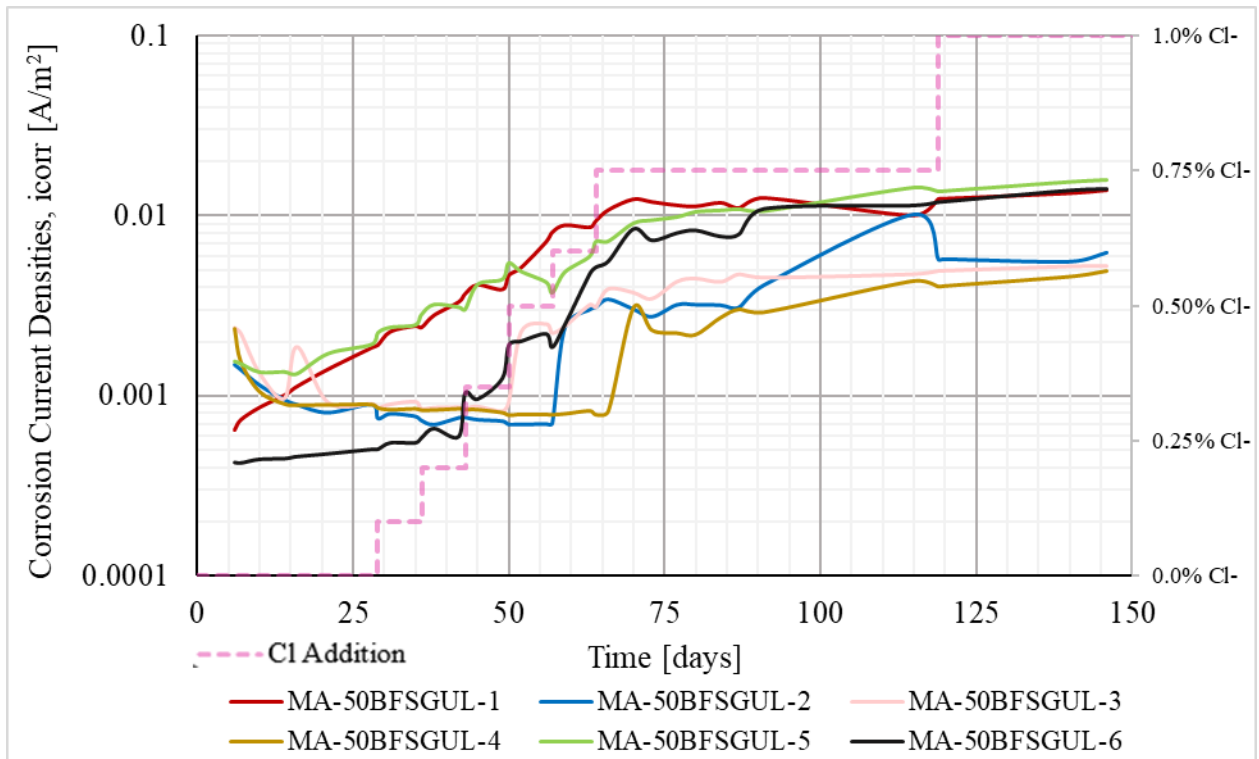


Figure B.12 Current densities, by LPR, and OCP for rebar specimens in 50BFGUL test solution

B-06

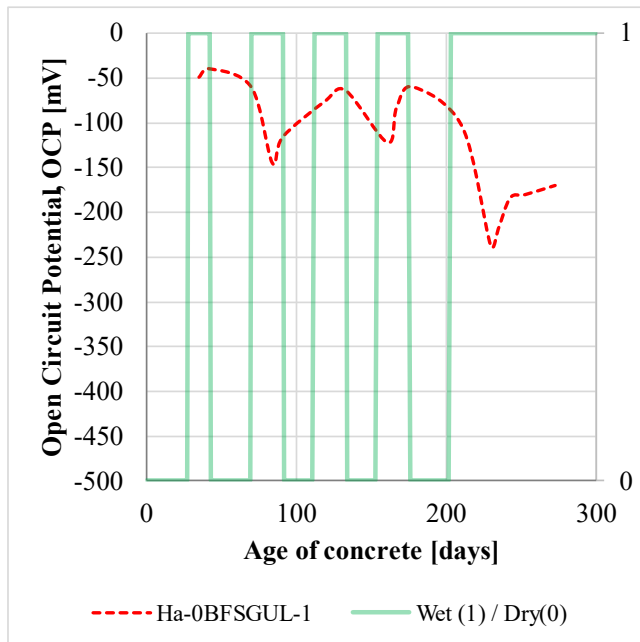
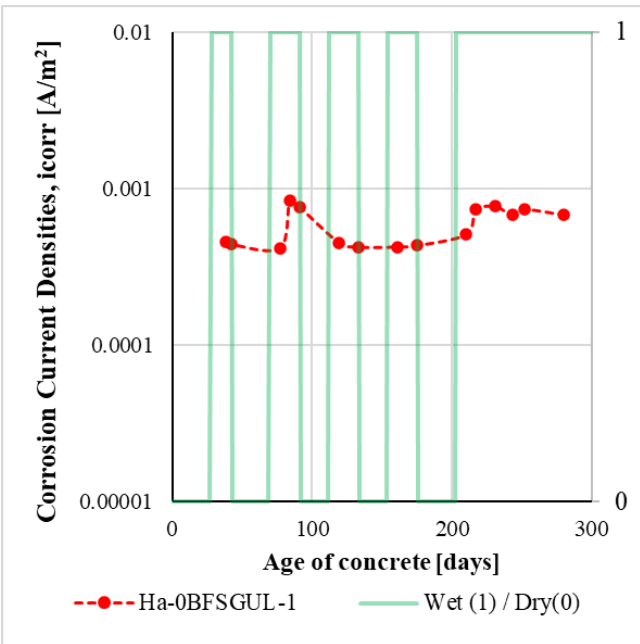
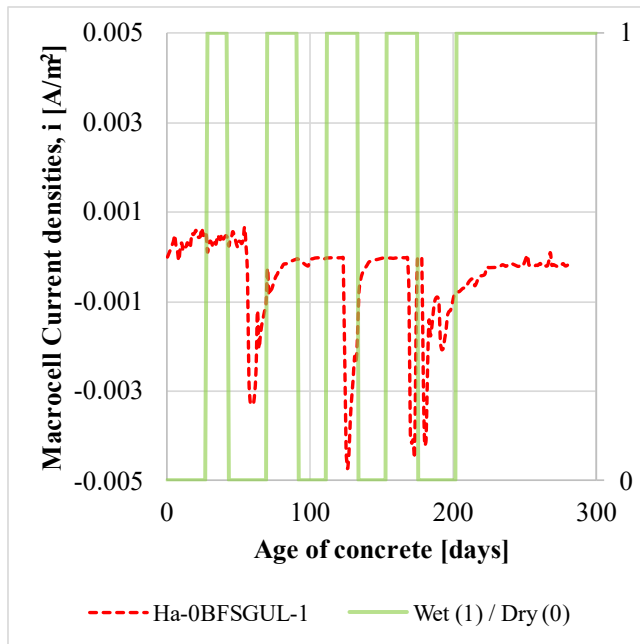
Appendix C - Extra Information on Tests based on Concrete Specimens

C.1 Electrochemical Test Measurements and XRF Data for Major Elements for Bars in Individual Autopsied Specimens

The following present the electrochemical test measurements and post-test analyses and photographs of the individual autopsied specimens :

- 1) For the autopsied concrete specimens, both macrocell and microcell corrosion measurements of the top and bottom bars are provided along with (before and after) photographs of the bars and their respective surrounding internal concrete surfaces.
- 2) Note that XRF information on the autopsied concrete specimens were measured within 24 hours after cutting with their conditions preserved by storing in sealed plastic Ziploc bags.
- 3) Note, as mentioned in text, the chloride concentration of the specimens, with chloride-contaminated wetting solutions in the ponding well (i.e. the specimens identified with 1, 2, 3 and 4 for Ha-0BFSGU, Ha-0BFSGUL, MA-0BFSGU and MA-0BFSGUL; and specimens identified with 1, 2, 3 for the slag-included mixes MA-25BFSGU, MA-25BFSGUL, MA-35BFSGU, MA-35BFSGUL, 50BFSGU and 50BFSGUL) was initially 3% wt. NaCl and changed to 5.75%NaCl at day 210 and onwards.
- 4) Note that specimens identified with 5 for MA-0BFSGU and MA-0BFSGUL, as well as specimens identified with 4 for any of the slag-included concrete mixes 25BFSGU, 25BFSGUL, 35BFSGU, 35BFSGUL, 50BFSGU and 50BFSGUL were not exposed to chlorides in the wetting solutions of their ponding wells.

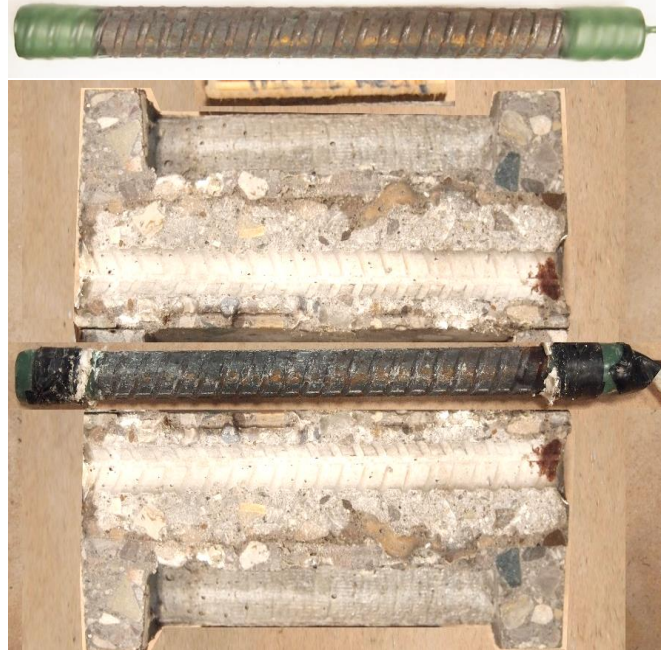
1a) Top Bar of Ha-0BFSGUL-1 concrete specimen (autopsied)



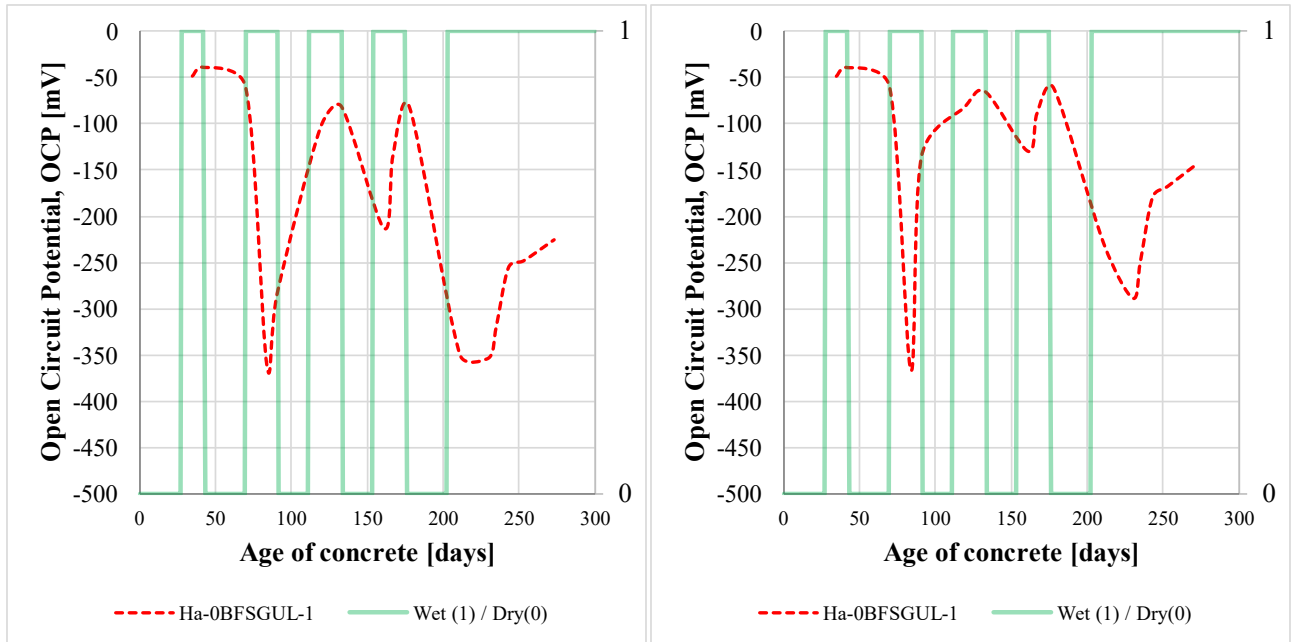
Specimen	Depth Point	Cl [%]	Fe [%]	Ca [%]	Al [%]	Si [%]	S [%]	Mg [%]
Ha-0BFSGUL-1	1	0.560	0.616	23.696	0.350	3.492	0.303	1.529
	2	0.240	0.717	24.154	0.506	6.720	0.777	1.200
	3	0.036	0.962	20.638	0.236	3.798	0.923	<LOD
	4	0.035	0.901	22.315	0.409	5.817	0.776	1.131
	5	0.044	1.216	21.234	0.598	5.832	0.717	<LOD
	6	0.059	0.557	16.519	<LOD	2.810	0.557	<LOD

Note: <LOD = Below limit of detection by XRF

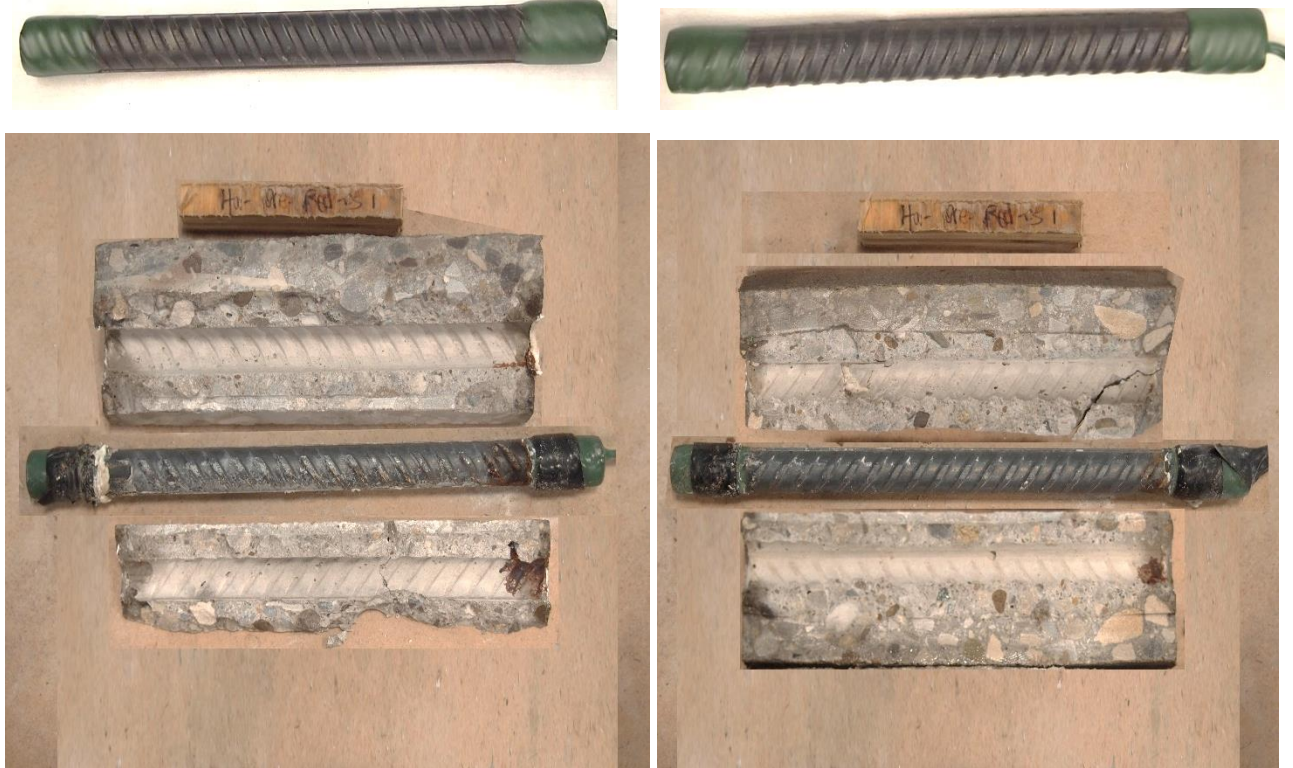
BEFORE



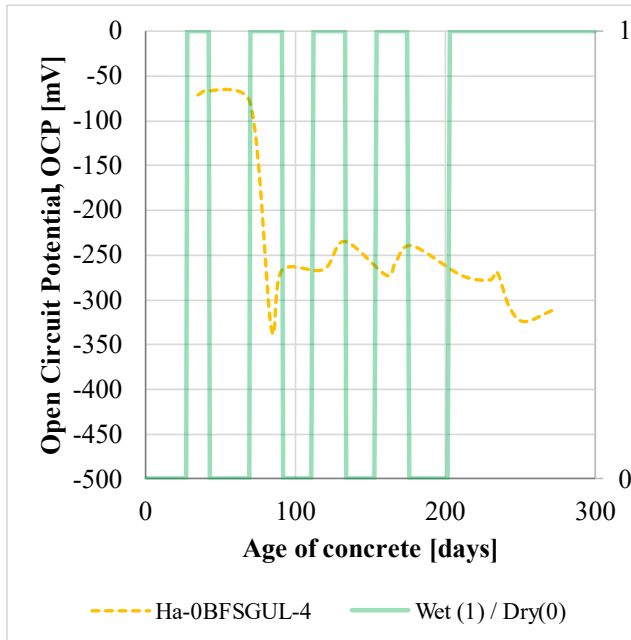
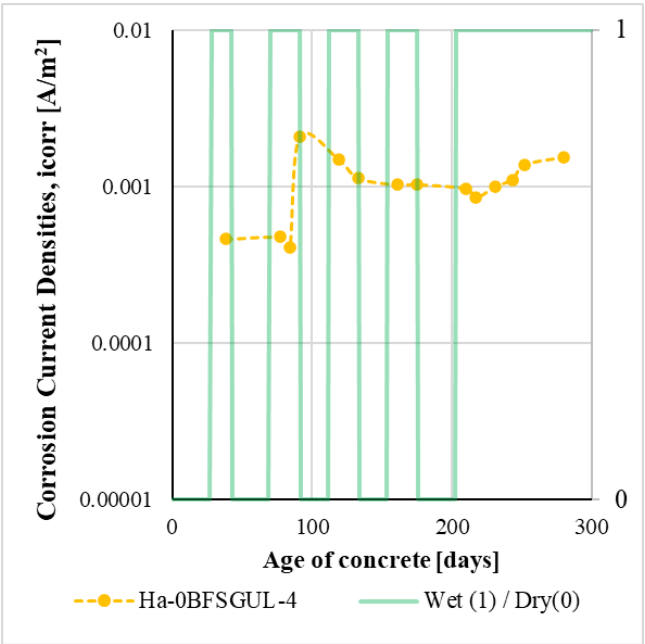
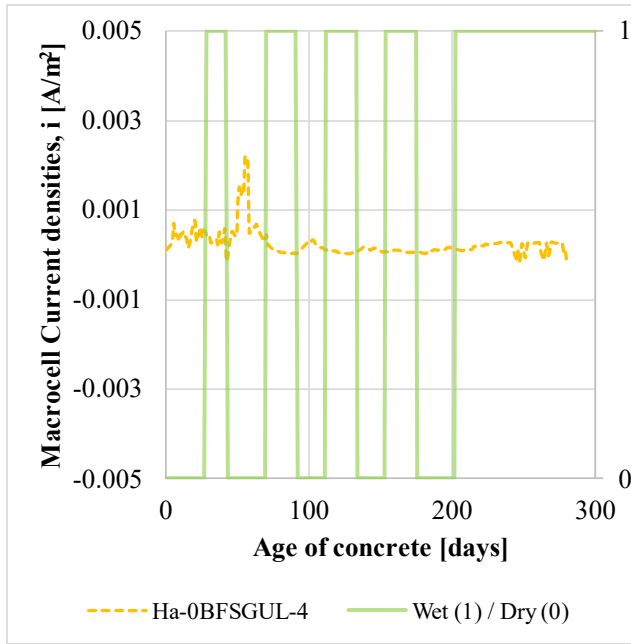
1b) Bottom Bars of Ha-0BFSGUL-1 concrete specimen (autopsied)



BEFORE



2a) Top Bar of Ha-0BFGUL-4 concrete specimen (autopsied)

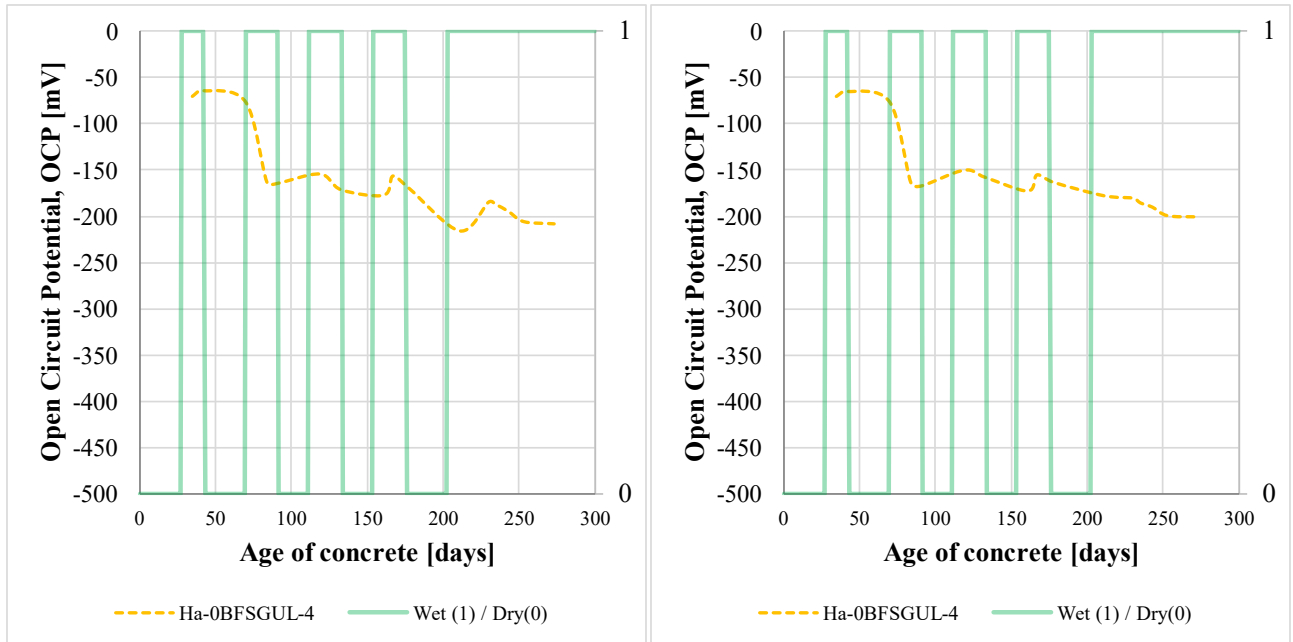


Specimen	Depth Point	Cl [%]	Fe [%]	Ca [%]	Al [%]	Si [%]	S [%]	Mg [%]
Ha-0BFGUL-4	1	-	-	-	-	-	-	-
	2	0.173	1.938	18.515	0.305	3.273	0.918	<LOD
	3	0.036	1.099	24.100	0.923	8.140	0.511	2.327
	4	0.013	0.878	16.886	<LOD	0.716	0.146	<LOD
	5	-	-	-	-	-	-	-
	6	-	-	-	-	-	-	-

Note: <LOD = Below limit of detection by XRF



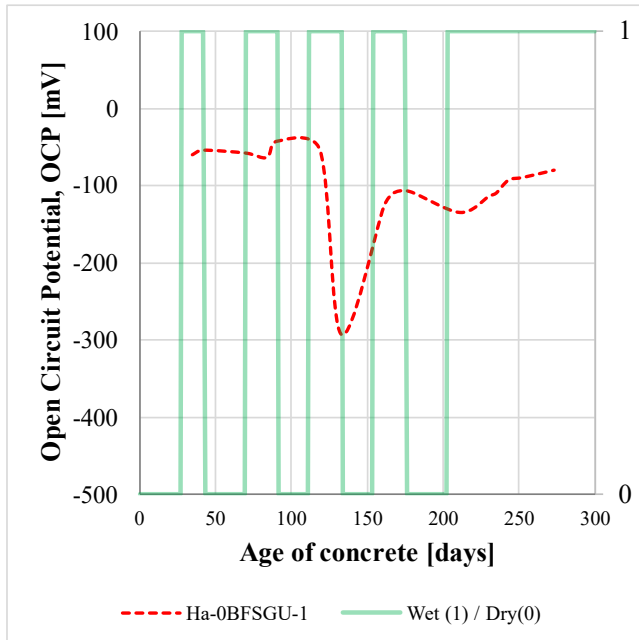
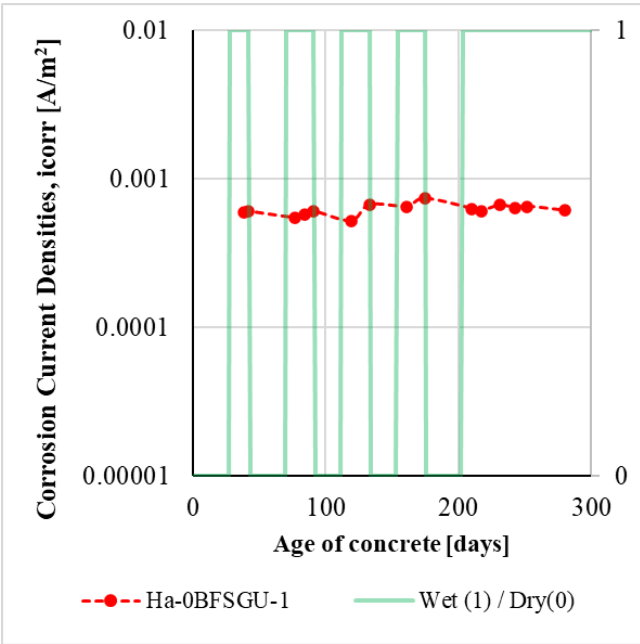
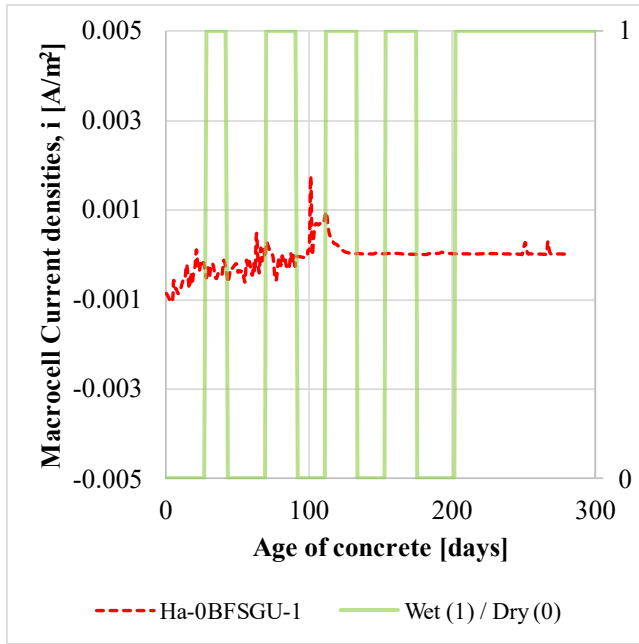
2b) Bottom Bars of Ha-0BFGUL-4 concrete specimen (autopsied)



BEFORE



3a) Top Bar of Ha-0BFSGU-1 concrete specimen (autopsied)



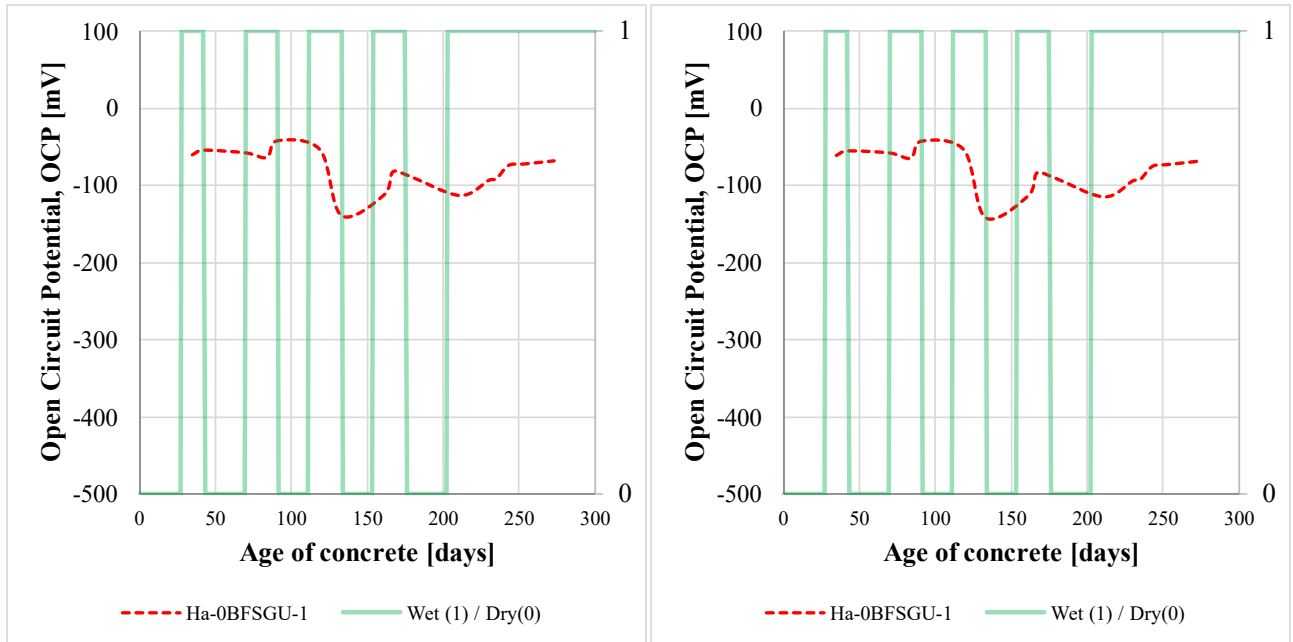
Specimen	Depth Point	Cl [%]	Fe [%]	Ca [%]	Al [%]	Si [%]	S [%]	Mg [%]
Ha-0BFSGU-1	1	0.617	0.545	22.276	0.432	4.673	0.305	2.043
	2	0.119	0.881	23.035	0.564	6.996	0.766	1.727
	3	0.052	1.228	18.156	0.259	2.777	0.850	<LOD
	4	0.043	1.355	24.570	0.723	8.402	1.058	1.076
	5	0.040	0.949	24.430	0.318	4.136	1.079	<LOD
	6	0.049	0.973	25.199	0.563	6.193	1.063	1.108

Note: <LOD = Below limit of detection by XRF

BEFORE



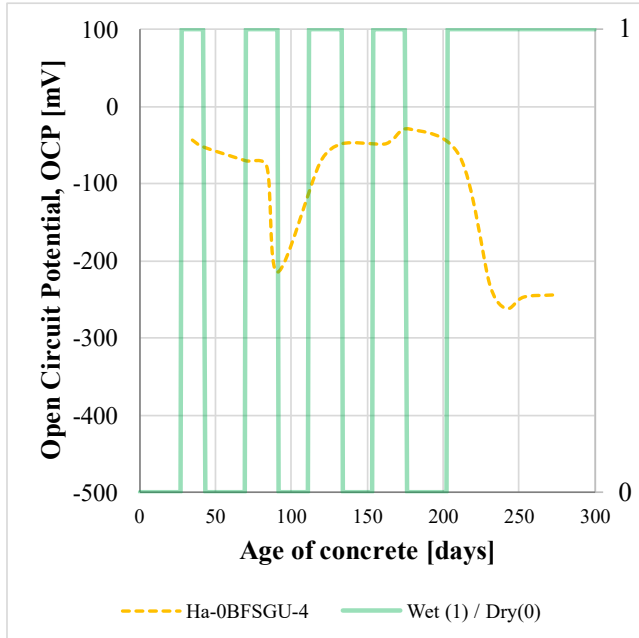
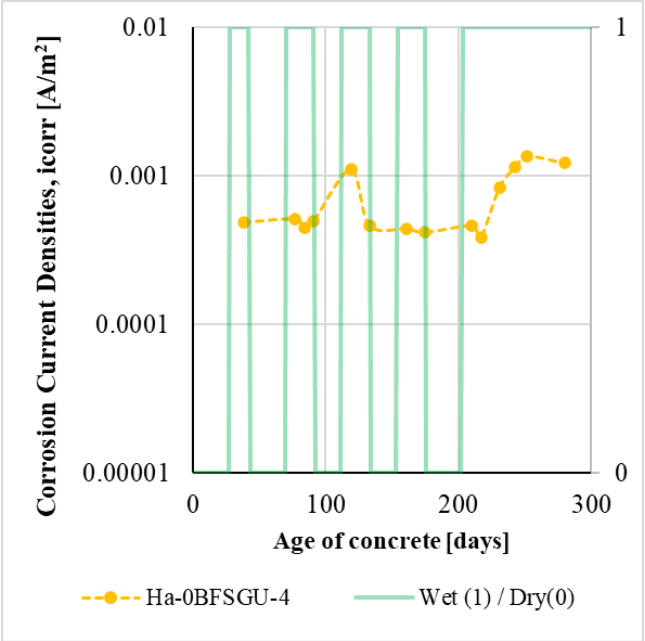
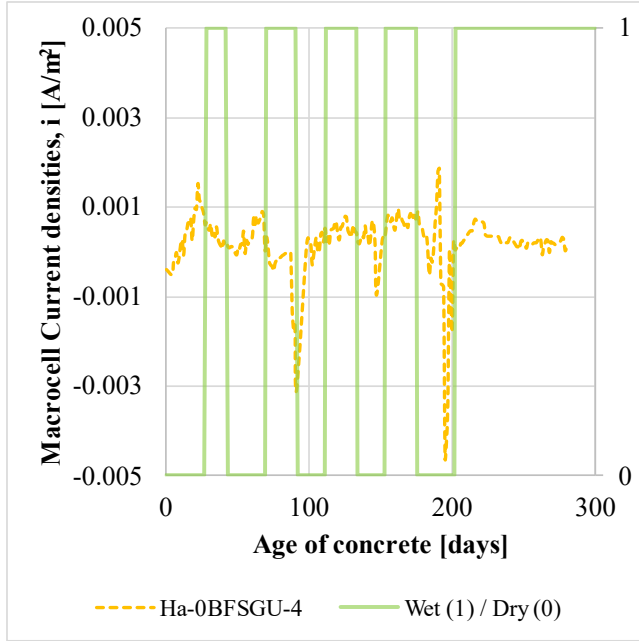
3b) Bottom Bars of Ha-0BFSGU-1 concrete specimen (autopsied)



BEFORE



4a) Top Bar of Ha-0BFSGU-4 concrete specimen (autopsied)



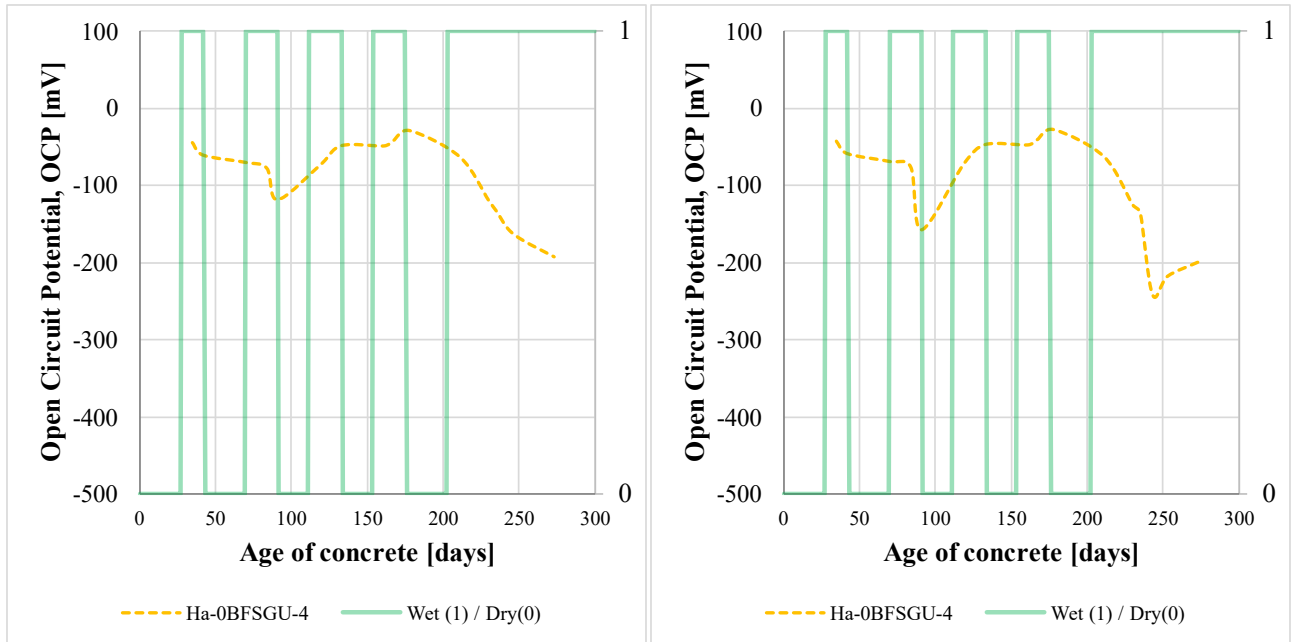
Specimen	Depth Point	Cl [%]	Fe [%]	Ca [%]	Al [%]	Si [%]	S [%]	Mg [%]
Ha-0BFSGU-4	1	-	-	-	-	-	-	-
	2	0.595	1.711	16.091	0.689	6.703	0.801	<LOD
	3	0.064	1.005	18.793	0.385	4.330	0.759	<LOD
	4	0.038	0.559	23.061	0.401	4.964	0.525	1.481
	5	-	-	-	-	-	-	-
	6	-	-	-	-	-	-	-

Note: <LOD = Below limit of detection by XRF

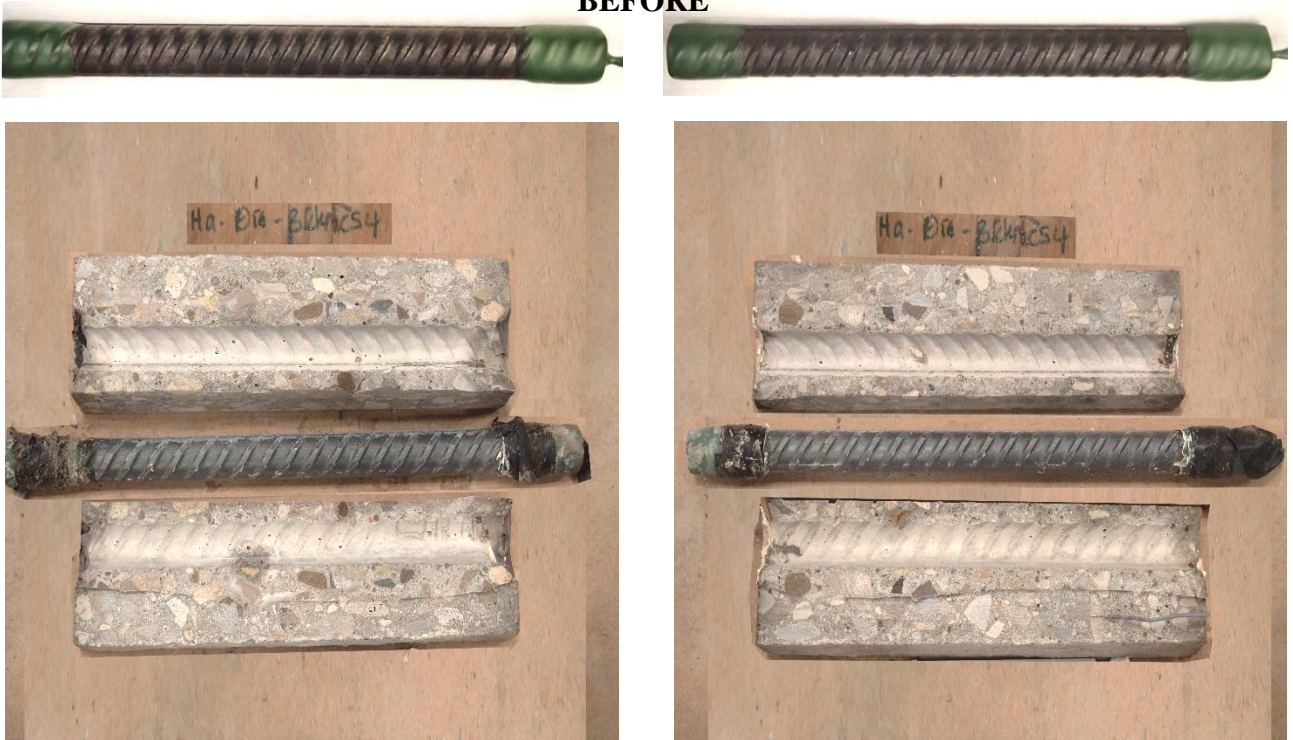
BEFORE



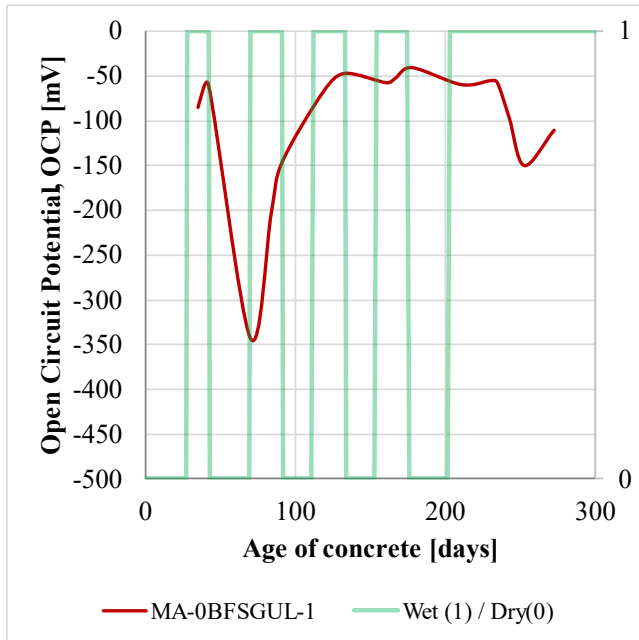
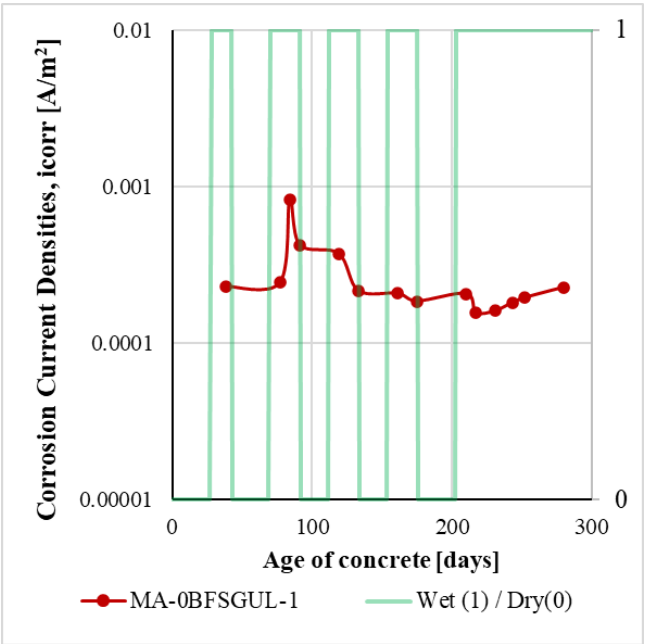
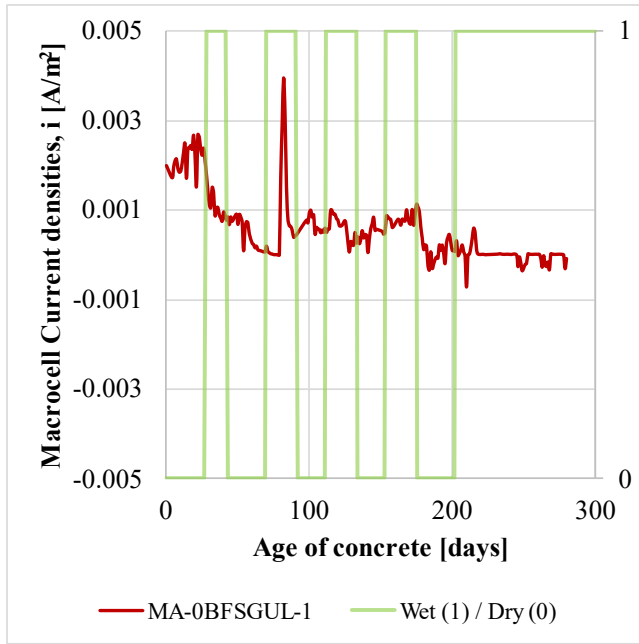
4b) Bottom Bars of Ha-0BFSGU-4 concrete specimen (autopsied)



BEFORE



5a) Top Bar of MA-0BFSGUL-1 concrete specimen (autopsied)



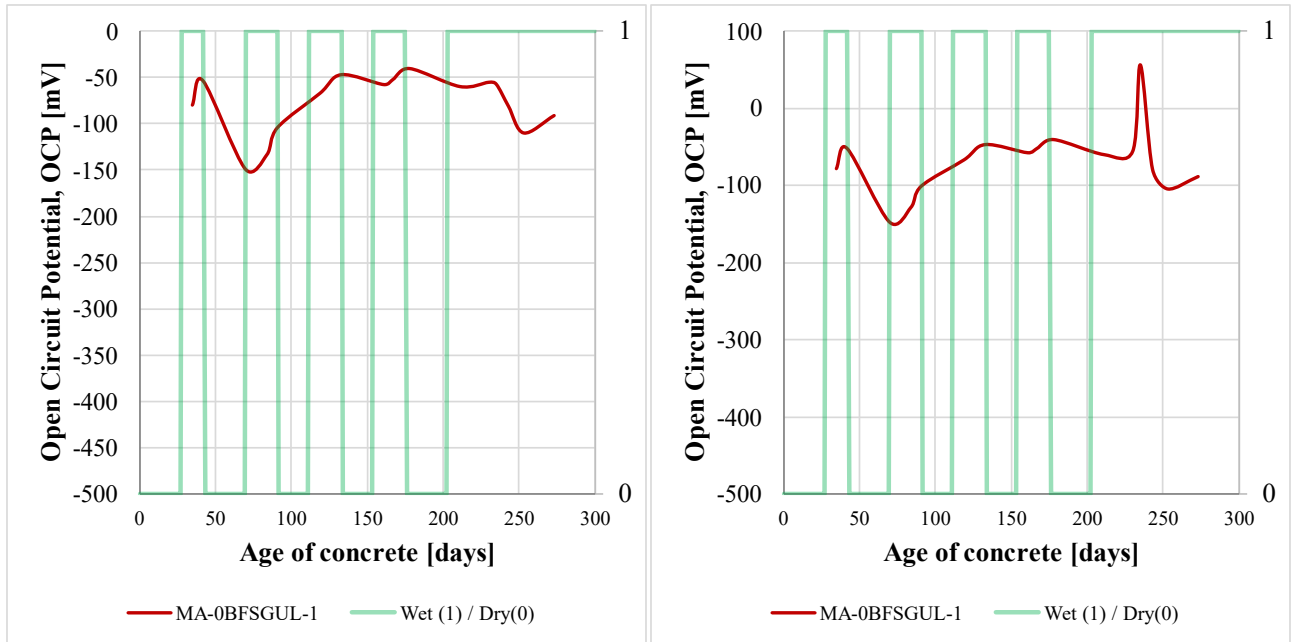
Specimen	Depth Point	Cl [%]	Fe [%]	Ca [%]	Al [%]	Si [%]	S [%]	Mg [%]
MA-0BFSGUL-1	1	-	-	-	-	-	-	-
	2	0.037	0.715	21.405	0.357	3.765	1.013	<LOD
	3	0.052	0.327	12.203	<LOD	3.965	0.193	<LOD
	4	0.060	0.462	18.509	0.299	5.085	0.475	1.172
	5	-	-	-	-	-	-	-
	6	-	-	-	-	-	-	-

Note: <LOD = Below limit of detection by XRF

BEFORE



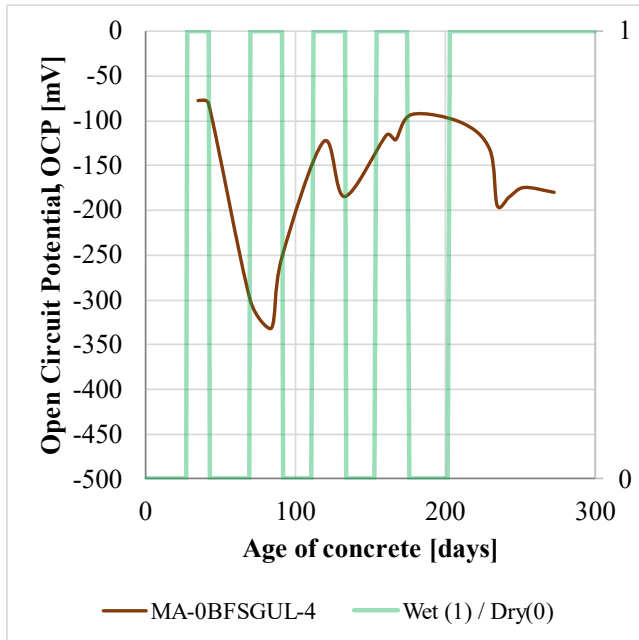
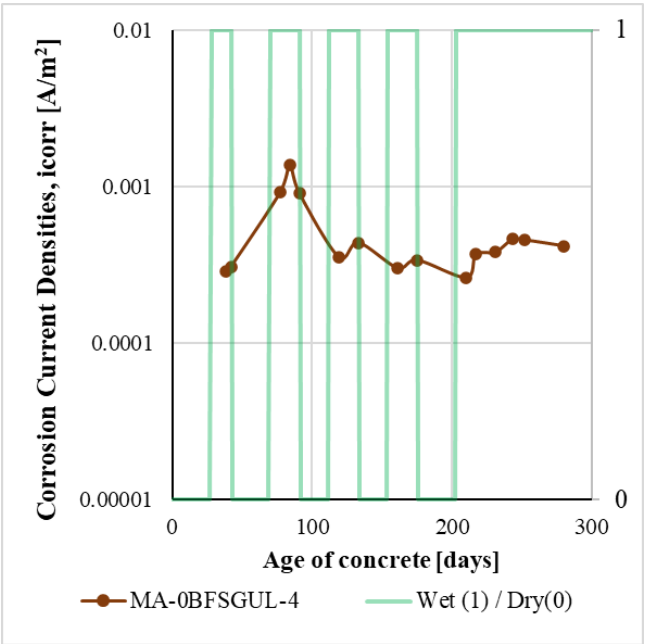
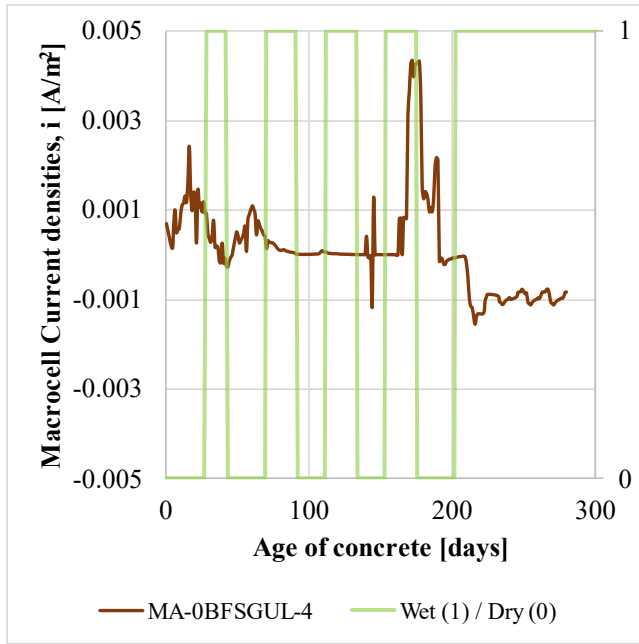
5b) Bottom Bars of MA-0BFGUL-1 concrete specimen (autopsied)



BEFORE



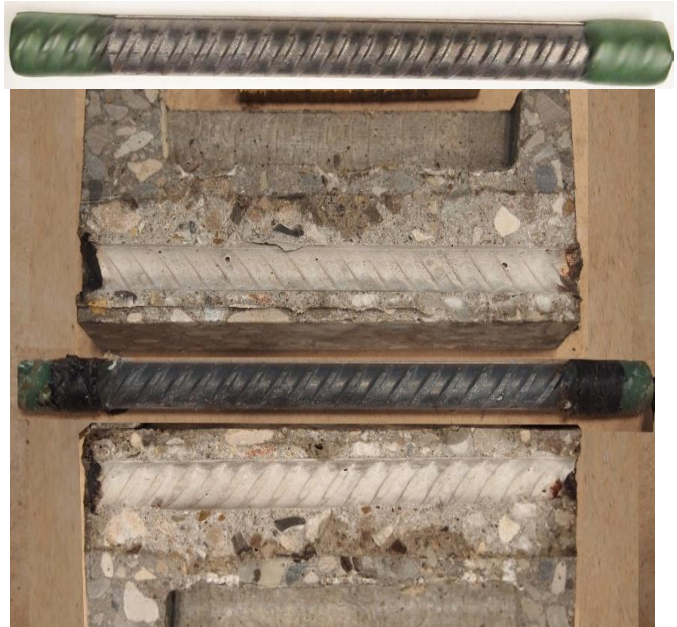
6a) Top Bar of MA-0BFGUL-4 concrete specimen (autopsied)



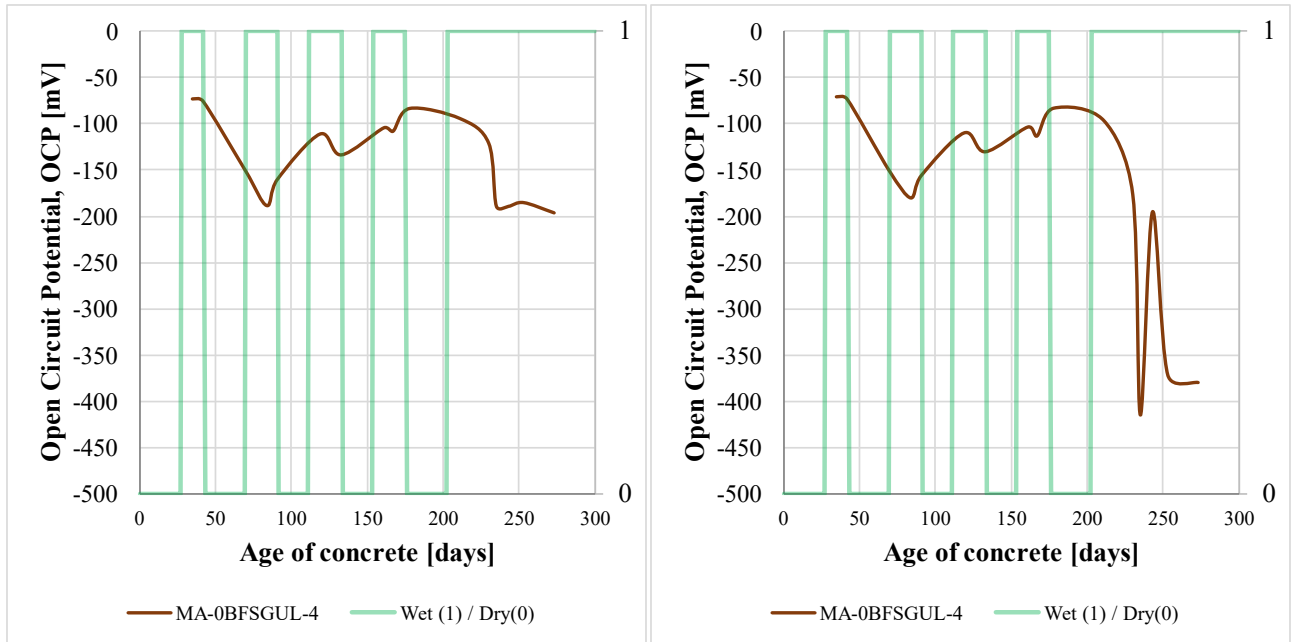
Specimen	Depth Point	Cl [%]	Fe [%]	Ca [%]	Al [%]	Si [%]	S [%]	Mg [%]
MA-0BFGUL-4	1	0.651	1.693	16.254	0.847	10.538	0.339	1.783
	2	0.180	0.882	25.061	0.868	9.060	0.868	1.460
	3	0.039	0.679	19.553	0.265	3.092	0.869	<LOD
	4	0.032	0.897	24.331	0.564	5.940	0.985	<LOD
	5	0.042	0.715	21.886	0.384	3.907	0.878	<LOD
	6	0.036	0.780	21.928	0.568	4.331	0.954	1.932

Note: <LOD = Below limit of detection by XRF

BEFORE



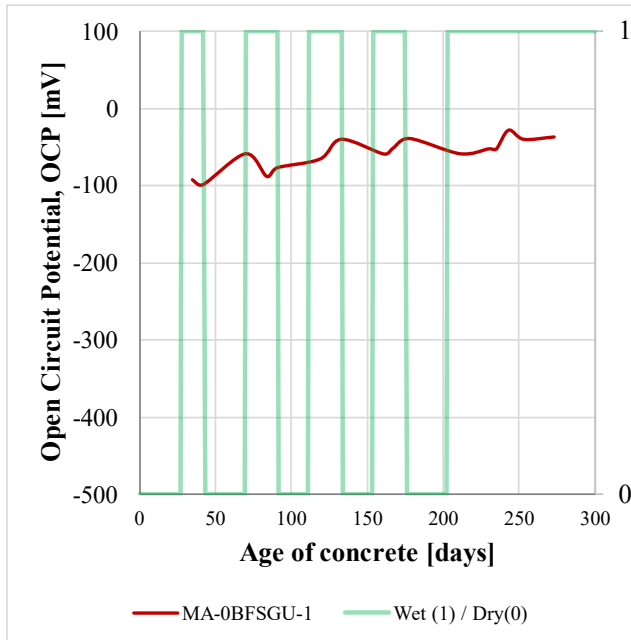
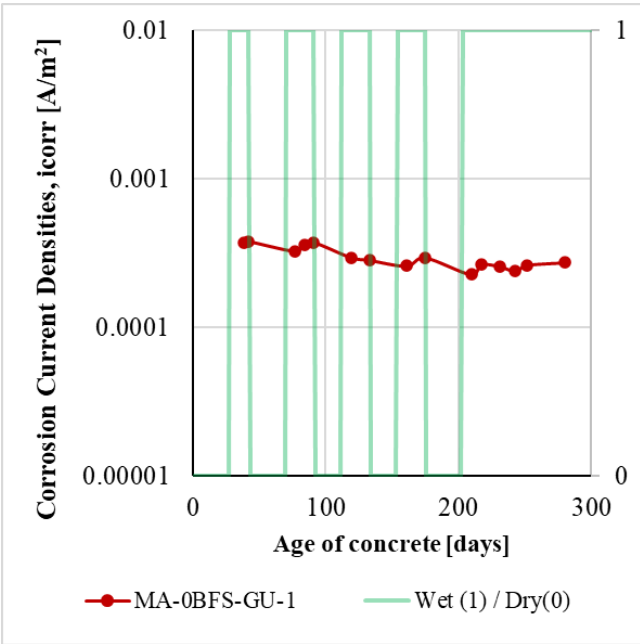
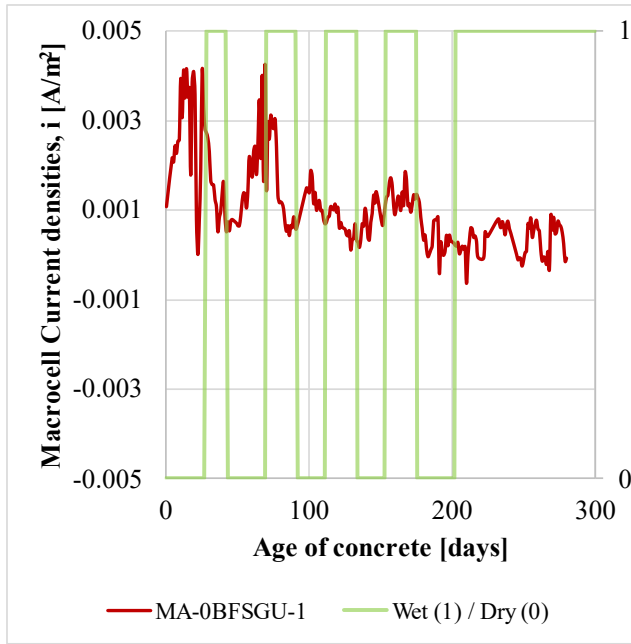
6b) Bottom Bars of MA-0BFGUL-4 concrete specimen (autopsied)



BEFORE



7a) Top Bar of MA-0BFSGU-1 concrete specimen (autopsied)

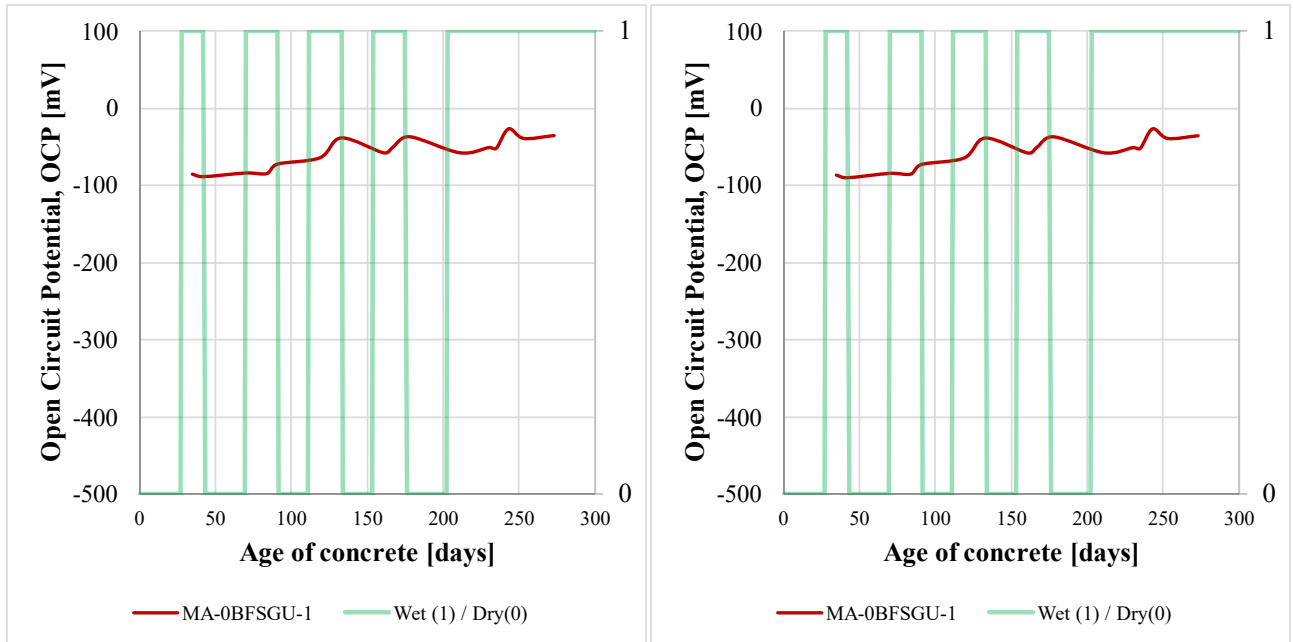


Specimen	Depth Point	Cl [%]	Fe [%]	Ca [%]	Al [%]	Si [%]	S [%]	Mg [%]
MA-0BFSGU-1	1	-	-	-	-	-	-	-
	2	0.049	0.984	16.568	0.609	7.741	0.996	<LOD
	3	0.031	0.710	22.035	<LOD	2.422	0.768	<LOD
	4	0.072	0.381	7.937	<LOD	2.099	#DIV/0!	<LOD
	5	-	-	-	-	-	-	-
	6	-	-	-	-	-	-	-

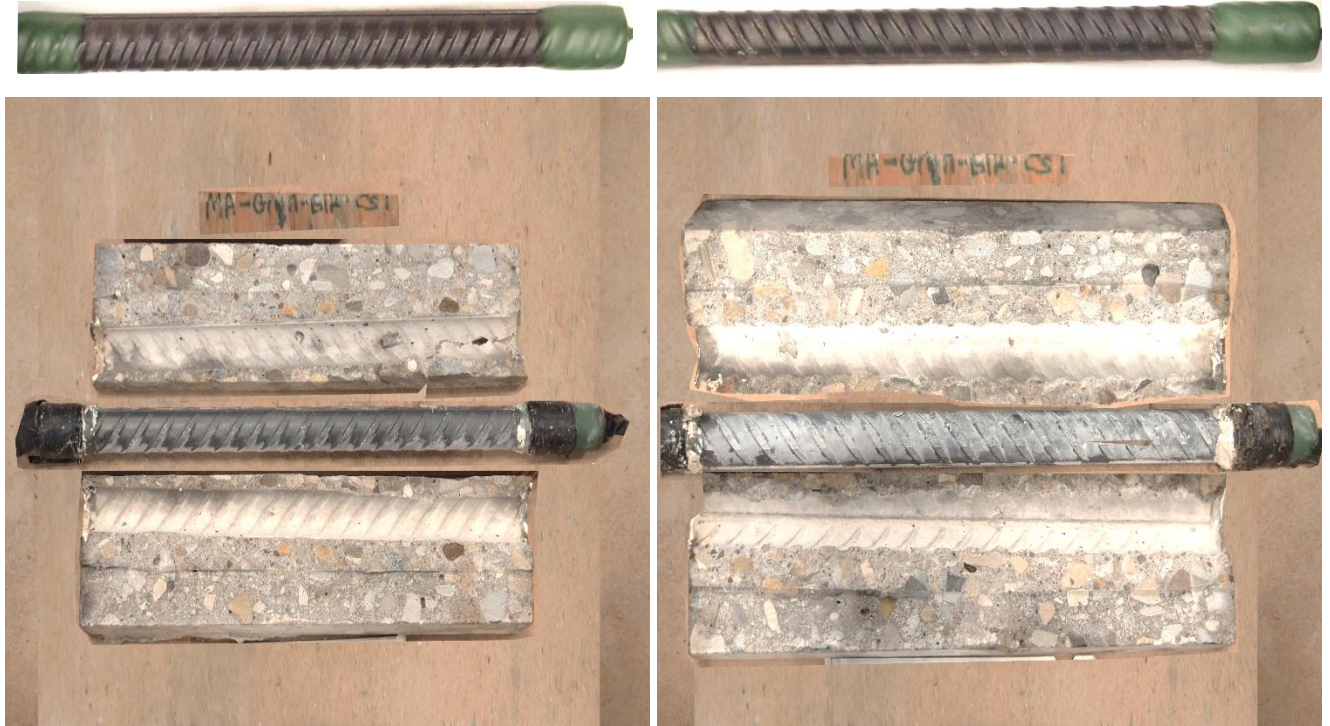
Note: <LOD = Below limit of detection by XRF



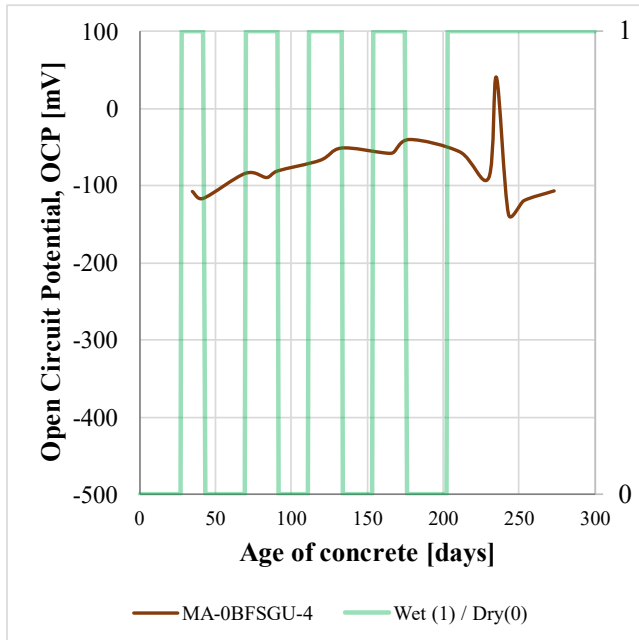
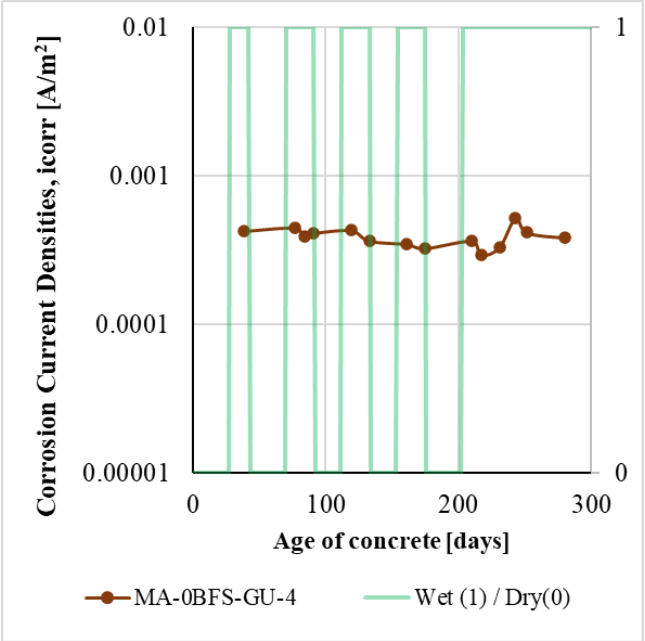
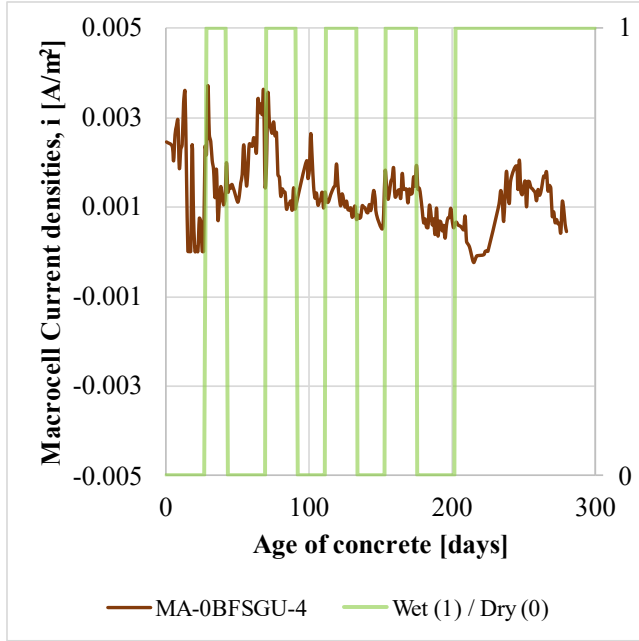
7b) Bottom Bars of MA-0BFSGU-1 concrete specimen (autopsied)



BEFORE



8a) Top Bar of MA-0BFSGU-4 concrete specimen (autopsied)



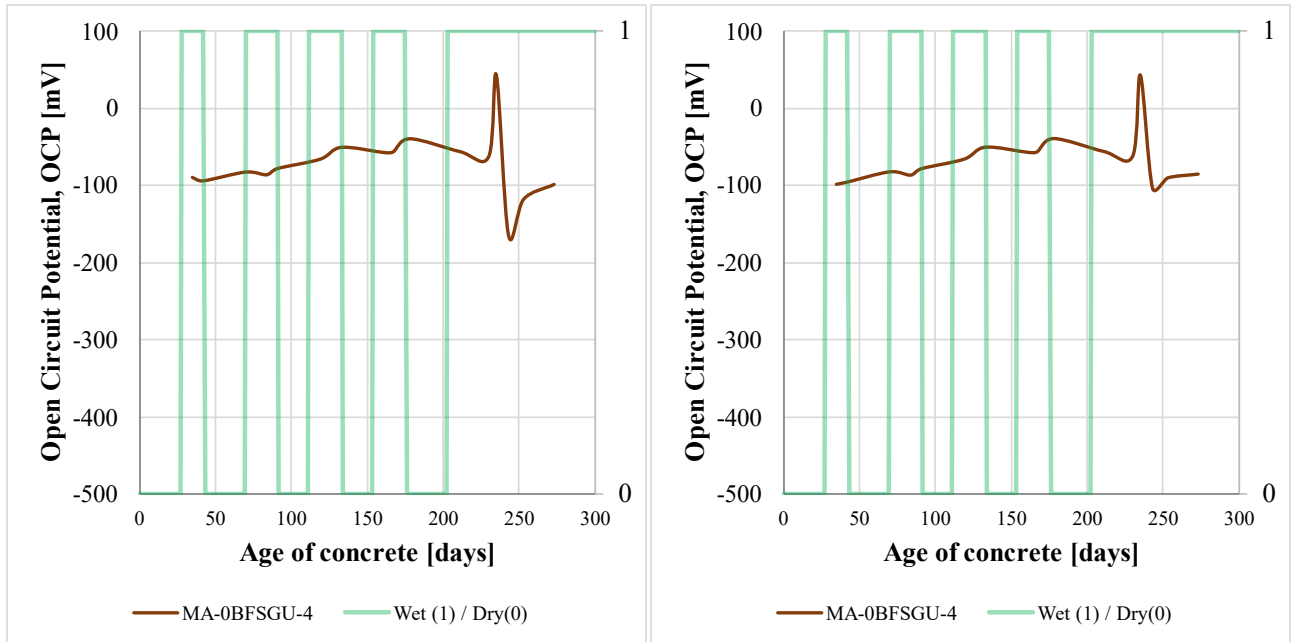
Specimen	Depth Point	Cl [%]	Fe [%]	Ca [%]	Al [%]	Si [%]	S [%]	Mg [%]
MA-0BFSGU-4	1	0.803	0.872	23.036	0.583	7.868	0.500	1.004
	2	0.178	0.895	24.348	0.707	8.497	0.873	1.167
	3	0.038	0.722	21.143	<LOD	2.726	0.957	<LOD
	4	0.043	1.250	24.188	0.578	7.169	0.999	<LOD
	5	0.050	0.758	22.739	0.432	3.230	0.886	<LOD
	6	0.043	0.770	22.287	0.346	3.404	0.872	<LOD

Note: <LOD = Below limit of detection by XRF

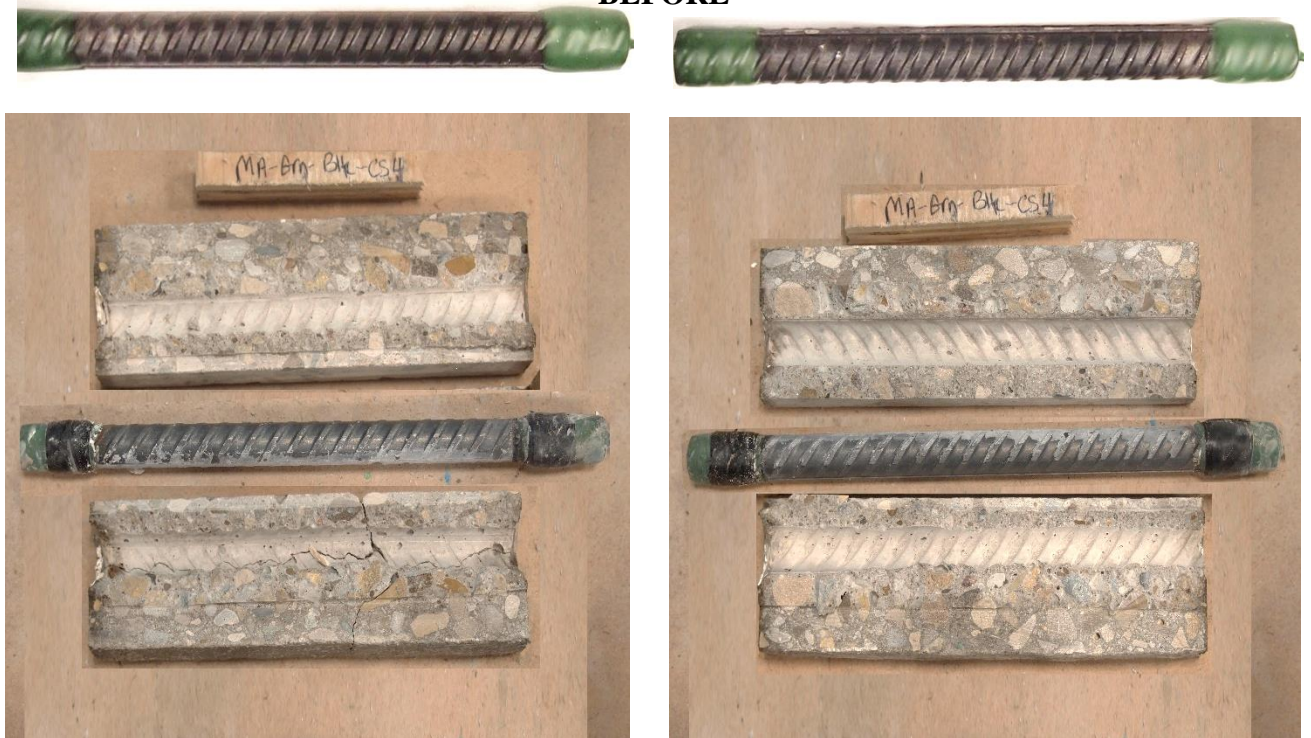
BEFORE



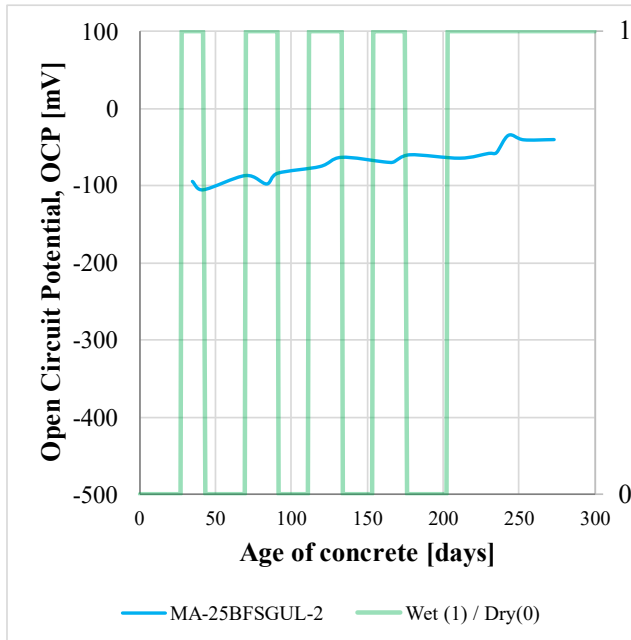
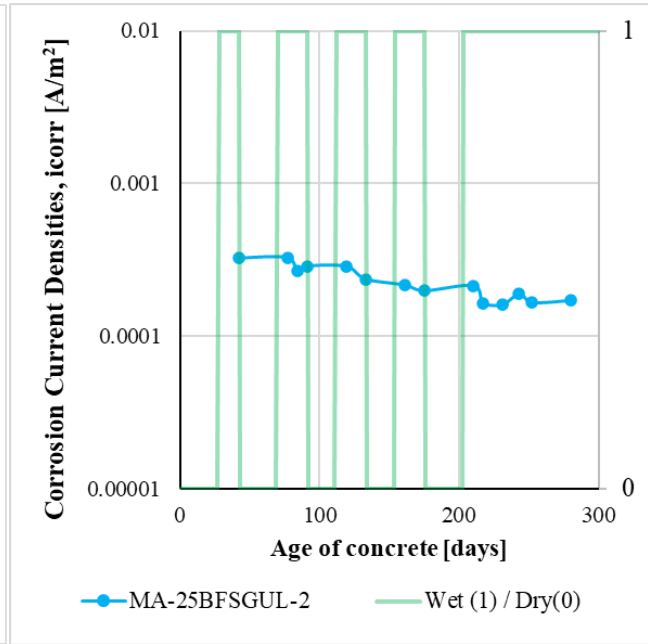
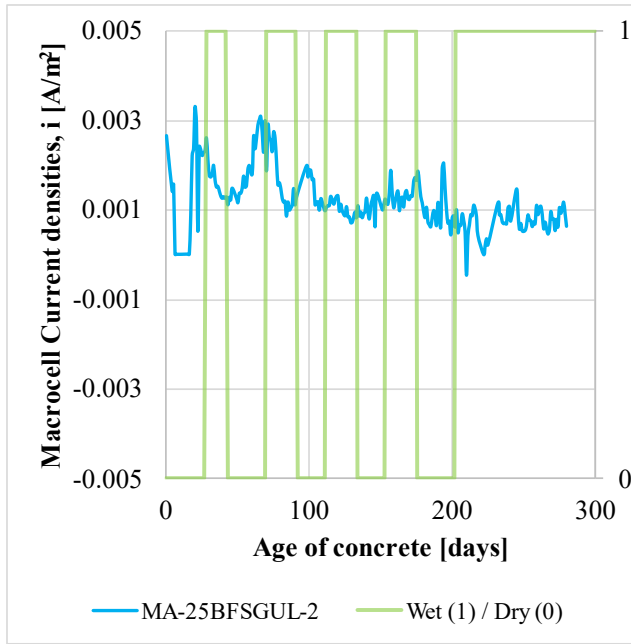
8b) Bottom Bars of MA-0BFSGU-4 concrete specimen (autopsied)



BEFORE



9a) Top Bar of MA-25BFGUL-2 concrete specimen (autopsied)



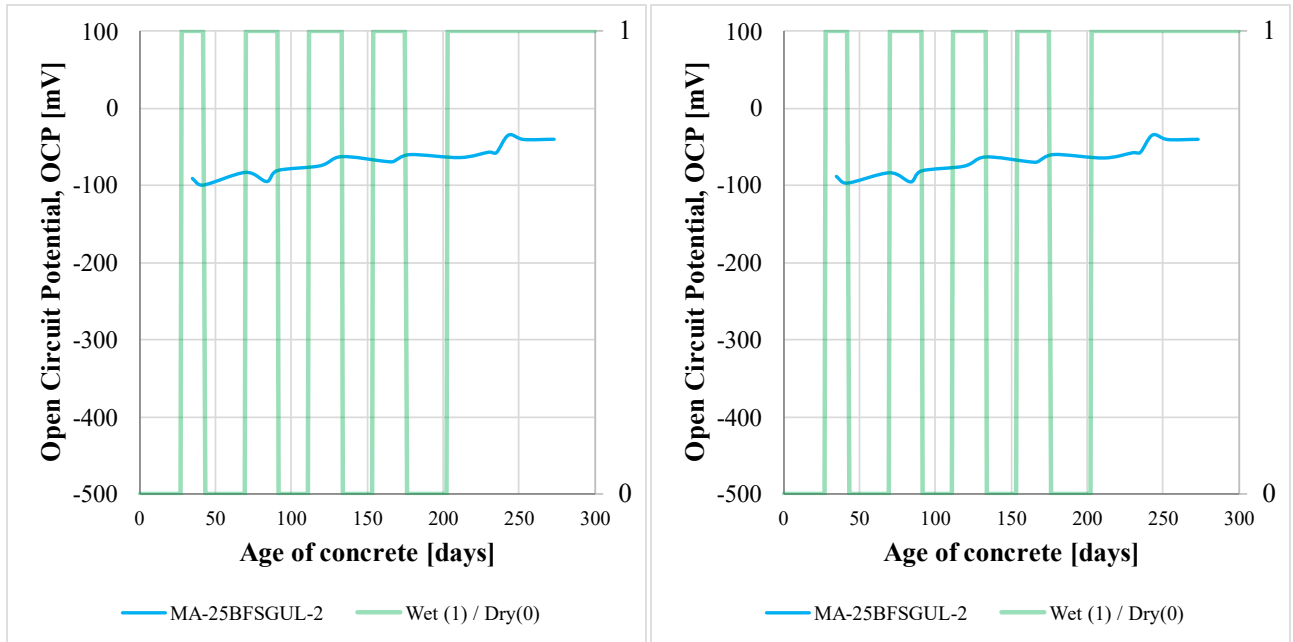
Specimen	Depth Point	Cl [%]	Fe [%]	Ca [%]	Al [%]	Si [%]	S [%]	Mg [%]
MA-25BFGUL-2	1	0.870	0.575	20.502	0.533	6.749	0.369	1.533
	2	0.197	0.747	21.961	0.945	9.737	0.834	1.101
0	3	0.045	0.521	16.879	0.210	3.575	0.636	<LOD
	4	0.033	0.781	20.608	0.875	9.352	0.819	<LOD
	5	0.044	0.741	20.484	0.505	5.612	0.949	<LOD
	6	0.034	0.865	23.702	0.559	6.675	1.118	0.935

Note: <LOD = Below limit of detection by XRF

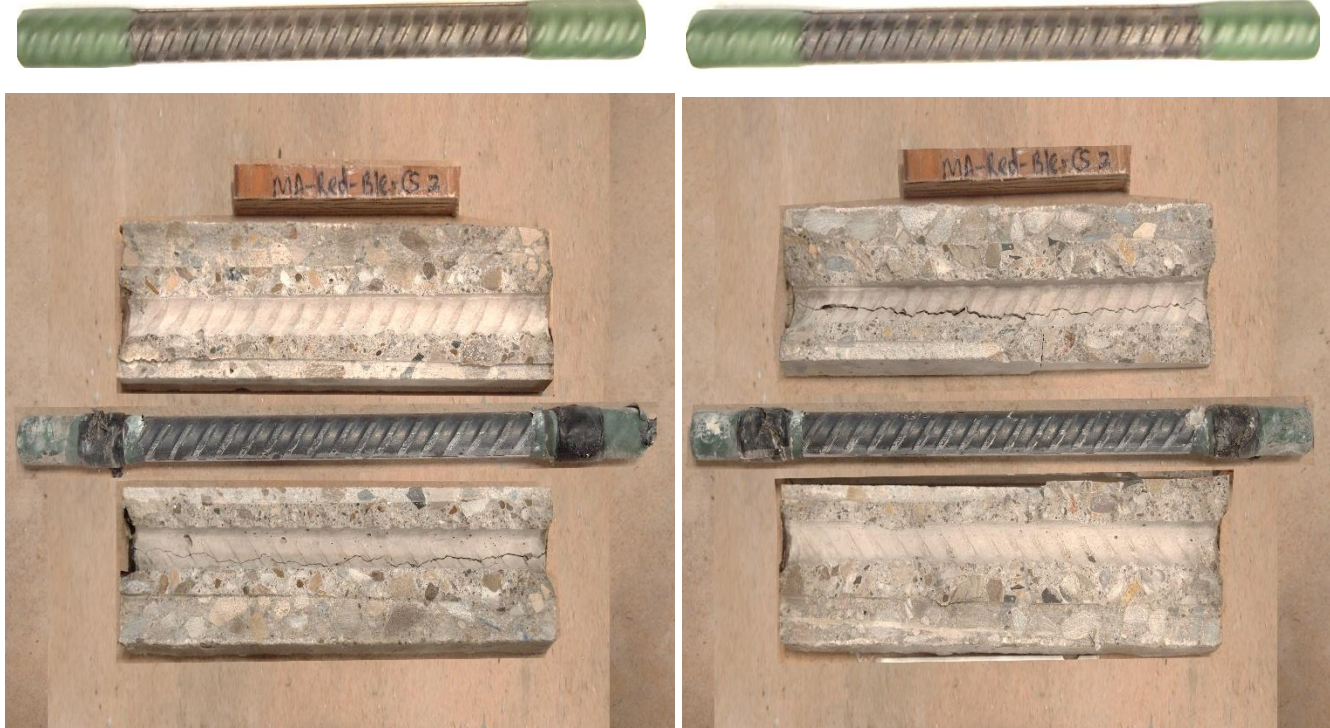
BEFORE



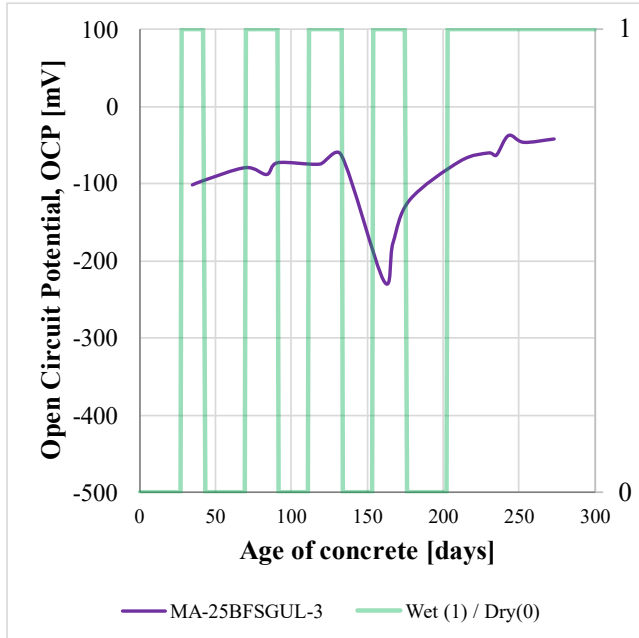
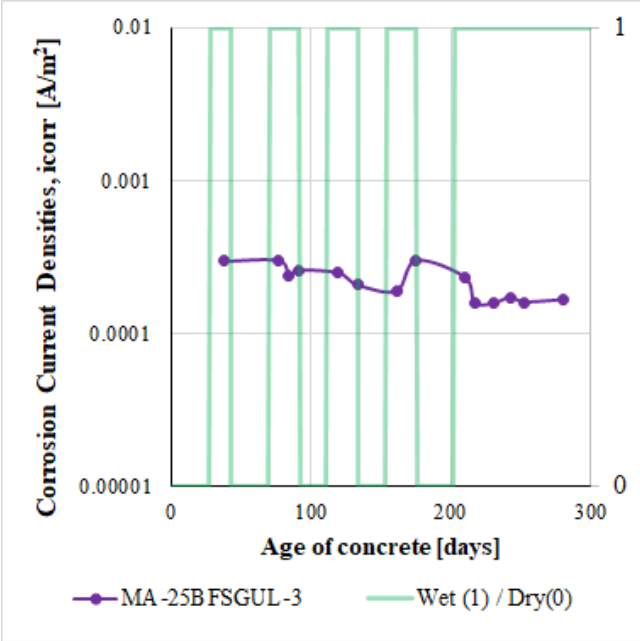
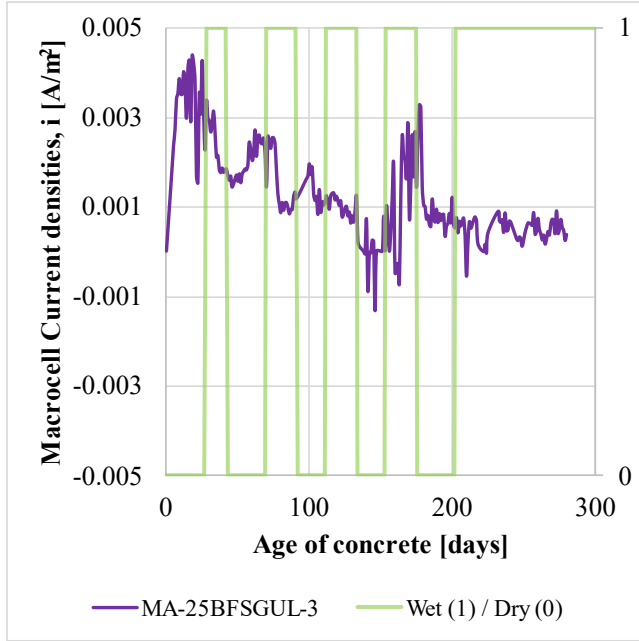
9b) Bottom Bars of MA-25BFGUL-2 concrete specimen (autopsied)



BEFORE



10a) Top Bar of MA-25BFGUL-3 concrete specimen (autopsied)



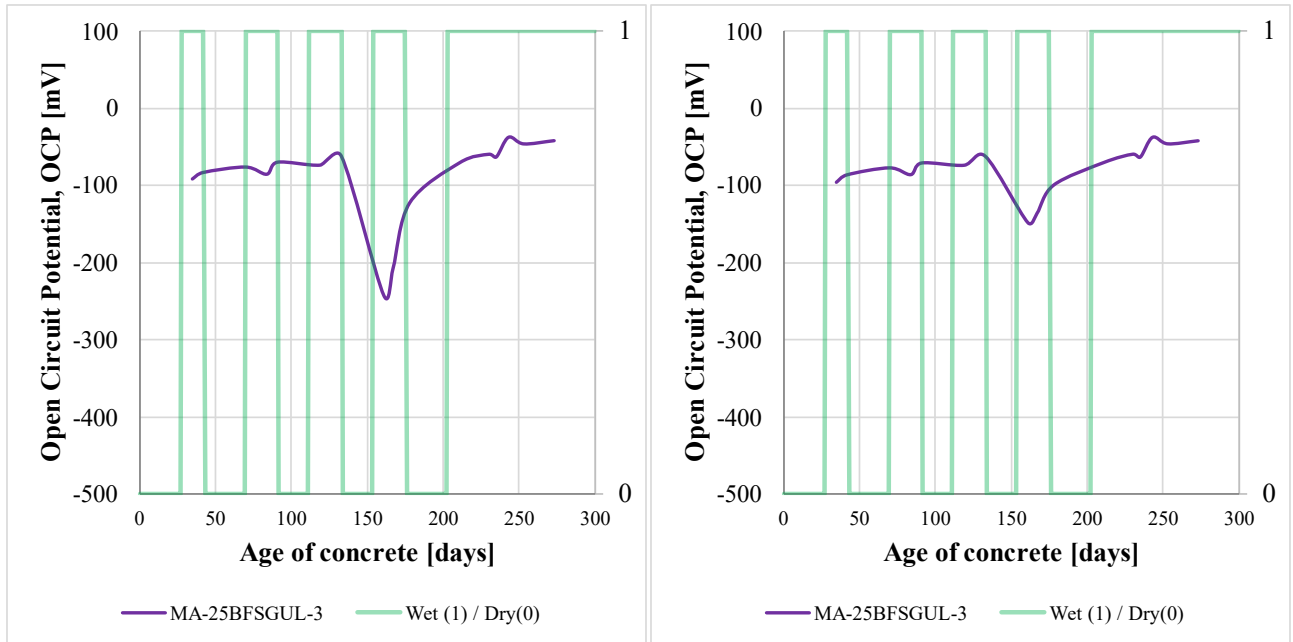
Specimen	Depth Point	Cl [%]	Fe [%]	Ca [%]	Al [%]	Si [%]	S [%]	Mg [%]
MA-25BFGUL-3	1	0.730	0.618	27.085	0.780	7.363	0.321	1.177
	2	0.199	0.861	23.914	0.719	7.562	0.662	1.902
	3	0.029	0.614	22.970	0.634	6.373	1.018	<LOD
	4	0.029	0.742	20.726	0.313	4.024	0.854	<LOD
	5	0.032	0.557	22.062	0.655	7.749	0.704	<LOD
	6	0.035	0.835	22.676	0.464	5.855	1.103	<LOD

Note: <LOD = Below limit of detection by XRF

BEFORE



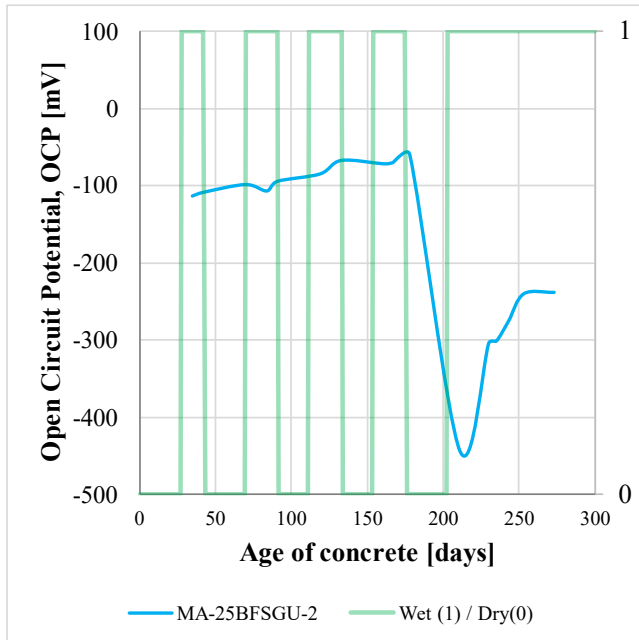
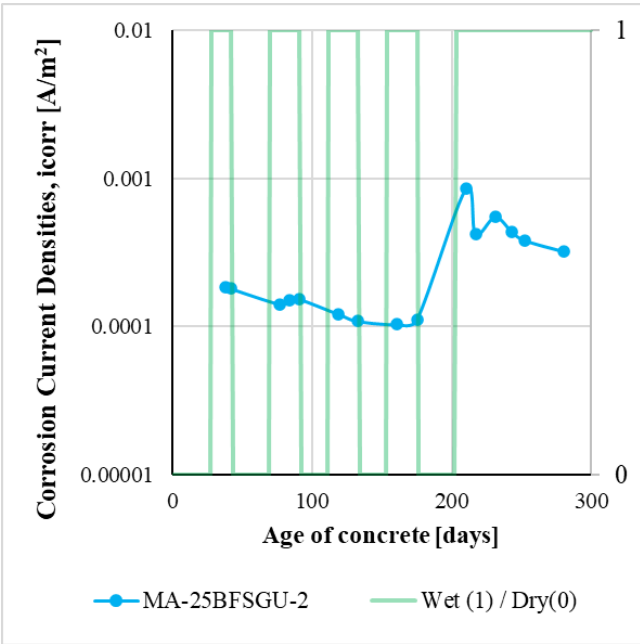
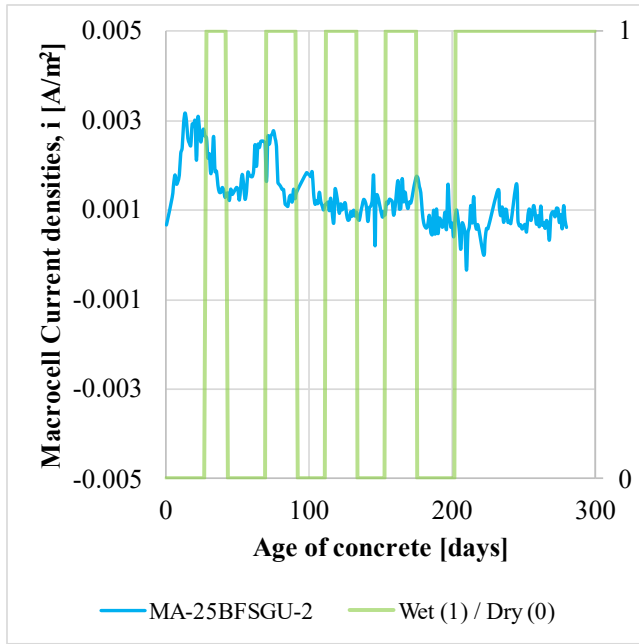
10b) Bottom Bars of MA-25BFGUL-3 concrete specimen (autopsied)



BEFORE



11a) Top Bar of MA-25BFSGU-2 concrete specimen (autopsied)



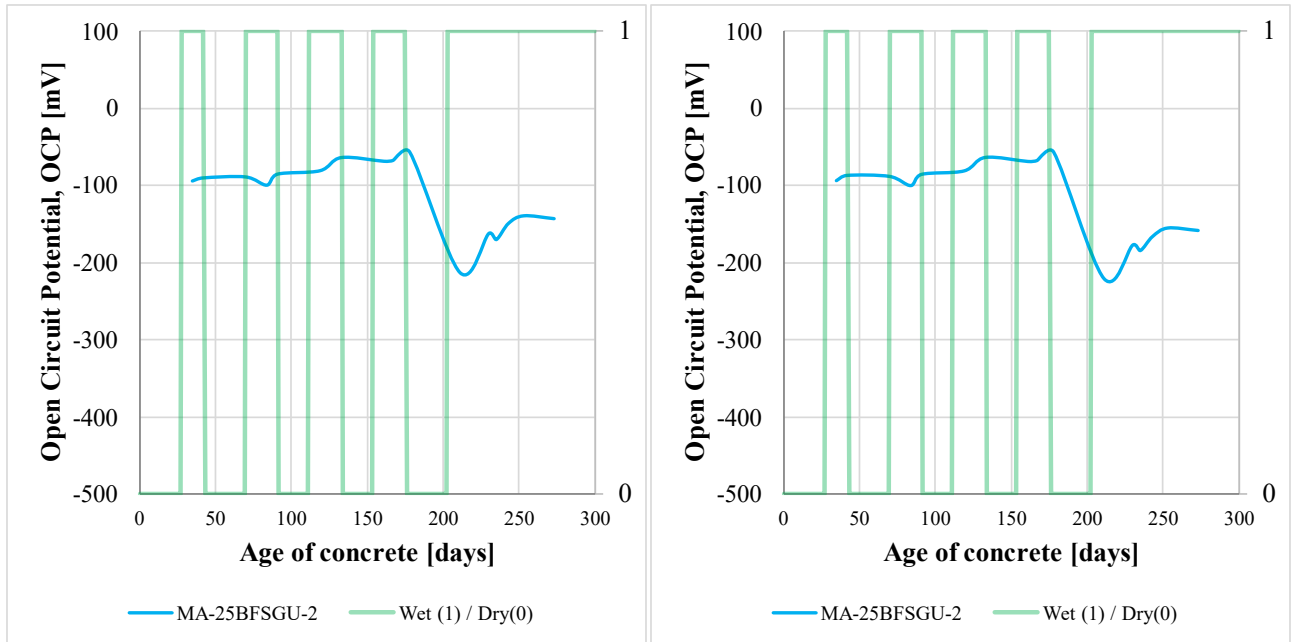
Specimen	Depth Point	Cl [%]	Fe [%]	Ca [%]	Al [%]	Si [%]	S [%]	Mg [%]
MA-25BFSGU-2	1	0.664	0.727	20.856	0.429	4.689	0.349	1.265
	2	0.055	0.799	20.883	0.690	8.160	0.707	0.864
	3	0.049	0.622	16.486	<LOD	3.304	0.716	<LOD
	4	0.039	0.801	23.084	0.651	7.105	0.906	1.785
	5	0.039	0.817	23.158	0.583	5.957	1.164	<LOD
	6	0.039	0.871	23.461	0.525	5.571	1.181	<LOD

Note: <LOD = Below limit of detection by XRF

BEFORE



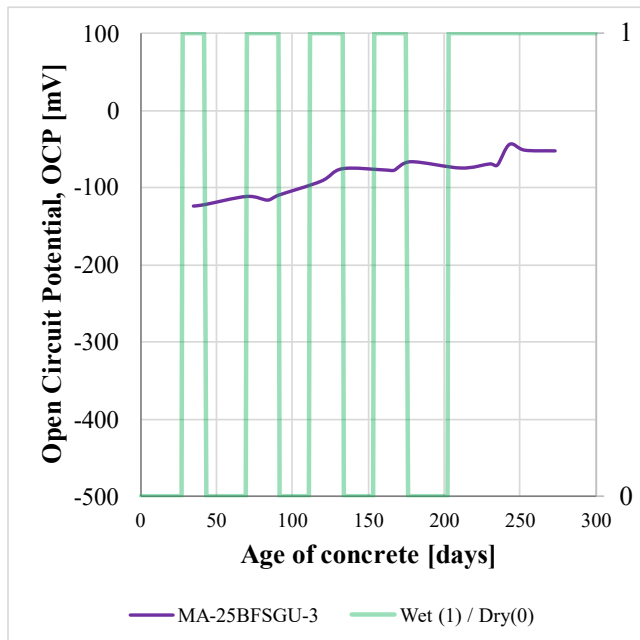
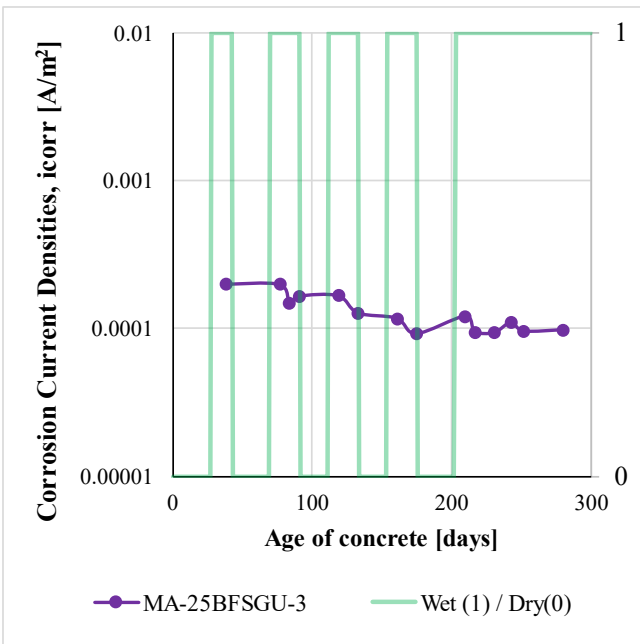
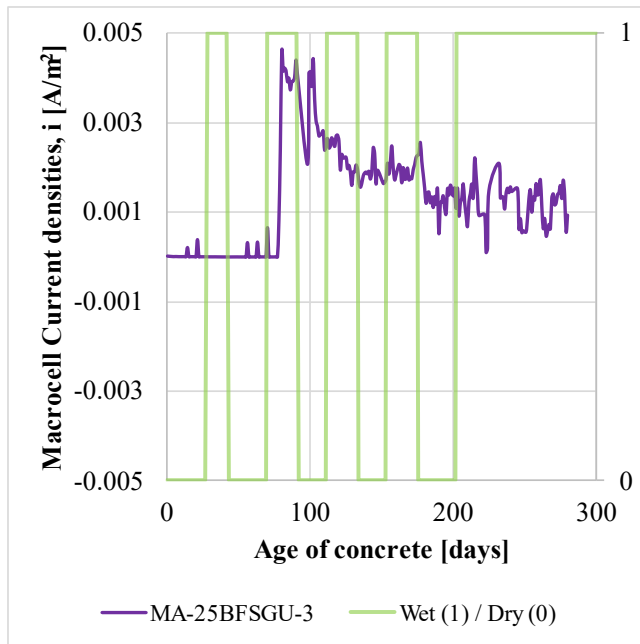
11b) Bottom Bars of MA-25BFGU-2 concrete specimen (autopsied)



BEFORE



12a) Top Bar of MA-25BFSGU-3 concrete specimen (autopsied)



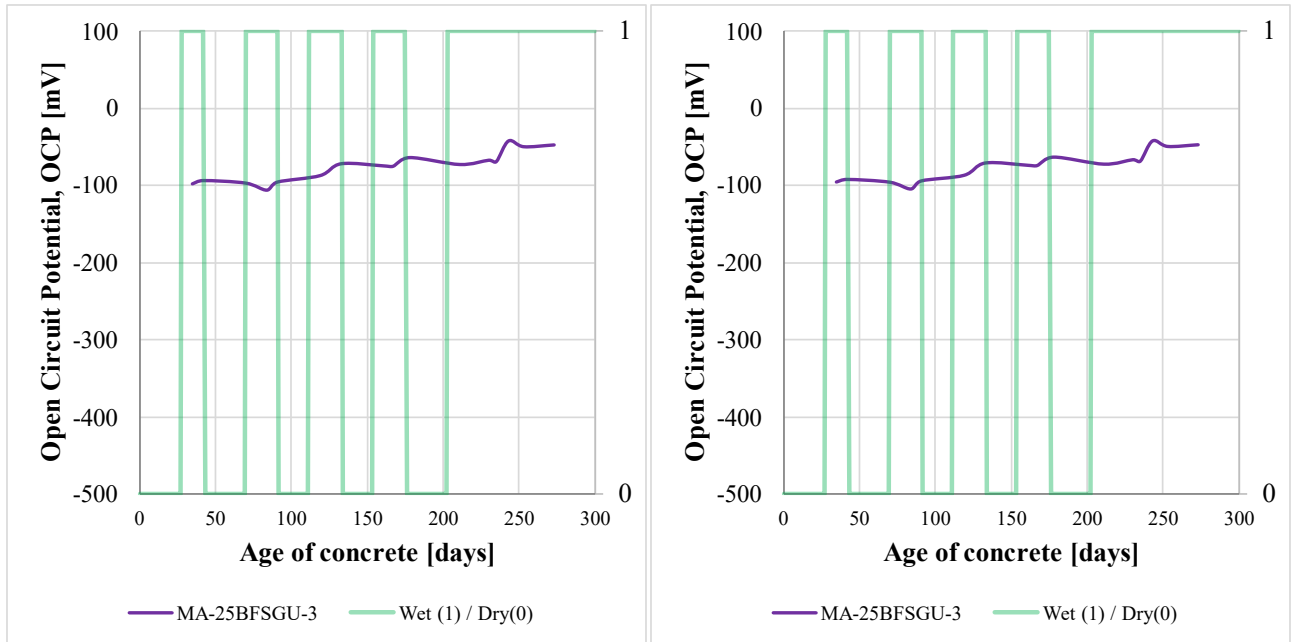
Specimen	Depth Point	Cl [%]	Fe [%]	Ca [%]	Al [%]	Si [%]	S [%]	Mg [%]
MA-25BFSGU-3	1	0.594	0.745	22.105	0.614	6.880	0.610	<LOD
	2	0.120	0.650	25.580	0.867	7.273	0.598	3.674
	3	0.033	0.735	19.486	0.484	5.460	0.920	1.153
	4	0.031	1.110	23.739	0.563	6.398	1.200	<LOD
	5	0.033	0.713	20.367	0.643	8.161	0.775	<LOD
	6	0.041	0.656	21.044	0.386	5.145	0.921	<LOD

Note: <LOD = Below limit of detection by XRF

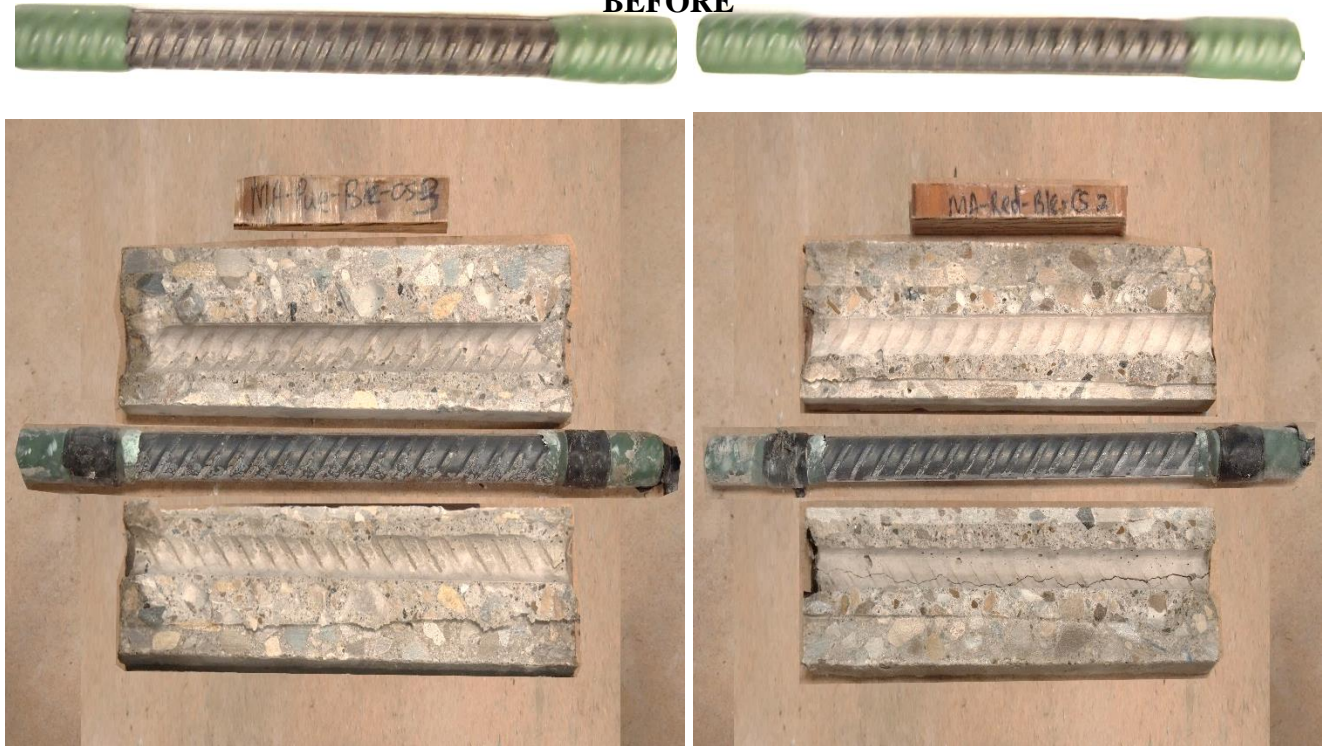
BEFORE



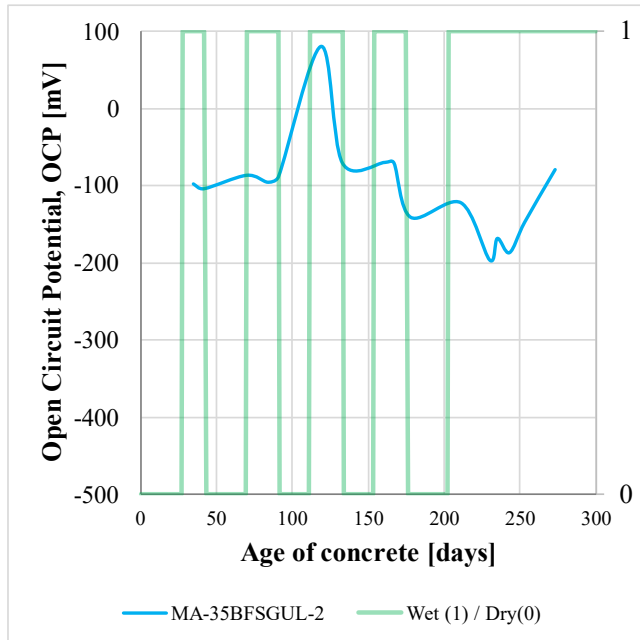
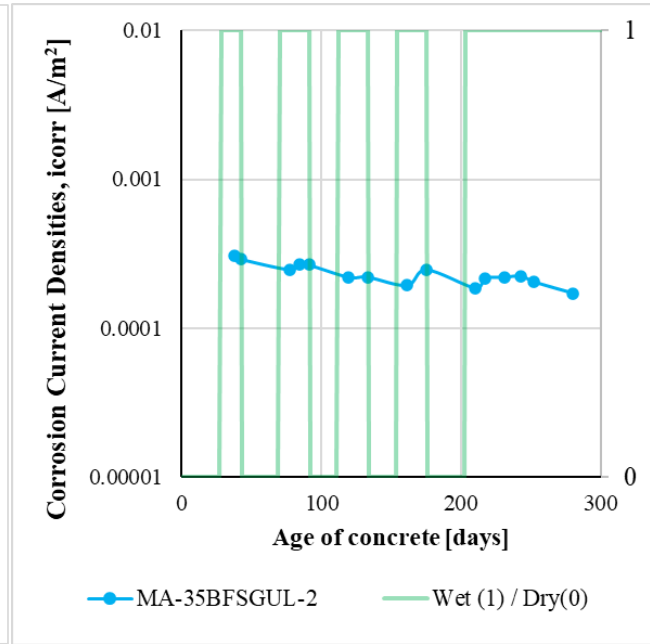
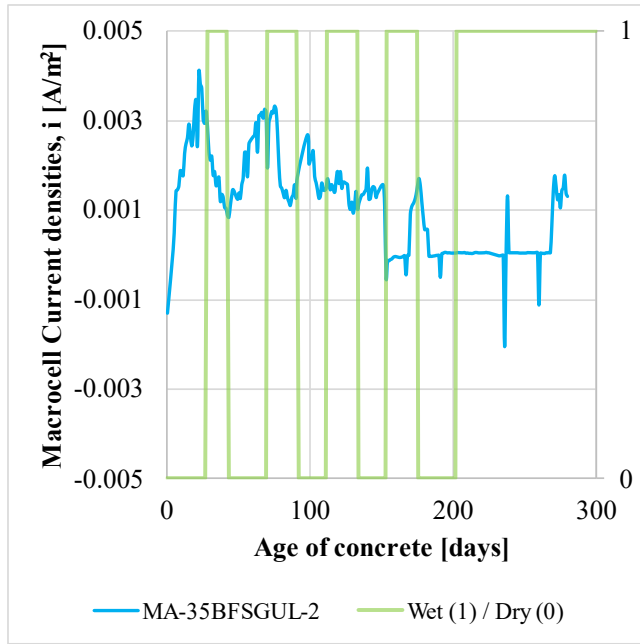
12b) Bottom Bars of MA-25BFGU-3 concrete specimen (autopsied)



BEFORE



13a) Top Bar of MA-35BFGUL-2 concrete specimen (autopsied)



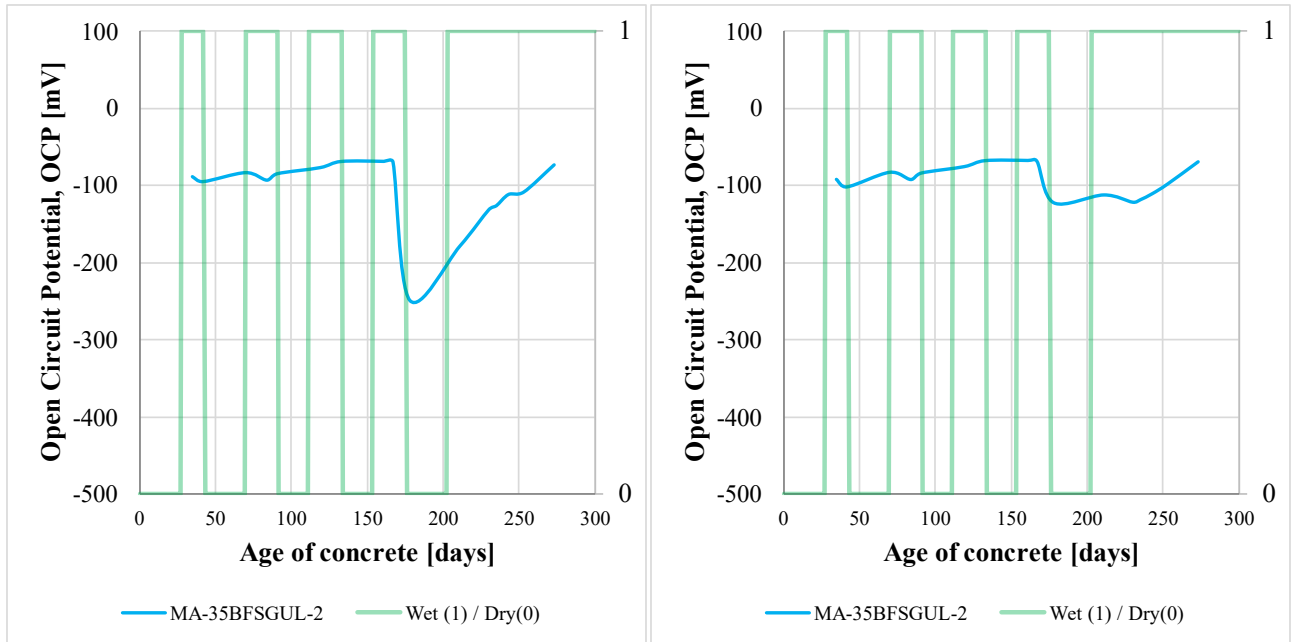
Specimen	Depth Point	Cl [%]	Fe [%]	Ca [%]	Al [%]	Si [%]	S [%]	Mg [%]
MA-35BFGUL-2	1	0.796	0.519	21.688	0.373	6.041	0.347	1.164
	2	0.148	0.779	22.268	0.932	11.940	0.773	1.093
	3	0.038	0.599	21.126	0.581	4.782	0.853	<LOD
	4	0.031	0.875	21.883	0.802	9.088	0.761	0.986
	5	0.033	0.658	22.680	0.461	5.894	1.017	<LOD
	6	0.034	0.566	20.727	0.423	5.100	0.873	<LOD

Note: <LOD = Below limit of detection by XRF

BEFORE



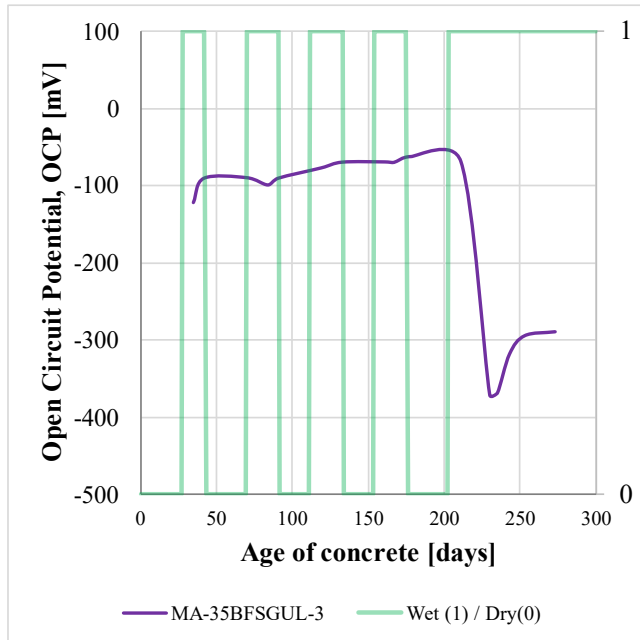
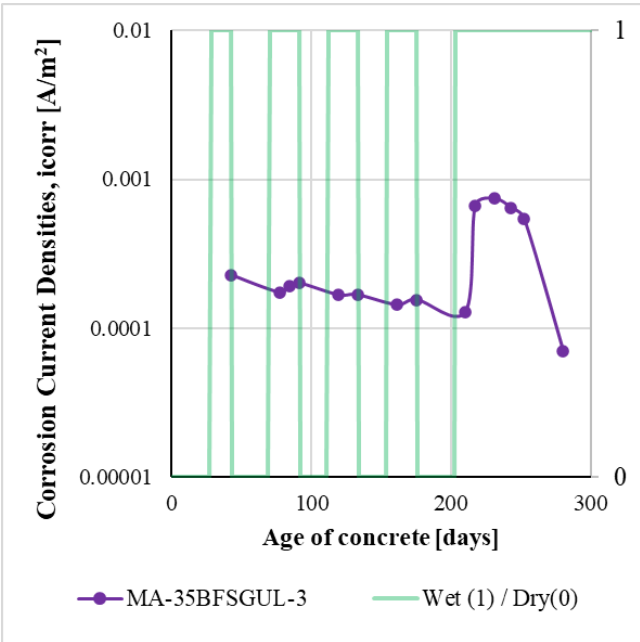
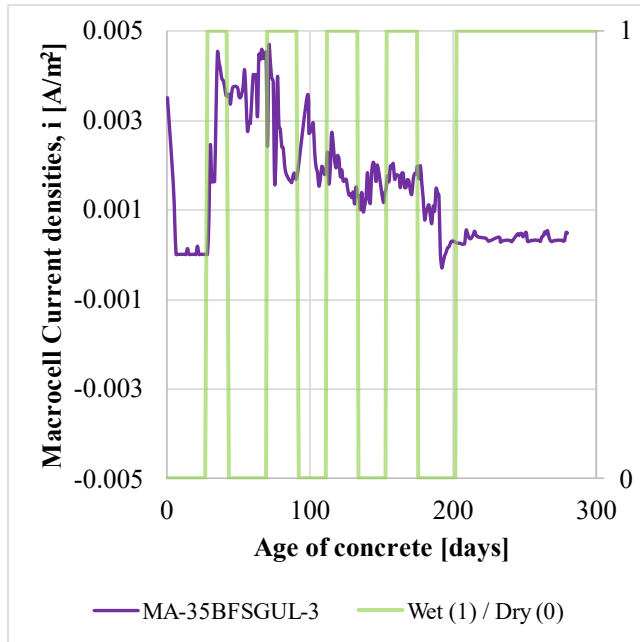
13b) Bottom Bars of MA-35BFSGUL-2 concrete specimen (autopsied)



BEFORE



14a) Top Bar of MA-35BFGUL-3 concrete specimen (autopsied)



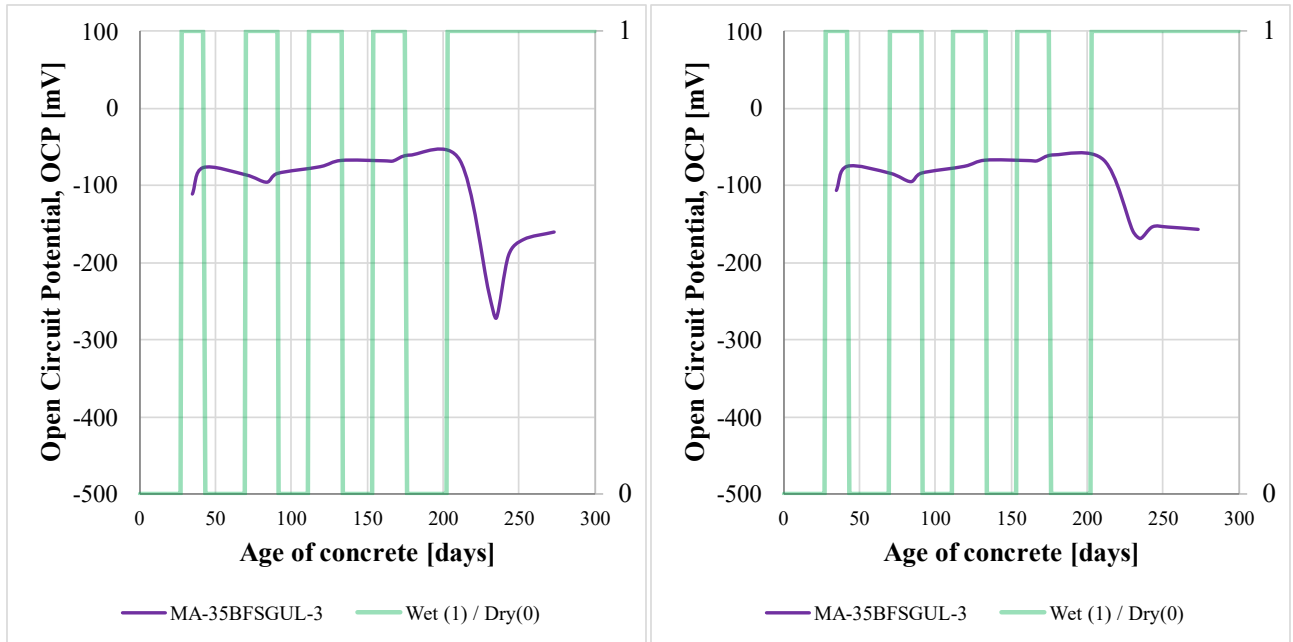
Specimen	Depth Point	Cl [%]	Fe [%]	Ca [%]	Al [%]	Si [%]	S [%]	Mg [%]
MA-35BFGUL-3	1	0.712	0.304	22.427	0.321	4.434	0.259	2.414
	2	0.506	0.626	18.666	0.973	19.444	0.813	1.337
	3	0.034	0.597	21.233	0.434	5.296	0.987	<LOD
	4	0.033	0.570	18.961	0.280	3.583	0.601	<LOD
	5	0.032	0.837	24.948	0.603	7.059	0.353	0.892
	6	0.031	0.794	27.460	0.891	8.423	0.723	1.241

Note: <LOD = Below limit of detection by XRF

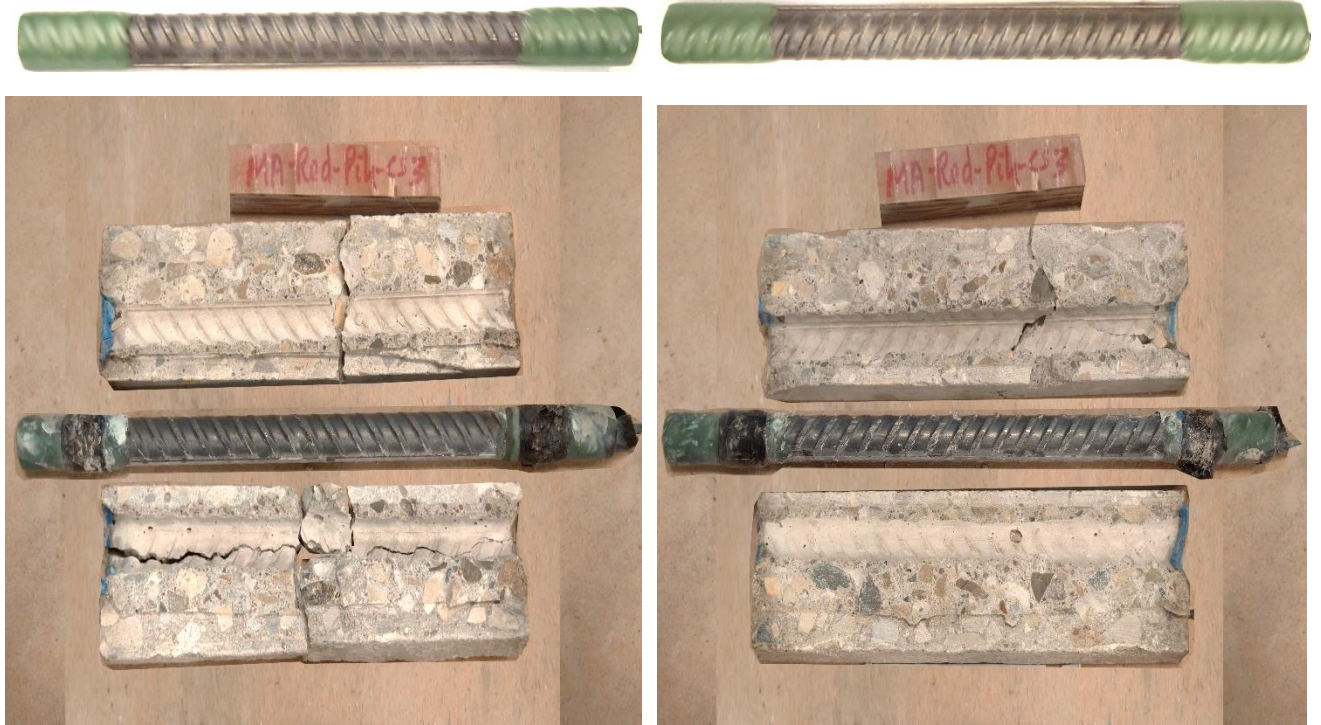
BEFORE



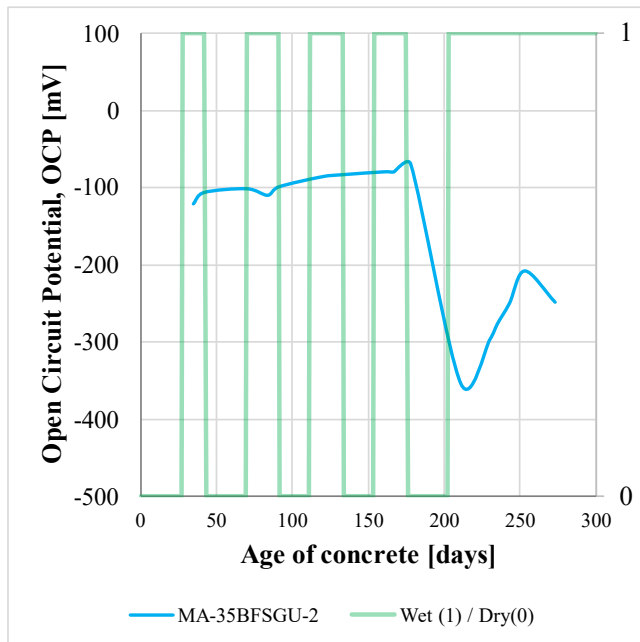
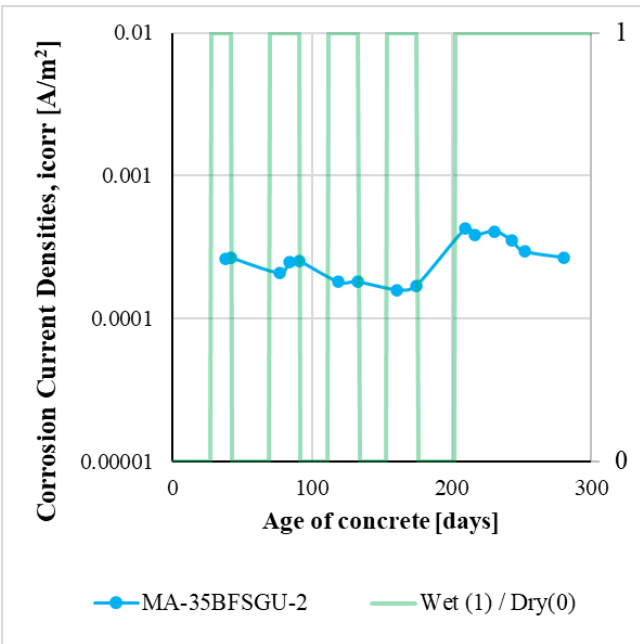
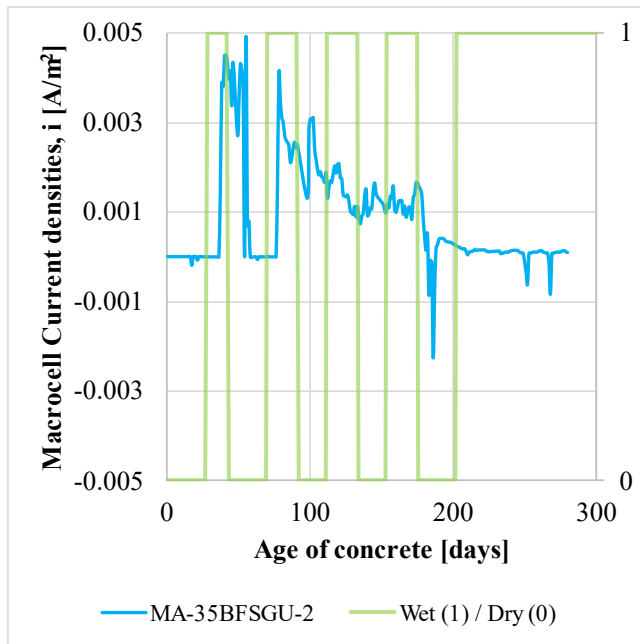
14b) Bottom Bars of MA-35BFGUL-3 concrete specimen (autopsied)



BEFORE



15a) Top Bar of MA-35BFGU-2 concrete specimen (autopsied)



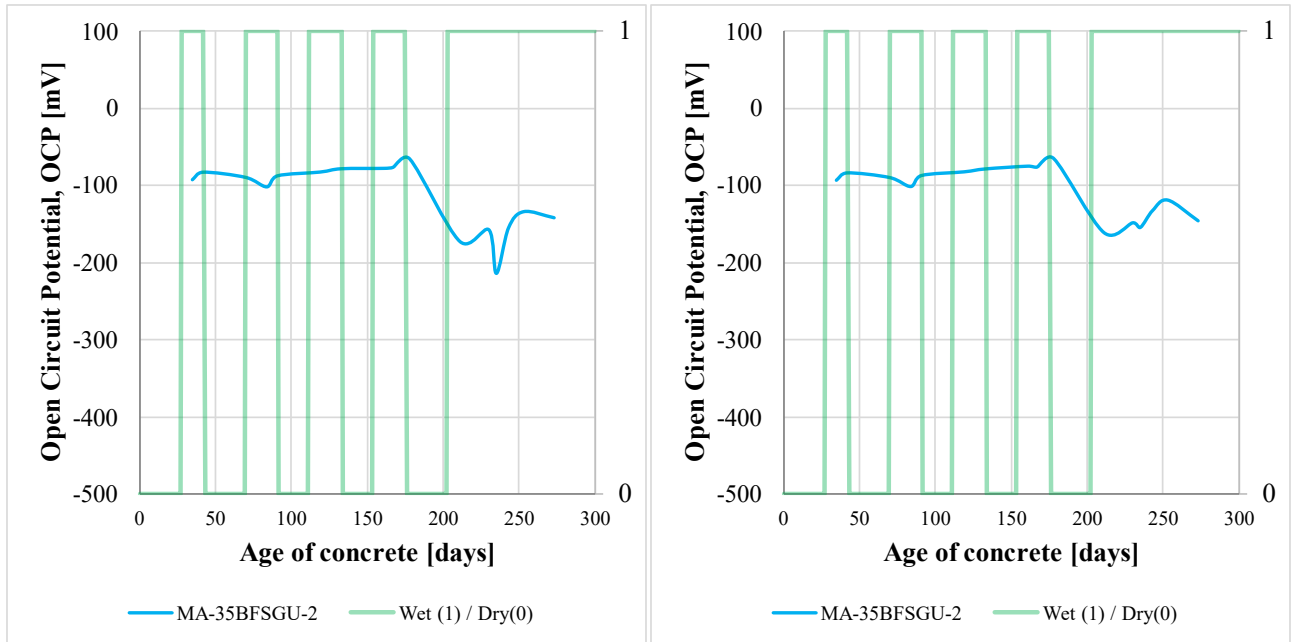
Specimen	Depth Point	Cl [%]	Fe [%]	Ca [%]	Al [%]	Si [%]	S [%]	Mg [%]
MA-35BFGU-2	1	0.760	0.557	17.011	0.342	9.350	0.368	0.947
	2	0.075	1.121	22.530	1.078	11.378	0.942	1.421
	3	0.037	0.584	17.920	0.256	3.600	0.777	<LOD
	4	0.044	0.964	22.174	0.723	8.444	0.966	<LOD
	5	0.051	0.673	18.751	0.508	4.499	0.876	<LOD
	6	0.045	0.679	17.708	0.420	4.173	0.753	1.303

Note: <LOD = Below limit of detection by XRF

BEFORE



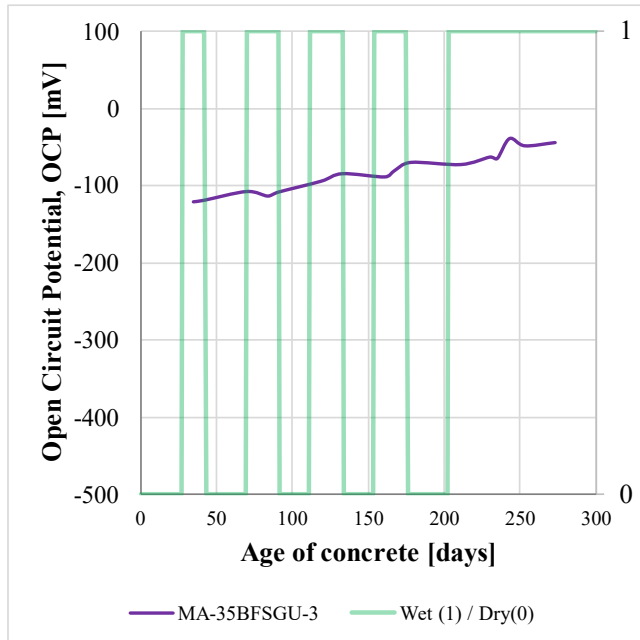
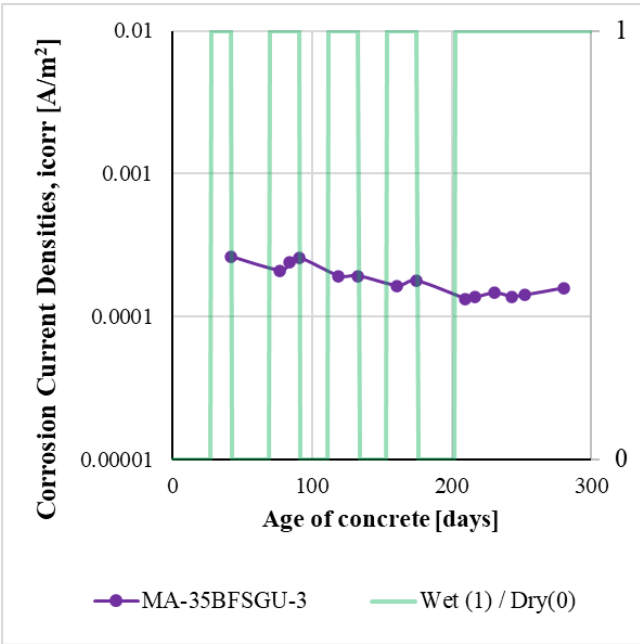
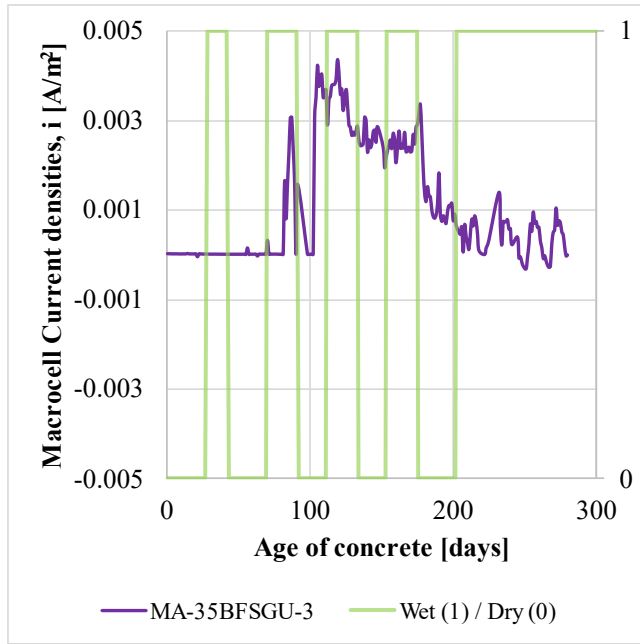
15b) Bottom Bars of MA-35BFGU-2 concrete specimen (autopsied)



BEFORE



16a) Top Bar of MA-35BFGU-3 concrete specimen (autopsied)



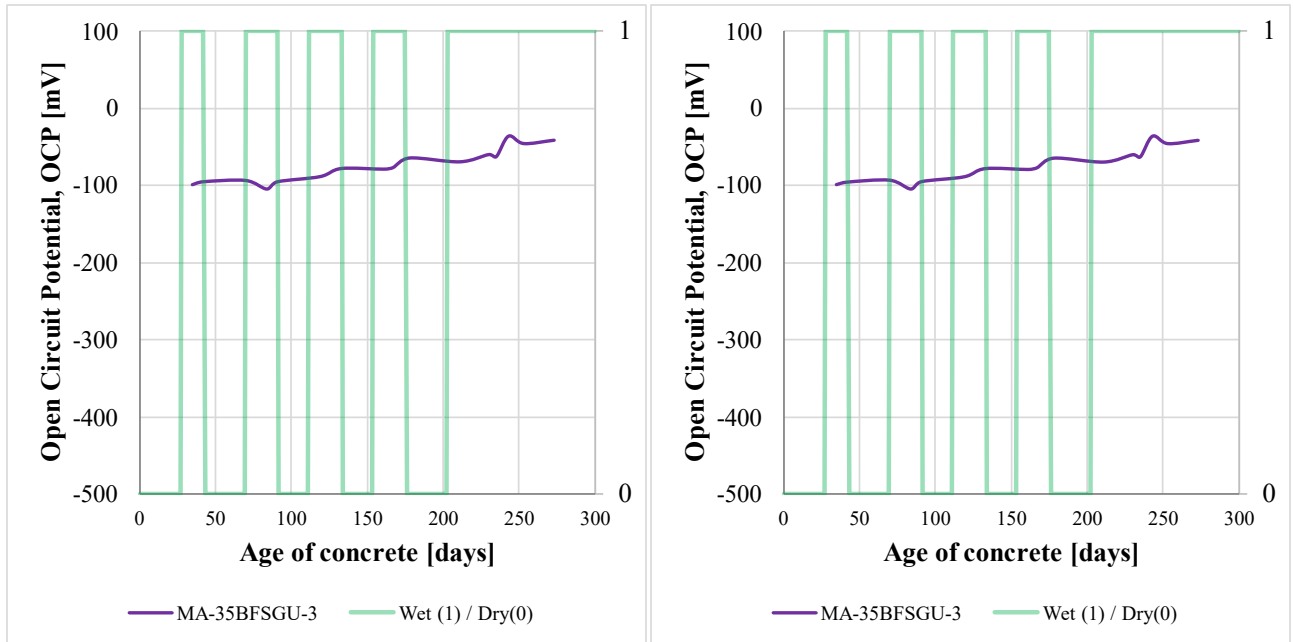
Specimen	Depth Point	Cl [%]	Fe [%]	Ca [%]	Al [%]	Si [%]	S [%]	Mg [%]
MA-35BFGU-3	1	0.614	1.106	27.222	0.976	10.667	0.407	1.429
	2	0.102	0.757	22.933	0.784	7.148	0.506	2.551
	3	0.038	0.740	22.416	0.546	7.435	1.016	<LOD
	4	0.045	0.628	18.522	0.346	4.945	0.829	<LOD
	5	0.041	1.002	23.887	1.159	8.821	0.599	3.233
	6	0.052	0.378	20.252	0.328	3.983	0.489	<LOD

Note: <LOD = Below limit of detection by XRF

BEFORE



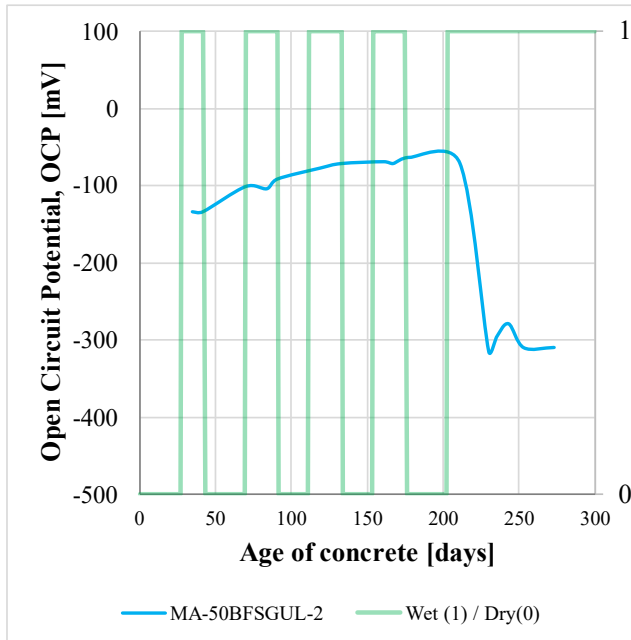
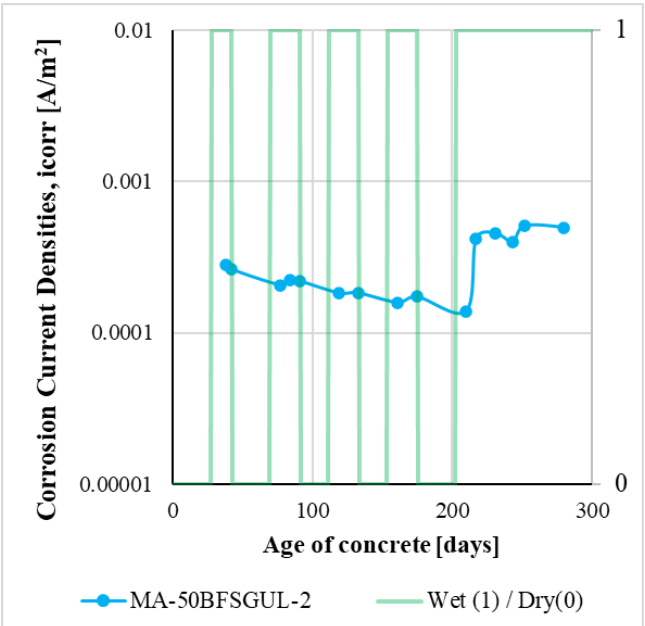
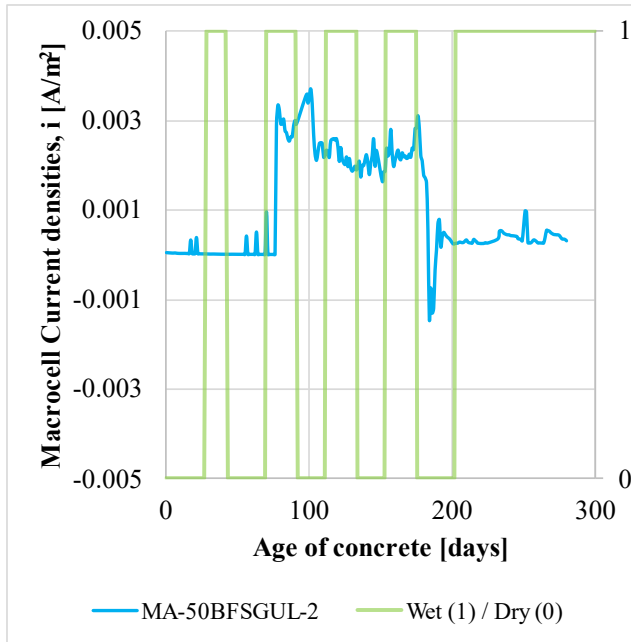
16b) Bottom Bars of MA-35BFSGU-3 concrete specimen (autopsied)



BEFORE



17a) Top Bar of MA-50BFGUL-2 concrete specimen (autopsied)



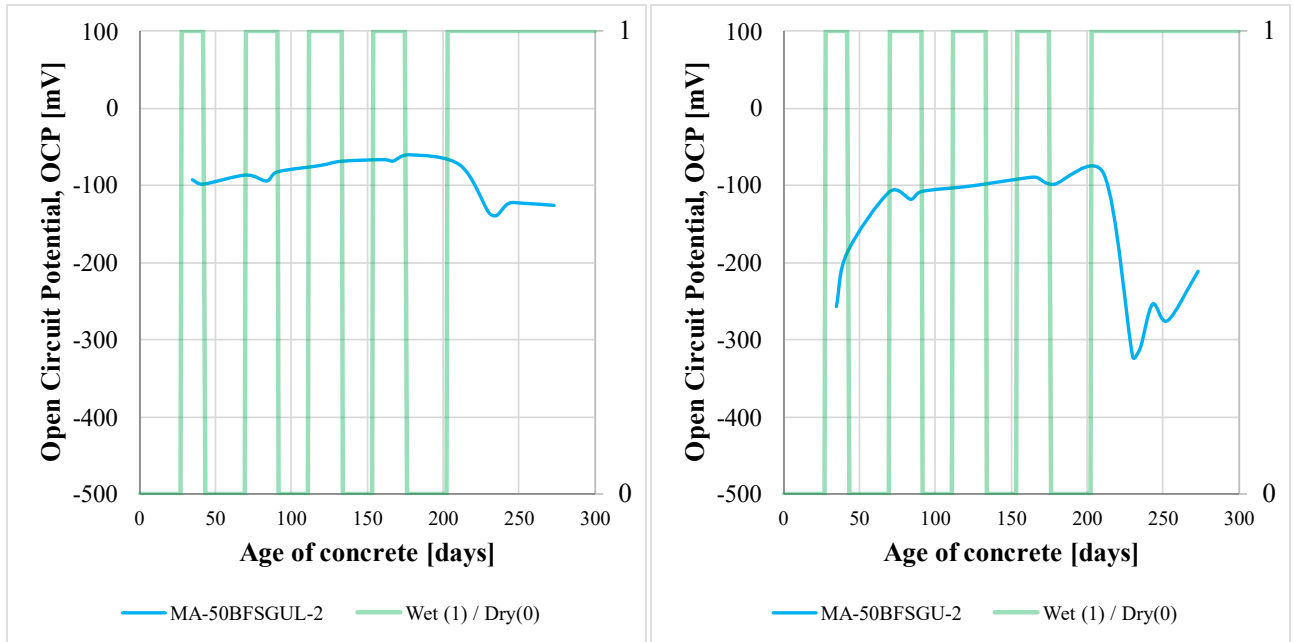
Specimen	Depth Point	Cl [%]	Fe [%]	Ca [%]	Al [%]	Si [%]	S [%]	Mg [%]
MA-50BFGUL-2	1	0.870	0.575	20.502	0.533	6.749	0.369	1.533
	2	0.197	0.747	21.961	0.945	9.737	0.834	1.101
	3	0.045	0.521	16.879	0.210	3.575	0.636	<LOD
	4	0.033	0.781	20.608	0.875	9.352	0.819	<LOD
	5	0.040	0.652	20.840	0.581	6.265	0.956	<LOD
	6	0.060	0.562	16.942	0.480	5.157	0.666	<LOD

Note: <LOD = Below limit of detection by XRF

BEFORE



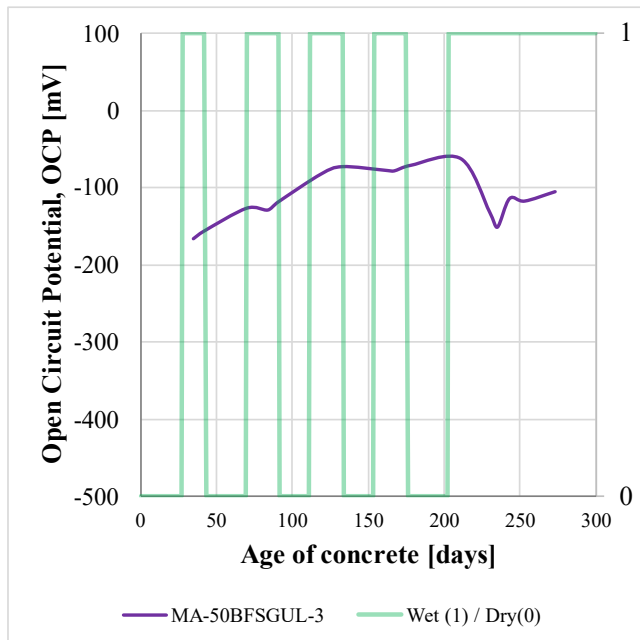
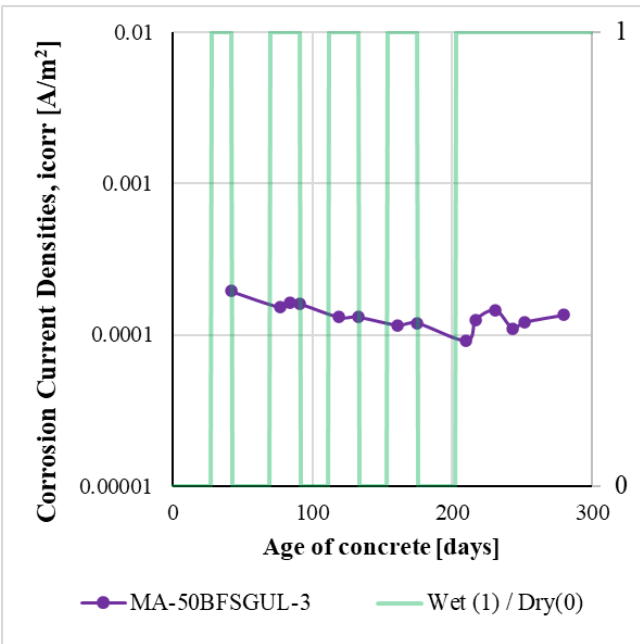
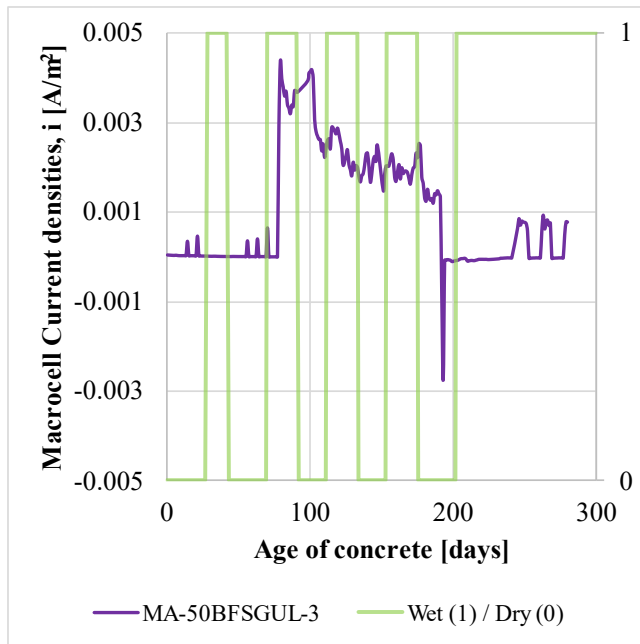
17b) Bottom Bars of MA-50BFGUL-2 concrete specimen (autopsied)



BEFORE



18a) Top Bar of MA-50BFGUL-3 concrete specimen (autopsied)



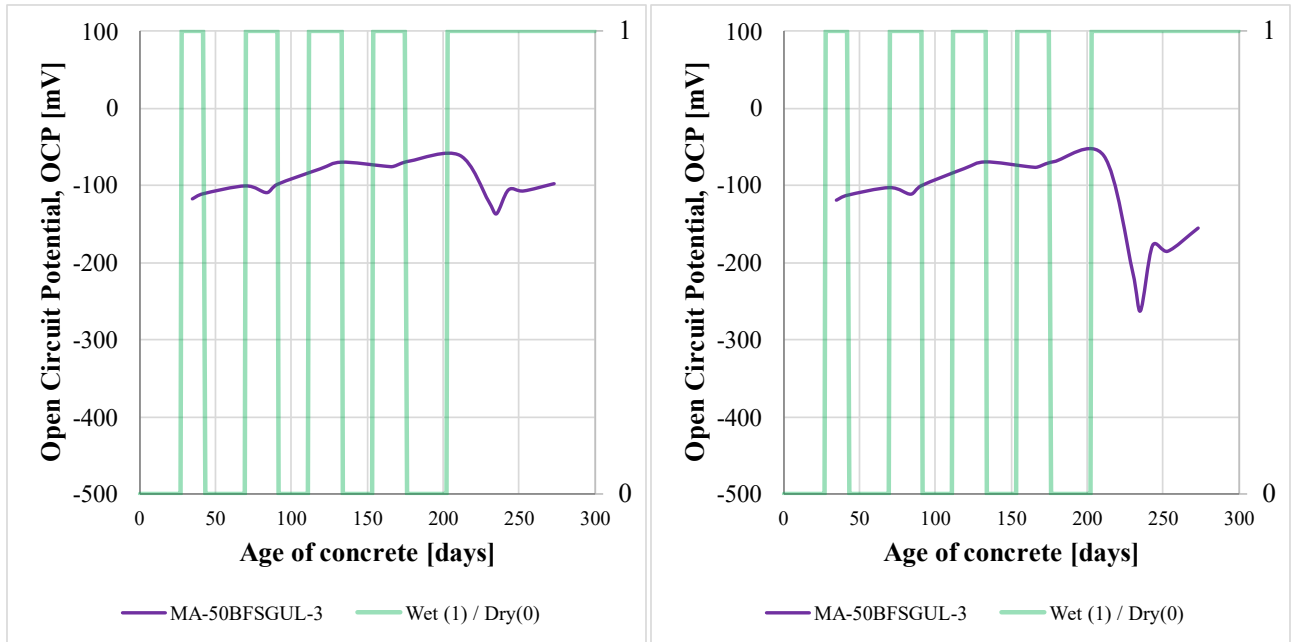
Specimen	Depth Point	Cl [%]	Fe [%]	Ca [%]	Al [%]	Si [%]	S [%]	Mg [%]
MA-50BFGUL-3	1	0.565	0.599	18.458	0.440	5.400	0.286	1.298
	2	0.313	0.756	20.808	0.880	8.755	0.651	1.964
	3	0.036	0.572	20.954	0.585	6.305	0.748	2.011
	4	0.030	0.624	17.769	0.247	3.650	0.671	<LOD
	5	0.036	0.732	19.479	0.720	8.001	0.637	0.863
	6	0.048	0.487	19.541	0.519	6.541	0.551	1.059

Note: <LOD = Below limit of detection by XRF

BEFORE



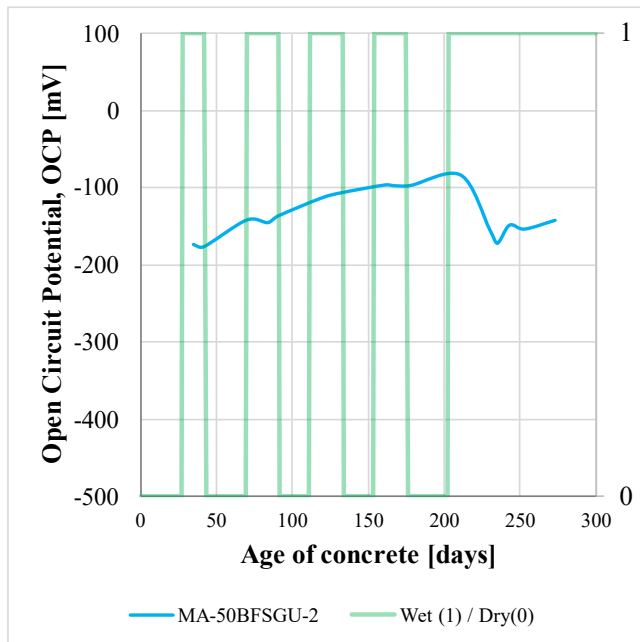
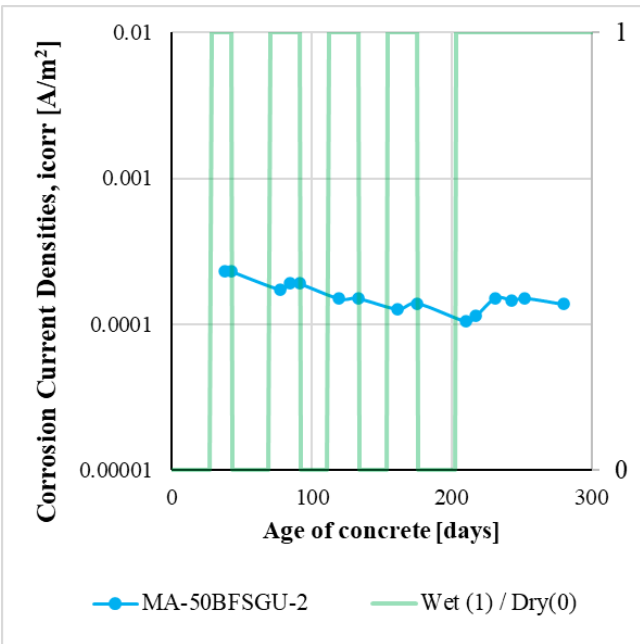
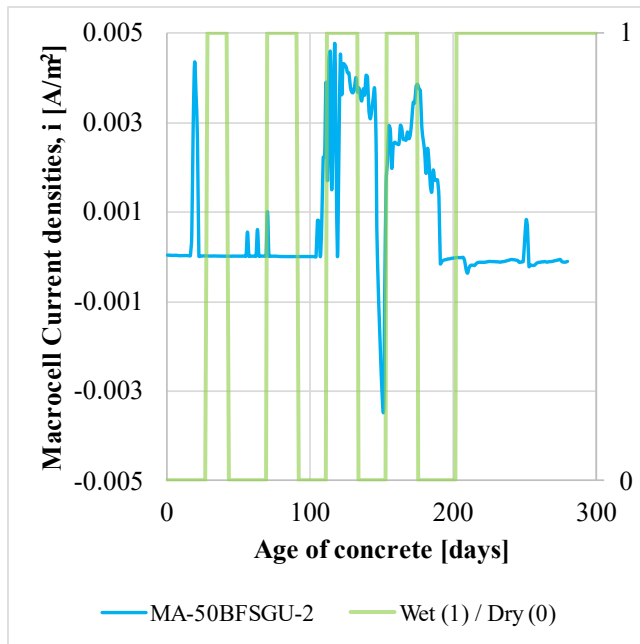
18b) Bottom Bars of MA-50BFGUL-3 concrete specimen (autopsied)



BEFORE



19a) Top Bar of MA-50BFGU-2 concrete specimen (autopsied)



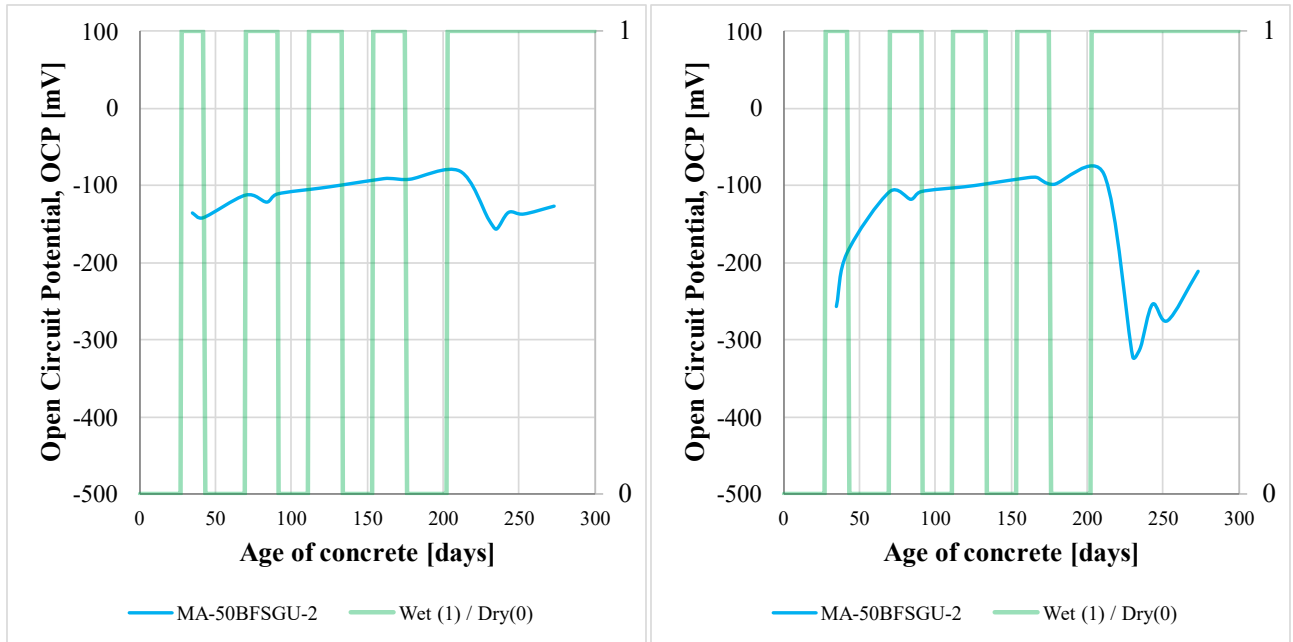
Specimen	Depth Point	Cl [%]	Fe [%]	Ca [%]	Al [%]	Si [%]	S [%]	Mg [%]
MA-50BFGU-2	1	0.704	0.722	19.839	0.577	6.975	0.259	1.565
	2	0.171	0.703	25.217	0.719	8.134	0.692	0.876
	3	0.038	0.511	15.348	<LOD	3.240	0.596	<LOD
	4	0.046	0.651	19.741	0.596	7.179	0.670	<LOD
	5	0.049	0.739	20.057	0.394	5.380	0.907	<LOD
	6	0.057	0.471	13.622	<LOD	3.084	0.483	1.837

Note: <LOD = Below limit of detection by XRF

BEFORE



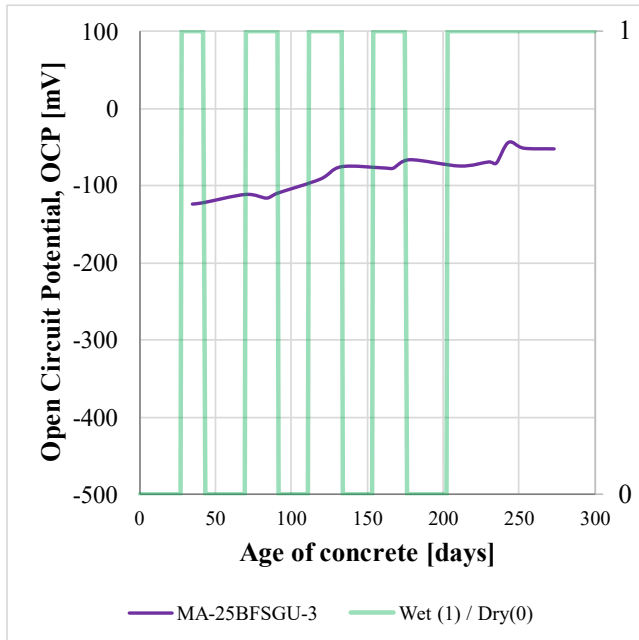
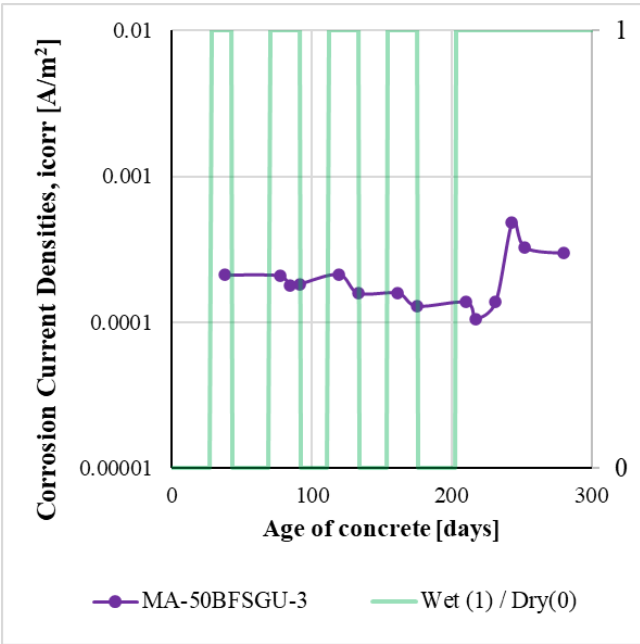
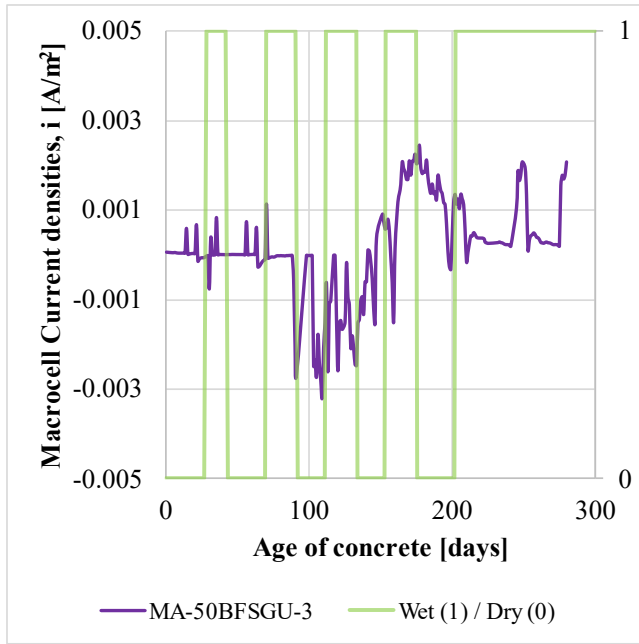
19b) Bottom Bars of MA-50BFGU-2 concrete specimen (autopsied)



BEFORE



20a) Top Bar of MA-50BFSGU-3 concrete specimen (autopsied)



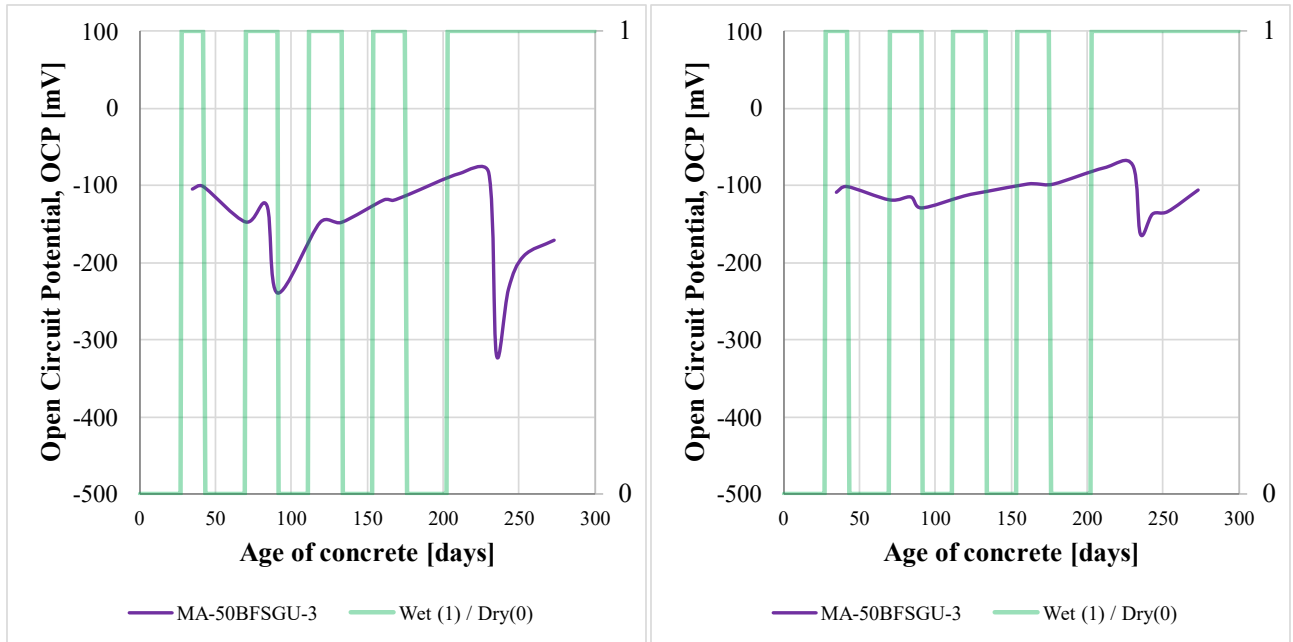
Specimen	Depth Point	Cl [%]	Fe [%]	Ca [%]	Al [%]	Si [%]	S [%]	Mg [%]
MA-50BFSGU-3	1	0.743	0.712	20.528	0.875	8.936	0.380	1.746
	2	0.082	0.661	22.315	1.259	11.122	0.680	1.980
	3	0.035	0.738	20.336	0.857	9.227	0.915	1.032
	4	0.052	0.503	14.163	<LOD	2.818	0.467	<LOD
	5	0.044	1.557	17.778	1.065	11.679	0.618	1.106
	6	0.053	0.543	18.510	0.434	5.814	0.549	<LOD

Note: <LOD = Below limit of detection by XRF

BEFORE



20b) Bottom Bars of MA-50BFSGU-3 concrete specimen (autopsied)



BEFORE



C.2 Sketch of Layout of Concrete Specimens in Monitoring Room

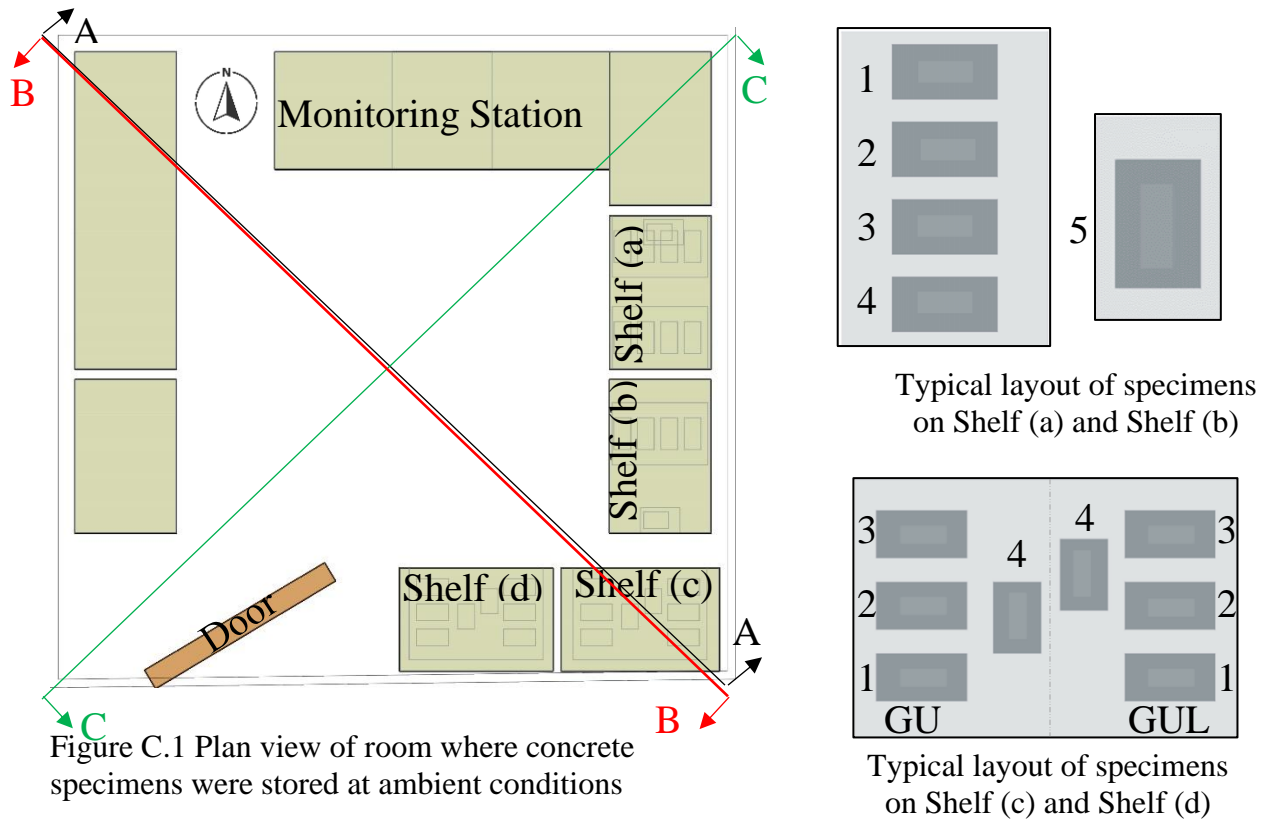


Figure C.1 Plan view of room where concrete specimens were stored at ambient conditions

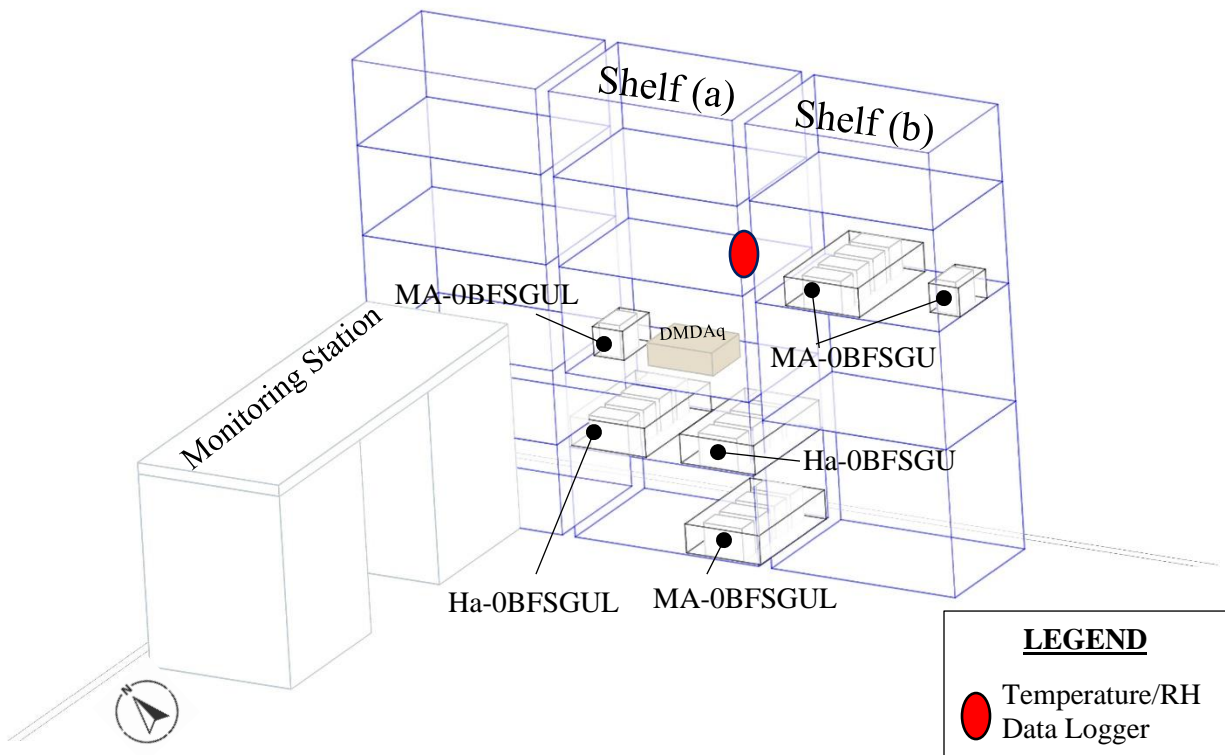


Figure C.2 A-A Section view of monitoring room

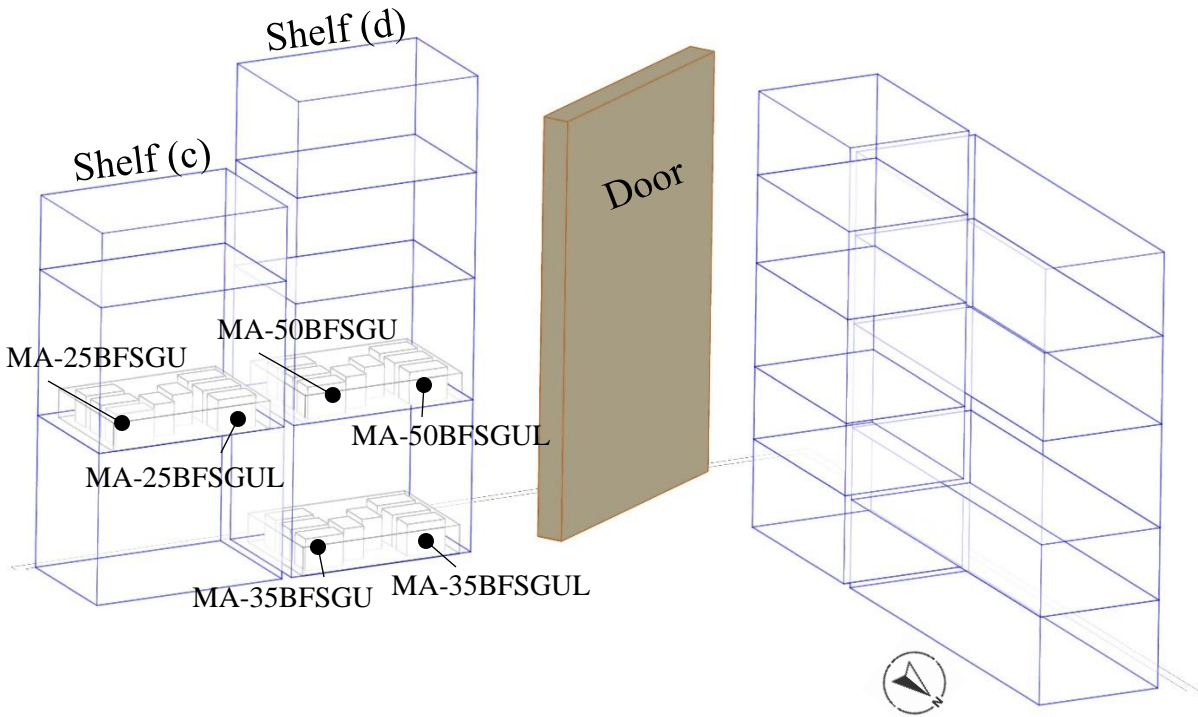
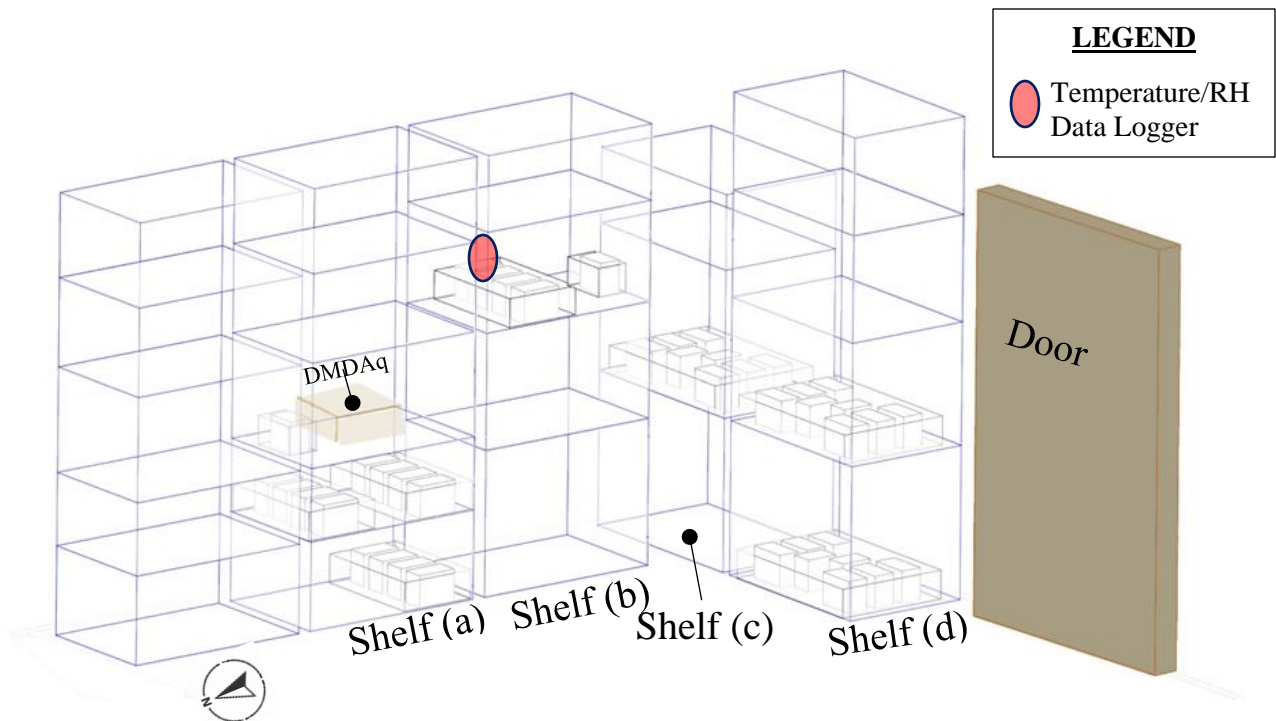


Figure C.3 B-B Section view of monitoring room



LEGEND
 ○ Temperature/RH Data Logger

Figure C.4 C-C Section view of monitoring room